UNIVERSIDAD DE ALCALÁ
ESCUELA POLITÉCNICA SUPERIOR

Electrónica Sistemas Electrónicos Avanzados. Sistemas Inteligentes

UNIVERSITÉ DE TOUNIS EL MANAR
L'ÉCOLE NAT. D'INGENIEUR DE TUNIS

Systéme de Communication

Local Positioning System with Ultrasonic Beacons for 3D Environments

Author:
Khaoula Mannay

Supervisors:
Dr. Jesús Ureña Ureña and Dr. Álvaro Hernández Alonso
Dr. Mohsen Machhout and Dr. Taoufik Aguili

2020
Doctoral Thesis

إلى والديّ وإخوتي

لولا دعمكم ، تفهمكم ، تشجيعكم و حبكم لما كان هذا العمل ممكنًا

شكرا لكم

To my parents and brothers,
Without your support, your understanding, your encouragement and your loves,
this work would not have been possible,
Thank you.

À mes parents et frères,
Sans vos soutiens, vos compréhensions, vos encouragements et vos amours,
ce travail n'aurait pas été possible,
Merci.

A mis padres y hermanos,
Sin su apoyo, su comprensión, su aliento y sus amores, este trabajo no hubiera sido posible,
Gracias.

Acknowledgements

First of all, I would like to thank my Tunisian thesis director Pr. Mohsen Machhout and my Tunisian co-Tutor Pr. Taoufik Aguili because they believed in me and incorporate me as a researcher within their Laboratories EμE-FSM at the university of Monastir and SysCom-ENIT at the University of Tunis El Manar, then for their advice and supports during the course of this thesis, as well as all the researcher's group of those labs.

I would like, also, to acknowledge my Spanish director Pr. Jesús Ureña, and my co-tutor Pr. Álvaro Hernández for admitting to supervise me, to allow me to be a part of an interesting research topic, as well to be a member of the Laboratory Geintra-group at the University of Alcala. Also, for their welcomes and supports during the courses of the stay, as well as their attitudes and commitments in the thesis work. Listening to the various problems topic (sociocultural, administrative and technic and etc.), discussing the possible solutions, then offering me improvements and differences that have enriched my learning to complete my work as well to improve my personality by discovering more about other culture (the fact that the lab presents a cultural diversity due to the number of nationalities that integrate it). I enjoyed our discussion times talking about different point of view and our weekly meetings.

I would also like to thank the other current and past members of the GEINTRA-US&RF group, especially David, Santiago, Rubén, Martin, Edel, Elena, Sara, Jorge, Sergeo, Miguel Angel and etc. who have made me have a very good time both in the meals and in the meetings we organize.

I can't forget the professors José M. Villadangos, Maria Carmen Pérez, Juan Jesús García, Juan Carlos García, Ana Jiménez and the rest of the teachers who belong to the research. It is a pleasure to have worked with them because they are an excellent working team by sharing their ideas, initiatives and advises.

In these acknowledgements, I cannot forget the role that my parents and my brothers presented. They have been my principal inspiration to be the best version of me. For everything they have done and sacrificed to support me and to help me to draw a big smile in my face, my heart and my life too, Just Thank you my All.

Abstract

This PhD Thesis contributes with the development and improvement of Indoor Location and Positioning Systems (ILPS), which are used to locate, position and track people, as well as mobile and/or connected targets, such as robots or smartphones, not only inside buildings in the lack of GNSS (Global Navigation Satellite Systems) signals, but also in constrained outdoor situations with reduced coverage. Indoor positioning applications and their interest are growing in certain environments, such as commercial centres, airports, hospitals or factories. Several sensory technologies have already been applied to indoor positioning systems, as infrared, Wi-Fi, light, cameras, or radiofrequency, where ultrasounds are a common solution due to its low cost and simplicity.

This thesis deals with the development of 3D positioning systems based on ultrasounds. So, its contributions are divided into three blocks. The first one proposes a 3D Ultrasonic Local Positioning System (ULPS), based on a set of three asynchronous ultrasonic beacon units, capable of transmitting coded signals independently, and on a 3D mobile receiver prototype. The proposal is based on the aforementioned beacon unit, which consists of five ultrasonic transmitters oriented towards the same coverage area and has already been proven in 2D positioning by applying hyperbolic multilateration. Those beacon units are manually calibrated and placed in strategic and known positions of three perpendicular walls (generally in the centre of the ceiling and two perpendicular walls). This approach has been characterized and experimentally verified, trying to maximize the coverage zone, at least for typical sizes in most common public room and halls.

The second block deals with several fusion methods, to obtain the final estimated position of the mobile receiver existing inside the positioning space, assuming a low accumulative error, after merging the particular results from each beacon unit. Two merging ways have been presented and implemented: the loosely and the tightly coupled fusions. For the loosely coupled method, three algorithms have been applied: the Maximum Likelihood Estimation (MLE) fusion algorithm, the Linear Kalman Filter (LKF) and the Adaptive Kalman Filter (AKF). These algorithms fuse the positions obtained from several ULPSs to get a final more accurate position. With regard to the tightly coupled fusion methods, three algorithms have also been applied, which are based on: the Extended Kalman Filter (EKF) for only one ULPS; three EKFs for the three independent ULPS; and finally only one EKF for all the set of three ULPSs.

On the other hand, the third block proposes a preliminary SoC architecture based on a FPGA device for the receiver stage, so it can be deployed on board a mobile target (people, robot, drone, smartphones, etc.). The architecture involves a specific hardware peripheral, connected to the processor, which is in charge of implementing the low-level processing of the ultrasonic signals (particularly a BPSK demodulation and a transmission encoding with Kasami sequences).

Finally, all the proposals aforementioned have been verified by simulations and experimental tests, contributing to the design and improvement of the ultrasonic LPSs as well as to the deployment of these systems in several real environments. Simulations and experimental tests have been satisfactory, achieving a positioning accuracy in the range of centimetres in the zone where the coverages from the three ultrasonic beacon units are available, whereas it is in the range of decimetres whether the coverage from one or more beacon units is missing. Particularly, two different experimental environments have been considered: a small volume with many furniture (Lab), and a large and empty volume (Hall); tests have been carried out at points distributed in the environment to consider those cases of interest.

Résumé

Cette thèse de doctorat contribue au développement et à l'amélioration des systèmes de localisation et de positionnement intérieurs (ILPS), qui sont utilisés pour localiser, positionner et suivre des personnes, ainsi que des cibles mobiles et/ou connectées, telles que des robots ou des smartphones, non seulement à l'intérieur des bâtiments en l'absence de signaux GNSS (Global Navigation Satellite Systèmes) mais aussi dans des situations extérieures contraignantes avec une couverture réduite. Les applications de positionnement en intérieur et leur intérêt se développent dans certains environnements, tels que les centres commerciaux, les aéroports, les hôpitaux ou les usines. Plusieurs technologies sensorielles ont déjà été appliquées aux systèmes de positionnement intérieur, comme l'infrarouge, le Wi-Fi, la lumière, les caméras ou la radiofréquence, où les ultrasons sont une solution courante en raison de leur faible coût et de leur simplicité.

Cette thèse porte sur le développement de systèmes de positionnement 3D basés sur les ultrasons. Ainsi, ses contributions sont divisées en trois blocs. Le premier propose un système de positionnement local à ultrasons en 3D (ULPS), basé sur un ensemble de trois unités de balises à ultrasons asynchrones, capables de transmettre des signaux codés indépendamment, et sur un prototype de récepteur mobile en 3D. La proposition est basée sur l'unité de balise susmentionnée, qui consiste en cinq émetteurs ultrasoniques orientés vers la même zone de couverture et a déjà fait ses preuves en matière de positionnement 2D par application de la trilatération hyperbolique. Ces unités de balises sont calibrées manuellement et placées dans des positions stratégiques et connues de trois parois perpendiculaires (généralement au centre du plafond et de deux parois perpendiculaires). Cette approche a été caractérisée et vérifiée expérimentalement, en essayant de maximiser la zone de couverture, au moins pour des tailles typiques dans la plupart des salles et des halls publics.

Le deuxième bloc traite plusieurs méthodes de fusion, pour obtenir la position estimée finale du récepteur mobile existant à l'intérieur de l'espace de positionnement, en supposant une faible erreur cumulée, après avoir fusionné les résultats particuliers de chaque unité de balise. Deux méthodes de fusion ont été présentées et mises en œuvre : la fusion à couplage lâche et la fusion à couplage serré. Pour la méthode à couplage lâche, trois algorithmes ont été appliqués : l'algorithme de fusion par estimation de probabilité maximale (MLE), le filtre de Kalman linéaire (LKF) et le filtre de Kalman adaptatif (AKF). Ces algorithmes fusionnent les positions

obtenues à partir de plusieurs ULPSs pour obtenir une position finale plus précise. En ce qui concerne les méthodes de fusion à couplage étroit, trois algorithmes ont également été appliqués, qui sont basés sur : le filtre de Kalman étendu (EKF) pour un seul ULPS ; trois EKF pour les trois ULPSs indépendants ; et enfin un seul EKF pour les trois ULPSs.
D'autre part, le troisième bloc propose une architecture SoC préliminaire basée sur un dispositif FPGA pour l'étage récepteur, afin qu'il puisse être déployé à bord d'une cible mobile (personnes, robot, drone, smartphones, etc.). L'architecture implique un périphérique matériel spécifique, connecté au processeur, qui est chargé de mettre en œuvre le traitement de bas niveau des signaux ultrasonores (notamment une démodulation BPSK et un codage de transmission avec des séquences Kasami).

Enfin, toutes les propositions susmentionnées ont été vérifiées par des simulations et des tests expérimentaux, contribuant à la conception et à l'amélioration des LPS ultrasoniques ainsi qu'au déploiement de ces systèmes dans plusieurs environnements réels. Les simulations et les tests expérimentaux ont été satisfaisants, permettant d'atteindre une précision de positionnement de l'ordre de quelques centimètres dans la zone où les couvertures des trois unités de balises à ultrasons sont disponibles, alors qu'il est de l'ordre de quelques décimètres lorsque la couverture d'une ou plusieurs unités de balises soit manquante. En particulier, deux environnements expérimentaux différents ont été considérés : un petit volume avec beaucoup de mobilier (Lab), et un grand volume vide (Hall) ; où des tests ont été effectués à des points répartis dans l'environnement pour examiner les cas intéressants.

Resumen

Esta tesis doctoral contribuye al desarrollo y mejora de los sistemas de localización y posicionamiento en interiores (ILPS), que se utilizan para localizar, posicionar y rastrear personas, así como objetivos móviles y/o conectados, como robots o teléfonos inteligentes, no sólo en el interior de edificios en ausencia de señales de GNSS (Sistemas Globales de Navegación por Satélite), sino también en situaciones exteriores limitadas con cobertura reducida. Las aplicaciones de posicionamiento en interiores y su interés están creciendo en determinados entornos, como centros comerciales, aeropuertos, hospitales o fábricas. Ya se han aplicado varias tecnologías sensoriales a los sistemas de posicionamiento en interiores, como el infrarrojo, el Wi-Fi, la luz, las cámaras o la radiofrecuencia, en los que los ultrasonidos son una solución común debido a su bajo coste y simplicidad.

Esta tesis trata del desarrollo de sistemas de posicionamiento 3D basados en ultrasonidos. Sus contribuciones se dividen en tres bloques. El primero propone un Sistema de Posicionamiento Local por Ultrasonidos en 3D (ULPS), basado en tres unidades de baliza asíncrona de ultrasonidos, capaces de transmitir señales codificadas de forma independiente, y en un prototipo de receptor móvil en 3D. La propuesta se basa en la mencionada unidad de baliza, que consta de cinco transmisores de ultrasonidos orientados hacia la misma zona de cobertura y que ya ha sido probada en el posicionamiento 2D mediante la aplicación de la multilateración hiperbólica. Esas unidades de baliza se calibran manualmente y se colocan en posiciones estratégicas y conocidas de tres paredes perpendiculares (generalmente en el centro del techo y dos paredes perpendiculares). Este enfoque se ha caracterizado y verificado experimentalmente, tratando de maximizar la zona de cobertura, al menos para los tamaños típicos en la mayoría de las salas y espacios públicos.

El segundo bloque trata de varios métodos de fusión, para obtener la posición final estimada del receptor móvil existente dentro del espacio de posicionamiento, suponiendo un bajo error acumulativo, después de fusionar los resultados particulares de cada unidad de baliza. Se han presentado e implementado dos formas de fusión: la fusión de acoplamiento loosely y la de acoplamiento tightly. Para el método de acoplamiento débil se han aplicado tres algoritmos: el algoritmo de fusión de la Estimación de Máxima Verosimilitud (MLE), el Filtro Lineal de Kalman (LKF) y el Filtro Adaptativo de Kalman (AKF). Estos algoritmos fusionan las posiciones obtenidas de los diversos ULPSs para obtener una posición final más precisa. En

cuanto a los métodos de fusión fuertemente acoplados, también se han aplicado tres algoritmos, que se basan en: el Filtro de Kalman Extendido (EKF) para un solo ULPS; tres EKF para los tres ULPSs independientes; y finalmente un solo EKF para los tres ULPSs.

Por otra parte, el tercer bloque propone una arquitectura preliminar SoC basada en un dispositivo FPGA para la etapa receptora, de manera que pueda ser desplegada a bordo de un objetivo móvil (personas, robot, dron, smartphones, etc.). La arquitectura implica un periférico de hardware específico, conectado al procesador, que se encarga de implementar el procesamiento de bajo nivel de las señales ultrasónicas (en particular una demodulación BPSK y una detección de transmisiones codificadas con secuencias Kasami).

Por último, todas las propuestas mencionadas se han verificado mediante simulaciones y pruebas experimentales, lo que ha contribuido al diseño y la mejora de los LPS ultrasónicos, así como a la implantación de estos sistemas en varios entornos reales. Las simulaciones y pruebas experimentales han sido satisfactorias, logrando una precisión de posicionamiento en el rango de centímetros en la zona en que se dispone de las coberturas de las tres unidades de baliza ultrasónicas, mientras que está en el rango de decímetros cuando falta la cobertura de una o más unidades de baliza. En particular, se han considerado dos entornos experimentales diferentes: un pequeño volumen con muchos muebles (Lab), y un volumen grande y vacío (Hall); se han realizado pruebas en puntos distribuidos en el entorno para considerar los casos de interés.

Contents

List of Tables

List of Figures

Glossary

ABS	*Anti-lock Braking System*
AKF	*Adaptive Kalman Filter*
AOA	*Angle of Arrival*
AOD	*Angle of Departure*
API	*Application Programming Interface*
BLE	*Bluetooth Low Energy*
BPSK	*Binary Phase-Shift Keying*
CDF	*Cumulative Probability Function*
CDMA	*Code Division Multiple Access*
EKF	*Extended Kalman Filter*
FPGA	*Field Programmable Gate Array*
ID	*IDentifier*
IMU	*Inertial Measurement Unit*
IP	*Intellectual Propriety*
IPS	*Indoor Positioning System*
ISM	*Industrial Scientific and Medical*
GDOP	*Geometric Dilution of Precision*
GLONASS	*GLObal NAvigation Satellite System*
GNSS	*Global Navigation Satellite System*
GPS	*Global Positioning System*
GSM	*Global System of Mobile*
ISI	*Inter-Symbol Interferences*
IR	*Infrared*
KF	*Kalman Filter*
k-NN	*k-Nearest Neighbor*
LBS	*Location-Based Services*
LPS	*Local Positioning System*
LED	*Light-Emitting Diode*

MAI	*Multiple Access Interference*
MEMS	*Micro-Electro-Mechanical Systems*
MLE	*Maximum Likelihood Estimation*
NFC	*Near Field Communication*
NNSS	*Nearest Neighbor in Signal Space*
PC	*Personal Computer*
PDA	*Personal Digital Assistant*
PDOP	*Position (3D) Dilution of Precision*
PDR	*Pedestrian Dead Reckoning*
PL	*Programmable logic*
RF	*Radio Frequency*
RFID	*Radio-Frequency Identification*
RSS	*Received Signal Strength*
RSSI	*Received Signal Strength Indicator*
SNR	*Signal to Noise Ratio*
SD memory	*Secure Digital Memory Card*
SOC	*System on Chip*
Std	Standard deviation
TDOA	*Time Difference of Arrival*
TDMA	*Time Division Multiplexing Access*
TOA	*Time of Arrival*
TOF	*Time of Flight*
UART	*Universal Asynchronous Receiver Transmitter*
ULPS	*Ultrasonic Local Positioning System*
US	*Ultrasonic Signal*
USB	*Universal Serial Bus*
UWB	*Ultra-wideBand*
VDOP	*Vertical Dilution of Precision*
VLC	*Visible Light Communication*
WLAN	*Wireless Local Area Network*
WSN	*Wireless Sensor Network*
2D	*2 Dimension*

3D *3 Dimension*

Nomenclature

σ_m	*Standard deviation in the distance measurements.*
σ_x	*Position variances in X.*
σ_y	*Position variances in Y .*
σ_z	*Position variances in Z.*
$\Delta d_{ij,k}$	*Difference of distance of the position to the i^{th} beacon using the beacon j as a reference at instant k.*
A	*Transition matrix.*
A_k	*Derivative with respect to each component of the state vector of the relationship between the previous and current state k adding the a priori information.*
B_{ij}	*Coordinates of the i^{th} beacon of the j^{th} ULPS.*
$B_{ij,k}$	*Coordinates of the i^{th} beacon of the j^{th} ULPS at instant k.*
C	*Velocity of sound in air (here assumed 340m/s).*
c_i	*Kasami code.*
$d_{ij,k}$	*Distance of the receiver position to the i^{th} beacon using the beacon j as a reference at instant k.*
d_i	*Distance of the receiver position to the i^{th} beacon.*
d_j	*Distance of the receiver position to the j^{th} beacon.*
$d[n]$	*Demodulated signal.*
fs	*Sampling frequency.*
H_k	*Derivative matrix related to the state vector of the relationship, between the state vector and the measurements at instant k.*
I	*Identity matrix.*
K	*Kalman gain.*

K_k	*Kalman Filter gain at instant k.*
k	*Instant k.*
L	*Length of the Kasami codes.*
M	*Length of the modulation symbol.*
N	*Number of ULPSs.*
P_k	*Covariance matrix of the state vector at instant k.*
P_A	*Estimated position from the receiver* R_A.
P_B	*Estimated position from the receiver* R_B.
P_C	*Estimated position from the receiver* R_C.
P_1	*Estimated position of ULPS-1.*
P_2	*Estimated position of ULPS-2.*
P_3	*Estimated position of ULPS-3.*
P_i	1^{st} *Set of ground truth positions of the mobile receiver.*
P'_i	2^{nd} *Set of ground truth positions of the mobile receiver.*
Q	*Process noise matrix.*
Q_k	*Covariance matrix related to a process equation.*
R	*Radius of the big base of the ULPS coverage volume.*
R	*Radius of the small base of the ULPS coverage volume.*
R	*Measurement noise matrix.*
R_k	*Covariance matrix related to a measurement noise matrix at instant k.*
R_A	*Receiver A.*
R_B	*Receiver B.*
R_C	*Receiver C.*
r_A	*Received ultrasonic signal in* R_A.

r_B	*Received ultrasonic signal in* R_B.
r_C	*Received ultrasonic signal in* R_C.
$r[n]$	*Acquired signal.*
$s[n]$	*Modulation symbol.*
$t_i[n]$	*Correlated signal.*
v_k	*Measurement noise, zero-mean white noise related to a measurement equation at instant k.*
w_k	*Process noise, zero-mean white noise related to a process equation at instant k.*
X_k	*Estimated position on the current state.*
X_{k-1}	*Estimated position on the previous state.*
z	*Beacons height variations from the ULPS' plane (0 cm for* B_2 *and* B_4*, 10 for* B_3 *and* B_5*, 20 cm for* B_1*).*
Z_k	*Vector that contains measurement information at instant k.*
z_1	*Distance between the 1st ground truths positions of the mobile receiver and the floor.*
z_2	*Distance between the 2nd ground truths positions of the mobile receiver and the floor.*

Chapter 1

Introduction

1.1 Indoor Positioning Systems

Localization and positioning systems are classified into global positioning systems and local positioning systems. Global positioning systems provide world-wide position estimations. The available global positioning systems is the Global Navigation Satellite System (GNSS). Its characteristics are the availability, coverage plus the compact size and the cheap price of the receivers. However, it does not fit all scenarios and applications due to the required accuracy as well as the degradation and the lack of satellite signals in closed environments (e.g. inside buildings). In those specific scenarios, Local Positioning Systems (LPS), called also Indoor Positioning System (IPS), are employed. Its local coverage varies significantly regarding the technology, the emitter architecture and its dimension, the used configuration and the units density in the systems based on sensors network to cover large areas or spaces [Men2019].

So, the IPS is a system capable of detecting, tracking, and localizing multiple targets accurately in an indoor environment. Typical applications of LPS include resource management, robot localization, environment monitoring, and people-tracking for purposes of special supervision, public safety, etc. Several preceding works addressed these tasks in extended indoor environments, like train/bus stations, airports, hospitals, universities, or commercial centers. So, the interest in developing systems able to positioning mobile targets is increasing [Mau2012].

The high interest for IPS has driven a developing a number of research works during the past 15 years or more. For instance, Table 1 gives the number of picked published reviews for the last five years according to [Men2019].

Year	2015	2016	2017	2018	2019
Number of reviews	12	16	13	13	7

Table 1.1. Distribution of publications about indoor positioning systems [Men2019].

The common LPS classification depends on technology (e.g. RF, Wi-Fi, light, ultrasonic, etc.), which defines the physical variables measured by the system, as well as on techniques (e.g. Angle of Arrival (AoA), Time of Flight (ToF), Time Difference of Flight (TDoF), Received Signal Strength (RSS), etc.), which are applied to measure those physical variables used to get the position estimates of the mobile target.

Positioning systems in 2D, such as the LOCATE-US unit based on ultrasonic technology and developed by the GEINTRA group of the University of Alcala, present good accuracy in the centimeter range. For 3D positioning systems, a sensor network is utilized, based on several beacon units installed in particular orientations to cover as much as possible all the space, trying to have a homogeneous ultrasonic coverage, which is a main parameter to have a stable accuracy. The final position estimates are obtained fusing data from the available beacon units at each time. That is why several fusion methods have been studied and applied (e.g. Maximum Likelihood Estimation (MLE), Extended Kalman Filter, etc.), trying to achieve a good accuracy over time in all the space. In general terms, the accuracy range for ultrasonic systems in 3D positioning can be also in the centimeter and the decimeter ranges even for large coverage areas.

1.2 Thesis Context and Objectives

Most of the research work done within this Thesis was developed under the structure of the research projects TARSIUS (ref. TIN2015-71564-c4-1-R) and SOC-PLC (ref. TEC2015-64835-C3-2-R) supported by the Spanish Ministry of Economy, Innovation and Competitiveness, as well as by LOCATE-US (ref. CCG2016/EXP-078), Echo-Drone3D (ref. CCGP2017-EXP/050) and LocActiv (ref. CCGP2017-EXP/053, and UAH-AE2017-4) sponsored by the University of Alcala and the María de Guzman grant of this University.

The Thesis was also been economically supported by the University Of Tunis el Manar by the mobility program and the national PhD grant, as well as by a Lab grant from the Electronic and Micro-Electronic Lab of the University of Monastir to allow research stays at the School of Engineering from the University of Alcala.

The motivations of those projects are the need of research in localization technologies and multi-sensors fusion techniques that allow complementing or replacing the Global Navigation Satellite System (GNSS) in the lack of its signals or in places where this system is not accessible (e.g. indoor environments), as well as extending the 2D Local Positioning System (LPS) to 3D

Local positioning System to get an accurate position in the space, granting them a deployment of services based on localization that are needed by the society.

Specific 3D configuration is used to study mobile positions and its tracking in the space, firstly in a room range, then in a large space. This configuration is basically composed of several emitter units. A final position is got after various fusion methods of the different received signals. After that, a comparison is made between those fusion methods to find the most accurate merging technique.

The principal challenges deal with different development levels within the localization and positioning systems:

- Migration from 2D emitters to 3D emitters.
- Migration from 2D receivers to 3D receivers.
- Study and analysis of a suitable 3D configuration for beacons.
- Fusion of the data coming from the sensors.
- Implementation of the positioning algorithm in a SoC architecture.
- Experimental tests for the proposal

To achieve the challenges described above, in this project the technology used is ultrasonic. Its expected accuracy range for the 2D and 3D positioning is from centimeters to decimeters, thus the purposes of this work are:

- Specification of the 3D configuration of an Ultrasonic Local Positioning System (ULPSs) for positioning of a mobile target in the space, which requires complex processing techniques.
- Development of robust localization, positioning algorithm as well as the use of several fusing techniques of data issued from various sources.
- Comparison between those fusion techniques, tightly coupling and loosely coupling methods, to get accurate positions.
- Extension of the 3D ULPSs configuration to large environments that need stronger emitted signals plus larger coverage areas.
- Implementation of the developed positioning algorithms in a SoC, facing the complexity of the algorithm and the limited resources of the hardware board to keep the positioning accuracy in the real-time operation.

1.3 Thesis Structure

This thesis has been divided into the following chapters, in addition to this introductory one:

- Chapter 2: Backgrounds.

This chapter contains a review of indoor positioning systems from low- to high-level algorithms, at first. Then, we present a review of relevant works related to indoor localization technologies (e.g. RF, mechanical, light and US), emphasizing on ultrasonics, since the proposals of this thesis are based on this indoor positioning technology. Later, we introduce the most important positioning techniques and different localization methods using ranging information: geometric methods, cost function minimization and fingerprinting. Then, we show ranging techniques based on Time of Arrival (TOA) and Time Difference of Arrival (TDOA). After that, we describe various characteristic of the positioning system. Later a description of the different 3D positioning systems based on ultrasounds is provided. Finally, a general description of the fusion algorithms is indicated, such as MLE, KF or EKF.

- Chapter 3: General view of the proposal

In this chapter, the ULPS is detailed for its two principal parts: transmitters and receivers, the different modules they have, and how each module is operating (modulation schemes, correlation, coding, medium access technique, etc.). The needs to migrate from one single emitter system to combined systems, and from a single receiver (2D receiver) to a multi-receiver case (3D receiver), are also considered.

- Chapter 4 : Multi-Sensor fusions performances

In this chapter the Gauss Newton algorithm is detailed to locate and position mobile targets in the space, using data from different single ULPS placed and oriented to several directions. Later, a combination of several configurations of a set of ULPS, to better cover the workspace and to extend the system from a small room to a large-size room, for synchronised (spherical method) and no synchronized units (hyperbolic methods). In addition, a Position Dilution of Precision (PDOP) and an accuracy study were done for single and combined units, based on the Cumulative Distribution Function (CDF) for positioning error, on Standard Deviation Error (STD), as well as on mean error.

- Chapter 5: Experimental results

In this chapter, we present a set of experimental results, which validate the studied proposals behaviours and performances; moreover, it shows its feasibilities. The 3D indoor positioning system is used to prove empirically the positioning algorithms as well as the fusion methods to improve it in the space as presented in previous chapters. Also, a description of the developed SoC architecture is presented with the BPSK demodulation and the five correlations functions to compute the arriving time of the received ultrasonic signals with a set of five Kasami codes. This arriving times have been previously used with the Gauss-Newton positioning function.

- Chapter 6: Conclusions and future works

This chapter shows the most relevant conclusions derived from the development of this thesis, including references to publications (indexed international journals and conferences). Finally, we discuss about future research lines that could be followed after the proposals and results obtained here.

Chapter 2

Background

In the age of automation, smart systems and smart cities, the ability to navigate persons, smartphones and smart devices in indoor/outdoor environments has become important for many applications. The GNSS provides good location estimates and afford high accuracy rate in the outdoor positioning. Nevertheless, it cannot be used in indoor environments due to their weak signals in the lack of line of sight between the satellites and the mobile devices and the fail of entering and spreading those signals inside buildings. So, to locate mobile devices indoors without counting on the direct radio frequency signal from GNSS satellites, indoor positioning systems are needed [Sert2012].

Thus, an indoor positioning system (IPS) is a network of devices used to position, locate, and track smartphones, people, smart devices or robots in the absence of GNSS signals inside buildings, due to the wide number of applications that can be provided to society.
There is a large number of applications that can benefit from the indoor location systems, due to the advances in wireless technologies and the consequent proliferation of wireless devices in indoor buildings. There are two kinds of application, 2D applications for mobile devices and navigation of smart robots and 3D applications which use the 3D position to deliver context-dependent information with a mobile device, as well as for navigation purposes. The most important examples for 3D indoor location and position systems are smartphones, persons, 3D industrial robots and drones as shown in Fig. 2.1 [Kol20017]. In general, applications involved in IPS are:

- *Location-Based Services in Indoor Environments (LBS)*: is the highest commercial application of the mass market, which uses the geographical position to deliver context-dependent information accessible with a mobile device. In Fig. 2.1.b there is an example of a delivery by drone for the Amazon company, to obtain information on cinema, concerts or events, to navigate to right places (mall, office,...), to navigate to the right transport platform (train, bus stop,…), etc.
- *Environmental Monitoring:* to observe some natural phenomena (heat, pressure, humidity and air pollution).

- *Police and Firefighters: to* provide benefits in law enforcement, rescue services, and fire service. Fig. 2.1.a) shows an example of fire detection by drone and Fig. 2.1.d) a police surveillance by drone.
- *Intelligent Transportation:* to provide a seamless navigation through extension of road guidance inside parking garages for example.
- *Museums:* to track visitors, observe and study the visitor behavior and location-based user guiding.
- *Logistics and Optimization:* to have information about location of assets and staff members. To position cargo management systems at airports, ports and rail traffic.
- *Guiding of the Vulnerable People*: to aid the visually impaired to navigate and walk in combination with public transport.
- *Surveying and Geodesy:* to survey the building interior, capture the setting out and geometry of new buildings and reconstruct them.
- *Underground Construction:* to be applied in dusty, dark, humid and space limited environments for and longwall mining.
- *Scene Modeling and Mapping:* to have 3D modeling of natural scenes and geometric modeling for physical simulation, mapping of hazardous sites and cultural heritage preservation.
- *Industry:* to develop intelligent systems for more or less fully automatic manufacturing as shown in Fig. 2.1.g) (robotic guidance, industrial robots, robot cooperation or smart factories).
- *Private Homes:* to detect lost items, physical gesture games, locate based services at home and locate persons (old people with Alzheimer disease or children...) using smart phones for example as presented in Fig. 2.1.e) and Fig. 2.1.f).
- *Medical Care:* to locate tracking of medical personnel in emergency situations, patient and equipment, Also helping the injured in emergency cases as shown in Fig. 2.1.c) where a drone is used to take the medical box to the accident site
- *Motion Capturing:* to rely on the detection of physical gestures and the capability to locate and track body parts (animated films, location-based gaming).

a) Drone in a wildfire b) Package delivery system c) Emergency Medical d) police surveillance

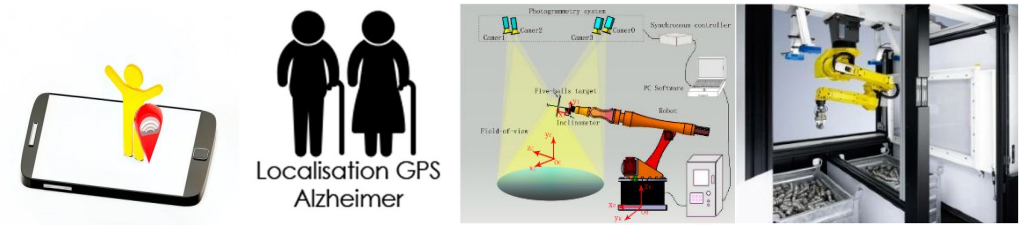

e) Smartphones f) People localization g) Industrial robot positioning

Fig. 2.1. Examples for Indoor Positioning Systems.

Also, several technologies have been introduced, tested and implemented to improve the location, positioning, tracking and navigation indoors. Among them there are Radio Frequency (RF), photonic, mechanical, sonic waves, and other technologies [Tor2010]. The RF technologies often include Ultra-wideband (UWB), Bluetooth, Wireless Local Area Network (WLAN), Wireless Sensor Network (WSN), Near Field Communication (NFC) and Radio-Frequency Identification (RFID) [Sak2017] [Tor2010] [Zaf2019].

Moreover, positioning techniques utilized in IPSs combine the signal properties and positioning algorithms. The common signal properties are Time of Arrival (TOA), Angle of Arrival (AOA), Angle of Departure (AOD), Received Signal Strength Indication (RSSI) and Time Difference of Arrival (TDOA); whereas the positioning algorithms are trilateration, triangulation, fingerprinting and proximity [Sak2017] [Tor2010] [Zaf2019].

In this chapter, a background of the IPSs will be detailed, various technologies and techniques will be described, as well as their characteristics and differences existing in systems and fusion algorithms.

2.1 Categories of Indoor Positioning Systems

IPSs are divided into different groups according to two main criteria, among others. The first one is based on the infrastructure and the second is based on the positioning algorithms.

Based on infrastructure, two types of indoor positioning systems can be defined. On one hand, the infrastructure-based ones, where the target's location is determined by the installed network infrastructure in the testbed, as well as the device used to transmit the signal, the devices used for measurements and the estimation. Three models are developed, the terminal-based systems

where the signals are sent by base stations, the mobile terminals collect the signals, store them and estimate their location. It provides the location of the mobile terminal to the users only (privacy oriented). In the terminal assisted systems, the signals are also sent by the base stations but the mobile terminals only collect the signals and send them to a network server for the estimation process. Finally, in the network-based systems, the signals are sent and collected by both base stations and mobile terminals. Then, the data are sent to a network server where data will be stored and the location will be estimated. This property is beneficial in reducing the computation cost and power consumption on the mobile terminals [Zek2011] [Ro2015] [Xie2017].

On the other hand, the other type is the infrastructure-less or decentralized positioning systems, where special devices act as base stations spread all over the targeted areas in a grid or arbitrarily distributed in an ad-hoc setup. The purpose of developing these systems is to authorize localization without prior knowledge about the building layout. This is important in situations where the WLAN infrastructure of a building gets damaged due to the fire, etc. Two models are developed, terminal-based systems (the beacons send signals to a server terminal to calculate the target's location) and collaborative systems (the beacons send the signals in order to perform the estimation process) [Lor2004] [Zek2011] [Kum2013] [Bak2013].

Regarding the positioning algorithms involved, there are two principal positioning algorithms, deterministic and probabilistic algorithms, applying various ways to model the signal properties [Kol2017]. Deterministic algorithms attempt to find the minimum statistical signal distance between a detected RSSI location vector and the location vectors of the various calibration sample points. This can be equal or different from the minimum physical distance between the actual device physical location and the recorded location of the calibration sample. The sample point with the minimum statistical signal distance between itself and the detected location vector is generally regarded as the best raw location estimate contained in the calibration database, this single value is the average RSS. The applied deterministic methods are the Nearest Neighbor in Signal Space (NNSS); the target's location is estimated by applying the Euclidian distance algorithm between the nearest value of the stored signal and the current one; and the k-Nearest Neighbor (k-NN), k is set of number of signal properties. k-NN works by first searching for the k-values in the radio map having the lowest error mean with the current signal property [Kol2017] [Gu2016].

On the other hand, probabilistic systems is an approach to calculate the conditional probability distribution to get the estimated location of the mobile target using the Bayes Theorem based

on a likelihood function [Daw2010]. Some approaches estimate empirical parametric distributions (Gaussian, Exponential, Lognormal, etc.), which do not require extensive storage and computation resources due to the simple use of statistical parameters. Nevertheless, these empirical distributions do not fit the observed distributions so well. Histogram-based and nonparametric methods fit better the real distribution as they cannot assume the shape of the signal distributions. But they need large storage and computation resources, so it is difficult to be implemented in functional localization systems [Ji2016].

2.2 Positioning Techniques

Several positioning methods determine the estimated positions of mobile targets from various basic measurements, such as distances, angular observations, proximity and signal strength etc. Those methods can be combined, one with each other, or used separately.

2.2.1 Proximity Detection

Proximity provides position information, employing a grid of antennas with known positions to estimate a rough localization. When a mobile target is detected in motion, the nearest antenna is employed to calculate its position. If the mobile target is identified by more than one antenna, the strongest antenna signal is employed to calculate its position. The estimated position is computed using the RSSI, which is frequently applied in proximity to estimate the distance between mobile targets to acquire its position information. This technique is employed in IR, RFID and Bluetooth systems. To achieve a secure and a large coverage area, a large number of readers are needed, which could lead to high cost and complex systems [Wa2014] [Sak2017].

2.2.2 Triangulation and Lateration

Triangulation is a positioning technique based on angle measurements to calculate the position of the mobile object when signals are emitted from (or received at) fixed points in the space. This technique regularly needs the use of antenna arrays in the transmitter and receiver to measure the AOA and AOD, as shown in Fig. 2.2.b). Various estimation algorithms can be employed, such as multiple signal classification and estimation of signal parameters by rotational invariance techniques, to calculate the AOA and AOD. Localization of the mobile receiver in 2D is probable if the AODs from two transducers are known or the AOAs at the two transducers are known. Furthermore, this process fails for the localization of the mobile receiver if it is aligned with the transducers so no triangle can be set in this case [Zek2011] [Rod2017].

Lateration refers to calculate the position of the subject based on its relative distance to several previously-known fixed points in space. Many distances are obtained indirectly by measuring parameters which are proportional to a distance measurement. Always, a 2D/3D position is computed with redundancy from more than two/three distance measurements to nearby nodes, as presented in Fig. 2.2.a). Lateration can be applied on a set of distances and no matter what distance estimation method has been used [Zek2011].

In this way, Time of Flight (TOF) systems employ a precise measurement of the arrival time of a signal transmitted from an emitter to various receivers, where the distance between the mobile device and each receiver can be defined from the elapsed propagation time of the signal travelling between them, as the velocity of the travelling signal is known. The TOF technique requires exact knowledge of the transmission start time and must ensure that all the emitters devices, as well as the receiver device, are accurately synchronized with an exact time source. Knowing both propagation speed and measured times, it is feasible to measure the distance between the mobile and the transmitter devices. This distance will be considered as a radius of a circle presenting the area around the transmitters. The intersection of more than three circles is the location of the mobile receiver [Zek2011].

Similarly, Time Difference of Arrival (TDoA) technique utilizes relative time measurements at every receiver device. So, TDoA does not demand the use of synchronized time sources at the point of transmission to solve timestamps and estimate the receiver location, so the transmission with an unknown offset time is permitted. Its implementations are based on a mathematical theory identified as hyperbolic lateration. In this procedure, at least three/four no synchronized received signals are required for 2D/3D positioning [Zek2011].

2.2.3 Fingerprinting

Fingerprinting techniques call pattern recognition techniques, working in two stages, offline and online. In the offline stage, the test bed is covered by a set of predetermined or random points or reference points. At every reference point, the user must collect a set of readings, each set contains the coordinates of that point and signal to noise ratio (SNR) or the received signal strength (RSS) values from multiple APs and then store these readings in a server or in the target device. Then, in the online stage and when the target's location is needed, the target collects a set of RSS readings and tries to match them with the stored fingerprints from the offline data Fig. 2.2.c) presents this technique [Zek2011] [Jim2010].

2.2.4 GNSS Augmentation

GNSS augmentation is a method to enhance the positioning, navigation and tracking system's performances as accuracy, security, availability and continuity through the assimilation of external information into the estimation process of the user position. Real-time kinematic and precise point positioning were extended for high-accuracy positioning for specific applications to improve the GNSS capability. The term ‘‘GNSS augmentation’’ is used to specifically describe the wide-area augmentation by the use of additional satellite-broadcast correction messages [Cho2017] [Sab2013].

2.2.5 Dead Reckoning

Dead reckoning is a relative positioning method where the current position and the heading position are estimated by integrating the velocity or acceleration over a time step and adding that value to the previously known position and heading. The positioning error grows with traveled distance (drift), so it has to be combined with an absolute positioning system such as GPS to stop the error from growing infinitely. The error for dead reckoning is often measured as a percentage of the traveled distance [Jim2010] [Zek2011].

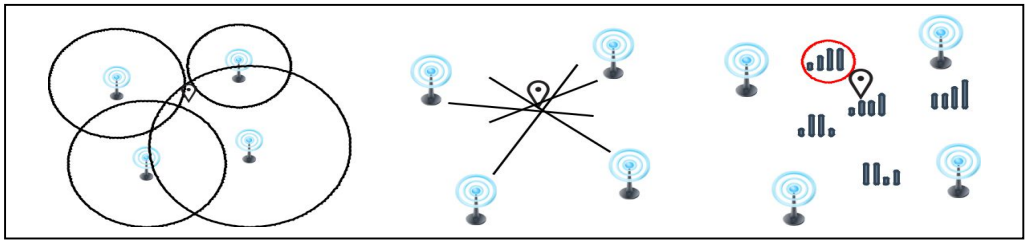

a) Lateration b) Angulation c) Fingerprinting

Fig. 2.2. Most common methods for positioning used in IPS.

2.3 Sensory Technologies of IPS

Location and positioning systems employ several parameters to obtain an accurate position. The technology is one of the critical parameters, which depend on the applications. While several technologies have grown, the most common ones are the focus of this section [Bat2018].

2.3.1 Radio Frequency

One of the solutions used to estimate the position of a mobile target in the context by measuring one or more properties of the signals emitted by a transmitter and hosted by a mobile station. These properties depend on the travelled distance by the transmitted signal and the properties of the environment [Sak2017] [Bat2018].

RFID (Radio-Frequency Identification) system has several essential elements, including RFID tags, the RFID readers and the communication between them. The RFID reader is to read the data transmitted from RFID tags. RFID readers and tags apply a defined RF and protocol to send and receive data. In addition, the RFID tags are active or passive operating with or without battery. They reflect the RF signal emitted to them from the reader and add information by modulating it. But, their ranges are limited, where the reading range is 1–2 m, and the reader's cost is high. Active RFID tags are small transceivers, which can actively emit their ID in reply to an interrogation. Its advantages are the small antennae and longer ranges, which can reach tens of meters. [Lu2017] [Sak2017] [Rai12].

Bluetooth (IEEE 802.15) operates in the 2.4-GHz ISM band. Its range is short (about 10–15 m). Bluetooth is a "lighter" standard, extremely ubiquitous and embedded in most electronic devices such as phones, personal digital assistants (PDAs), etc. In addition, it supports other networking services in addition to IP. Bluetooth tags are tiny size transceivers. Each tag has a unique ID, which is employed for locating the Bluetooth tag. This technology is mainly used in small-scale positioning as a single-room. The biggest advantages of this technology are small size and easy to integrate in PDA, PC and mobile phones, so easy to be familiarized [Sak2017] [Wa2013] [Rai12].

WLAN (IEEE 802.11) Wireless local area network standard, is working in the 2.4-GHz Industrial, Scientific and Medical (ISM) band, has a range of 50–100 m and IEEE 802.11 is the principal local wireless networking standard. So, it is the most economical solution providing suitable connectivity and high-speed links, moreover it can be implemented easily in software. The accuracy of the WLAN positioning systems applying RSS is around 3 to 30 m, with an update frequency in the range of some seconds [Me2012] [Mau2012].

UWB –Ultra Wide Band is a new communication technology and has great differences with traditional communication technologies. It sends and receives extremely narrow pulses to transmit data, which needs a wide bandwidth. UWB can be applied for accurate indoor

positioning, as finding the location of a robot motion tracking or battlefield soldiers. UWB systems matched with traditional narrowband systems have numerous advantages, such as the penetrating of objects/walls and low power consumption, stability to multi-path effects, large security, moderate complexity, highly accurate positioning, etc. Hence, UWB technology can be employed into indoor stationary or moving objects and people location, navigation and tracking. Also, it provides highly positioning accuracy [Sil2018].

Cellular-Based is a technique that uses a global system of mobile/code division multiple access (GSM/CDMA, LTE, 5G) mobile cellular networks to estimate the location of outdoor mobile clients. However, the accuracy of the method using cell-ID or enhanced observed time difference is low in the range of 50–200 m. The accuracy is higher in densely covered areas (expected around 1m with 5G) and lower in rural environments. Indoor positioning based on a mobile cellular network is conceivable if the building is covered by numerous base stations or one base station with strong RSS received by indoor mobile clients [Dar2018].

2.3.2 Mechanical Technology

Odometer is a rotary encoder attached to a wheel axis or a motor shaft that outputs a square or sine wave when it turns. The encoders for robot applications are optical but there are brushes or magnetic encoders used in ABS brakes. Optical encoders can be absolute or relative. The relative ones are simpler and cheaper where a light beam is aimed at a photodetector and is interrupted a number of times per revolution. The employed technique to calculate the displacement along the vehicle's trajectory is the dead reckoning [Kit2010] [Bat2018].

Inertial Navigation works by sensing acceleration and orientation in the three axes and integrating over time. An inertial measurement unit (IMU) is composed of accelerometers, gyroscopes and magnetometers. An accelerometer detects acceleration in a certain direction and is found in many consumer electronics devices (smartphones). In an IMU three accelerometers are mounted orthogonally to each other. Three gyroscopes measures orientation and three magnetometers measure the components of the earth magnetic field giving an absolute orientation. For robot applications, micro-electro-mechanical systems (MEMS) IMUs consisting of microchips on a small printed circuit board are practical to use since they are compact and cheap. Inertial navigation has the same disadvantages as odometry: an increasing error over time and bad precision at low accelerations but there is no wheel slippage and is easier to set up [Ge2007] [Hel2018].

Visual Odometer works by determining movement with computer processing of visual information from high-resolution images taken by video cameras. It can be fused with other methods like wheel encoders and GPS. Algorithms that make use of multiple cameras usually perform better compared to monocular systems [Kit2010].

2.3.3 Optical Technology

Cameras have become a dominating technique for positioning systems which covers a wide area of applications at all ranges of accuracy, with its principal application area in the sub-mm region. The success of optical methods starts with the development and miniaturization of actuators (lasers) and especial progress in the technology of detectors (CCD sensors). In addition, there has been an improvement in data transmission rates and computational capabilities, as well as the development of algorithms in image processing.
Optical indoor positioning systems can be classified into ego-motion systems, where the mobile target can be located with static cameras, measuring the image coordinates via angular information and applying the Angle of Arrival (AoA) technique, called also stereo-vision approach. The other group is the synthetic stereo vision approach, where the mobile device is the camera in this case. So, the scene is examined sequentially from diverse locations by the same camera and image depths can be measured in a similar manner to the stereo-vision approach [Sah2015] [Rai12].

In this group, light refers to the phenomena of electromagnetic radiation at wavelengths inside the visible range, which spreads generally between 380 and 750 nanometres, where the visible light, ultraviolet and infrared light exist.

Visible Light Communication (VLC) and *V.L. Positioning (VLP)* are LED-based positioning systems that employ visible light signals to transmit data. VLC uses IEEE 802.15.7 standard, where the installed LED-lamps on the ceiling will serve as anchor nodes to give a highly accurate location with a minimum calculated error. Each LED-light gets its unique address which represents its coordinate and unique ID; as well as the receiving nodes transmit the LED-ID to estimate the position. VLP can use triangulation, proximity or fingerprinting as a positioning technique. The advantages of VLP are cost-effective due to longer life expectancy, low energy consumption, reusing the current lighting system in the building, no electromagnetic interference and more secure, etc. Nevertheless, this technology is sensitive to lens distortion,

ambient light, time measurement error and flickering. Furthermore, it is so difficult to achieve synchronization between LED-lights anchor nodes and mobile devices [Mou2018] [Raj2014].

In *Infrared System (IR)*, its principle is that the IR modulated ray emission is recognised by the optical sensor situated in the indoor positioning receiver. Although the IR has a simple structure, almost high accuracy and a low-cost indoor, it can be only used in the line of sight case. The two main limitations of IR systems are short sightlines and transmission distance [Bre2017].

2.3.4 Acoustic Technology

Ultrasonic positioning technology proposes a distance ranging methods. Ultrasonic ranging takes distance method by trilateration positioning algorithm to determine the location of objects. The accuracy of the ultrasonic positioning system is high, also its hardware structure is simple and with a low cost. However, this system has to deal with multipath effects and must provide direct lines of sight between the emitter units and the mobile objects, even in complex environments, in order to receive adequate signals. Also, it can be affected by Doppler effects and, also, the environment's noise. Finally, it needs a large infrastructure to cover an extensive area. [Mau2012] [Med2013] [Kap2020].

Audible sound has a frequency below 20 kHz. It is an easily deployable positioning system using sound cards of standard devices to be a low cost and a simple system, but it has low bit rates and delays caused by the soundcards. To avoid those delays, calibration of various transmitters must be done. To minimize intrusiveness due to the audible signals, positioning is estimated on request, using the TOA multilateration technique. The accuracy of the sound positioning systems, used for several navigation and tracking applications, is in the cm range [Mau2012] [Med2013].

2.3.5 Hybrid Technologies

Hybrid systems combine two technologies or more, in order to enhance the accuracy and precision of the location estimation. Depending on applied technologies by the positioning systems, they will have particular advantages or disadvantages. An example of hybrid systems, combining more than one technology (as RF, IR, Wi-Fi, US, UWB, etc.) and more than one technique (TDoA, AoA, ToA, RSS etc.), is the indoor GPS. In this system, the user position is essentially defined by at least four transmitters and a receiver [Pue2013].

A battery-operated transmitter employs laser and infrared light to transmit one-way position data and elevation from the transmitter to the receiver. The receiver has photodiodes inside its module and senses the transmitted laser and infrared light signals. The signal is transferred over a wireless network link producing mobility to users. The 3D position of the optical receiver is then determined by the method of triangulation. Indoor GPS depends on a clear line of sight and calibration points. As both technologies allow centimetre range positioning accuracy separately, when they are combined the accuracy range is significantly higher [Kho2009].

2.4 Positioning Metrics

In order to find an appropriate positioning technology for a specific application, the performance parameters and categories require d to fit users 'demands are detailed below.

2.4.1 Accuracy

Accuracy of a positioning system is the closest calculated position (to the real one) that can be achieved to a target object or the degree of conformance between the estimated or measured position and the ground-truth position at a given time. The accuracy depends on many factors such as the used technology, techniques system configuration etc. Fig. 2.3 presents a summary of the used technologies and their accuracy, where every system has its own accuracy so the higher the accuracy, the better the positioning is. However, the accuracy is still the very challenging area of research in this field [Sak2017] [Men2019] [Rai12].

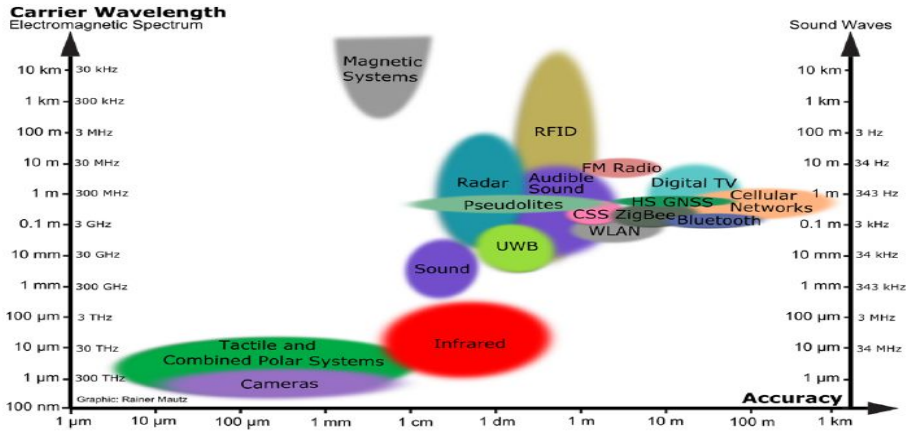

Fig. 2.3. Indoor technologies according to on accuracy and carrier wavelength [Rai12].

2.4.2 Range of Coverage

Each positioning system works in a different range, which depends on the used technology, the number of the transducer units, their configuration and the environment nature. The most efficient systems cover the largest range. Ranges of existing systems go from 5 meters to 50 meters. Providing a system that has coverage of more than 60 meters is a challenge by itself [Sak2017] [Men2019] [Rai12].

2.4.3 Security

The security of a system is the extent of guard against undesirable occurrence such as the privacy invasion, robbery, physical damage, as well as the information's corruption. The protection quality from unauthorized access or uncontrolled effects should be given. For positioning systems, security requires locating, positioning, monitoring and communicating with individuals (e.g. passengers, employees) or with devices (e.g. smartphones, drones, industrial robots), to find the positions of the desired mobile object or person at all times and all positions when it is necessary. So, it is an important positioning factor in personal networks. However, the security of indoor positioning systems has not been a major concern in most of the initial research in this area, where the Beep System is an example of a secure indoor positioning system. [Men2019] [Mau2012] [Sak2017].

2.4.4 Complexity

The complexity can be attributed to hardware, software, and operation factors (software: computing complexity of the positioning algorithm; hardware: the complexity of implementation). About the calculation of the positioning, the algorithm is performed on a centralized server-side, the positioning could be calculated quickly (powerful processing capability, sufficient power supply). The effects of complexity are evident if it is carried out on the mobile target (mobile targets lack strong processing power, long battery life). Since positioning techniques are various, so they own various complexities. Positioning algorithms with low complexity are better not only in term of processing time but also in term of battery life for autonomous systems and devices [Men2019] [Mau2012] [Sak2017].

2.4.5 Precision

The location precision considers how systematically the system works (a measure of the robustness of the positioning technique since it reveals the variation in its performance over many trials). Also, the location precision is the standard deviation in the location error or the geometric dilution of precision (GDOP). It is also the distribution of the distance error between the estimated location and the true location. The cumulative probability functions (CDF) of the distance error are employed for measuring the precision of a system [Men2019] [Mau2012] [Sak2017].

2.4.6 Robustness

A positioning technique with high robustness could operate commonly even in the absence of some signals, or when some of the RSS value or angle/distance parameter are not available. Sometimes, the signal from a transmitter unit is totally blocked or damaged. The unique information to estimate the position is the signal from other measuring units. So the positioning techniques have to use the incomplete information to compute the location [Men2019] [Mau2012] [Sak2017].

2.4.7 Scalability

The scalability character of a system guarantees the normal positioning function when the positioning field gets larger. The positioning performance degrades when the distance between the transmitter and receiver increases. A positioning system needs to scale on two axes: geography and density. The geographic scale is related to the area or the space to be covered. And the density scale is based on the number of location units per geographic area and per time period. The larger the area or space covered is, the more the units that are needed. Wireless signal channels can become congested and more calculation is needed to perform location positioning. Another measure of scalability is the dimensional space or the configuration of the system. Some systems can support both 2-D and 3-D spaces [Men2019] [Mau2012] [Sak2017].

2.4.8 Cost

For an indoor positioning system, the costs comprise various features, including expenses, time and space consumption, energy dissipation, etc. The capital expense is essentially related to hardware costs, which depend on the specific applications. Then, time costs include

maintenance and deployment times. Also, the space consumption essentially refers to the unit density of the system (emitters and receivers), its number of units and distribution in the workspace.

In addition, the energy consumed is relevant due to the limited energy of the mobile terminal battery life. Generally, low-cost indoor positioning systems become more popular due to their large area of application and acceptable accuracy [Men2019] [Mau2012] [Sak2017]. Table 2.1 summarizes accuracy and coverage of the main positioning technologies.

Technology	***Accuracy***	***Coverage (m)***	***Measuring Principle***	***Applications***
Light	Depends on technique and setup. 1 mm < average < 2 m	IR 1 – 5 Psudolight 10 – 1000	Thermal imaging, active beacons carrier phase ranging	People detection, tracking GNSS challenged pit mines
Computer Vision	For odometry, from 0.25% to 8.5% of path length For maker-based solutions, average < 1 m	1 – 10	Angle measurements from images	Metrology, robot navigation Pedestrian navigation
Acoustic	For ultrasound, average < 1 cm For audible sound, average < 10 cm	2-10	Distances from time of arrival	Hospitals, tracking
Magnetic Fields	For artificial fields, average < 1 m For the natural field, average < 5 m 0.3–1.5% of walked distance	1-20	Fingerprinting and ranging	Hospitals, mines
PDR	Average as low as 2 m for specific environments, but commonly above 5 m For SLAM, average 1 m to 10 m	10-100	Dead reckoning	Pedestrian navigation, LBS
UWB	Commonly, average < 50 cm	1-50	Body reflection, time of arrival	Location based services
WiFi	For fingerprinting, average < 5 m are common For time-based techniques, average < 2 m For CSI techniques average < 2 m	20-50	fingerprinting	Pedestrian navigation, LBS
BLE	Average between 2 m to 5 m	10-1000	fingerprinting, proximity	Person tracking
RFID	Average < 2 m	1-50	proximity detection, fingerprinting	pedestrian navigation
Cellular	Average < 50 m	10-1000	fingerprinting, proximity	Person tracking

WSN	Average < 2 m but higher values can be found	10-1000	fingerprinting, proximity	Person tracking
ZigBee	Average < 5 m	10-1000	fingerprinting, proximity	Person tracking

Table 2.1. Summary and comparison of indoor positioning technologies [Men2019] [Rai12].

2.5 Some Existing 3D Ulrasonic Positioning Systems

Ultrasonic positioning systems have been admitted as an interesting technology for indoor applications, mainly for some advantages, such as suitable accuracy, low power and low cost [DeA2015] [Yuc2012]. Thus, some 3D ultrasonic positioning systems have been developed earlier using diverse configurations, as reviewed in [Se2012] [Li2019]. They are based on two main proposals: emitters are located at fixed positions and receivers are moving in the space, and vice-versa. The general positioning methods used are trilateration or multilateration [Kap2016] [Kap2020] [S2012] [DeA2015] [Pri2009]. These methods are based on the determination of the times of arrival (TOA) [Se2012], time differences of arrival (TDOA) [DeA2015], angle of arrival (AOA) [S2012], or also on hybrid techniques [Pri2009] to measure the distances or distance differences between emitters and receivers, and then estimate the receivers' positions. In the case of multiple position estimates are obtained, the final position estimate is usually performed as the mean of all the obtained ones [Li2019] [Pri2009] [Lop2012].

Concerning the first proposal, where the emitters are located at known positions and the receivers are moving in the environment, 3D positioning systems have been developed with diverse configurations, positioning techniques and number of beacons. Some configurations consist of beacons fixed at the ceiling corners [LoP2012], where three autonomous beacons, synchronized with the receiver, are used for a hybrid method based on AOAs and TOAs; also, the deployment of four beacons at the ceiling corners is introduced in [Suz2009]. Other configurations are made by a set of beacons placed in the ceiling as in [Kap2016]. It presents a set of six synchronized beacons in the ceiling, pointing to the centre of the room to measure TDOAs. Moreover, four beacons are synchronized with a fixed microphone in [Se2012], in order to estimate the distances between the emitters and the receiver. In addition, a set of four beacons can be placed in only one plane (or slightly out of the plane to avoid coplanarity) to point to the desired workspace [Sc2010] [DeA2015]. The main constrain in almost coplanar

structures is the measure of the position in the axis perpendicular to this specific plane. To overcome this constraint, some preceding works have also introduced the deployment in different or parallel planes [Pri2009] [Se2012] [Lop2012].

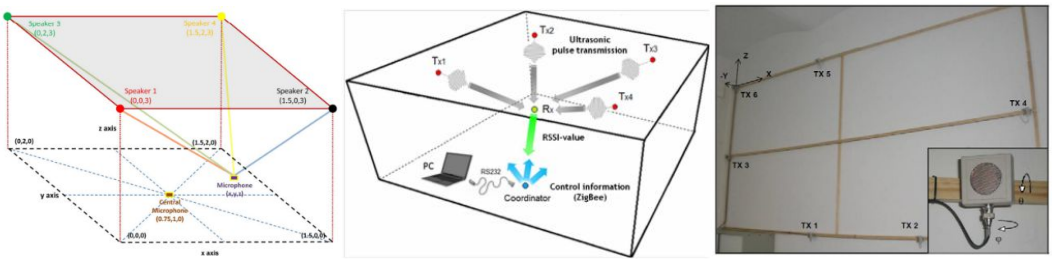

Fig. 2.4. Three different 3D ultrasonic positioning systems with fixed emitters and mobile receivers [LoP2012] [Se2012] [Sc2010].

Concerning the second proposal, a 3D positioning system is proposed in [Sat2011], based on five ultrasonic emitters installed on a mobile user, and five ultrasonic receivers placed and fixed at known locations. This system utilizes a trilateration positioning technique and the Extended Phase Accordance Method as a tracking algorithm to measure the distance to the mobile target, also a time division multiplexing access (TDMA) communication link, so a trigger pulse is used to synchronize the emitters and the receivers. In [Na2010] this proposal is also developed, by setting a receiver with four coplanar beacons located perpendicularly to the mobile emitters. Furthermore, a 3D positioning system presented in [Khy2012] is composed of a single mobile emitter and a set of six fixed and coplanar receivers at known positions, to use a linear ultrasonic chirp, and the phase correlation approach to calculate the corresponding TOAs, additionally with a spherical trilateration technique to calculate the estimated positions.

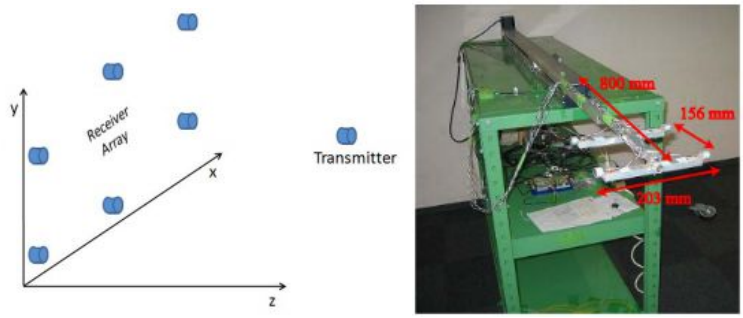

Fig. 2.5. Two different 3D Ultrasonic Positioning Systems with fixe location of the receivers and mobile emitters [Khy2012] [Na2010].

2.6 Multi-Sensors Fusion

To compute the estimated position of a mobile target in the space, various independent sensors can be used. Then, to get an accurate estimation a fusion of data coming from those sensors must be applied. As a definition, multi-sensor data fusion is an intense domain in recent research activities. Its purpose is to fuse complementary information accessible from different sensors to generate more accurate results for data processing problems. It refers also to the acquisition, processing and combination of data collected by various learning sources and sensors. Many factors can contribute to improve the execution of the development of the system efficiency, such as reliability, robustness, extended coverage, increased confidence, shorter response time, etc. [Hall2001] [V1997].

2.6.1 Multi Sensors Fusion Architectures

Accuracy and efficiency tend to be the two mains in positioning, tracking and navigation applications. Separate positioning technologies, techniques and systems provide a diverse spectrum of data that can be fused. Besides, depending on the sensors concerned and the application, the level where the fusion of sensor data is implemented should be designed respectively [Hall2001] [V1997]. Data fusion can be performed at a variety of levels from the observation level to state vector and the decision level, which explains the utilization of several categories or configurations of fusion data sensors [Nur2017] [Gro2015] [Hel2018]. In addition, multiple sensors can be, also, integrated into three main architecture scenarios.

Centralized architectures, also called *measurement fusion integration architectures*. All the raw data (observations or sensor measurements) from separate sensors are sent to a single module to be fused, and a global or combined measurement is obtained. This method provides high fusion accuracy to the estimation problem but a large number of states requires high processing data rates that cannot be maintained in real-time applications. Another limitation of this method is the lack of robustness when the sensor or central filter fails. That is why parallel structures can usually provide improved failure detection and correction, redundancy control, and reduced costs for multi-sensor system integration [Nur2017] [Sal2008].

Decentralized/distributed integration *architectures*, called also *state-vector fusion integration architectures*, in which the filtering process is distributed between some local fusion modules working in parallel to get individual sensor-based state estimates and one master module combining these local estimates to produce an improved global state estimate. The advantages

of this method are higher robustness due to the parallel implementation of fusion modules and lower computation load and communication cost at each fusion module. It is also suitable for modular systems where diverse sensory processing can be implemented as separate units. The distributed fusion is conceptually more complex and requires higher bandwidth compared with centralized fusion [Nur2017] [Sal2008].

Hierarchical architecture comprises a combination of distributed and decentralized nodes, to generate a hierarchical scheme, where the data fusion process is carried out at several levels in the hierarchy [Cas2013].

Generally, a decentralized data fusion system is more complicated to implement due to computation and communication demands. Though in practice, the choice of the appropriate architecture depends on the system characteristics, as well as the requirements, demand, data availability, existing networks, node processing capabilities, and structure of the data fusion system [Cas2013].

2.6.2 Fusion Algorithms

Several fusion techniques exist for all the abstraction levels of sensor data, which depend on the desired application and resources. A general factor for estimation methods is the use of a model for approximating the position from the measurement data. The input data has noise and its error distribution depends on the measured parameter. In estimation methods, the input data are the sensors measurements. Maximum Likelihood and Kalman filter variants belong to the estimation methods.

- Maximum Likelihood Estimation

Maximum Likelihood Estimation (MLE*)* is a classical fusion approach where the estimation is optimal in the reason that it includes all the important information on the state $\boldsymbol{x}$ available from the sensor measurements $\boldsymbol{z}$, allowing proper probabilistic modelling of sensor measurements and target motion. In the positioning case, the fusing algorithm for two independent sensors is described below, where (z_1, z_2) are two independent measurements of state x, and the positioning error can be modelled as $p(z_1|x) = N(x, \sigma_1)$ and $p(z_2|x) = N(x, \sigma_2)$. The final estimated position x_{MLE} after fusion can be obtained from (2.1) [Del]:

$$x_{MLE} = \frac{\sigma_1^{-2} \cdot z_1 + \sigma_2^{-2} \cdot z_2}{\sigma_1^{-2} + \sigma_2^{-2}}$$

And, as the statistical information is additive, the new standard deviation σ will be: (2.1)

$$\sigma^{-2} = \sigma_1^{-2} + \sigma_2^{-2} \quad (2.2)$$

Where σ_i is the standard deviation of the measurements z and i={1, 2} the index of sensor.

Kalman filter variants or Bayesian filter work well with low-level abstraction data. This raw data is often described using dynamic quantities. It consists of two steps: prediction and correction. Both steps use a model. Prediction model estimates the next time step. State vector and its covariance go put through the model.

Measurement model determines how the measurements influence the states. The prediction result is compared with the measurements and is weighted accordingly. Kalman filter can manage situations where the tracking target performs in a linear model movement. Extended Kalman filter is capable to follow a mobile target whose movement can be non-linear, Fig. 2.6 shows the different types of the Bayesian Filters [Nur2017] [Hau2012].

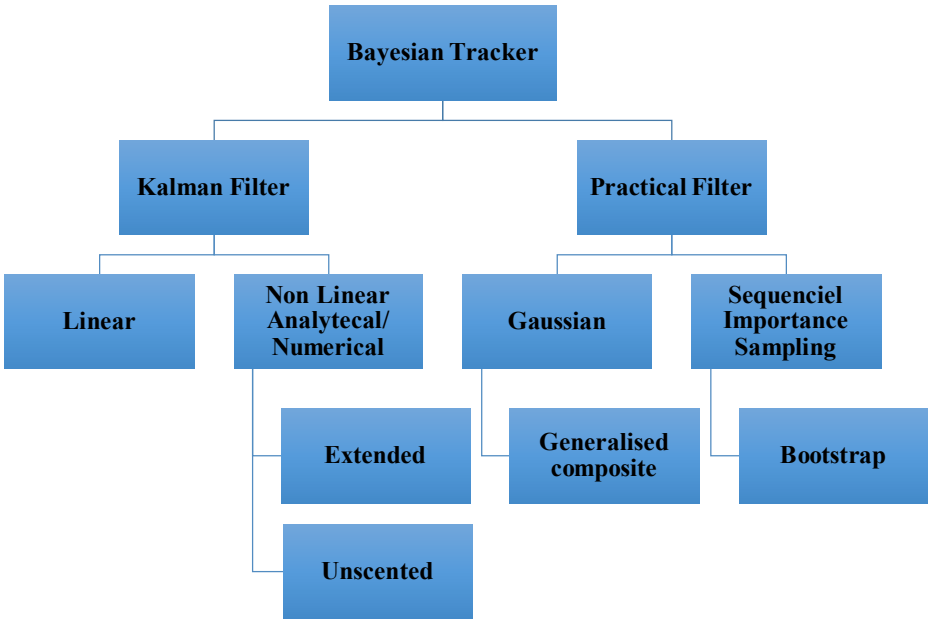

Fig. 2.6. The division of estimation and inference filters [Hau2012].

- Kalman Filter

Kalman filter (KF) is the optimal solution for the estimation of systems with known dynamics and Gaussian noise in case of linear problems according to the minimum variance criterion. In the positioning case, the fusing algorithm for two independent sensors is described below. The

Kalman Filter is one of the most common and practical methods used in Markov chain state estimation. It employs preceding and succeeding information to determine the target states. So, the Kalman filter is used to fuse estimated positions applying a loop of two steps: prediction and updating, trying to converge into the correct estimated position after *n* iterations [Kal1961].

- The state model of the filter is

$$\begin{aligned} \boldsymbol{X_k} &= \boldsymbol{A}.\boldsymbol{X_{k-1}} + w_{k-1} \\ \boldsymbol{Z}_k &= \boldsymbol{H}.\boldsymbol{X_k} + v_k \end{aligned} \tag{2.3}$$

Where $\mathbf{X_k}$ is the estimated position on the current state, $\mathbf{X_{k-1}}$is the estimated position on the previous state; $\mathbf{Z_k}$ is the measurement values; w_{k-1} is the process noise; and v_k is the measurement noise. Then a recursive loop between predictions and updates hold on to converge to the final estimated position. Eq. (2.4) presents the prediction step and Eq. (2.5) presents the correction steps.

- Time update

$$\begin{aligned} \boldsymbol{X_k} &= \boldsymbol{A}.\boldsymbol{X_{k-1}} \\ \boldsymbol{P_k} &= \boldsymbol{A}.\boldsymbol{P_{k-1}}.\boldsymbol{A^T} + \boldsymbol{Q} \end{aligned} \tag{2.4}$$

- Measurement update (correction)

$$\boldsymbol{K_k} = \boldsymbol{P_k} \ . \ \boldsymbol{H^T}(\boldsymbol{H} \ . \ \boldsymbol{P_k} \ . \ \boldsymbol{H^T} + \boldsymbol{R})^{-1} \tag{2.5}$$

$$\boldsymbol{X_k} = \boldsymbol{X_{k-1}} + \boldsymbol{K_k} \ . \ (\boldsymbol{Z_k} - \boldsymbol{H} \ . \ \boldsymbol{X_k})$$

$$\boldsymbol{P_k} = (\boldsymbol{I} - \boldsymbol{K_k} \ . \ \boldsymbol{H}) \ . \ \boldsymbol{P_k}$$

Where $\mathbf{K_k}$ is the Kalman Filter gain; $\mathbf{Q}$ and $\mathbf{R}$ are successively the process noise matrix and the measurement noise matrices; $\mathbf{A}$ and $\mathbf{H}$ are constant transition matrices; and $\mathbf{P_k}$ is a dynamic matrix at instant *k*. Those matrices and their sizes are specific with the desired system.

- Adaptive Kalman Filter

The Adaptive Kalman Filter (AKF) is based on the Kalman Filter and used to adaptively estimates and adjusts noise matrices $\mathbf{Q}$ and R at each step of prediction an updating to improve the predictions at the instant *k*. Those matrices become dynamic noise matrices $\mathbf{Q_k}$ and $\mathbf{R_k}$, then improve the dynamic state estimation accuracy of the filter [Moh1999] [Yan2006]. All the

initial values are similar to the Kalman Filter case, except the noise matrix that becomes$\mathbf{Q_0}$ initially, *N* is a positive constant. The final $\mathbf{Q_k}$ is computed using (2.6) and $\mathbf{R_k}$ is computed using $\mathbf{Q_k}$, so it is also a dynamic matrix.

$$\boldsymbol{Q_k} = \left|diag\left(\left(\frac{N-1}{N}\right).\boldsymbol{Q_{k-1}} + \left(\frac{1}{N}(\boldsymbol{P_k} - \boldsymbol{A}.\boldsymbol{P_{k-1}}.\boldsymbol{A^T}) + \frac{1}{N-1}(w_{k-1} - w_k).(w_{k-1} - w_k)^T\right)\right)\right| \tag{2.6}$$

Where $w_k = \frac{(N-1)}{N} w_{k-1} + \left(\frac{1}{N}\right) w_k$,

- Extended Kalman Filter

Extended Kalman Filter is used for estimation system in non-linear problems, such as the positioning. The modifications are based on the use of Jacobian matrices for linearizing the equations. Due to this linearization, the estimation is not optimal (as the Kalman Filter) but depending on the application the estimation presents enough precision and it can be accepted for positioning purposes [Co1964] [Kil2014]. The method is summarized in the following stages:

The state $\mathbf{X_k}$ and measurement $\mathbf{Z_k}$ are given by (2.7) and (2.8).

$$\boldsymbol{X_k} = f\left(\boldsymbol{X_{k-1}}, \Delta d_{ij,k}\right) + w_k \tag{2.7}$$

$$\boldsymbol{Z_k} = h(\boldsymbol{X_k}) + v_k \tag{2.8}$$

Where $\Delta d_{ij,k}$ is the increments of measurement between the iteration *k-1* and *k* given by the mobile receiver; w_k is the process noise; and v_k is the measurement noise at instant *k*.

- Prediction step is computed by (2.7) and (2.8) where $\mathbf{X_k}$ is the a priori estimation position.
- Update step

$$\begin{aligned} \boldsymbol{K_k} &= \boldsymbol{P_k}.\ \boldsymbol{H_k^T}.(\boldsymbol{H_k}.\ \boldsymbol{P_k}.\ \boldsymbol{H_k^T} + \boldsymbol{R_k})^{-1} \\ \boldsymbol{X_k} &= \boldsymbol{X_{k-1}} + \boldsymbol{K_k}.(\boldsymbol{Z_k} - h(\boldsymbol{X_k})) \end{aligned} \tag{2.9}$$

$$\boldsymbol{P_k = (I - K_k \,.\, H) \,.\, P_k}$$

Where $\mathbf{K_k}$ is the Kalman gain; $\mathbf{H_k}$is the matrix observations; $\mathbf{R_k}$ is the covariance matrix; $\mathbf{Z_k}$ the measurement vector and $\mathbf{P_k}$ is the error covariance matrix, at instant *k*.

2.7 Problem Statement and Thesis Objectives

As has been described in the preceding sections of this chapter, there are various propositions for 3D indoor positioning in term of technologies: RF, US, Wi-Fi, light, etc., and different architectures. The main problems in term of accuracy are firstly related to technology; where all of these technologies have not been the unique suitable for indoor positioning systems; then related to the coverage space, which is related to the system configuration. Positioning systems based on US signals need to dispose of an appropriate infrastructure usually based on US transmitters to estimate the position of the target. For 2D systems, emitters are installed on the ceiling and oriented to the floor to cover all the needed area, where more than one beacons unit also called ULPS can be used for an extended area. Therefore, the main objective of this thesis is the proposal of a 3D configuration for positioning and tracking of a mobile target in extended indoor space using a set of beacon units (ULPS, Ultrasonic Local Positioning) by applying fusion techniques.

The detailed goals to achieve in this work are:

• Proposal of a 3D sensor network architecture deploying multiple ULPSs, with several directions to properly cover extensive indoor spaces, then providing an accurate positioning system.

• Development of algorithms that allows positioning and navigating in the space using all or the maximum of signals coming from (ULPSs), so a mobile target can be located after the fuse of data from the various ULPSs. Two fusion methods are used:

- The loosely coupled method, where the Maximum Likelihood Estimation, the Kalman Filter and the Adaptive Kalman Filter are applied for the estimated positions then their accuracies will be compared.
- The tightly coupled method, where the Extended Kalman Filter is applied for one single ULPS, for three independent ULPSs and for three Combined ULPSs, also a comparison will be done for their accuracies.

- After receiving the ultrasonic signals, some of them are implemented in a System-on-Chip (SOC) architecture based on a Field-Programmable Gate Array (FPGA). The implementation is composed of three modules: the BPSK demodulation, the correlations and the peak detections. Those modules are applied to compute the TDOA. Those results will be used, later, in the GN Algorithm to compute the estimated positions.

Chapter 3

General View of the Proposal

As we have seen in preceding chapters, a LPS permits locating and tracking a mobile target with high accuracy in a reduced region, in the range of centimetres for 2D deployments. Usually, such systems are developed for 2D positioning as the mobile targets are supposed to navigate on the floor. In previous works, to locate a mobile target in an extensive area, using ultrasonic technology, a set of ultrasonic beacon units installed at the ceiling and oriented to the floor is deployed to cover the full region of localization and navigation [Gua2019].

There are other varieties of applications that require a 3D positioning, for instance, the positioning of drones, parts of the body of people, smartphones, industrial robots, etc. For this case, a set of ULPSs (Ultrasonic Local Positioning Systems) is deployed to cover the space of the location and navigation application with specific orientations and placements. So, the proposal consists of the use of various ULPS units, which cover the scanning region from diverse points of view in order to obtain an accurate estimation of the receiver's position in the space.

This chapter proposes a general background on the ULPSs, firstly developed with a structure and properties for 2D positioning, their principal technologies and characteristic, as well as a description of the 2D positioning configurations. Then the proposed 3D positioning is described in terms of configuration and implemented algorithms. The following sections of this chapter describe a single ULPS structure for 2D positioning, the architecture of the proposal for the 3D positioning, and the algorithms developed to get accurate estimated positions after the fusion of data coming from various ULPSs [Gua2014] [Ure2016] [Gua2019].

3.1 Ultrasonic Local Positioning System (ULPS)

ULPSs are intended to detect, position, navigate and also track, one or various mobile targets accurately in an indoor environment through ultrasonic technology. They are often used in various applications, such as people tracking, environment monitoring, resource management, robot localization and location-based services. Some 3D ultrasonic positioning systems have been developed previously using different configurations, and based on two main approaches: emitters are placed at fixed positions whereas receivers move in the environment, and vice versa

where the receivers are located at fixed positions whereas emitters are mobile in the environment. In this work, the first case is applied. So, the moving target is usually equipped with a miniature receiver to collect the ultrasonic emissions coming from several beacons of the ULPSs fixed in kown positions, in order to estimate its own position with enough precision. Fig. 3.1 shows a general scheme for an ultrasonic positioning system, where the beacons are set in various places of the environment to cover it well, and the receiver is moving and estimating its own positions by computing the distances from Time of Arrivals or Time Differences of Arrivals (ToA, TDoA) between receivers and emitters [Ure2018] [Man2018].

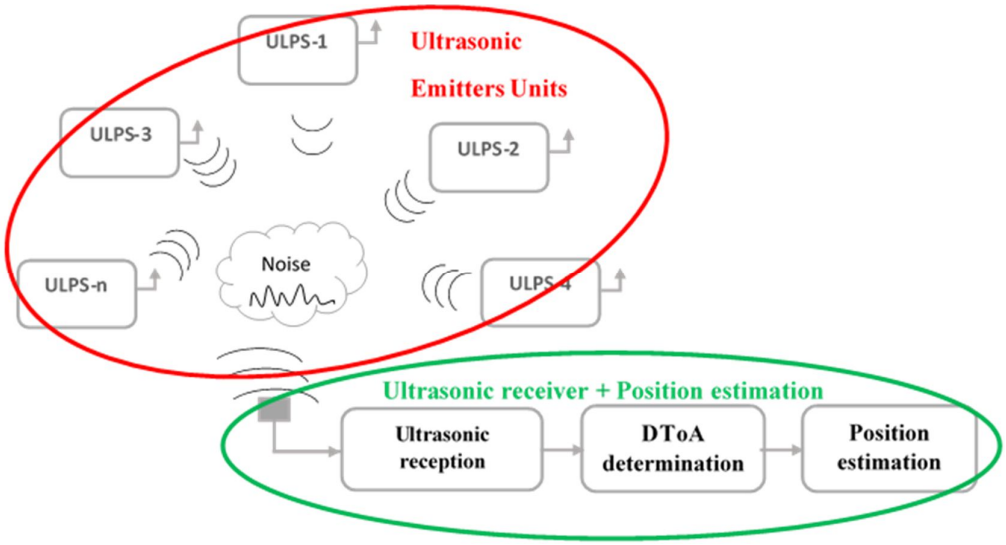

Fig. 3.1. Basic structure for an ultrasonic positioning and navigation system.

ULPS applications are often assigned to 2D positioning and navigation of mobile robots and vehicles, as well as to 3D positioning and navigation of smart devices, such as smartphones, persons, industrial robots, drones, etc. [Sam2009] [Ure2018]. The final accuracy of an ULPS in the position estimation depends on several parameters, as the sensory technology, the system configuration, and the coverage area properties, where the accuracy for 2D Ultrasonic Systems is in the centimetre range and for 3D Ultrasonic Systems is from the centimetre to the decimeter range. Related to this, a general parameter for an ULPS is the Geometric Dilution of Precision (GDOP), computed to specify the propagation and distribution of the distance error between the measurements and the estimated positions. For 3D positioning, the Position Dilution of Precision PDOP can be experimentally obtained, according to (3.1):

$$PDOP \approx \frac{\sqrt{\sigma_x^2 + \sigma_y^2 + \sigma_z^2}}{\sigma_m} \quad (3.1)$$

Where $\sigma_x^2, \sigma_y^2, \sigma_z^2$ are the position variances in X, Y and Z, respectively ; and σ_m is the standard deviation in the distance measurements (that can be for ultrasonic measurements $\sigma_m = 1\text{cm}$).

Another fundamental parameter is the maximum range of coverage, where common values for indoors zones are between 5 and 50 meters. Due to this, and for extended coverage zones, scalability is significant to assure an average positioning performance, as the positions estimation degrades with the distance between the receiver and transmitters [Roo2002] [PRI2005].

In this work, we deployed an LPS, which is composed of a multiple ultrasonic beacons unit to cover an extensive 3D indoor space, then to locate a mobile target. Every single beacon unit is composed of a set of five ultrasonic beacon emitters distributed as Fig. 3.2 shows. The structure and characteristics of this system are based on the previous project LOCATE-US developed by the GEINTRA group in the Electronics Department from the University of Alcalá [Her2017] [Pro2014]. These works present the design and implementation of the ULPS after selecting the appropriate beacon unit distribution and ultrasonic emissions.

3.2 2D Positioning System Approach

The 2D positioning system, developed in previous works mentioned before (LOCATE-US), are generally used to locate mobile target or robot on the floor, whereas the receiver's devices must be installed above the mobile targets. Furthermore, the ultrasonic beacons unit are installed at the ceiling and oriented to the floor, to cover it as much as possible. For extended area, more than one ULPS can be used. Fig. 3.2.a) shows an example of a 2D positioning and navigating system based on one ULPS, and a mobile robot where an ultrasonic receiver is installed. In addition, Fig. 3.2.b) shows a 2D positioning for an extended area where several ULPSs are installed in the ceiling to track a mobile robot on the floor [Gua2.014] [Ure2016] [Gua2019].

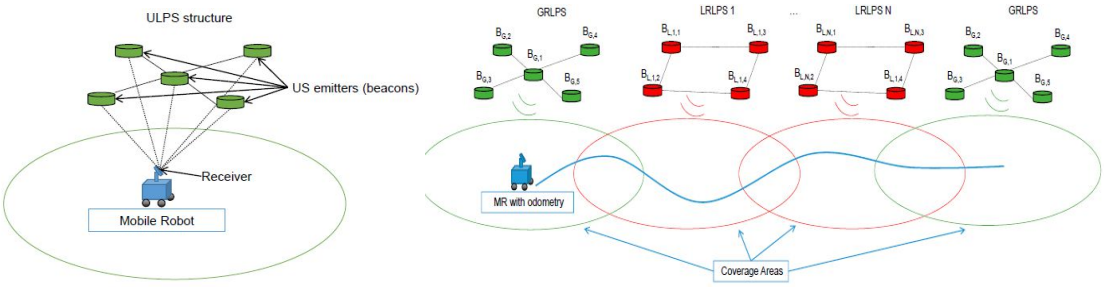

a) b)

Fig. 3.2. 2D ultrasonic positioning system using a) a single ULPS and a single receiver for small area, b) several ULPSs and a single receiver for extended area [Gua2019].

3.2.1 General View of LOCATE-US

LOCATE-US ULPS is a compact, light and portable ultrasonic beacon architecture (hereinafter denoted as ULPS). A single ULPS is formed by five emitters beacons (B_i, where i=1,2,…5) [Pro2014], placed at the centre and at the four corners to form a square with a side of $1/\sqrt{2}$ m, as can be observed in Fig. 3.3. The five beacons have the same orientation and are coplanar to facilitate the simultaneous reception in the receiver of all the emissions, despite the fact that this beacons' structure may not be good from the point of view of PDOP. Usually, for 2D positioning, the ULPS is placed at the ceiling emitting top-down to cover approximately an area of 40 m^2 on the floor for a height of 3.5 m, since the total aperture angle of each emitter beacon is 120º. To overcome audible artefacts, the ULPS operates around 41 kHz [Pro2014].

Many ULPSs can be easily deployed to cover wide indoor areas, where the receiver to be located is moving around. Particular calibration techniques have been used in order to facilitate this deployment. Each emitter of the ULPS use both protocols, the code division multiple access (CDMA) and the time division multiple access (TDMA), to generate the corresponding emissions, encoded with a different code, with suitable auto-correlation characteristics and low mutual interference characteristics with the others. The emitters for a single ULPS are controlled to configure the ultrasonic transmission in term of modulation schemes, sampling frequency and code patterns to be transmitted. Several ULPSs can be efficiently deployed to cover extended indoor areas. The accuracy obtained is in the centimetre range for 2D applications, even in extensive areas. At the reception, a non-limited number of receivers can compute and estimate its own position by measuring TDOAs from the incoming ultrasonic signals, inside the coverage area with an independent and autonomous way. That is why it is not necessary to synchronize the beacons and the receivers [Ure2016] [Ure2018].

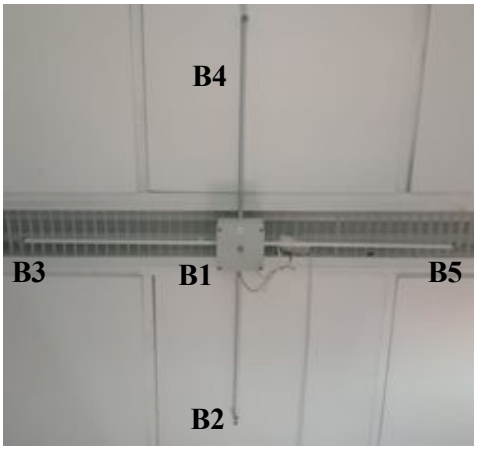

Fig. 3.3. General view of Locate-Us (2D ULPS).

The ultrasonic receiver is a small and portable device, which can be installed above the mobile target pointing down-top. It contains some low-cost components: an omnidirectional MEMS PU0414HR5H-SB microphone with a suitable response at 41.67 kHz to receive the ultrasonic signal; a STM32F103 module to filter the received signals with a high-pass filter and an analog-digital converter with a sampling rate of 100 kHz. In addition, it has a buffer memory with 10000 samples to save at least one complete period from every acquired signal from all the ultrasonic emitters. Also, an UART interface is used to send periodically the emitted signal to the processing module. This prototype provides accurate positioning of the receiver in a horizontal plane, generally considered for 2D location. Fig. 3.4 presents the 2D ultrasonic receiver, showing its small size and its main hardware components [Ampl2012] [Ue2018].

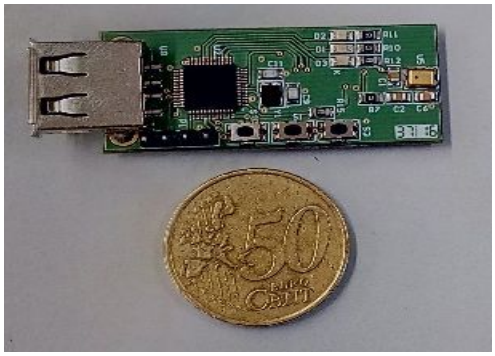

Fig. 3.4. General aspect of the receiver prototypes: single-receiver (2D receiver).

The receiver consists of a microphone and a signal acquisition module connected to a laptop to process the received information. The omnidirectional MEMS microphone receives the ultrasonic signals, with a similar strength from all the different beacons as well as minimizing the near-far effect (thanks to the beacons' distribution). Moreover, all the ultrasonic links have similar channel model and, consequently, all the inter-symbol (ISI) or multiple-access interferences (MAI) can be provided with the same algorithms to get similar results. Then, the received signal is digitized and processed to carry out a set of correlations with each one of the code patterns in the emitted signals. In the case of a single ULPS, five correlations are needed. From the different peaks of the correlator outputs, also five peaks or more –if more of one period of the emission is acquired (related to the buffer size of the receiver), the system computes the TDOAs. Finally, the 2D receiver's position is obtained by means of a hyperbolic trilateration algorithm. The position can be computed and updated at a frequency of 5 Hz, which depends on the length of the used codes. The diagram block of the reception phase for 2D positioning is presented in Fig. 3.5 [Ure2016] [Ure2018].

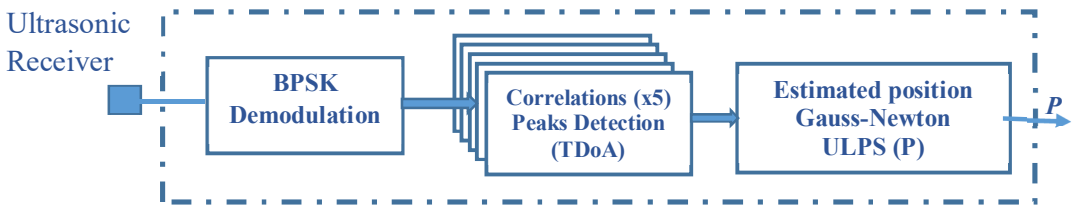

Fig. 3.5. 2D ultrasonic positioning system using a single ULPS and a single 2D receiver.

3.3 3D Positioning System Approach

3.3.1 Devices Adaptations

The 2D positioning system provides good results, where its accuracy is in the centimetre range. To extend the use of this system for the 3D positioning keeping the configuration in Fig. 3.2, where the emitters are installed on the ceiling, two main limitations hold on. Firstly, it provides higher errors in the perpendicular coordinate to the plane where ULPS is installed. Secondly, it becomes hard to reach the total volume of a room, especially for the close regions to the ULPSs and room corners. This is due to the form of the coverage volume of each ULPSs, as explained above and can be observed in Fig. 3.6, and to the coplanar effect of the five beacons per ULPS as shown in Fig. 3.3.

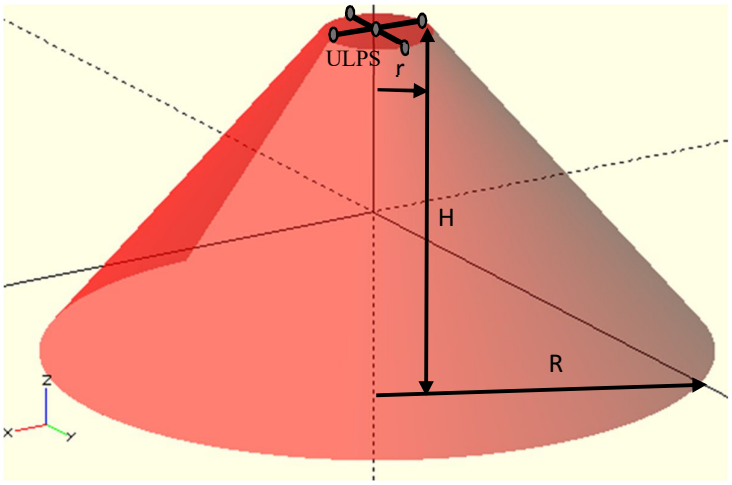

Fig. 3.6. Coverage area for one ULPS installed at the ceiling.

Moreover, Fig. 3.6 presents an explanation of the coverage volume of a single ULPs, which is a truncated cone, where its big base is on the floor with a radius R=3.5 m. As well as, its small base is the ULPS perimeter with a radius r=0.5 m. The beacons unit can reach an area of 40 m^2 and a volume of 53 m^3 roughly when it is installed at a height H of 3.5 m.

To improve the 3D positioning capability of the ULPS, two solutions have been proposed: the first one is to use several ULPSs installed in different planes with various orientations to point to the centre of the space, in order to cover almost all the space. The second solution is to change the ULPS unit configuration and beacon distribution, to obtain a depth between beacons, so the beacons have been placed at different planes: B_2 and B_4 are in the base plane, B_3 and B_5 are moved by 10 cm apart, and B_1 is moved by 20 cm from the base plane, as shown in Fig. 3.7 [Her2017] [Man2018].

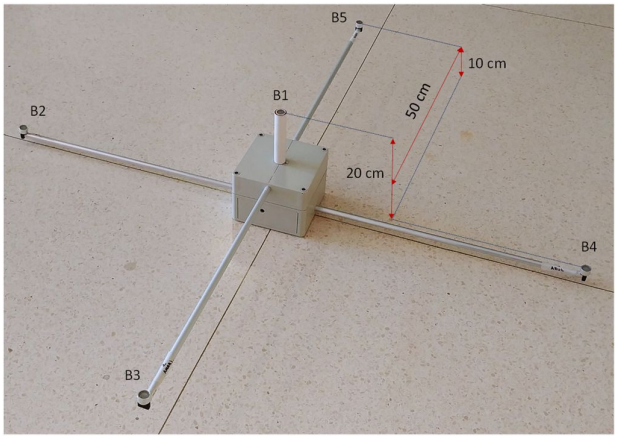

Fig. 3.7. View of the disposition of transducers in a single ULPS.

Also, in order to implement an accurate 3D positioning, a new receiver assembly has been designed. It is composed of three 2D receivers as the one shown in Fig. 3.4, placed in the three faces of a tetrahedron. This distribution has been adapted to capture ultrasonic transmissions coming from as many directions as possible. All the three receivers are wire-synchronized, whereas the general aspect of this 3D ultrasonic receiver described before is shown in Fig. 3.8. Three buffers (SD memory) have been added to each receiver to store the acquired signals, where the receiver R_A is the master and the receivers R_B and R_C are slaves. Each receiver is able to acquire up to 1s, so this acquisition window includes at least a complete transmission from various transducers from various ULPSs at different places and orientations [Ampl2012] [Ure2018] [Man2018].

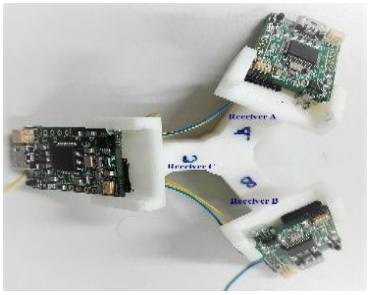

Fig.3.8. General aspect of the 3D receiver prototype based on three single receivers.

3.3.2 Proposed 3D Positioning System Configurations

As was indicated in previous sections, the configuration with a single ULPS at the ceiling means that the performance significantly degrades with the height variation, due to the poor Vertical Dilution of Precision (VDOP), which defines the performance only taking into account the typical deviation in the z coordinate. In order to improve these results, other beacons' organisations of several ULPSs have been conceived although conserving the basic structure of the ULPS, and its characteristics.

As a first configuration, three units are placed in the corresponding three perpendicular planes, which define most common indoor room's shape, so they cover most of the volume simultaneously, whereas other non-central areas are still scanned by at least one of them. Fig. 3.9.a) depicts the general aspect of this beacon distribution in a normal ordinary-size room. The first ULPS is installed on the floor or at the ceiling. The second two units are installed in two

perpendicular walls. Fig. 3.9.b) also shows the projection of this 3D configuration in the XY plane, as well as the *z* variation of the beacons in the different planes to avoid the co-planarity limits [Man2017] [Man2018] [Mann2018].

The second configuration is composed by four ULPS placed at four corners oriented as expected to the centre of the room, in the direction of the cube diagonals, for extended spaces as Halls. Fig. 3.9.c) presents the general aspect of the beacon unit distribution in an extended size space and Fig. 3.9.d) shows the projection of this 3D configuration in the XY plane, as well as the *z* variation of the beacon units.

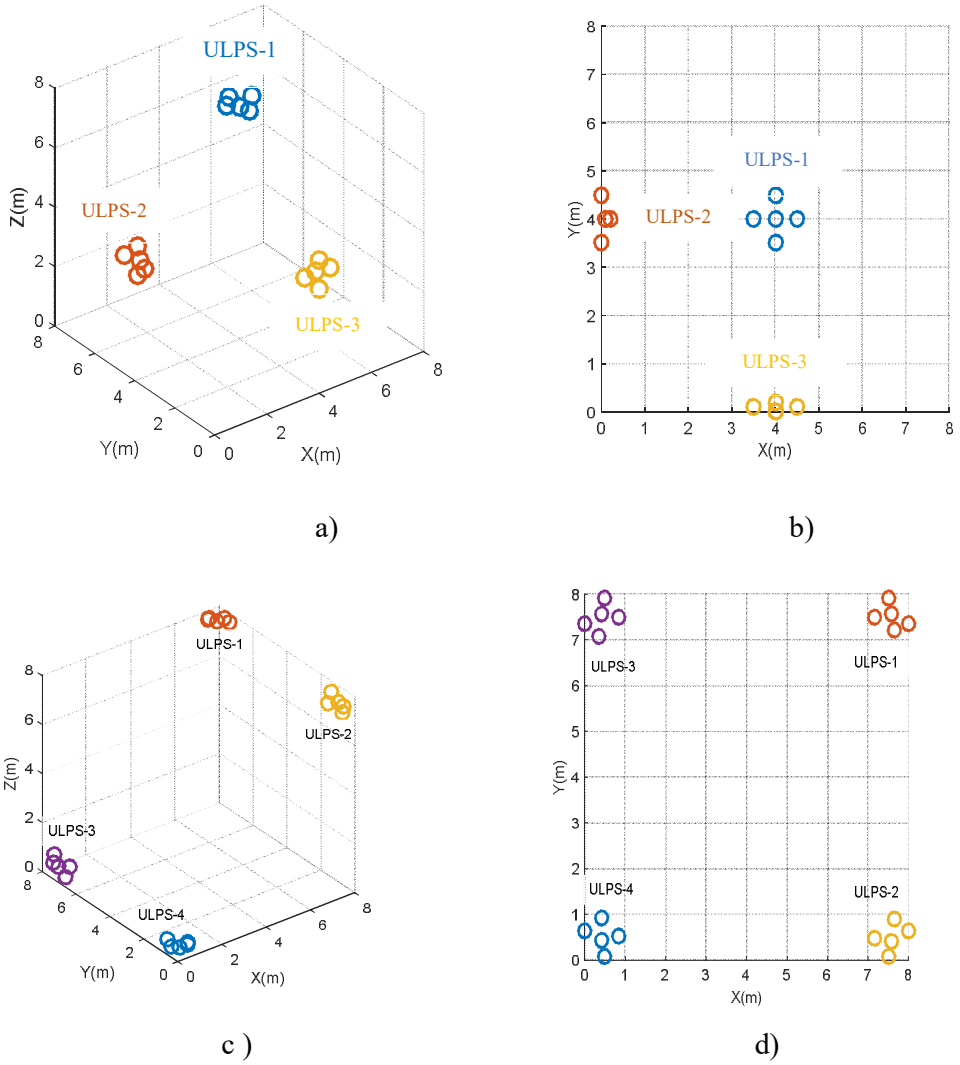

Fig. 3.9. Two proposed 3D positioning system configurations: a-b) first configuration using three ULPSs fixed on three perpendicular walls; and c-d) second configuration applying four ULPSs installed on the four corners of the two principal diagonals of the room.

3.3.3 3D Positioning System Algorithm

After acquiring the ultrasonic signals from n ULPSs, a set of a BPSK demodulations and correlations with the corresponding emitted 1024-Kasami sequences code is performed. These correlation functions are analysed in order to detect the maximum peak values of the received signals and, consequently, compute the TDOA between the mobile receiver and the beacons to estimate the receiver position by a Hyperbolic Gauss-Newton trilateration technique, since all the ULPSs' emissions are asynchronous. Take into account that, by processing the acquired signals from the ULPSs, each one will able to detect up to 5 transmissions per ULPS. As an example, Fig. 3.5 presents the positioning algorithm for a single-receiver prototype (2D receiver) and one ULPS [Ure2018]. To extend it to the three receivers' case (3D receiver prototype), the computational complexity will be multiplied by three. Furthermore, Fig. 3.10 resumes this processing for the 3D receiver prototype and n beacon units (ULPS-1, ULPS-2, ..., ULPS-n), where, in our case, n can be three or four [Man2017] [Man2018]. Finally, the number of estimated position is generally $3 \cdot n$ (where 3 is coming from the number of receivers). So, to improve the accuracy of the final position estimate, several fusion algorithms are used [Bha2019]. Two principal fusion methods groups exist, the loosely coupled fusion and the tightly coupled fusion. Each method uses a specific number of steps and diverse types of data. For the positioning case, the loosely coupled fusion is applied after estimating the mobile position from all the emitters, then they will be fused to get the final estimated position. On the other hand, the tightly coupled fusion is utilised to fuse distances coming from various beacons to update the previous positions [Nur2017]. Those methods will be explained next.

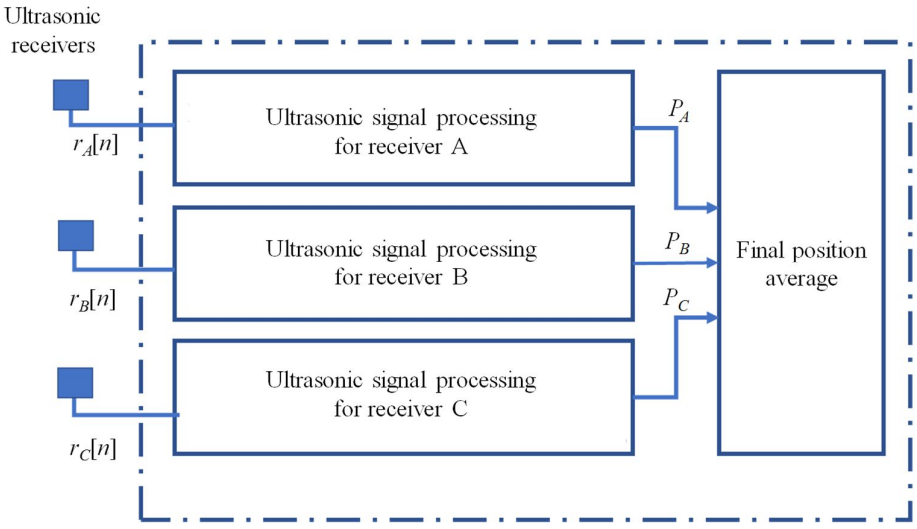

Fig. 3.10. General block diagram of the processing proposed for the multiple receiver prototype.

- Tightly Coupled Data Fusion

A tightly coupled approach is supposed to integrate the multi-sensors data for the position estimation. There are two ways to combine acquired data using specific filters, as the EKF.

The first way is fusing data in the prediction step of the filter (e.g. EKF), which employs the values given by the sensors as essentially a control input. So, some sensors are used in the prediction step, while the rest of the sensors are used in the update step to correct the prediction [Rhu2012]. The second way is known as the measurement fusion method [Gan2001]; it is the simplest form and consists of fusing data through the observation vector of the filter (e.g. EKF) [Ben2012], where the prediction step is totally based on a mathematical motion model, while the update and correction are performed employing the observations of the sensors [Mir2017].

In the implementation of the tightly approach used in this work, the second approach is used, due to the direct use and combination of each individual measurements, coming from the ultrasonic sensors, which are used as the observation vector. Thus, this vector consists of the TDOAs between the ultrasonic transmitters and the mobile receiver as explained in Fig. 3.11. The most relevant advantage is that it does not lose information coming from the pre-processing of the ultrasonic measurements.

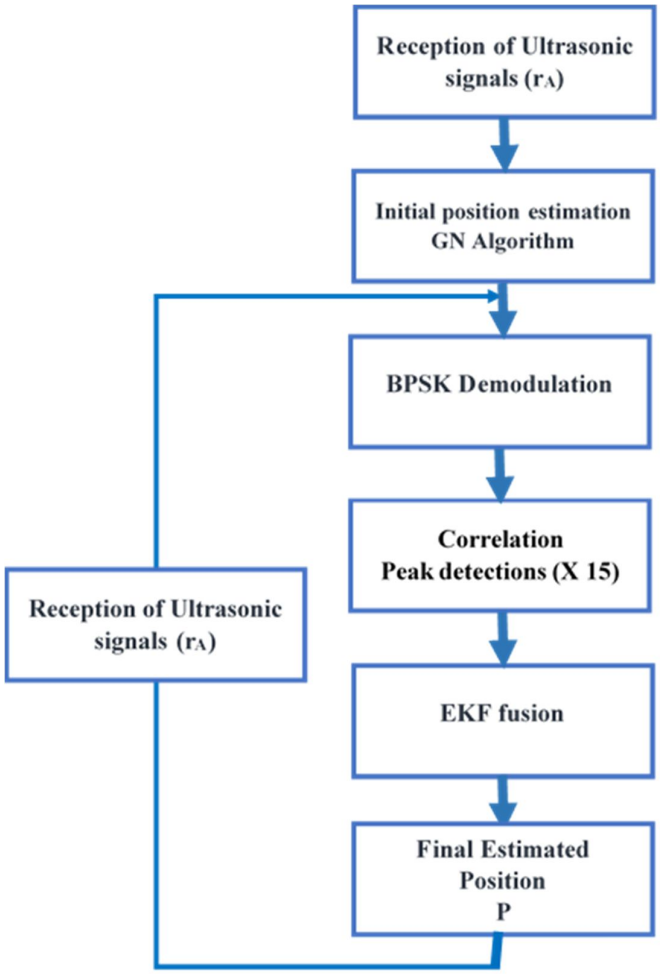

Fig. 3.11. Block diagram of a tightly multi-sensors fusion for one receiver RA and three ULPSs (15 incoming ultrasonic signals) for 3D positioning system.

- Loosely coupled data fusion

The loosely coupled approach, referred also as to decentralized one, is supposed to integrate estimated positions, obtained from the multi-sensors, to get the final one. The raw distance measurement is firstly computed by triangulation or least squares to get the positions' estimate, and, then, they are used as input data to be integrated into specific algorithms or filters. Since the loose coupling approach requires pre-processing of the raw measurement data, in some cases, part of the information is lost [Zen2019].

In this work, the ultrasonic measurements, coming from more than one ULPS, are used to obtain position estimates using the Gauss-Newton algorithm from the multi-lateration approach. These position estimates are consequently used as input position measurements in the sensor fusion

algorithms (KF, MLE, AKF), then merged to obtain the final position estimate output of the integrated system, in order to generate a fused position estimation with less noise, as well as more accuracy than the individual position estimations, as shown in Fig.3.12.

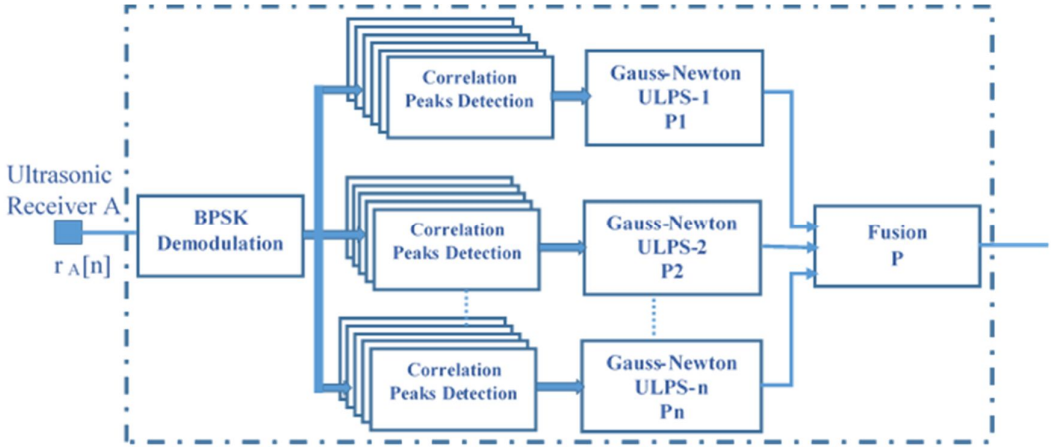

Fig. 3.12. Block diagram of a loosely multi-sensors fusion for one receiver RA for 3D positioning system.

3.4 Conclusion

In this chapter, a general illustration of the 2D Ultrasonic positioning system has been described in terms of the configurations of emitters and receivers. To use this system for 3D positioning, some drawbacks appeared, such as the non-coverage spaces in specific places of the room, or a large error of the estimated position in the perpendicular direction to the ULPS plane. Thereby, some modifications in the emitter and receiver architectures and new configurations are needed and proposed.

These new configurations are based on the use of a sensors network or multi-sensor configurations. The first one is composed of three ULPSs installed in three perpendicular planes: those positions of the ULPSs can be in the centre of each plan or shifted. The second one is composed of four ULPSs placed at four diagonal corners of a room. Also, a modification of the receiver architecture is done to adapt it to the new configurations and to be able to acquire signals from several directions.

Finally, to obtain the final estimated positions with enough accuracy, several fusion methods have been proposed. Some methods are based on the tightly coupled approach and others are

based on the loosely coupled approach. The next chapter will detail all the proposed algorithms and approaches, as well as some simulated results that will be also presented and discussed.

Chapter 4

Proposed Developments for 3D Positioning

In the previous chapter, we presented a general view of two suggested 3D configuration system for indoor positioning with ultrasonic signals in a large environment, these solutions are based on the deployment of various ULPSs with particular orientations and positions to cover all the space. Many algorithms have been proposed and developed to allow positioning and navigating of a Mobile Receiver in the space, which can be installed on a mobile target to estimate its positions autonomously. To cover extensive areas the used ULPSs must be calibrated to obtain a good estimated position.

As mentioned in the previous chapter, two different configurations are studied:

- Configuration A: three ULPSs placed at the centres of three perpendicular planes, the first plane is in the centre of XY-plane at z=8m, the second plane is in the YZ-plane at x=0m and the final plane is in XZ-plane at y=8m. All these ULPSs are emitting perpendicularly to the plane in which they are placed, particularly to the centre of the room (workspace), as shown in Fig. 4.1.a).

- Configuration B: four ULPSs located at four corners of the room at (8m, 8m, 8m), (8m, 0m, 8m), (0m, 8m, 0m) and (0m, 0m, 0m), sequentially. Each ULPS is emitting in the direction of the cube diagonal corresponding to the corner at which it is located, especially to the centre of the room, as shown in Fig. 4.1.b).

On the other hand, the mobile receiver is placed in a grid of positions, in the two different indoor environments, where all the ultrasonic emitters transmit simultaneously and independently. Two fusion methods have been used to merge data coming from the various ULPSs to get the accurate estimated position. The first method is based on the loosely coupling algorithms, fusing the obtained estimated positions from various ULPSs to get the final estimated position. The second method is based on a tightly coupled algorithm used to fuse data, such as distances, angles or difference of distances, to update the final positions. Usually, this method is used to track mobile targets.

This chapter is organized as follows: first section is an introduction of the proposal, in which we describe the two studied architectures of the system and introduce possible solutions; second and third sections show the proposed algorithms and the simulated results for a single ULPS, and then for three independent ULPSs in the different configurations; fourth section shows the proposed algorithms, as well as the simulated results, when applying multiple sensors fusion; and the last section discusses some conclusions.

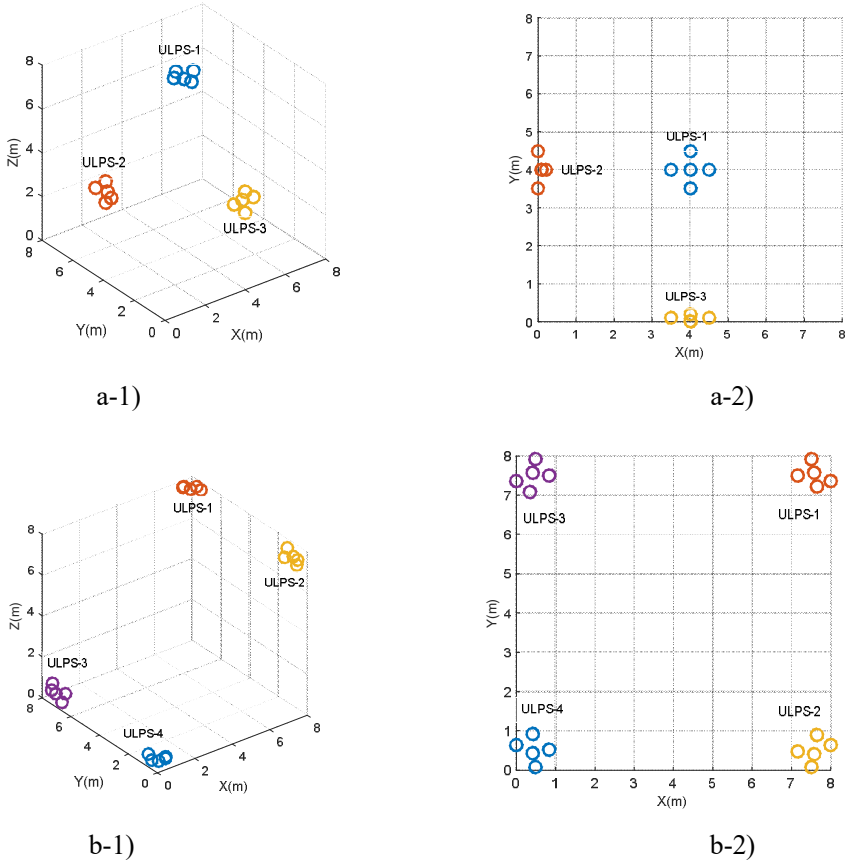

Fig. 4.1. Studied configurations: a) using 3 ULPSs installed in the centres of 3 perpendicular planes where a-1)) is the 3D view and a-2) is its projection on the XY-plane; and b) using 4 ULPSs installed on the 4 corners of the principal diagonal of the room, where b-1) is the 3D view and b-2) is also its projection on the XY-plane.

4.1 Configurations based on a Single ULPS

4.1.1 Positioning Algorithm: Gauss-Newton Algorithm

The ULPS operates with a set of transmitting elements (ultrasonic beacons) placed at known positions of the environment (room) and a mobile receiver, whose position is the one to be estimated. The mobile receiver location can be computed by spherical trilateration from the Times of Arrival (TOAs) of the emitted ultrasonic signals. Nevertheless, the mobile receiver needs to know the starting time of the transmission of beacons, which requires a synchronism trigger signal between the receiver and the beacons, what involves the use of additional hardware, i.e. Radio Frequency (RF) or Infrared (IR) transceivers in an ultrasonic ULPS. Moreover, the errors in the synchronization process increment the errors in the estimation of the mobile receiver position.

To avoid this problem of synchronization between the emitters and the receivers, it is possible to use a hyperbolic positioning algorithm. This algorithm needs the measure of the Time Differences of Arrival (TDOA) between a reference beacon and the others. So, hyperbolic trilateration permits asynchronous detection of emitted ultrasonic signals after using one more beacon which acts as a reference.

Both TOA and TDOA require to solve a non-linear system of equations to get the estimated position of the mobile receiver. Gauss-Newton algorithm (GNA) is used as the positioning algorithm, due to its suitable features, by an iterative minimization of the non-linear equation positioning system, as presented in Fig. 4.2.

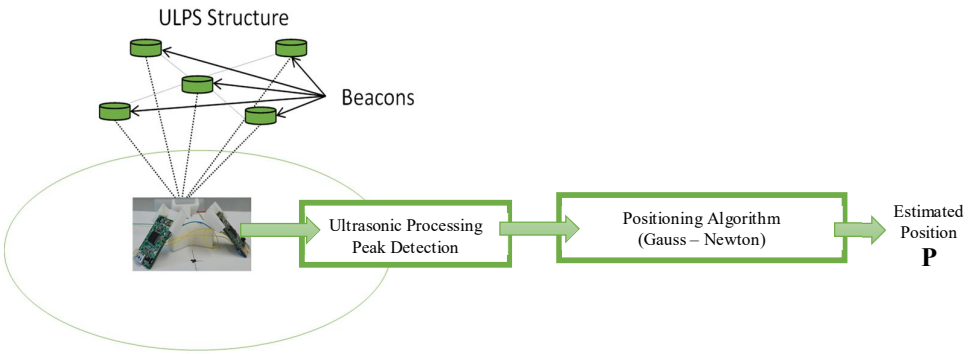

Fig. 4.2. General view of the ultrasonic positioning system based on one ULPS unit.

In indoor positioning systems, it is essential to evaluate its main quality parameters, which are the precision or the accuracy of the estimated positions. This parameter depends on some factors, such as the quality of measurements (signal strength, ranging distances, etc.), the geometry of the positioning system (beacons' geometry), as well as the positioning system configuration (the number of beacons, the orientations, the installation places of each emitted units, etc.) or some adverse effects (multipath, etc.). In order to study the positioning system in the 3D space, a room with a volume of 8×8×8 m^3 has been chosen as a workspace. One ULPS is installed at a known place: firstly in the centre of a wall at (0 m, 4 m, 4 m); then in the centre of the ceiling at (4 m, 4 m, 8 m) for configuration A; secondly in the high corner at (8 m, 8 m, 8 m) in configuration B as presented in Table 4.1 (circle marks represent the five ultrasonic beacons of a ULPS emitter and the diamonds are the estimated positions). The general shape of the coverage volume of the ULPS is a truncated cone, as explained in Fig. 4.3; its small base is the circle included the ULPS and its big base is in its parallel plane and its area depends on the distance (height) between those bases.

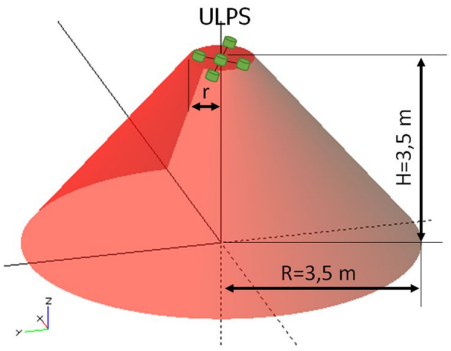

Fig. 4..3 Coverage volume form of one ULPS placed in the ceiling, which is a truncated cone: the small base radius r=0.5 m is the distance from the central beacon B1 to the others (B2, B3, B4 and B5) and the big base radius R=3.5 m corresponds to a heigh between the two bases of H=3.5 m.

Many iterations have been done for each ground-truth position (the cross marks), where the step between the ground-truth positions is 1 m for the three axes X, Y and Z. In Table 4.1 below, simulated results have been plotted where the receiver is in the X-Y plane for a height z=2 m. A cloud of estimated positions (diamond marks) is obtained for the different ULPS positions and for the two studied configurations.

Configuration A	*Configuration B*	
ULPS in the centre of the ceiling	*ULPS in the centre of the wall*	*ULPS in the corner*
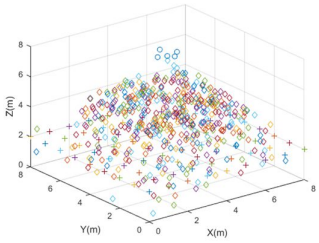	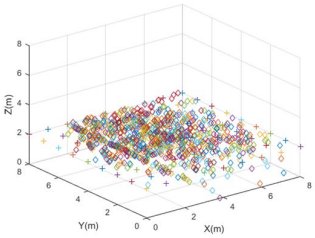	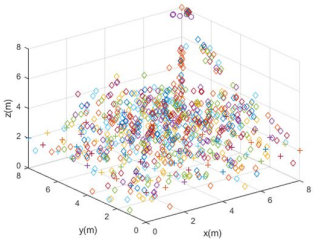
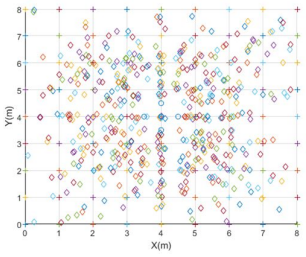	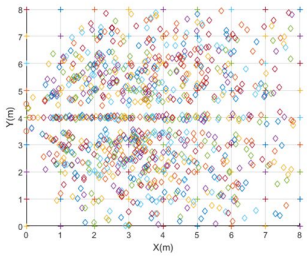	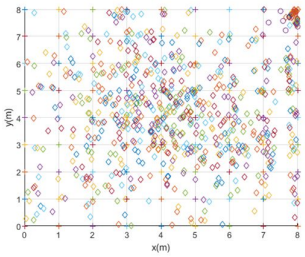
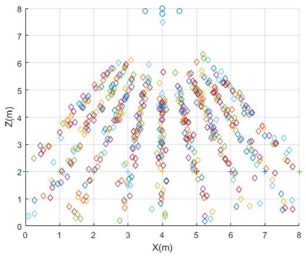	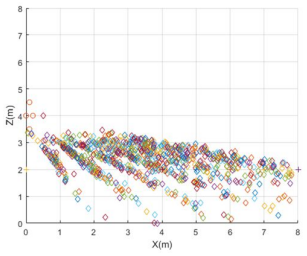	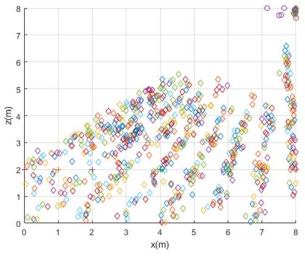
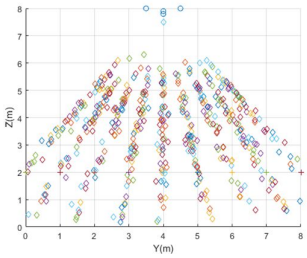	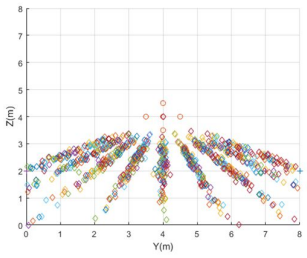	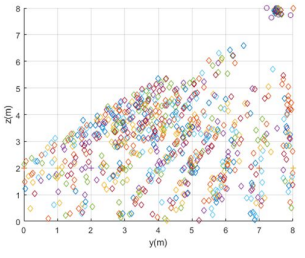

Table 4.1. Cloud of position points for a single ULPSs placed firstly at the centre of the ceiling (4 m, 4 m, 8 m) and at the centre of the wall (0 m, 4 m, 4 m) for configuration A; and at the high corner (8 m, 8 m, 8 m) for configuration B, when the receiver is in the XY-plane at a height z=2 m.

The dispersion of the estimated positions obtained differs according to the position of ULPS via various ground-truth positions of the receiver, also according to its height (the altitude of the receiver plane). But this dispersion is generally high, which results in uncertain positioning and subsequently a system of low precision for both configurations A and B. This dispersion can be used to compute the position variances in the space σ_x^2, σ_y^2 and σ_z^2 for the three axes X, Y and Z, respectively. Also, the standard deviation in the distance measurements have been set. Fig. 4.4 below presents the dispersion of the estimated position for one ULPS installed in the ceiling a) and in the high corner b), for three different heights z= 2 m, z= 4 m and z= 6 m. The dispersion related to the Z-axis is the largest one, whereas it decreases when the distance between the ULPS and the receiver plane reduces, and vice versa.

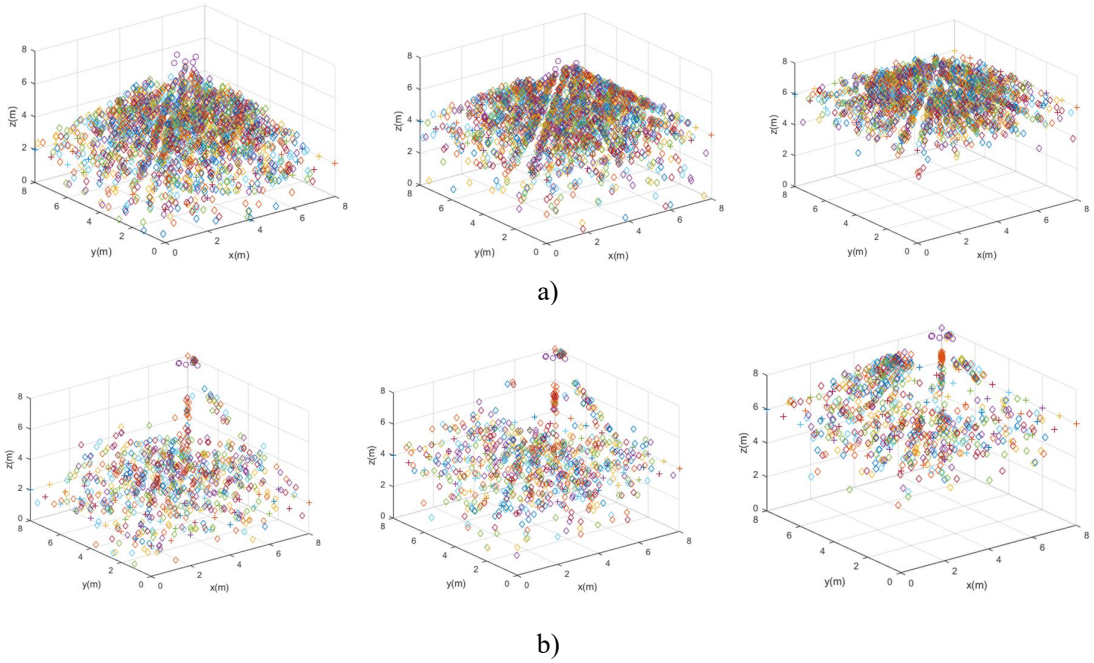

a)

b)

Fig. 4.4. Cloud of the obtained estimated positions from one ULPS: a) installed in the centre of the ceiling (4 m, 4 m, 8 m); b) installed at the high corner of the room (8 m, 8 m, 8 m) for different heights z=2 m, z=4 m and z=6 m.

When the positioning system is based on one ULPS, for a large 3D environment, the performance degrades considerably in the perpendicular direction of its installation position: in the ceiling ULPS case, the performance degrades in the vertical direction, which can be known as the Vertical Dilution of Precision (VDOP) and is related to the ULPS configuration and geometric architecture. Similarly, for the ULPS placed on the wall, the Z-axis dispersion is the lowest one and the X-axis dispersion is the highest one, as shown in Fig. 4.5.

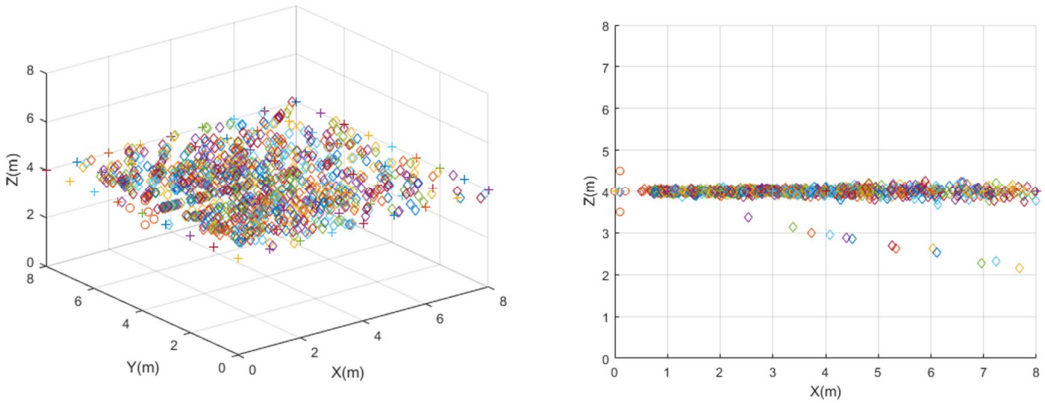

Fig. 4.5. Cloud of the obtained estimated positions from one ULPS installed at the centre of the wall (0 m, 4 m, 4 m) for the height z=4 m.

As a conclusion, the quality of the estimated positions depends on many factors, such as the geometry of the emitter unit, its position, orientation and distance to the receiver. So, to improve the obtained estimated position in terms of accuracy, as well as to reduce these errors due to the geometric effect, a combination of several ULPSs can be used.

4.1.2 PDOP Analyses for the Configuration based on a Single ULPS

The Position Dilution of Precision (PDOP) is used to describe the positioning system configuration in the terms of the positioning error caused by the relative positions, and the geometric distribution of the ULPS units, for a 3D positioning. The PDOP is decomposed in the horizontal dilution of precision (HDOP) and the vertical dilution of precision (VDOP), as explained in previous chapters. In this section, several simulations have been done to study the PDOP parameter for a single ULPS in both configurations A and B.

Table 4.2 shows the different PDOP values for the same XY plane for z=2 m for three different positions of the single ULPS. The PDOP values are high, above 100 for the ULPS installed on the wall, above 500 for the ULPS installed on the ceiling, and about 300 for the ULPS at the corner. The smallest PDOP values are always in the nearest area to the ULPS location. The contour map represents the PDOP in planes at a specific height. These values have been calculated for every point in the grid from the cloud of estimated positions after simulations, where each colour means a value of PDOP. So, the greater the PDOP is, the larger the positioning error is at that point. Then, with the PDOP map presentation, it is possible to have an idea about the error in each region of the space in a real situation with a particular ULPS configuration.

Configuration A		*Configuration B*
ULPS in the centre of the ceiling	*ULPS in the centre of the wall*	*ULPS at the corner*
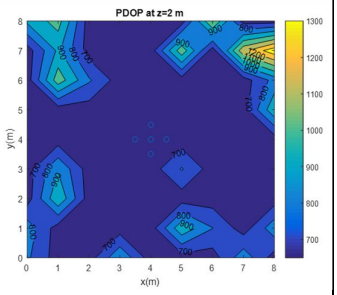	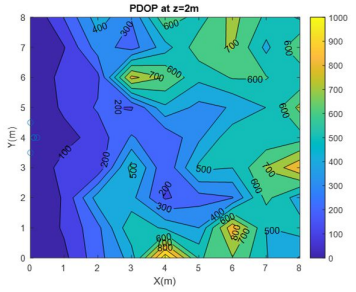	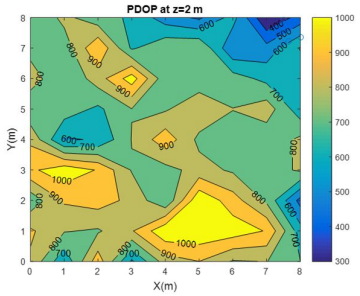

Table 4.2. PDOP distribution of a single ULPS placed in configuration A: in the centre of the ceiling (4m, 4m, 8m) and in the centre of the wall (4m, 4m, 4m); as well as in configuration B at the corner of the room (8m, 8m, 8m).

As can be observed in Fig. 4.6.a), the PDOP values differ in the three planes. In the configuration A, where the ULPS in installed in the centre of the ceiling, the PDOP values are smaller in the centre of every plane, and then they increase towards the sides of the room. For the first plane z=2m, the farthest plane from ULPS, the PDOP varies from 400 to 1100; whereas these values decrease in the middle of the room (z=4 m), where the PDOP is between 200 and 1100; and, finally, they range from 100 to 110 in the third plane z=6m, which is in the upper half of the room at the shortest distance from the ULPS. Similar conclusions can be derived from Fig. 4.6.b) with the ULPS placed at the corner (8 m, 8 m, 8 m) and pointing at the centre of the room. For the first plane z=2m, the PDOP values are between 400 and 1100; for z=4 m, they decrease to between 300 and 900; and between 100 and 1100 for z=6m, the lowest values due to the short distance between this plane and the ULPS location.

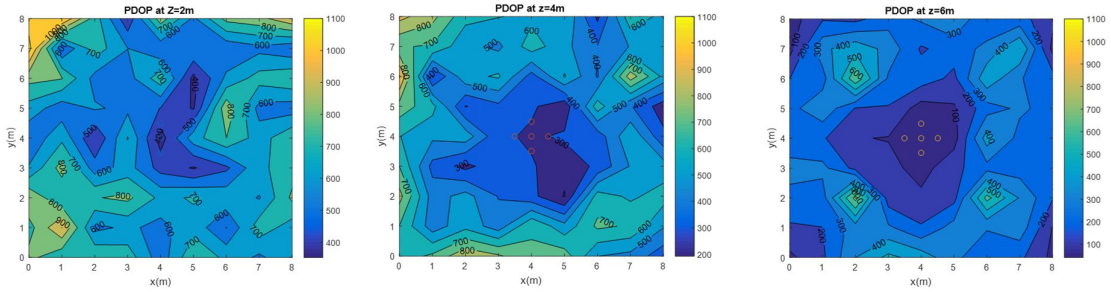

a)

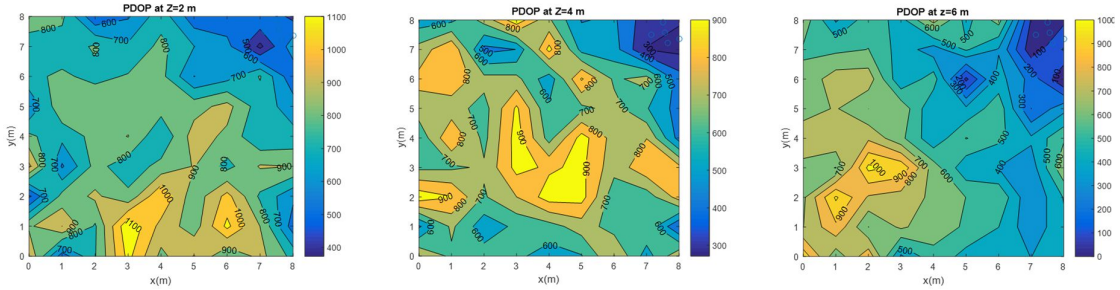

b)

Fig. 4.6. Colour map of PDOPs for different XY planes (z=2m, z=4m, z=6m), for a single ULPS placed: a) in the centre of the ceiling (4m, 4m, 8m) for the configuration A; and b) at the corner (8m, 8m, 8m) for the configuration B.

4.2 Configurations based on Synchronized ULPSs

In order to estimate the position of a mobile target in a 3D space, a single ULPS is not sufficient to cover all the space, assuming an 8x8x8m^3 volume, with high accuracy. The configuration with a single ULPS implies a significant degradation of the performance with the height variation, due to the poor Vertical Dilution of Precision (VDOP) and the typical deviation in the *z* coordinate. Then, the use of a single ULPS is not a fitting solution and a combination of several ULPSs is used (two, three and four ULPSs), placed as in previous configurations A and B for different heights.

Particularly, in this section several synchronized ULPSs are used, whereas the non-synchronized case will be studied later. Simulations for the estimated positions of the mobile receiver and PDOP values of different ULPSs configurations are done and plotted in all the volume of the large room, as presented in Tables below and in the index.

4.2.1 Two Synchronized ULPSs Configuration

In order to improve the positioning system in the space, two ULPSs emitter units have been validated by simulations. For configuration A, two units (ULPS-1 and ULPS-2) are installed in two perpendicular planes; ULPS-1 is in the centre of the ceiling (4 m, 4 m, 8 m) and ULPS-2 is in the centre of a wall (0 m, 4 m,4 m). As well as for configuration B, the two ULPSs are installed: firstly, in two opposed corners of a front diagonal of the room, respectively at (0 m, 0 m, 0 m) and (8 m, 0 m, 8 m); and then in two opposite corners of a main diagonal of the room, respectively at (0 m, 0 m, 0 m) and (8 m, 8 m, 8 m), to cover simultaneously most of the workspace volume.

The mobile receiver estimates its position synchronously by spherical trilateration from the distance measurements (TOA) between the beacons of each ULPS and the receiver. Then, a Gauss-Newton minimization algorithm computes the final estimated position. The complexity of the system increases, as the number of emitters does, since the number of equations to estimate the mobile receiver position increases, and it is multiplied by two after adding a second ULPS. Fig. 4.7 shows a simple view of the 3D positioning system based on two ULPSs.

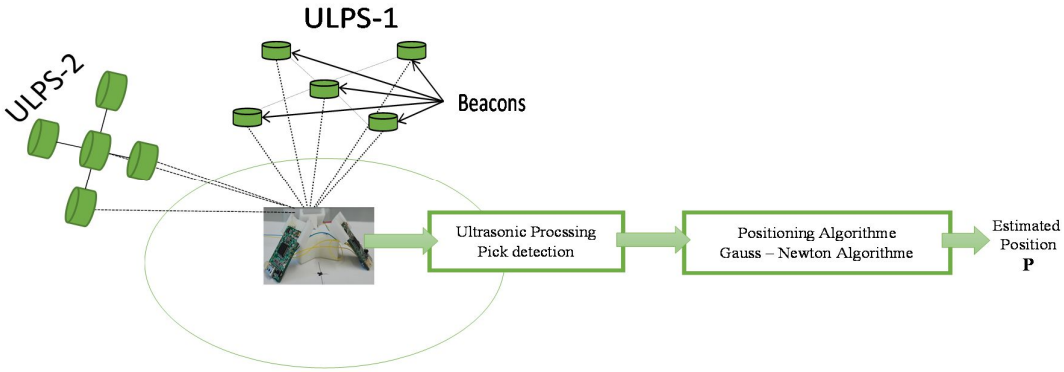

Fig. 4.7. General view of the positioning system using two ULPSs.

For a height of z=2 m, Table 4.3 presents a summary about the simulated results for the cloud of estimated positions for configurations A and B, as mentioned before. The estimated positions are a grid of ground-truth positions in XY-plane where z=2 m, which are separated by a step of 1m in the X-axis and Y-axis

.

Configuration A	*Configuration B*	
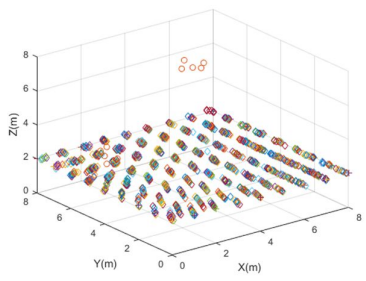	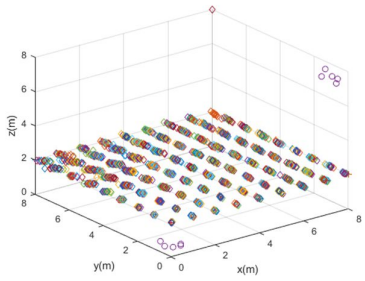	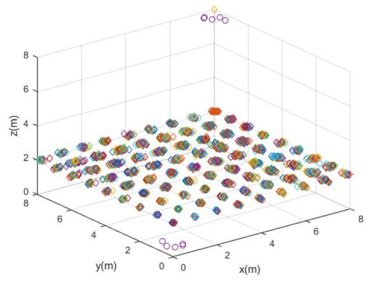

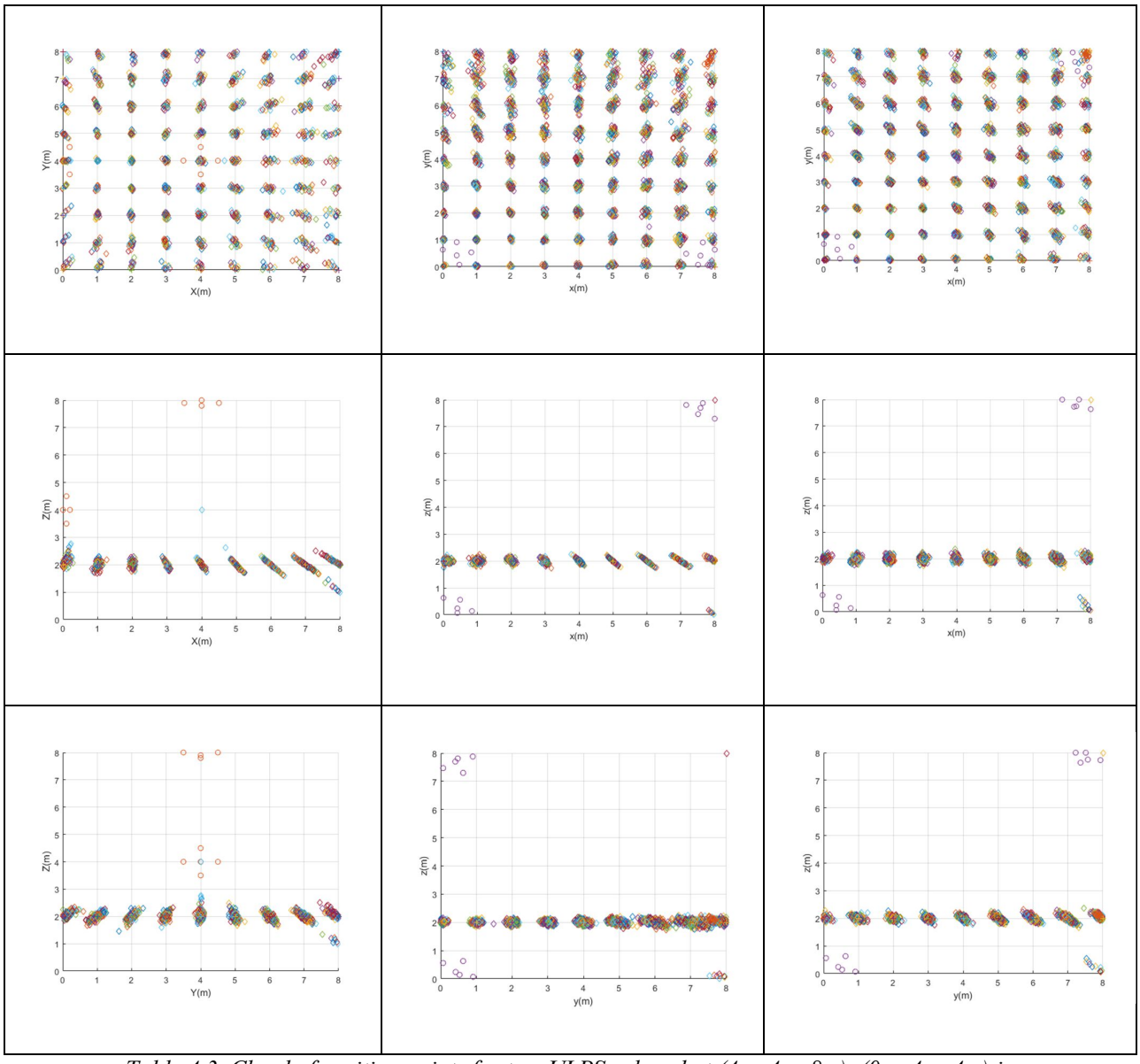

Table 4.3. Cloud of position points for two ULPSs placed at (4m, 4m, 8m), (0m, 4m, 4m) in configuration A, then at (0m, 0m, 0m) and (8m, 0m, 0m) as well as at (0m, 0m,0m) and (8m, 8m, 8m) in configuration B, for XY- plane (z=2m) in the down half of the workspace.

The dispersion of the obtained estimated positions was improved for the tree axes especially for the Z-axis. Moreover, this dispersion is not uniform, where in the neighbourhoods of the ULPSs the clouds of estimated positions are smaller than those clouds in the farthest zones. So, for configuration A the smallest cloud of estimated positions are in the intersection of the coverage spaces of ULPS-1 and ULPS-2. For configuration B, since the height of the mobile receiver is z=2 m, close to the ULPS-2 in the low corner, the cloud of the estimated position around that corner are smaller, which implies that the accuracy is higher also.

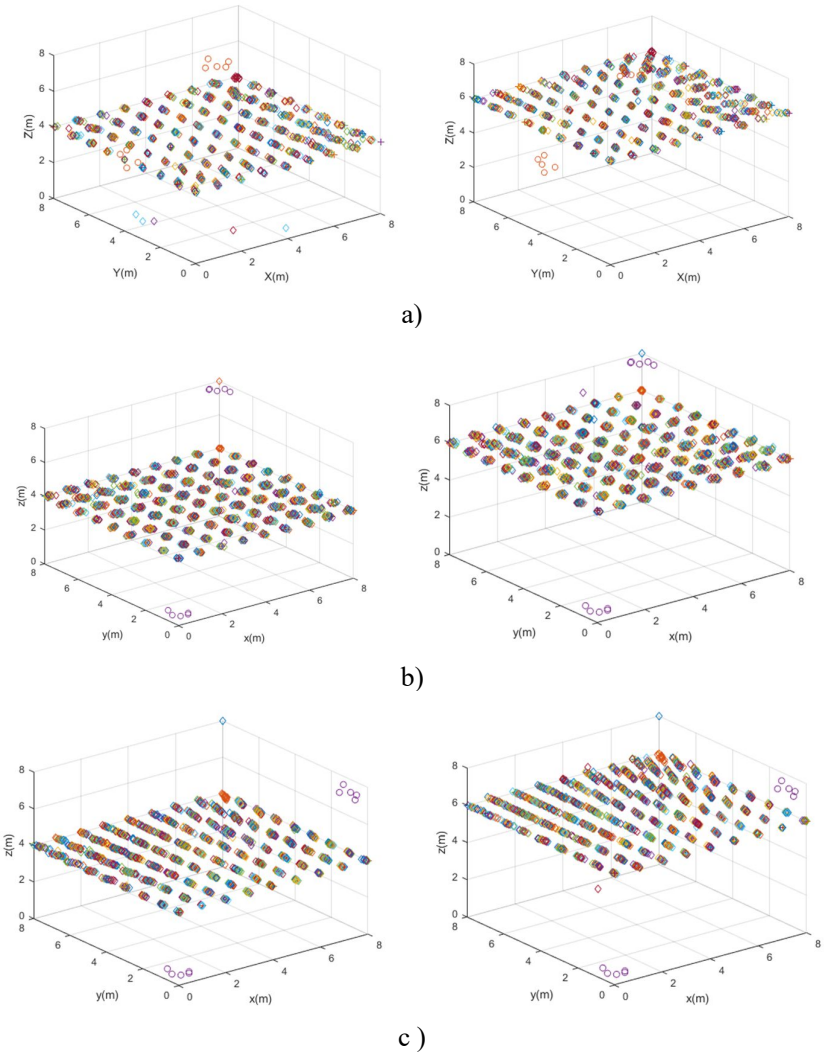

Fig. 4.8. Cloud of position points for two ULPSs placed at the two XY-planes z=4m and z=6m: in a) ULPSs are at (4m, 4m, 8m) and (0m, 4m, 4m) for configuration A; in b) ULPSs are at (0m, 0m, 0m) and (8m, 0m, 0m); and in c) ULPSs are at (0m, 0m,0m) and (8m, 8m, 8m) for configuration B.

Fig. 4.8 presents the cloud of estimated positions for those configurations at various heights. As a conclusion, the more accurate estimated positions are in the neighbourhoods of the ULPSs locations, also in the intersection of two ULPSs coverage volumes, in the middle and the upper half of the room.

To describe the positioning system configuration in the 3D space for the same XY-plane at z=2 m, the PDOP must be computed for both cases A and B using only two ULPSs. In configuration A, the PDOP value at the centre is the lowest one, equal to 15, whereas it increases as the ground-truth positions of the mobile receiver moves towards the boundaries of the room to reach a value of 40 or more. In configuration B, two configurations have been simulated: the

first one when the ULPSs are installed in the face diagonal of the room, as well as the second one with the ULPSs installed in the main diagonal of the room. The PDOP values are high, above 20 and below 220. Again, the smallest PDOP values are in the nearest zones to the ULPS locations, as plotted in the contour map of Fig. 4.9. So, at this height, the configuration A with two ULPSs presents better estimation of the mobile receiver positions, since its PDOP values are smaller than those for the two different ULPSs configurations in configuration B.

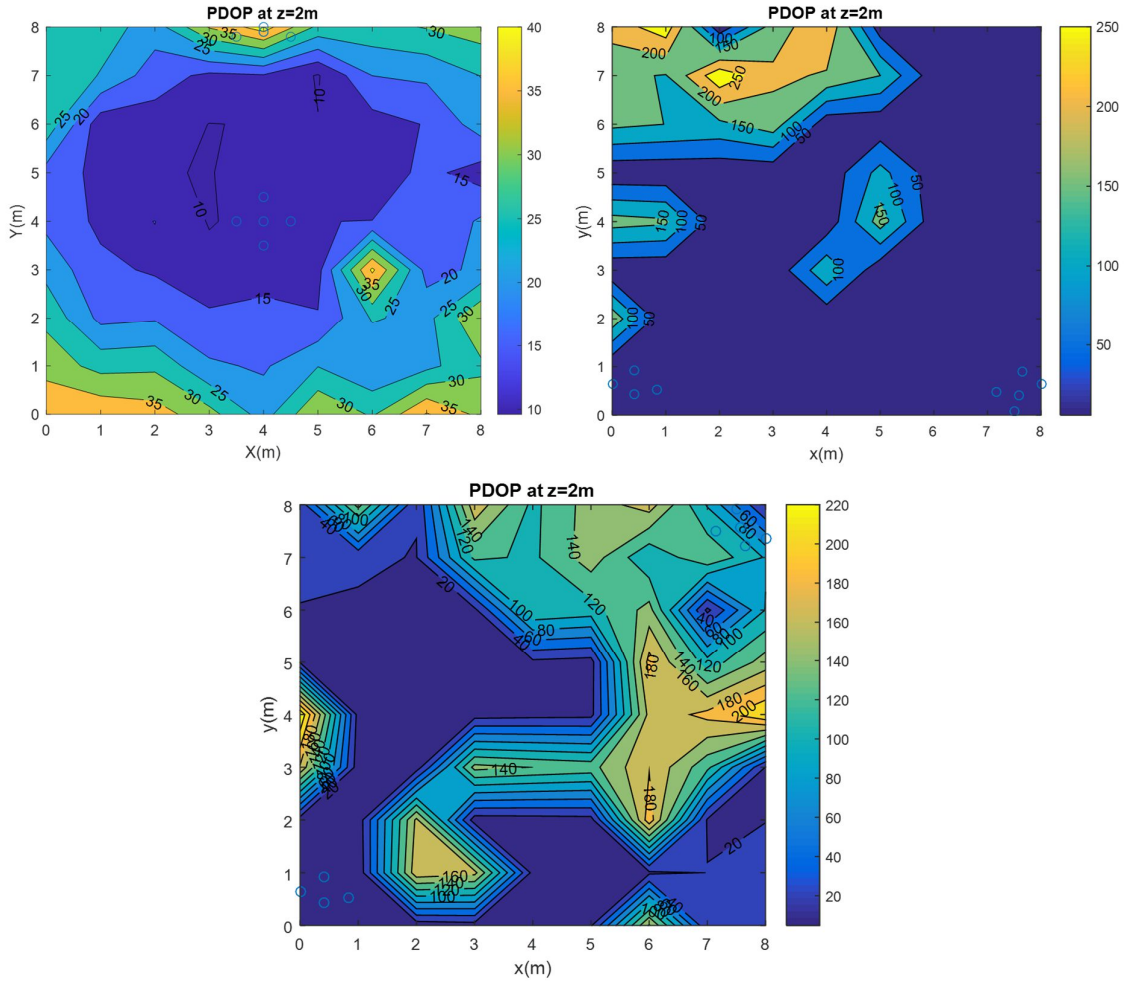

Fig. 4.9. PDOP values for two ULPSs in configurations A and B in the XY-plane at height z=2 m.

For the rest of the space, when the mobile receiver is in a cloud of ground-truth positions included in the XY-planes at z=4 m and z=6 m, the PDOP values for configuration A are below 40 in the middle of the room, and below 80 in the upper part of the room. The optimal PDOP values are at a middle height of the room, the same one as the ULPS-2, where there is a small intersection zone between the two ULPSs. For configuration B, the PDOP values are also high,

its maximum values are around 200 in the middle of the room and around 400 in the upper part of the room, as shown in Fig. 4.10. Configuration A presents better results for PDOP simulations again.

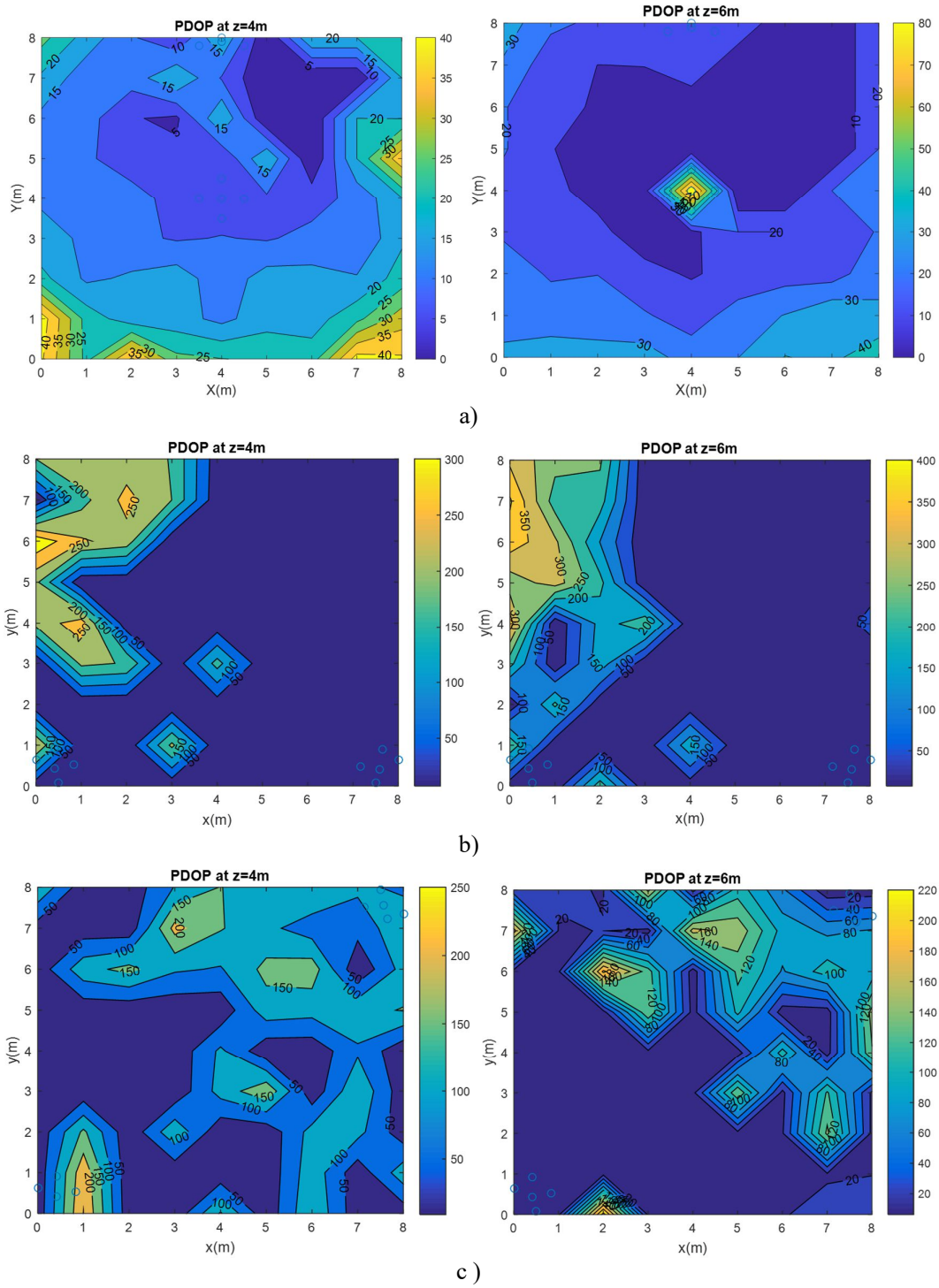

Fig. 4.10. PDOP values for two ULPSs in the XY-plane at heights z=4 m and z=6 m: a) when the ULPSs are at (4m, 4m, 8m) and (0m, 4m, 4m) for configuration A; b) when the ULPSs are at (8m,

0m, 8m) and (0m, 8m, 0m); and c) when the ULPSs are at (0m, 0m, 0m) and (8m, 8m, 8m) for configuration B.

4.2.2 Three Synchronized ULPSs Configuration

In order to cover the space better, a 3D configuration formed by three ULPS units is proposed and simulated hereinafter. Three units (ULPS-1, ULPS-2 and ULPS-3) are installed in three perpendicular planes; ULPS-1 is in the centre of the ceiling (4 m, 4 m, 8 m), ULPS-2 and ULPS-3 are in two perpendicular walls, at (0 m, 4 m, 4 m) and (4 m, 0 m, 4 m), respectively, for configuration A. On the other hand, in configuration B the three ULPSs are installed in three corners of two diagonal opposite corners of the room, at (0 m, 0 m, 0 m), (8 m, 8 m, 8 m) and (8 m, 0 m, 8 m), respectively. In these configurations, the three ULPSs units simultaneously cover most of the workspace volume. The centre of the room is covered by the intersection of the three ULPSs units' signals. The mobile receiver estimates its position synchronously with the three ULPSs by spherical trilateration from the distances measurements (TOA) between the beacons from every ULPS and the mobile receiver. Then, a Gauss-Newton minimization algorithm computes the final estimated positions. The complexity of the system increases more now, since the number of equations used to estimate the mobile receiver position also increases (as the number of ULPS units does), and is multiplied by three after adding the third ULPS.

In Table 4.4, we are assuming that the three ULPSs are synchronised, so the estimated positions are a grid of ground-truth positions at a height of z=2 m, including different presentations in the XY, YZ and the XZ-plane projections. As concluded in previous cases, the best results for the estimated positions are in the intersection of the coverage volumes of various ULPSs: in Case A the central region of the left half in the XY-plane (in the neighbourhood of the ULPS-2), in case B in the region between the three ULPSs corners.

Configuration A	*Configuration B*

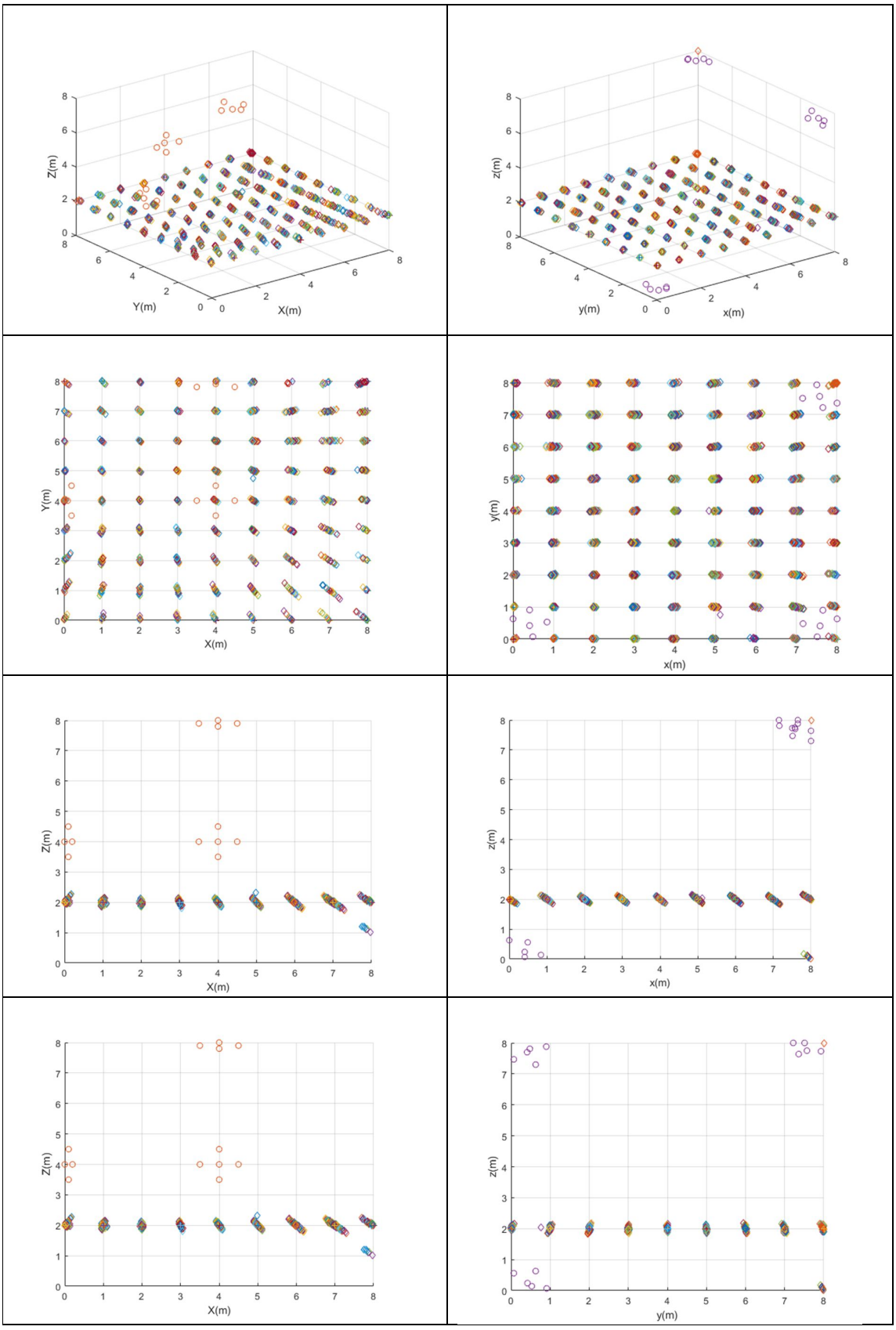
Z(m)
Y(m)
X(m)
z(m)
y(m)
x(m)
Y(m)
X(m)
y(m)
x(m)
Z(m)
X(m)
z(m)
x(m)
Z(m)
X(m)
z(m)
y(m)

Table 4.4. Cloud of position points for three ULPSs placed at (4 m, 4 m, 8 m), (0 m, 4 m, 4 m) and (4 m, 0 m, 4 m) for configuration A; and at (0 m, 0 m, 0 m), (8 m, 0 m, 0 m) and (8 m, 8 m, 8 m) for configuration B, as well as their plane projections (z=2m).

To generalize the conclusion obtained at height z=2 m, other simulations have been done for two other heights, in the middle of the room (z=4 m) and in the upper part of the room (z=6 m). The estimated positions are more accurate when they are in zones covered by a maximum number of ULPSs and close to their locations, as shown in Fig. 4.11.

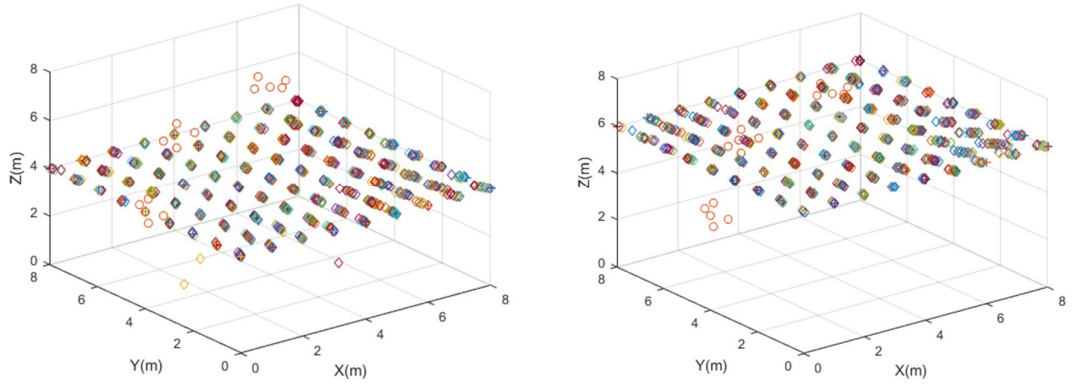

a)

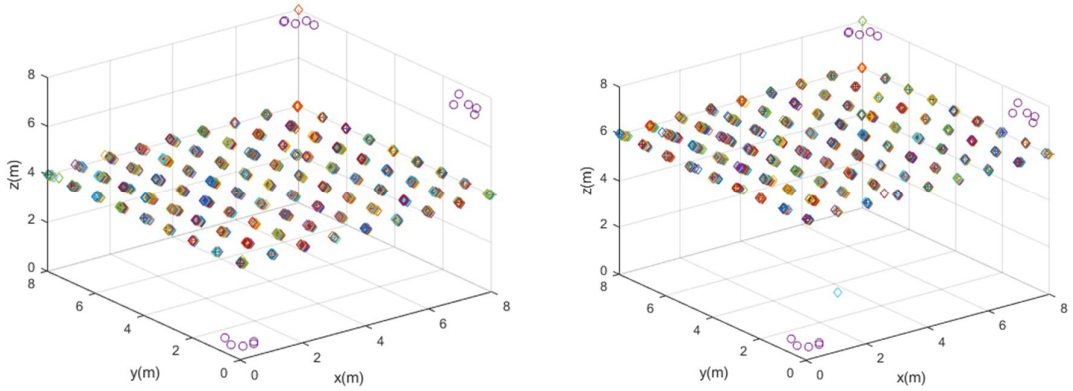

b)

Fig. 4.11. Cloud of position points for three ULPSs placed: a) at (4 m, 4 m, 8 m), (0 m, 4 m, 4 m) and (4 m, 0 m, 4 m) in configuration A; b) at (0 m, 0 m, 0 m), (8 m, 0 m, 8 m) and (8 m, 8 m, 8 m) in configuration B, for different XY-planes (z=4 m and z=6 m).

In this approach, the PDOP distribution values decreases more in both configurations (A and B) after adding a third ULPS, to become lower than 30 in configuration A, or even at the centre below 10 as it presents the intersection of all the ULPSs coverage volumes, as shown in Fig. 4.12.a). Then, in the configuration B, the PDOP values become below 25, where the lowest

PDOP values are in the neighbourhood of the ULPSs locations, as plotted in Fig. 4.12.b); especially in the middle of the room the PDOP is around 10 in both cases.

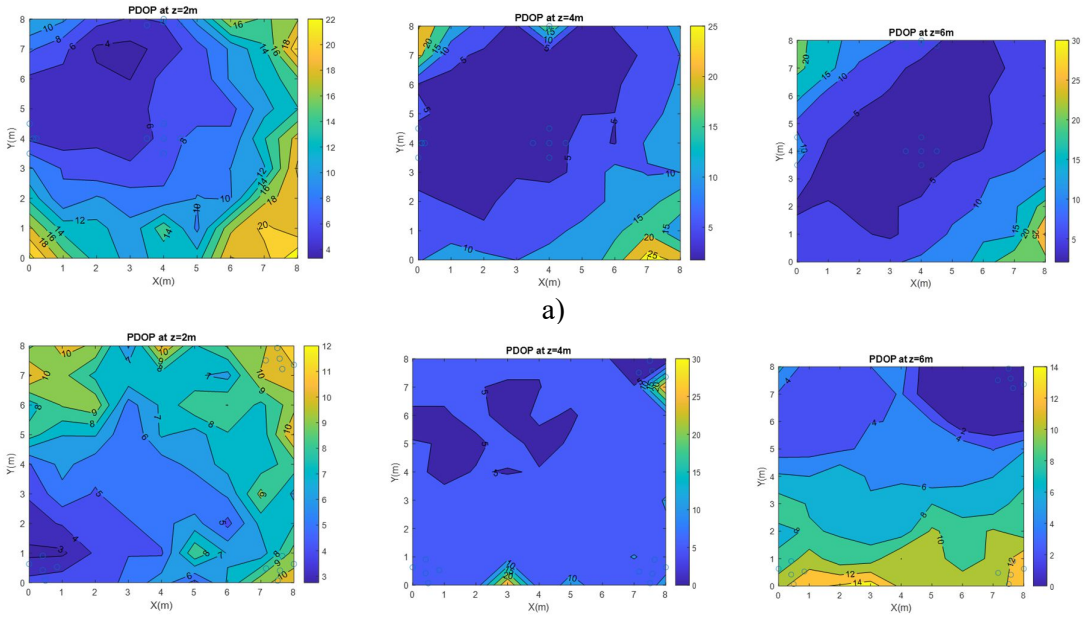

Fig. 4.12. PDOP values for three ULPSs in the XY-plane at z=2 m, z=4 m and z=6 m: a) the ULPSs are at (4 m, 4 m, 8 m), (0 m, 4 m, 4 m) and (4 m, 0 m, 4 m) for configuration A; b) the ULPSs are at (8 m, 8 m, 8 m), (0 m, 0 m, 0 m) and (8 m, 0 m, 8 m) for configuration B.

4.2.3 Four Synchronized ULPSs Configuration

To improve the coverage in large spaces, another 3D configuration formed by four synchronized ULPS units is proposed and simulated, where each two units, ULPS-1 at (8 m, 8 m, 8 m) and ULPS-2 at (0 m, 0 m, 0 m) whereas ULPS-3 at (8 m, 0 m, 8 m) and ULPS-4 at (0 m, 8 m, 0 m), are installed in the two opposite main diagonal corners of the room. In this configuration, the four ULPSs simultaneously cover most of the workspace volume, where the central subspace of the room is covered by the intersection of all the four ULPS units, then presented the best region in terms of accuracy. As for the corners of the room they are covered by one ULPS or sometimes not covered. The mobile receiver estimates its positions synchronously based on the four ULPSs by spherical trilateration using the distances measurements (TOA) between the beacons of every ULPS and the mobile receiver. As mentioned before, since we have a new ULPS unit, the complexity of the system increases. Fig. 4.13 presents the estimated positions when the mobile receiver is located in a grid of ground-truth positions at height z=2 m, as well as different plane projections. As it is concluded, the clouds of estimated positions are smaller and have almost the same size, which explains that

the dispersion of the estimated positions are better with this configuration, especially in the neighbourhoods of ULPS-3 (0 m, 0 m, 0 m) and ULPS-4 (0 m, 8 m, 0 m).

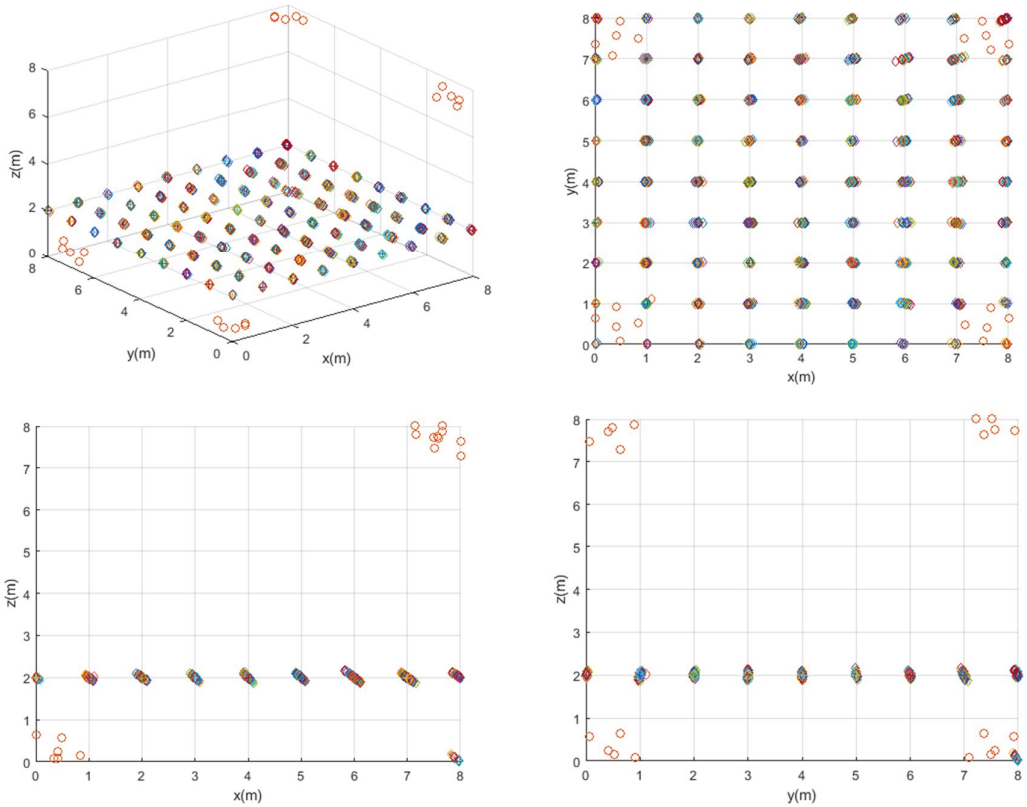

Fig. 4.13. Cloud of estimated positions for four ULPSs placed at the opposite two main diagonals of the room, at z=2 m.

Using this configuration, the cloud of the estimated positions are more or less equivalent in terms of dispersion in all the volume, especially in the middle of the room (z=4 m). Then for the upper half volume of the room, the best estimated positions are in the neighbourhoods of ULPS-1 (8 m, 0 m, 8 m) and ULPS-2 for z=6 m, as shown in Fig. 4.14.

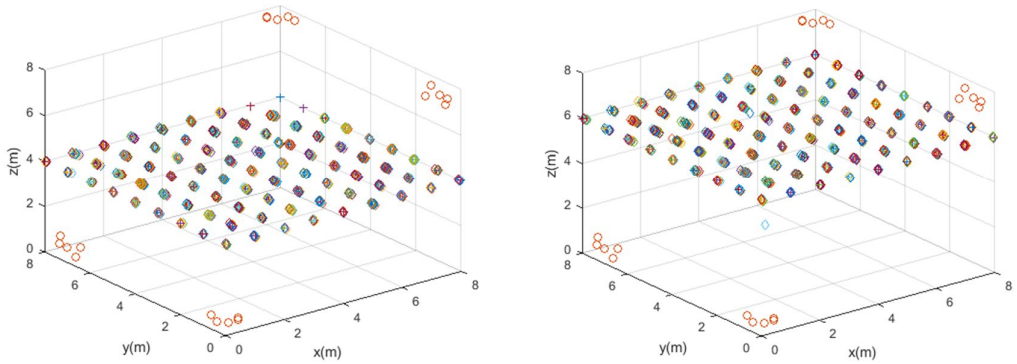

Fig. 4.14. Cloud of position positions for four ULPSs placed at (0 m, 0 m, 0 m), (8 m, 0 m, 8 m), (0 m, 8 m, 0 m) and (8 m, 8 m, 8 m) for heights z=4 m and z=6 m.

The PDOP values distribution decreases more and more after adding the fourth ULPS. They become lower than 30. In the centre the PDOP values are below 10, as here there is the intersection of all the ULPSs coverage volumes, shown in Fig. 4.15. Then, they become below 12 at z=2 m, below 9 when z=4 m and below 10 when z=6 m. The lowest PDOP values are still in the surroundings of the ULPSs locations. Also, the values are close to each other's in the three heights, which means that the distribution of the positioning error is in the same range.

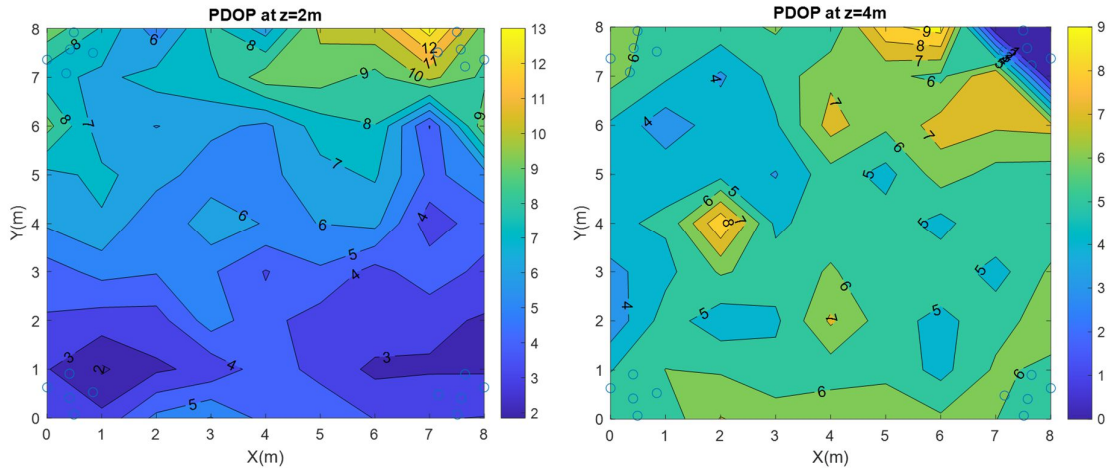

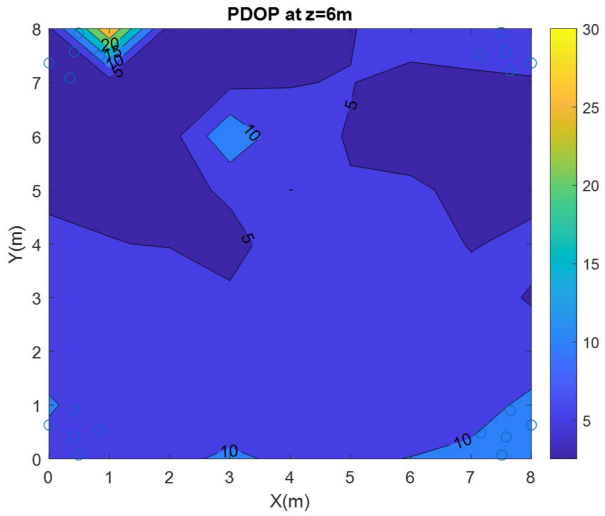

Fig. 4.15. PDOP values for four ULPSs in the XY-plane at z=2 m, z=4 m and z=6 m.

Summing it up, in order to review the results for the configurations analysed before for the whole volume, the Cumulative Distribution Function (CDF) of the estimated position error has been obtained in Fig. 4.17 for synchronized ULPSs, after simulating all the grid of the ground-truth positions for several heights, using 100 simulations per position. According to Fig. 4.16.a), in the 90% of the cases the error is below 0.7 m with only one ULPS, below 0.2 m with two ULPSs, and below 0.1m for three ULPSs at *z*=4 m, in the middle of the workspace. On the other hand, according to Fig 4.16.b), in the 90% of the cases the error is below 0.08 m for the different considered heights when using 4 ULPSs.

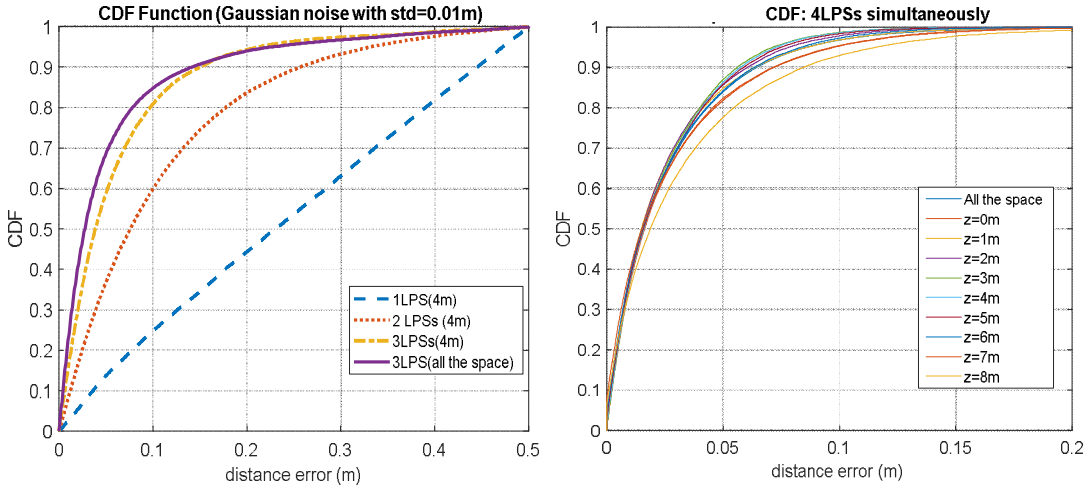

a) b)

Fig. 4.16. CDF for the position error: a) using one ULPS, two ULPSs and three ULPSs for z=4 m in configuration A; and b) using four ULPSs in configuration B.

4.3 Configurations based on Independent No-Synchronized ULPSs

For the unsynchronized ULPSs case, the Time Differences of arrival (TDOA) are determined, and then used to compute the estimated positions. Simultaneous measurements have been used to define all the differences of distances, which are derived from TDOAs. So, the positioning algorithm involves as many equations as measured distances minus one (four for each ULPS configured with five beacons). For the three ULPSs configuration, the positioning algorithm uses twelve equations, whereas, in the four ULPSs configuration, it utilizes sixteen equations. Then, the mobile receiver estimates its position asynchronously by hyperbolic trilateration from these DTOAs using a Gauss-Newton minimization algorithm.

4.3.1 Three No-Synchronized ULPSs Configuration

These three ULPS units (ULPS-1, ULPS-2 and ULPS-3) are placed in the corresponding three perpendicular planes, which define most common indoor rooms, so they cover most of the volume simultaneously, whereas other non-central areas are still scanned by at least one of them. Fig. 4.17 shows a representation about how the three different coverage areas overlap in the environment, according to the proposed distribution, whereas Fig. 4.18 depicts the general aspect of the ULPS units' distribution in the workspace and the dispersion of the estimated positions for the mobile receiver from the three independent ULPSs, called also configuration A.

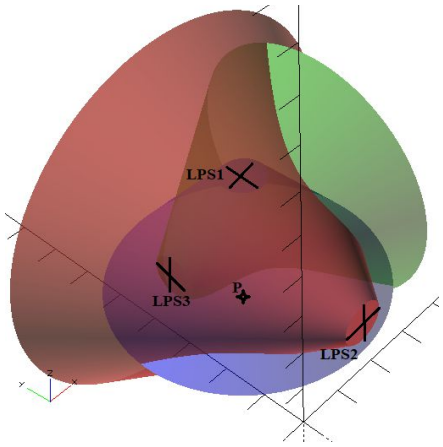

Fig. 4.17. 3D representation of the coverage space from the three ULPSs placed in perpendicular planes for configuration A (three ULPSs).

Several simulations have been done, just one ground-truth position of the mobile receiver is plotted in Fig 4.18. This plot shows the three dispersed sets of the estimated positions got from the three ULPSs, and their projections, at z=2 m. As it is well observed the high dispersion of each estimated position sets causes a high error of those estimated positions in the perpendicular directions of each ULPS.

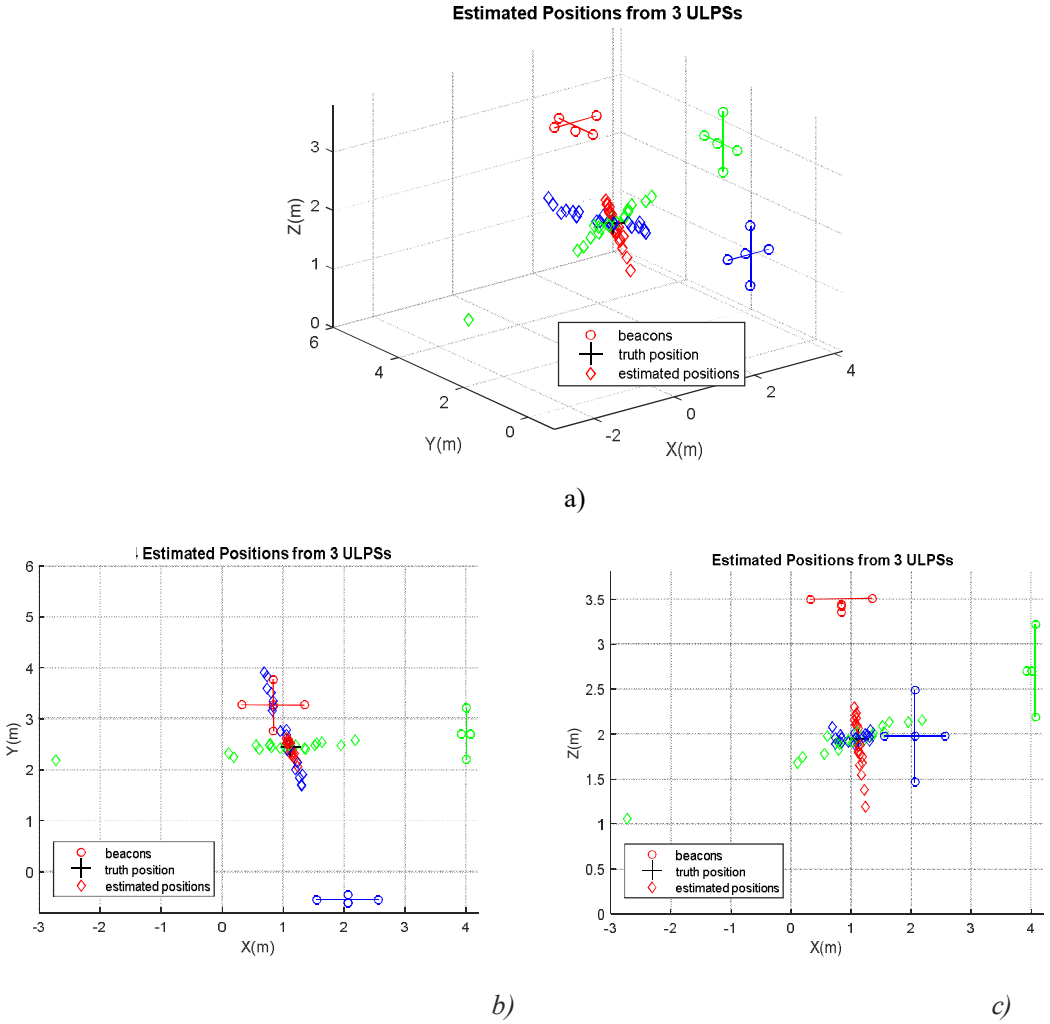

Fig. 4.18. Estimated positions from the three independent ULPSs at z=2 m: a) the 3D estimated positions of the receiver; b) the projection in the XY-plane; and c) in the XZ-plane.

4.3.2 Four No-Synchronized ULPSs configuration

In this configuration four ULPSs have been chosen and placed in the opposite main diagonal corners of the room, as explained before; furthermore, the ULPSs are not synchronised. Several simulations have been done for all the volume, although just one is plotted in Fig. 4.19 to show the four dispersed set of estimated positions got from the four ULPSs, and their projections at z=2 m.

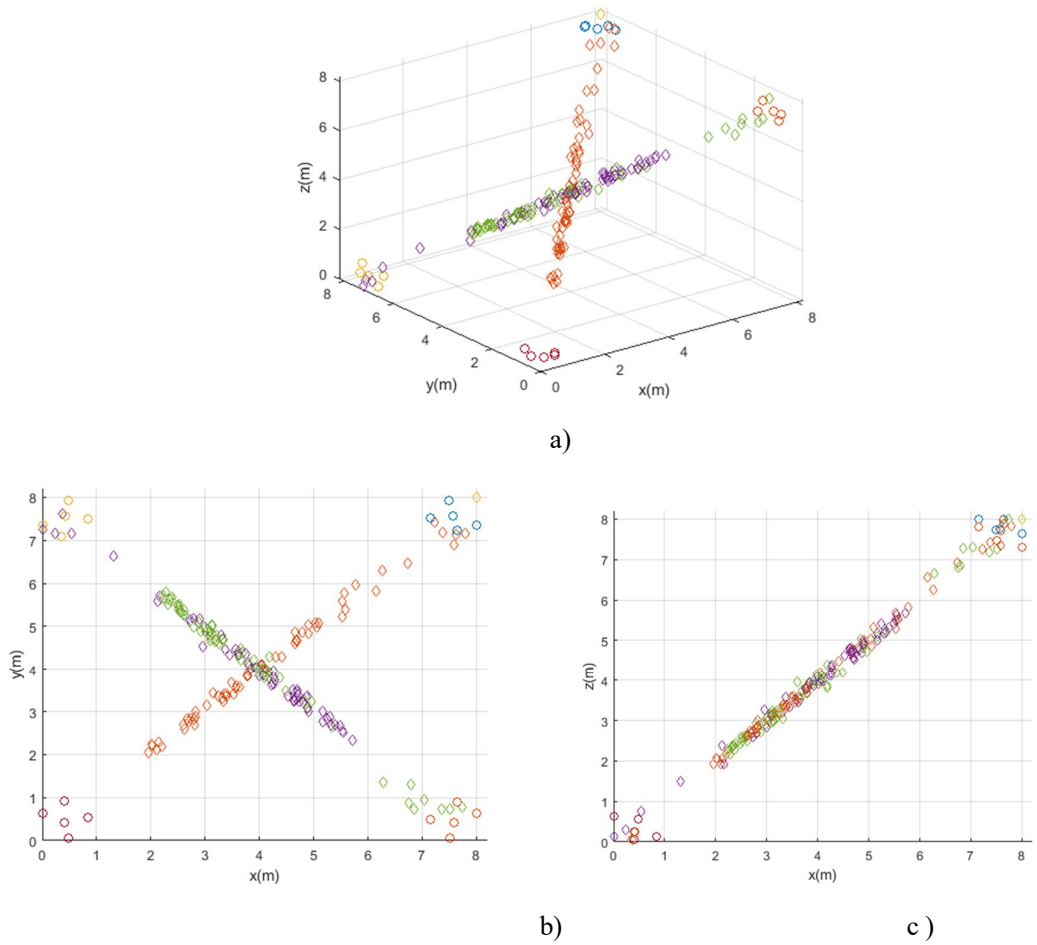

Fig. 4.19. Estimated positions from the four independent ULPSs at z=2 m: a) the 3D estimated positions of the receiver; b) the projection in the XY-plane; and c) in the XZ-plane.

The dispersion of the estimated positions coming from several ULPS in the asynchronous case presents a set of estimated positions obtained from the number of used ULPS, where it is not easy to compute the final estimated position of the mobile receiver. To resolve this problem some fusion methods have been defined and used in coming sections to merge and improve the final estimated positions.

4.3 Loosely-Coupled Fusion for Positioning Systems based on Multiple ULPS

After studying the proposed indoor positioning systems and distribution in a large space, hereinafter we will focus on the asynchronous combination of ULPSs, because it is easier to be

applied in terms of installation and deployment. This section is actually dedicated to improve the final estimated positions by applying different fusion algorithms, starting with those based on a loosely coupling.

4.3.1 Maximum Likelihood Estimation (MLE) Approach

As has been explained previously, estimating the mobile receiver positions with a single and independent ULPS is not a perfect solution, due to the high dispersion of the estimated positions in the space, especially in the perpendicular direction of the ULPS installation. To decrease this dispersion, the MLE fusion followed by an average of the estimated positions is applied here to the positions resulting from several ULPS deployed in the same environment. The hybrid MLE/mean fusion requires the use of the variances of each ground-truth position obtained from each ULPS. The first method is based on the determination of the variance after getting all the measurements. It is called an offline MLE/ mean fusion method; where the fusion process is done in only one step after getting all the measurements. The second method is composed of two steps, the study of the variances of all the ground-truth positions (using the offline method), storing them and, finally, using them in the online fusion.

The impact of the MLE approach in the positioning performance will be analysed by means of the PDOP, still considering the two scenarios or configurations described before, A and B. On the first offline stage, all the estimated positions from the independent ULPSs (three and four ULPSs) are obtained separately. This process has been repeated one hundred times at each position in the mentioned grids of the space. Then, these estimated positions are combined by the MLE fusion to get the final estimated positions, after getting all the set of measurements. However, in this case, this method has been used just to define the variance values of all the ground-truth positions that will be used in the online MLE stage, as a variance study of the workspace.

With those variance values, we can proceed with the online stage of the MLE approach, where both configurations A and B will be studied independently.

a. Configuration A: Three ULPSs

After computing the variances of all the receiver positions in the space, the PDOP study has been done to compare the various ULPS combination fusion: firstly, a combination of two ULPSs; secondly for the three ULPSs, as shown in Table 4.5, at various heights (z=2 m, z=4 m and z=6 m). In this configuration, ULPS-1 is placed at (4 m, 0 m, 4 m) in the floor, which is the same

case as the ULPS in the ceiling, just with an opposite PDOP distribution in the Z-axis. The PDOP values have been calculated for a hundred simulations at each point in the grid.

For the MLE fusion of two ULPSs, the PDOP values decrease compared to only one independent ULPS, to be lower than 100 in all the space and lower than 40 at the centre of the workplace. PDOP values keep decreasing after fusing the third ULPS, to be lower than 30 in all the space, especially to be lower than 15 at the centre of the workspace for all the heights, as plotted in Table 4.5. Also, the lowest PDOP values are always in the neighbourhood of the ULPSs installation areas.

z (m)	*Fusion of two ULPSs*	*Fusion of three ULPSs*
2	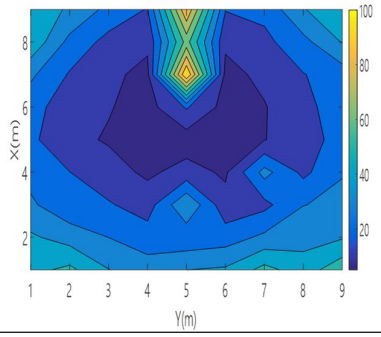	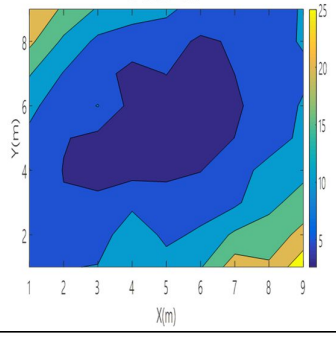
4	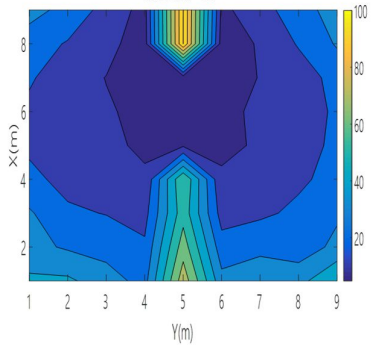	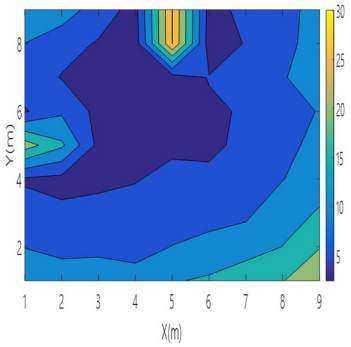
6	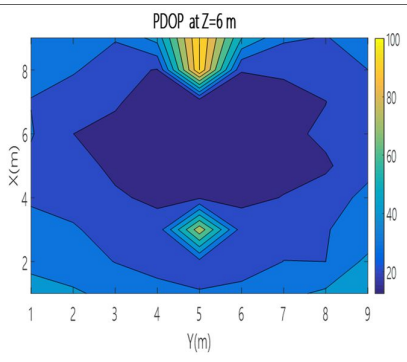	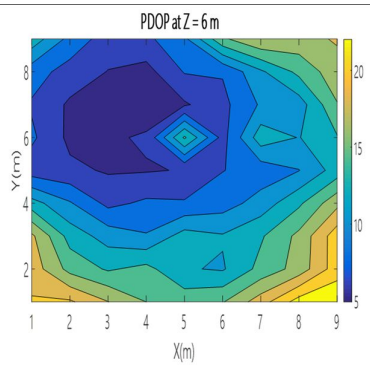

Table 4.5. PDOP values obtained by the MLE fusion using two ULPSs at (4 m, 4 m, 0 m) and at (4 m, 8 m, 4 m), and three ULPSs at (4 m, 4 m, 8 m), (4 m, 8 m, 4 m) and (0 m, 4 m, 4 m) for different XY planes (z=2 m, z=4 m, z=6 m) in configuration A.

Again, the distribution of the PDOP values in the unsynchronized ULPSs mode, employing the MLE/mean merging method is very close to the values of the synchronized ULPSs mode. Then, the 3D positions become more accurate than the single ULPS's positioning, in the analysed planes.

In order to summarize the obtained results for the case of three no-synchronized ULPSs, for the whole analysed volume, the Cumulative Distribution Function (CDF) of the position errors has been obtained, for all the points in the grid (100 simulations per each position). Fig. 4.20 shows the CDF of the fused positions errors for the unsynchronized ULPSs. For simultaneous measurements, in the 90% of the cases the error is below 0.8 m when using only one ULPS, below 0.7 m with two ULPSs, and below 0.5m for three fused ULPSs.

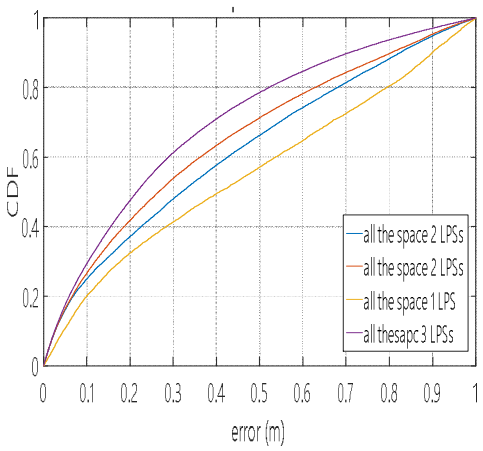

Fig. 4.20 CDF for the positioning errors in the whole volume using independent measurements (unsynchronized ULPSs) after the MLE fusion.

b. Configuration B: Four ULPSs

After computing the variance of all the receiver positions in the space for configuration B, the PDOP study has been analysed to compare the different ULPS combination: as before, firstly, a combination of two ULPSs, secondly for the three ULPSs, and finally for four ULPSs, as shown in Table 4.6, at various heights (z=2 m, z=4 m and z=6 m). In this configuration, the ULPSs are installed in the four corners of the principal diagonals of the workspace. The PDOP values have been calculated for a hundred simulations at each point in the grid.

For the MLE/Mean fusion of two ULPSs, the PDOP values are lower than 350 in all the space and lower than 200 in the corners where the ULPSs are installed. PDOP values keep decreasing after fusing the third ULPS, to be lower than 300 in all the space, and then 150 in the corners. Finally, the PDOPs values have a slight decrease after merging the fourth ULPS, as summarized in Table 4.6. Note that for two ULPSs the PDOP values are still as high as 300 in relatively large areas around the centre of the space.

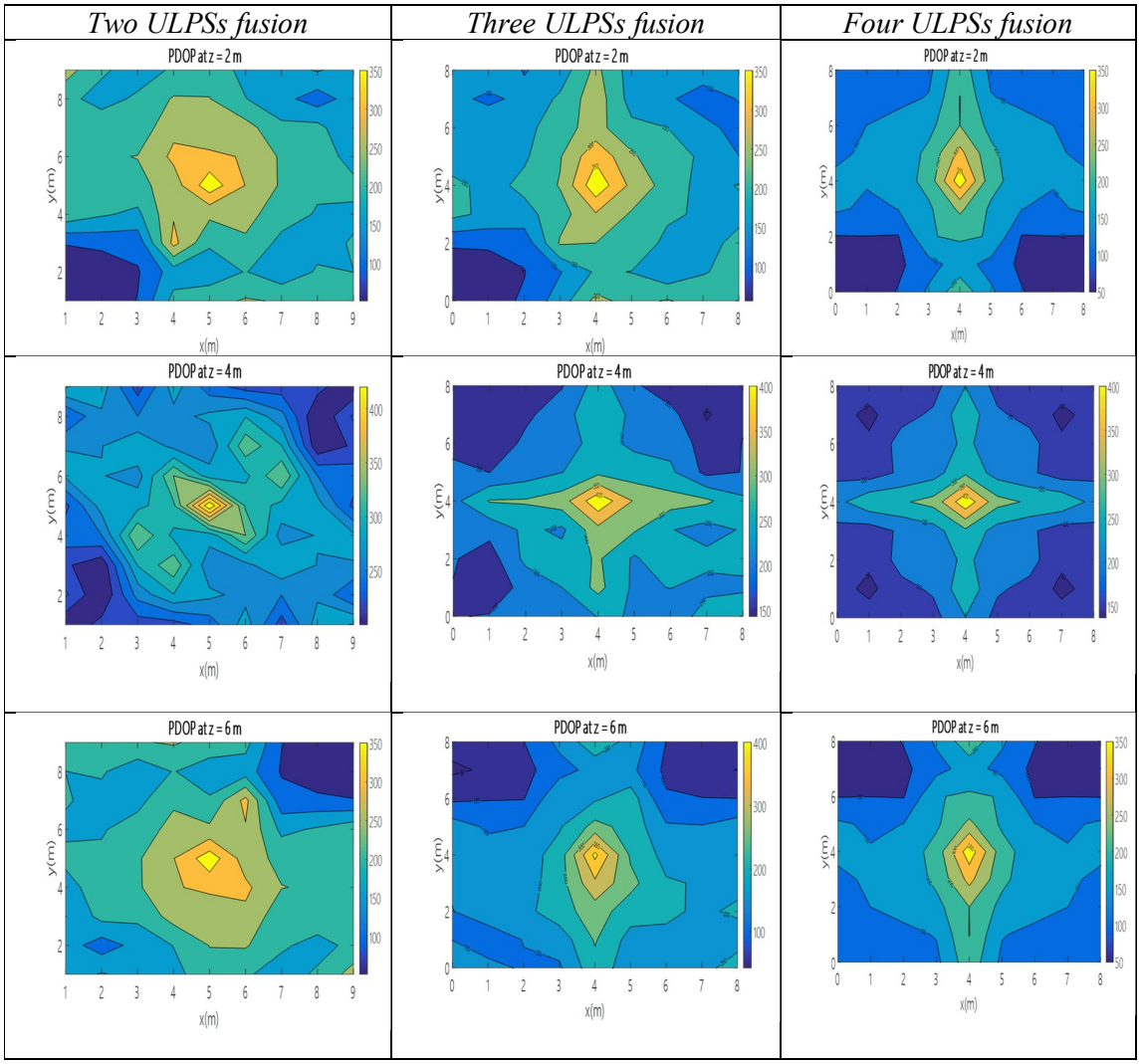

Table 4.6. PDOP values obtained by the MLE when using two ULPSs placed at (0m,0m,0m) and (8m,8m,8m), three ULPSs placed at (0m,0m,0m), (8m,8m,8m) and (0m,8m,0m), and finally four ULPSs placed at (0m,0m,0m), (8m,8m,8m), (8m,0m,8m) and (0m,8m,0m) for different XY-planes (z=2 m, z=4 m, z=6 m).

The error CDF, again obtained in all the points, for one hundred simulations at each position, for the distribution of four ULPSs previously described, can be observed in Fig. 4.21; the CDF error for one ULPS, as well as the CDF error after the fusion of two, three, and four ULPSs.

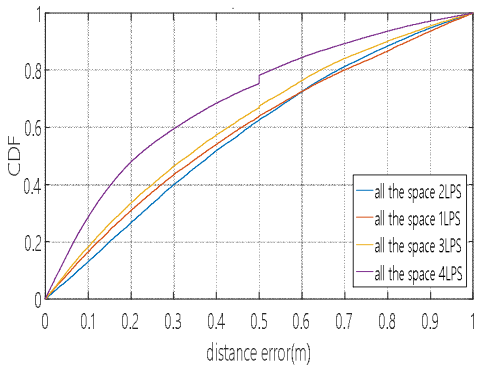

Fig. 4.21. CDF Error after MLE fusion in the whole space for 1, 2, 3 and 4 merged ULPSs.

In case of MLE fusion data from independent ULPSs, the CDF errors are below 0.85 m for one ULPS and below 0.7 m (for 90% of the cases) merging four ULPSs, as can be observed in Fig. 4.21. For all the positions in the analysed planes z=0 m, 1 m, 2 m …8 m, the error is quite similar for the 90% of the cases, below 0.7 m. That is, the performance of the system is similar in the whole volume.

c. Final ULPS Distribution Proposal

After the previous study, finally, the configuration A is the chosen configuration for a further analysis, where the system is composed by three ULPSs placed in perpendicular walls, following the real deployment that will be carried out in the later experimental tests. This choice is due to the better PDOP values provided.

Several simulation tests have been carried out for independent single ULPS (ULPS-1: the red one in the ceiling in Fig. 4.22). After that, other simulations have been done for three independent ULPSs (ULPS-1, the red one, ULPS-2, the blue one, and ULPS-3, the green one, in Fig. 4.22), where the receiver has been placed at positions P1-P7 for two different heights (z_1=1.35 m and z_2=1.93 m) in Fig. 4.22.a). This grid of positions has been chosen to cover a large area in the workspace, where each position represents a particular situation regarding the global coverage of the workspace. A second grid of positions P'1-P'7 in a small workspace has been also defined, where simulations and real tests have been carried out (see Fig. 4.22.b).

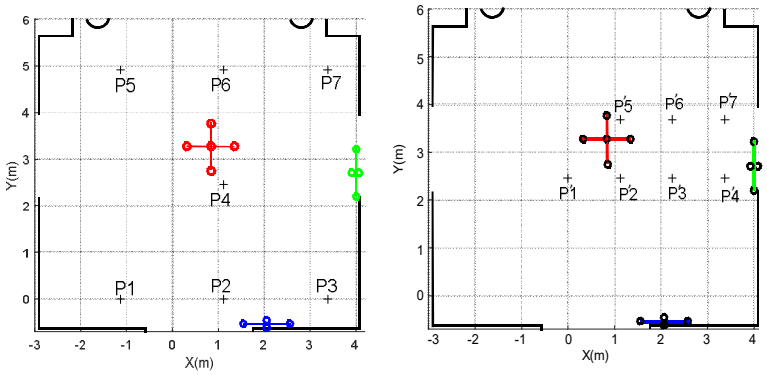

a) b)

Fig. 4.22. Workspace configuration and two grids of positions to be considered to evaluate the positioning performances: a) dispersed positions in a large area; and b) positions in a small area.

In the single ULPS case, five distances are obtained at the receiver, to estimate the 3D mobile receiver positions. Several estimated positions can be computed from the three ULPSs. To get the final estimated position, a combination of all these positions can be done applying the Maximum Likelihood Estimation (MLE) followed by the mean of the estimated positions (MLE/Mean), where the three independent measurements p_1, p_2 and p_3 are merged to get the measurement p of the receiver's estimated position.

At each ground-truth position P1-P7, thirty simulations have been carried out, using hyperbolic trilateration method with the Gauss-Newton positioning algorithm described before. The simulated results for a single ULPS-1 at both heights z_1 and z_2 are presented in Fig. 4.23, where the different positions P1-P7 have been plotted using different colors. As an example, the black diamonds correspond to the estimated positions for P1, which spread around the ground-truth position, with a significant dispersion along the ultrasonic emission direction.

This uncertainty in the resolution of coordinate z, which is the perpendicular axis to the plane where ULPS-1 is installed, rises as the distance between the ULPS and the mobile receiver positions increases. This is why those results for z_2 in Fig. 4.23.a) present more concentrated clouds of points than z_1 in Fig. 4.23.b), remarkably for the coordinate z. For the same reason, ULPS-1 is suitable for the estimation of coordinates x and y, with better performance for the positions in the centre of the coverage volume, as point P4 plotted with pink diamonds in Fig. 4.23. The same performances can be obtained for ULPS-2 and ULPS-3 that are installed on two perpendicular planes, so their most important dispersions are for the Y-axis and the X-axis, respectively [Man2020].

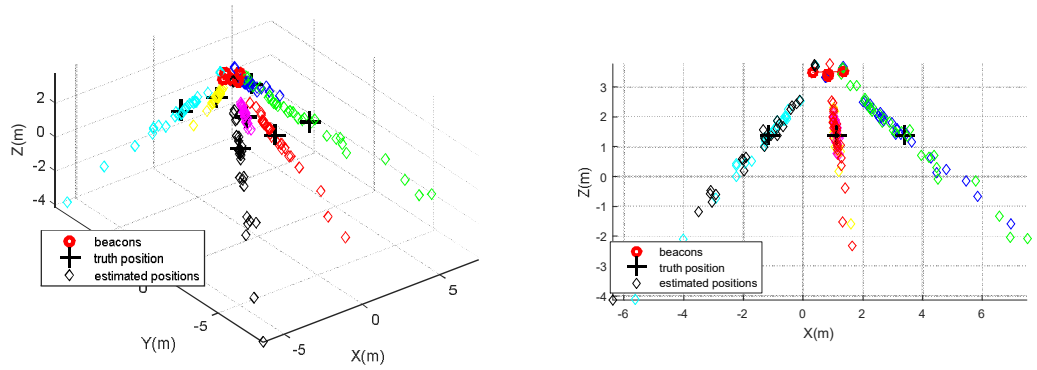

a)

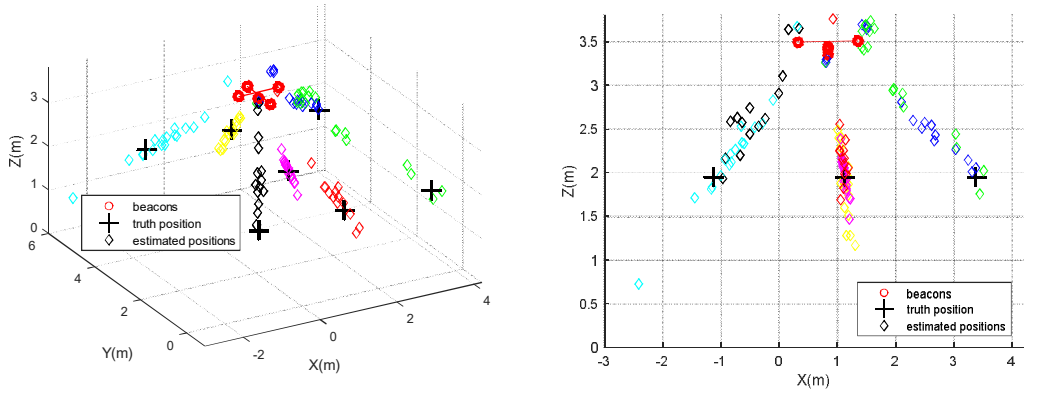

b)

Fig. 4.23. Positions estimated by simulation for ULPS-1 using a different colour for each simulated position (P1-P7): a) 3D representation for z_1=1.35 m and XZ-plane projection for z_1=1.35 m; b) 3D representation for z_2=1.93 m and XZ-plane projection for z_2=1.93 m.

Another study has been developed considering the PDOP for the ULPS-1 at z_1 and z_2 in Fig. 4.24. Both heights show a similar range of values, where the lowest PDOP values are below the ULPS-1 and the highest PDOP values are in the closeness of the transducers, as supposed in previous simulations. Moreover, the height z_2 provides lower PDOP values than z_1, as expected, since the PDOP raises as the distance between the ULPSs and the receiver positions does. Some results from the independent ULPS, in the ceiling, are presented in the Table 4.7 below, where the cloud of estimated positions and the PDOP values are given for z_1 and z_2.

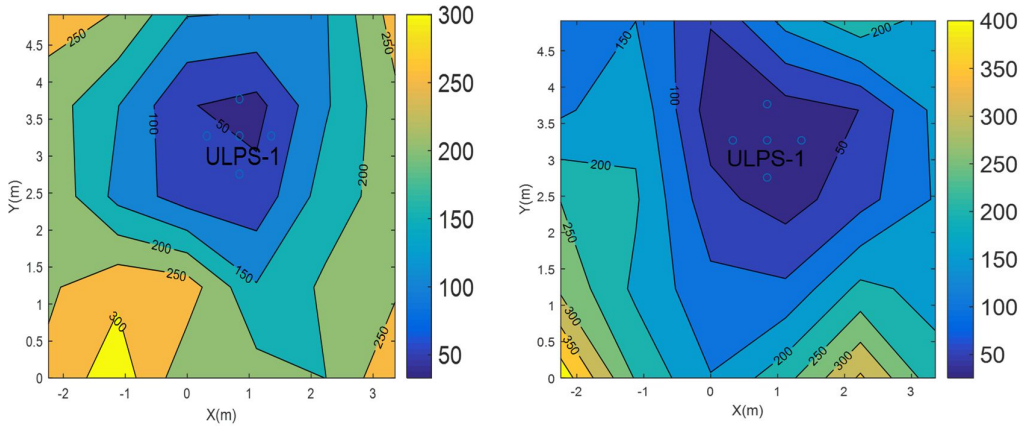

a) b)

Fig. 4.24. PDOP color map for ULPS-1: a) at z1=1.35 m; b) at z2=1.93 m.

For the three ULPSs in an independent way, the estimated positions after 20 iterations present a high dispersion in the emitted direction of each ULPS, as presented in Fig. 4.19 and in past results. The estimated positions are three sets of points with a high variation in the Z-axis for positions got from ULPS-1, in the Y-axis for ULPS-2, and, finally, in the X-axis for ULPS-3. So, the dispersion in all the three axes for the seven ground-truth positions is illustrated in Table 4.7. The most accurate position is for P1, in terms of the mean error, the standard deviation, and the CDF error for 90% of estimated positions, which is equal to 0.7 m. The poorest results are for P5 in the same terms as before, with a CDF error for 90% of estimated positions about 3.5 m. Generally speaking, the CDF error for 90% of estimated positions of all the grid of seven positions is about 1.9m.

Points	z_1						z_2					
	Mean error (m)			*Standard deviation (m)*			*Mean error (m)*			*Standard deviation (m)*		
	x	*y*	*z*	*x*	*y*	*z*	*x*	*y*	*z*	*x*	*y*	*z*
P1	1.091	1.819	1.187	0.908	1.553	0.970	0.713	1.207	0.753	0.611	1.004	0.607
P2	0.083	0.787	0.533	0.066	0.964	0.596	0.118	1.170	0.575	0.119	1.166	0.562
P3	1.416	1.798	1.242	1.484	1.949	1.314	1.219	1.579	0.996	0.690	0.877	0.589
P4	0.053	0.158	0.380	0.056	0.190	0.487	0.040	0.132	0.259	0.033	0.121	0.231
P5	0.745	0.628	0.891	0.532	0.451	0.667	0.648	0.544	0.563	0.796	0.645	0.670
P6	0.086	0.450	0.599	0.088	0.458	0.560	0.061	0.410	0.412	0.054	0.454	0.436
P7	4.539	4.946	1.287	2.040	1.308	1.132	4.607	4.988	0.535	1.264	0.840	0.563

Table 4.7. Mean positioning errors and standard deviations for the set of positions P1-P7 at z1=1.35 m and z2=1.93 m before the MLE/Mean fusion.

The variation of the position accuracy is due to various factors, such as the number of covering ULPS, the strength of the emitted signal, the distance from each ULPS, as well as its central axis. After analysing the behaviour of the ULPS-1 operating in an independent way, all the three ULPSs have been simulated together to analyse the behaviour in the same points P1-P7, considered again at z_1 =1.35 m and z_2 =1.93 m. The MLE/mean fusion approach has been performed to merge the estimated positions from the three ULPS. The estimated positions after fusion present variable accuracies, which depends on the region and the coverage zone. The estimated positions obtained in the crossing of three independent coverage areas of the three ULPSs are better in terms of accuracy, whereas those regions where only one ULPS is available are the most limited one regarding the accuracy. Table 4.8 describes the estimated positions after the whole fusion process for z_1=1.35 m and z_2=1.93 m. Also, it is possible to check how only points P1 and P5 (red and black diamonds, respectively) present higher dispersions than the others, mainly due to a longer distance to the ULPSs and/or to a coverage-limited zone, as presented in Table 4.8.

z (m)	*Estimated positions with MLE/Mean fusion*	*PDOP values*
z_1	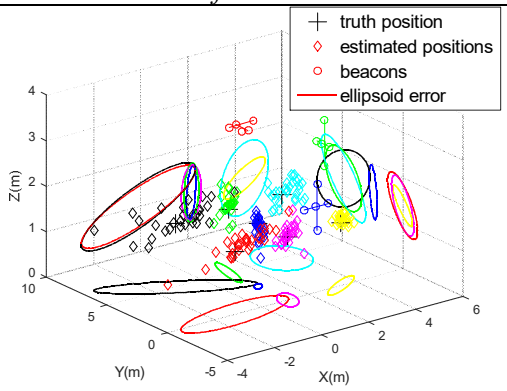	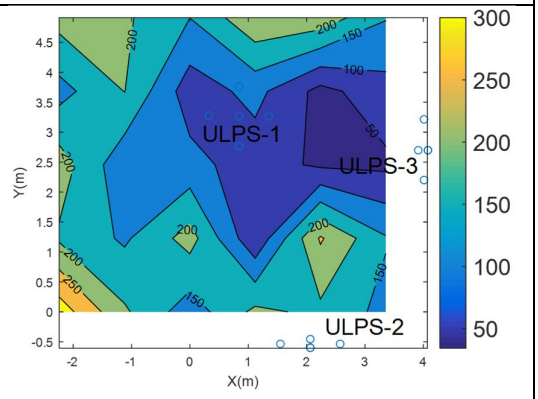
z_2	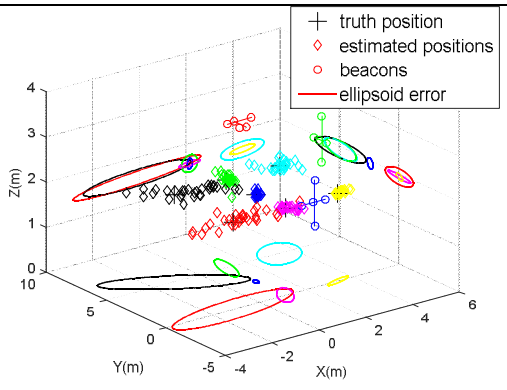	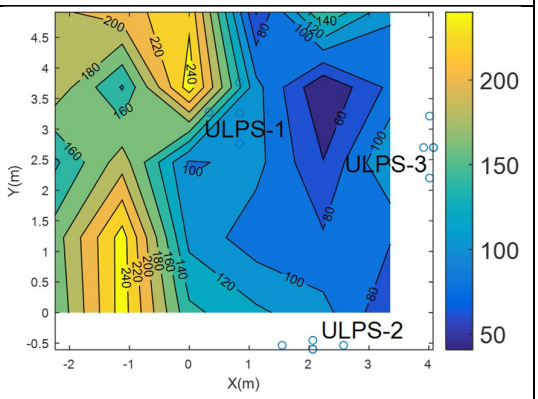

Table 4.8. Estimated positions for the considered positions (P1-P7) after fusion, including the projections of their corresponding error ellipsoids with a certainty of 95%, as well as PDOP values, at: z_1=1.35 m and z_2=1.93 m.

Similarly, the point P4 (blue diamonds) is still the most suitable one, with the smallest error ellipsoid for 95% of the estimated positions. Also, it is important to remark that the height z_2 is very close to the one at which the ULPS-2 is installed, thus providing a notable accuracy in the estimation of the coordinate *z*, with low dispersion. The PDOP estimation has been obtained by simulation for both heights, after fusion, and it is depicted in the same Table 4.8. The PDOP values vary from 50 to 250 for both heights, where the regions with high values are determined by the lack of one or two ULPSs' coverage.

In both cases, the zones with lower PDOP values match to the right areas, where the coverages from the three ULPSs are easily overlapped. Furthermore, the PDOP value is higher for z_2 at the left corners of the environment, where the coverage from the three ULPSs is more unlikely to be available simultaneously. Note that these areas with limited coverage are larger as the height increases. Nevertheless, in the central region where all the ULPS are available, the PDOP values at z_2 are still slightly better than at z_1 Furthermore, Table 4.9 presents those results by providing the mean error and the standard deviation per axis for the seven points considered (P1-P7). The smallest standard deviation and mean error, as well as the lowest error ellipsoid, is for P4, the most centred point in the covered volume (blue diamonds). On the other hand, the most critical results are obtained for P1 and P5 (red and black diamonds, respectively), distant away from the central axis of the three ULPSs.

Points	z_1						z_2					
	Mean error (m)			*Standard deviation (m)*			*Mean error (m)*			*Standard deviation (m)*		
	x	*y*	*z*	*x*	*y*	*z*	*x*	*y*	*z*	*x*	*y*	*z*
P1	0.503	0.046	0.220	0.780	0.520	0.281	0.056	0.031	0.008	0.121	0.159	0.017
P2	0.035	0.140	0.107	0.152	0.419	0.331	0.013	0.024	0.001	0.158	0.058	0.021
P3	0.025	0.023	0.022	0.227	0.166	0.100	0.001	0.034	0.010	0.034	0.105	0.041
P4	0.005	0.006	0.051	0.093	0.107	0.105	0.423	0.204	0.002	1.324	1.047	0.077
P5	0.066	0.002	0.080	0.761	0.664	0.246	0.012	0.029	0.017	0.082	0.288	0.049
P6	0.014	0.012	0.035	0.086	0.460	0.183	0.082	0.288	0.049	0.398	0.583	0.093
P7	0.031	0.282	0.088	0.400	0.94	0.260	0.482	0.001	0.016	0.716	0.432	0.050

Table 4.9. Mean positioning errors and standard deviations for points P1-P7 at z1=1.35 m and z2=1.93 m, after the MLE/Mean fusion.

In order to compare the accuracy of simulated results before and after MLE/mean fusion, the

Cumulative Distribution Function (CDF) has been calculated for the grid of positions. Table 4.10 provides the errors for 90% of the cases for the seven considered points (P1-P7) for z_1 and z_2, respectively. It is worth noting that the positioning error of the estimated positions obtained by simulation, before fusion, is in the range of decimetres or even metres, whereas the errors after fusion are in the range of centimetres or decimetres. Apart from the expected differences among the points and the heights, generally speaking, errors improve in all cases whether the three ULPSs are merged.

Positions	z_1				z_2			
	Before fusion (m)			*After fusion(m)*	*Before fusion (m)*			*After fusion(m)*
	ULPS-1	*ULPS-2*	*ULPS-3*	*3- ULPSs*	*ULPS-1*	*ULPS-2*	*ULPS-3*	*3-ULPSs*
P1	2.499	1.875	3.288	1.071	2.314	1.089	4.547	0.99
P2	2.357	0.941	2.338	0.540	1.828	0.501	2.448	0.235
P3	3.497	0.71	1.191	0.504	2.531	0.216	1.4	0.205
P4	0.438	0.75	1.639	0.174	0.455	1.123	0.967	0.119
P5	1.543	4.43	2.035	1.256	1.688	3.189	2.96	1.395
P6	0.716	1.431	1.639	0.432	0.465	1.693	2.769	0.455
P7	7.047	4.684	5.26	1.163	5.134	5.286	5.181	0.804

Table 4.10. CDF positioning error for 90% of estimated positions P1-P7 before and after MLE/Mean fusion at z1=1.35 m and at z2=1.93 m.

After studying the set of points (P1-P7) in Fig. 4.22.a), a specific small area is used hereinafter to apply all the fusion methods, loosely and tightly coupled methods, and then compare them. Fig. 4.22.b) presents the second set of points (P'1-P'7), where the X-axis step is 1.12 m and the Y-axis step is 1.28 m.

Positions	z_1				z_2			
	Before fusion (m)			*After fusion (m)*	*Before fusion (m)*			*After fusion (m)*
	ULPS-1	*ULPS-2*	*ULPS-3*	*3-ULPSs*	*ULPS-1*	*ULPS-2*	*ULPS-3*	*3-ULPSs*
P'1	0.543	1.757	2.084	0.27	0.783	1.098	3.57	0.236
P'2	0.476	0.97	2.57	0.225	0.771	0.844	1.192	0.108
P'3	0.90	1.041	1.95	0.273	0.919	1.173	1.128	0.102
P'4	1.098	1.008	0.215	0.265	1.37	1.326	0.682	0.22
P'5	2.282	2.203	3.096	0.385	2.27	2.591	2.249	0.112
P'6	0.546	1.817	1.109	0.324	0.807	1.855	0.68	0.153
P'7	2.879	2.557	2.457	0.529	3.086	2.68	2.484	0.646

Table 4.11. CDF positioning error for 90% of estimated positions P'1-P'7 before and after MLE/Mean fusion at z1=1.35 m and at z2=1.93 m.

For this second simulated set of positions (P'1-P'7), simulations before fusion for independent ULPSs and after MLE/mean fusion have been done. The Cumulative Distribution Function (CDF) has been calculated to define the error for 90% of the cases for the seven points (P'1-P'7) at z_1 and z_2. Table 4.11 presents those results. It is clear to see that the positioning error of the estimated positions obtained by simulations for independent ULPSs before MLE/mean fusion is always in the decimetres and sometimes metres range, while the errors after the MLE/mean fusion are in the range of centimetres or decimetres, as it was explained for the first set of positions (P1-P7). Also, the error results in lower values at z_2 than at z_1, as expected. After fusion, for z_1, the most accurate positions are P'1, P'2, P'3, and P'4, where the CDF errors for 90% of estimated position are below 0.27 m, whereas, for the rest of positions, the CDF errors for 90% of estimated position are below 0.52 m. So, the first row of positions are more accurate than the second row; this result is due to the farther distance from this row to ULPS-2. At z_2, this error decreases below 0.23 m, except for the point P'7 whose CDF error for 90% of estimated position is 0.64 m. The highest errors here are for P'7 (0.64 m), P'1 (0.23 m) and P'4 (0.22 m) due to their limited coverage by the three ULPSs, as they are located high and, in the corners, farther way from the ULPS-1 and ULPS-2. The mean CDF error for 90% of estimated position at z_1 is 0.344 m, and 0.201 m at z_2, which summarize the accuracy of the positioning system in those studied areas.

4.3.2 Linear Kalman Filter Approach

In this Section, a Linear Kalman Filter (KF) is used to merge the estimated positions obtained from the three ULPSs, after applying the GN algorithm. This filter is based on a loop of two steps: prediction and updating. This algorithm tries to converge into the correct estimated position after a number of iterations.

The state model of the filter is (4.1):

$$\boldsymbol{X_k} = \boldsymbol{A} \,.\, \boldsymbol{X_{k-1}} + w_{k-1} \qquad (4.1)$$
$$\boldsymbol{Z_k} = \boldsymbol{H} \,.\, \boldsymbol{X_k} + v_k$$

Where $X_k = (x_k, y_k, z_k)$ is the estimated position at the current state k; $X_{k-1} = (x_{k-1}, y_{k-1}, z_{k-1})$ is the estimated position at the previous state k-1; $\mathbf{Z_k}$ is the estimated positions obtained from the GN algorithm; w_{k-1} is the process noise; and v_k is the measurement noise. After initializing the

initial position vector $\mathbf{X_0}$ and the transition matrix $\mathbf{P_0}$ a recursive loop between predictions and updates allows to converge to the final estimated position. Equation (4.2) presents the prediction step and Equation (4.3) the correction steps.

$$\boldsymbol{X_k = A \,.\, X_{k-1}} \tag{4.2}$$

$$\boldsymbol{K_k = P_k \,.\, H^T (H.P_k \,.\, H^T + R)^{-1}}$$

$$\boldsymbol{X_k = X_{k-1} + K_k \,.\, (Z_k - H \,.\, X_k)}$$

$$\boldsymbol{P_k = A \,.\, P_{k-1} \,.\, A^T + Q} \tag{4.3}$$

$$\boldsymbol{P_k = (I - K_k \,.\, H).\, P_k}$$

Where $\mathbf{K_k}$ is the Kalman Filter gain; **Q** and **R** the process noise matrix and the measurement noise matrix, respectively; **A** and **H** are constant transition matrices; and **P** is a dynamic matrix. Those matrices and their sizes are specific with the desired system. To apply the Kalman Filter to fuse the independent estimated positions and get the final position, the covariance matrices of the process and measurement must be fixed experimentally. In our case, the measurement matrix is the covariance of the estimated position related to the specific ULPS. So, the measurement matrix is specific for each position. The process noise **Q** is fixed experimentally as $\frac{R}{10}$ and computed using (4.5), so it is also specific for each position. For the hyperbolic case, it is assumed that the noise is Gaussian, as it is applied for the differences of distances, the noise is correlated and Ri is defined as (4.4) :

$$R_i = \begin{pmatrix} \sigma_{x,i}^2 & 0.5\,\sigma_{y,i}^2 & 0.5\,\sigma_{z,i}^2 \\ 0.5\,\sigma_{x,i}^2 & \sigma_{y,i}^2 & 0.5\,\sigma_{z,i}^2 \\ 0.5\,\sigma_{x,i}^2 & 0.5\,\sigma_{y,i}^2 & \sigma_{z,i}^2 \end{pmatrix} \tag{4.4}$$

and $$Q = \begin{pmatrix} \frac{\sigma_{x,i}^2}{10} & 0.05\,\sigma_{y,i}^2 & 0.05\,\sigma_{z,i}^2 \\ 0.05\,\sigma_{x,i}^2 & \frac{\sigma_{y,i}^2}{10} & 0.05\,\sigma_{z,i}^2 \\ 0.05\,\sigma_{x,i}^2 & 0.05\,\sigma_{y,i}^2 & \frac{\sigma_{z,i}^2}{10} \end{pmatrix} \quad (4.5)$$

Where *i=(1-3)* is the index of the ULPS (ULPS-1, ULPS-2 and ULPS-3), and $(\sigma_{x,i}^2, \sigma_{y,i}^2, \sigma_{z,i}^2)$ are the variances of each position for the three-axis *x*, *y* and *z* related to the various ULPSs.

After applying the Linear KF to fuse the estimated positions obtained from the three ULPSs on the set of seven positions (P'1-P'7), the results have been plotted in Table 4.12 below at both heights z_1=1.35 m and z_2=1.93 m. Results after fusion are always better, especially for z_2, where the estimated positions present variable accuracies. At z_1, the most accurate estimated positions are for P'1, P'2, P'3, P'5 and P'6 (cyan, black, green, red and yellow circles, respectively); also, they present the smallest error ellipsoid for 95% of the estimated positions. On the other hand, the least accurate estimated positions are for P'4 (pink circles) and P'7 (blue circles), as they present the highest error ellipsoid for 95% of the estimated positions. Similar conclusions can be derived for z_2, with errors even lower. This effect is related to the distance between those positions and ULPS-2.

z_1	z_2
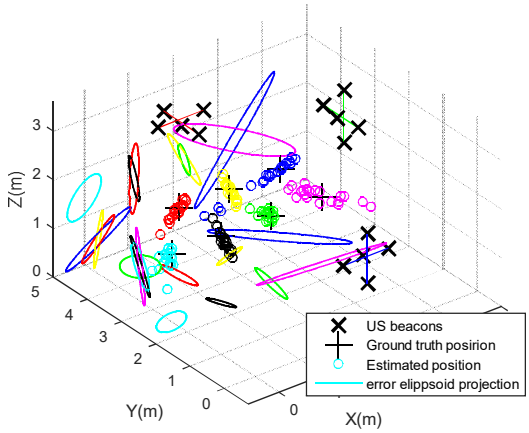	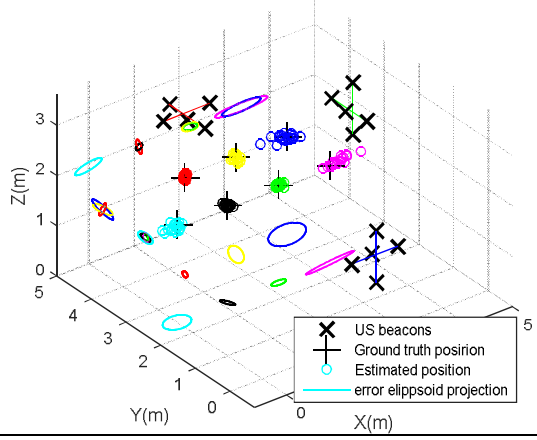

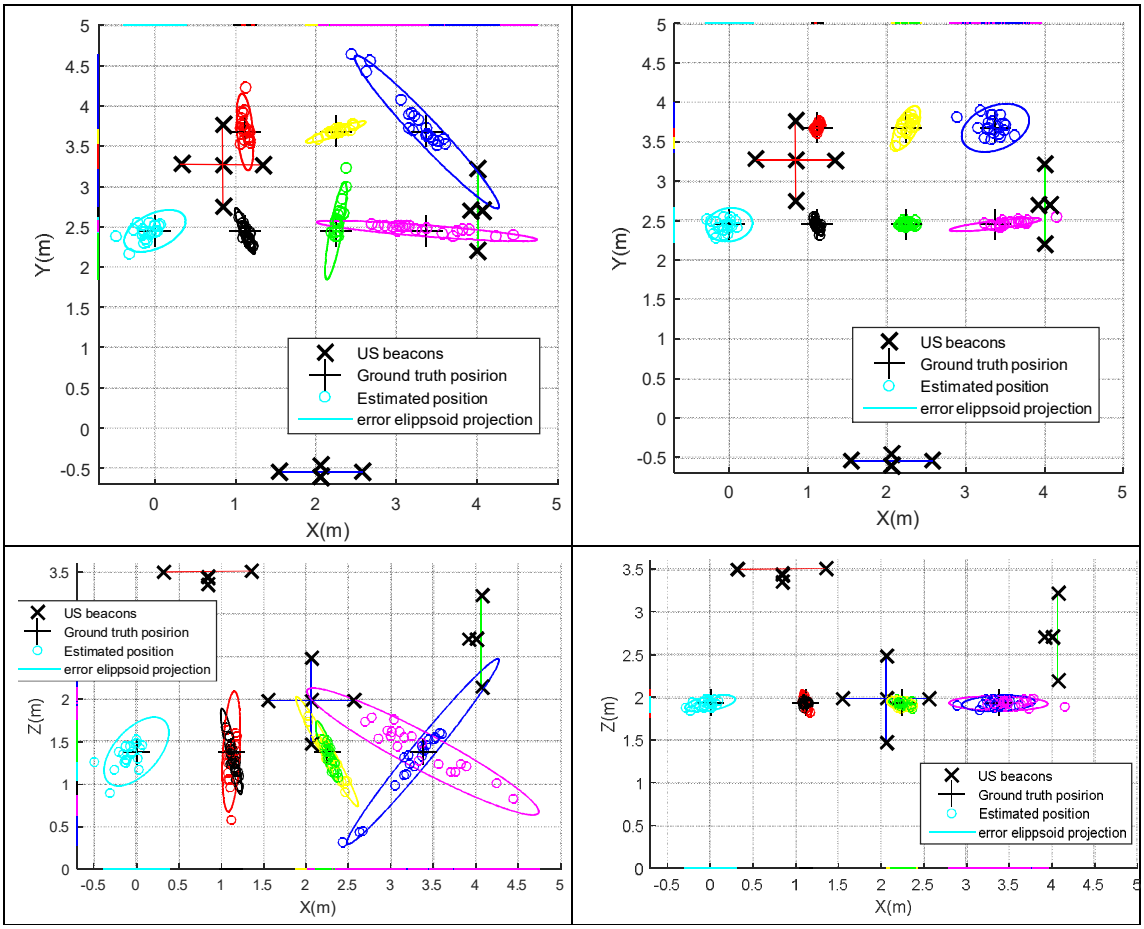

Table 4.12 Estimated positions after the Linear KF fusion for the points (P'1-P'7), including the projections of their corresponding error ellipsoids with a certainty of 95% in the XY and XZ-planes, at z_1 =1.35 m and z_2=1.93 m.

Table 4.13 presents those results by providing the mean error and the standard deviation per axis for the seven points considered (P'1-P'7). The lowest mean errors and standard deviation, as well as the smallest errors ellipsoid, are for P'2, P'3, P'5 and P'6, the most centred points in the covered volume. On the other hand, the worst results are obtained for P'1, P'4 and P'7, further away from the central axis of the three ULPSs.

% Points	z_1						z_2					
	Mean error (m)			*Standard deviation(m)*			*Mean error (m)*			*Standard deviation(m)*		
	x	*y*	*z*	*x*	*y*	*z*	*x*	*y*	*z*	*x*	*y*	*z*
P'1	0.120	0.068	0.109	0.122	0.062	0.122	0.090	0.061	0.090	0.082	0.045	0.082
P'2	0.107	0.083	0.161	0.300	0.064	0.300	0.089	0.036	0.089	0.298	0.035	0.298
P'3	0.041	0.190	0.041	0.041	0.192	0.041	0.042	0.024	0.042	0.036	0.014	0.036
P'4	0.404	0.044	0.233	0.258	0.026	0.258	0.204	0.028	0.204	0.186	0.023	0.186
P'5	0.030	0.124	0.186	0.021	0.128	0.021	0.017	0.028	0.017	0.012	0.023	0.012
P'6	0.103	0.034	0.180	0.080	0.033	0.080	0.052	0.081	0.052	0.036	0.057	0.036
P'7	0.232	0.233	0.271	0.263	0.289	0.263	0.114	0.089	0.114	0.105	0.062	0.105

Table 4.13. Mean positioning errors and standard deviations for points P1-P7 at z_1=1.35 m and z_2=1.93 m after a KF fusion.

To compare the accuracy of simulated results before and after a KF fusion, the Cumulative Distribution Function (CDF) has been calculated for all the positions. Table 4.11 presented the CDF errors for 90% of cases for the individual ULPSs, and Table 4.14 provides the errors for 90% of estimated positions for the seven points (P'1-P'7) after fusion. The positioning error of the estimated positions obtained by simulation is in the range of centimetres or decimetres. At height z_1, the most accurate positions are P'1, P'2, P'3, P'5 and P'6, where the CDF error for the 90% of cases is below 0.34m, and the least accurate ones are P'4 and P'7, where the error is 0.7 m in the 90% of cases. Results improve at z_2, where the CDF errors for all the positions (P'1-P'7) become below 0.29 m for 90% of cases. As a conclusion, the mean of the CDF error for the 90% of estimated positions is below 0.313 m at z_1 and 0.104 m at z_2.

Points	z_1	z_2
P'1	0.208	0.134
P'2	0.221	0.054
P'3	0.245	0.061
P'4	0.522	0.292
P'5	0.349	0.071
P'6	0.322	0.108
P'7	0.751	0.168

Table 4.14. CDF errors (m) for the points P'1-P'7 in the 90% of the cases after the KF fusion.

4.3.4 Adaptive Kalman Filter Approach

The adaptive Kalman filter (AKF) approach is based on the Linear Kalman Filter with a dynamic noise matrix $\mathbf{Q_k}$ to improve the predictions at the instant *k*.

All the initial values are kept as the Linear Kalman Filter case, except the noise matrix that becomes Q_0 initially, *N* is a positive constant in this case it was equal to 10, and ΔQ is the noise error covariance. The final Q_k is computed using (4.6).

$$Q_k = |diag(\alpha . Q_{k-1} + \Delta Q_k)| \tag{4.6}$$

$$\Delta Q_k = \frac{1}{N}(P_k - AP_{k-1}A^T) + \frac{1}{N-1}(\hat{w}k - w_k)(\hat{w}k - w_k)^T$$

Where $\alpha = \frac{N-1}{N}$, and $w_k = \alpha \ . \ w_{k-1} + \left(\frac{1}{N}\right) . w_k$

$$Q_0 = \begin{pmatrix} \frac{\sigma_{x,i}^2}{10} & 0.05\ \sigma_{y,i}^2 & 0.05\ \sigma_{z,i}^2 \\ 0.05\ \sigma_{x,i}^2 & \frac{\sigma_{y,i}^2}{10} & 0.05\ \sigma_{z,i}^2 \\ 0.05\ \sigma_{x,i}^2 & 0.05\ \sigma_{y,i}^2 & \frac{\sigma_{z,i}^2}{10} \end{pmatrix}$$

The AKF is applied to fuse the obtained estimated positions from the three independent ULPSs for the seven positions (P'1-P'7). Table 4.15 presents the fusion results at z_1=1.35m and z_2=1.93m. Similar conclusions can be derives, where the best estimated positions are P'1, P'2, P'3, P'5 and P'6 (cyan, black, green, red and yellow circles, respectively), and they also present the smallest error ellipsoid for 95% of the estimated positions, whereas the worst ones are P'4 (pink circles) and P'7 (blue circles).

z_1	z_2
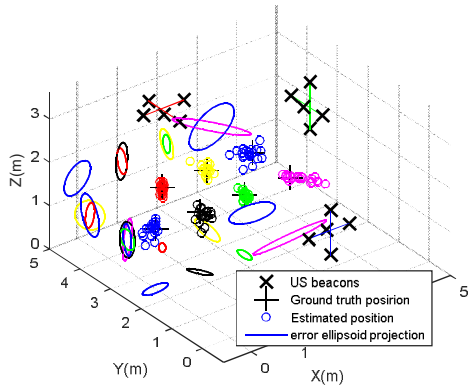	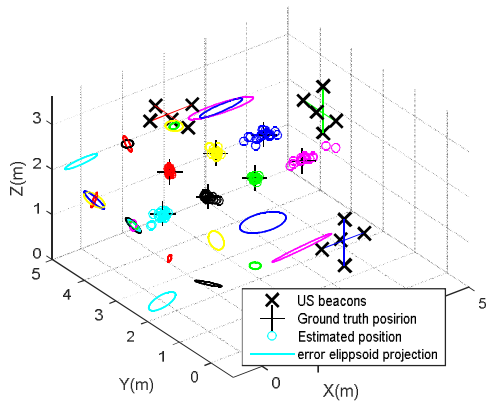

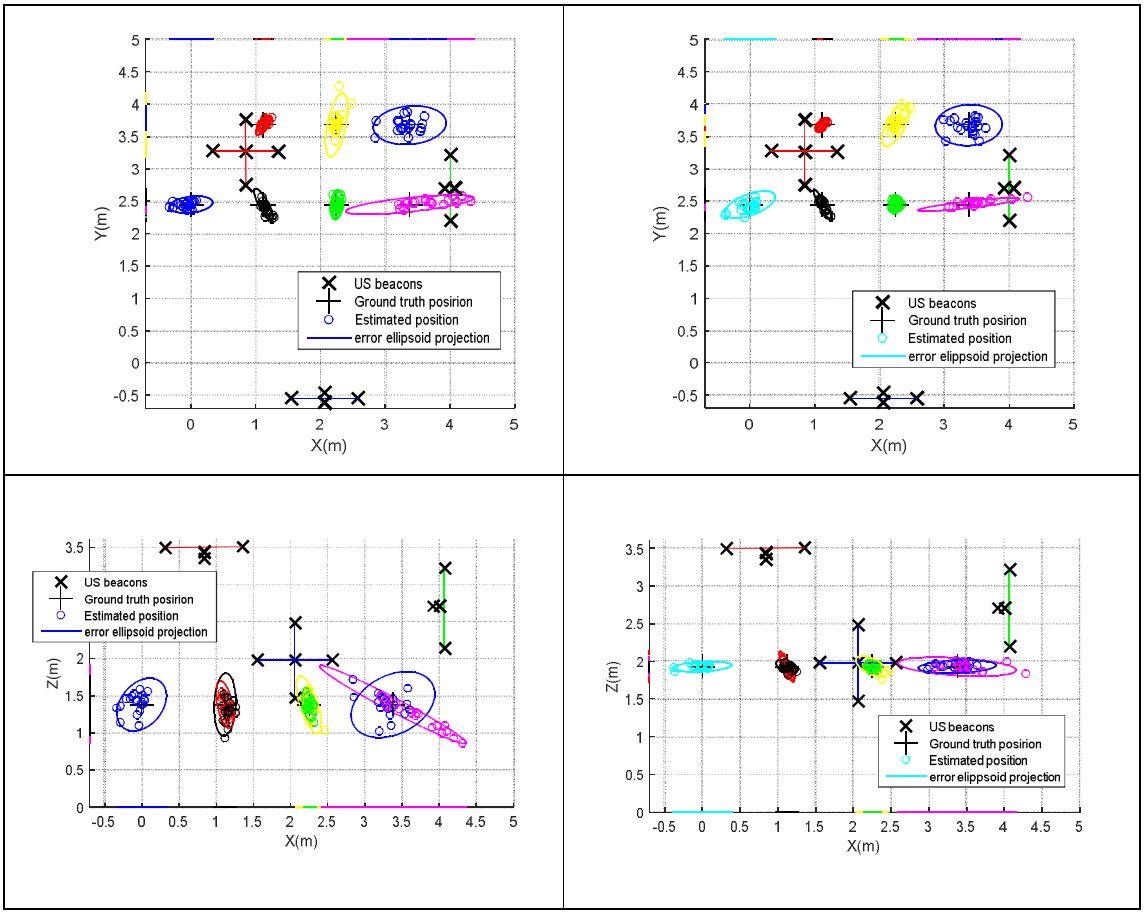

Table 4.15 Estimated positions after the AKF fusion for the considered points (P'1-P'7), including the projections of their corresponding error ellipsoids with a certainty of 95% in the XY and XZ planes, at z_1 =1.35 m and z_2=1.93 m.

From Table 4.15, the mean error and the standard deviation per axis are defined for the seven points (P'1-P'7) and illustrated in Table 4.16.

Points	z_1						z_2					
	Mean error (m)			*Standard deviation (m)*			*Mean error (m)*			*Standard deviation (m)*		
	x	*y*	*z*	*x*	*y*	*z*	*x*	*y*	*z*	*x*	*y*	*z*
P'1	0.121	0.066	0.110	0.088	0.036	0.074	0.116	0.086	0.045	0.139	0.044	0.027
P'2	0.082	0.065	0.124	0.243	0.051	0.102	0.071	0.043	0.024	0.119	0.059	0.042
P'3	0.031	0.103	0.099	0.029	0.118	0.058	0.036	0.032	0.023	0.223	0.030	0.016
P'4	0.270	0.032	0.131	0.295	0.025	0.117	0.173	0.031	0.028	0.039	0.025	0.025
P'5	0.031	0.138	0.231	0.023	0.074	0.115	0.017	0.022	0.036	0.187	0.023	0.016
P'6	0.149	0.061	0.280	0.141	0.061	0.250	0.028	0.075	0.032	0.012	0.013	0.024
P'7	0.178	0.210	0.255	0.221	0.272	0.303	0.153	0.086	0.027	0.120	0.066	0.026

Table 4.16. Mean positioning errors and standard deviations for points P'1-P'7 at z_1=1.35 m and z_2=1.93 m after an AKF fusion.

Furthermore, the Cumulative Distribution Function (CDF) has been determined for all the grid of positions (P'1-P'7) and presented in Table 4.17 at z_1 and z_2, respectively, after the AKF fusion. The positioning error of the estimated positions reached by simulation is already in the range of centimetres or decimetres. Results applying the KF are similar to results obtained after the AKF, but the second approach presents better accuracy caused by the update values of the noise matrix. At z_1, P'1, P'2, P'3, P'5 and P'6 have an error below 0.3 m for the 90%, whereas in P'4 and P'7 is less than 0.6 m. As an outcome, the mean of the CDF error for the 90% of estimated positions is below 0.27 m at z_1 and 0.101 m at z_2.

Points	z_1	z_2
P'1	0.205	0.169
P'2	0.208	0.073
P'3	0.139	0.072
P'4	0.306	0.168
P'5	0.306	0.054
P'6	0.426	0.111
P'7	0.622	0.214

Table 4.17. CDF error of the points P'1-P'7 for the 90% of the cases after an AKF.

Summing it up, in this Section three loosely coupled methods have been applied to fuse three ULPSs' estimated positions for a set of seven ground-truth positions (P'1-P'7) at two different heights. Estimated positions obtained independently from three ULPSs present a large dispersion in the three axes. Their error range is in the centimetres order to reach the metres in some cases. To decrease these errors, various fusion methods have been applied. The estimated positions after fusion present better results, with errors in the range of decimetres to reach in some positions centimetres. The more accurate positions at z_1 are for the MLE fusion approach and at z_2 for AKF fusion.

4.5 Tightly-Coupled Fusion Algorithms for Positioning Systems based on Multiple ULPS

In this section, an Extended Kalman Filter (EKF) will be applied to estimate the positions of the mobile receiver in the space. This filter is based on the fusion of the differences of distances between the beacons and the mobile receiver, to update its position. First of all, the initial

position is estimated using the Gauss-Newton algorithm, then the rest of the positions will be updated using the distance ranges. For a single ULPS, the number of the differences of distances needed is up to four. For three ULPSs this number is up to twelve.

The EKF is based on a loop of two steps: prediction and updating, (4.9) and (4.10). This algorithm tries to converge into the correct estimated position after several iterations based on (4.7), (4.8) and (4.11).

This algorithm linearizes the state vector and its covariance matrix, applying several observations. Those observations are computed from the US measurements and presented as the differences in distances between the mobile receiver and the beacons *i* and *j* (Δd_{ij}). Equations (4.7) and (4.12) are computed from the TDOA, where *c* is the velocity of sound in air: 340m/s.

$$\Delta d_{ij} = c.TDOA \tag{4.6}$$

The state $\mathbf{X_k}$ and measurement $\mathbf{Z_k}$ are given by (4.7) and (4.8).

$$\boldsymbol{X_k} = f\left(\boldsymbol{X_{k-1}}, \Delta d_{ij,k}\right) + w_k \tag{4.7}$$

$$\boldsymbol{Z_k} = h(\boldsymbol{X_k}) + v_k \tag{4.8}$$

Where Δd_{ij} is the increment of distance between the iteration *(k-1)* and *k* by the mobile receiver; w_k is the process noise related to each beacons' state vector and $\mathbf{Q_k}$ is the covariance matrix of the previous state at instant *k*; v_k is the measurement noise and $\mathbf{R_k}$ is its covariance matrix at instant *k*.

$$\boldsymbol{X_k} = f\left(\boldsymbol{X_k}, \Delta d_{ij,k}\right) \tag{4.9}$$

$$\boldsymbol{P_k} = \boldsymbol{A_k} \,.\, \boldsymbol{P_{k-1}} \,.\, \boldsymbol{P_k^T} + \boldsymbol{Q_k}$$

Where $X_k = \left[x_{k-1} + \Delta d_{ij,k}, y_{k-1} + \Delta d_{ij,k}, z_{k-1} + \Delta d_{ij,k} \right]^T$; $\mathbf{X_k}$ is the a priori estimation of the state vector based on the previous estimation $\mathbf{X_{k-1}}$; $\mathbf{A_k}$ is the derivative with respect to each

component of the state vector of the relationship between the previous and the current stage; and $\mathbf{P_k}$ is the a priori covariance matrix.

$$\boldsymbol{K} = \boldsymbol{P_k} \,.\, \boldsymbol{H_k^T} \,.(\boldsymbol{H_k}.\boldsymbol{P_k}.\, \boldsymbol{H_k^T} + \boldsymbol{R})^{-1}$$

$$\boldsymbol{X_k} = \boldsymbol{X_k} + \boldsymbol{K} \,.(\boldsymbol{Z_k} - h(\boldsymbol{X_k})) \qquad (4.10)$$

$$\boldsymbol{P_k} = (\boldsymbol{I} - \boldsymbol{K}.\boldsymbol{H_k}) \,.\, \boldsymbol{P_k}$$

Where $\mathbf{H_k}$ represents the derivative related to the state vector of the relationship between the state vector and the measurements; $\mathbf{Z_k}$ is a vector that contains the observations (distances or difference of distances) computed from (4.11); *K* is the filter gain computed from (4.10) and **I** is de identity matrix.

$$Z_k = \begin{pmatrix} \Delta d_{21,k} \\ \Delta d_{31,k} \\ \dots \\ \Delta d_{i1,k} \end{pmatrix} \qquad (4.11)$$

Where $_i$ is the index of the beacons ($_i$ =1.. 4); 1 is the 1st beacons and it presents is the reference one for only one ULPS and *j* is the index of the ULPS (*j*=1..3). $P_i = (x_i, y_i, z_i)$ and $P_j = (x_j, y_j, z_j)$ are the beacons coordinates and $P = (x, y, z)$ is the mobile receiver coordinate.

$$\Delta dij = di - dj = \sqrt{(x - xi)^2 + (y - yi)^2 + (z - zi)^2} - \sqrt{(x - xj)^2 + (y - yj)^2 + (z - zi)^2} \qquad (4.12)$$

The components of the observation matrix **H**, the Jacobin matrix, are defined by (4.12) and (4.13).

$$\begin{cases} \frac{\partial h_i(x_k)}{\partial x_k} = \frac{x_k - x_i}{\Delta d_{i1,k}} \\ \frac{\partial h_i(y_k)}{\partial y_k} = \frac{y_k - y_i}{\Delta d_{i1,k}} \\ \frac{\partial h_i(z_k)}{\partial z_k} = \frac{z_k - z_i}{\Delta d_{i1,k}} \end{cases} \quad (4.13)$$

Two different position systems have been tested. The first one is based on a low sampling frequency at the ultrasonic emitters, whereas the second system applies a high sampling frequency. Some results and conclusion are detailed below to describe its performance.

4.5.1 Low Sampling Frequency Approach

The emission period of the ultrasonic units is 50 ms, assuming that the mobile receiver moves with a step of 1.119 m per period so it will be 2.238m/s. Additionally, three different alternatives have been simulated, all of them are based on the Extended Kalman Filter (EKF): for only one ULPS which is placed on the ceiling (ULPS-1); three independent EKF (three parallel EKF), one EKF per ULPS; only one EKF for all the three ULPSs to fuse all the distances and obtain the final estimated position.

a. <u>One ULPS: on the ceiling</u>

An EKF is used to fuse only one single ULPSs' emitted signals (ULPS-1), installed on the ceiling. Therefore, after receiving the five ultrasonic transmissions, the algorithm detects the peaks of those five signals and compute the differences of distances (TDOA) to be used later to compute the initial position using the Gauss-Newton algorithm. Thereafter, this position will be updated by the EKF using the range of distances computed from the TDOA. In this case, the EKF matrices size is up to 4x4 to estimate the new positions. Fig 4.26 presents a sample prototype of the fully applied algorithm.

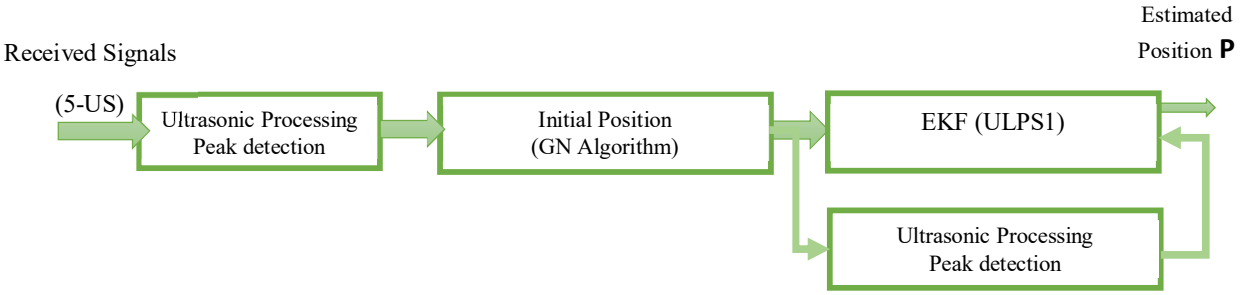

Fig. 4.26. Block schema for One EKF for one ULPS

Assuming that the distribution of the estimated positions is Gaussian, where the mean is the ground-truth position and the σ is its variance in the space, three different variances σ have been employed, (0.02 m, 0.2 m and 0.5 m), to see the behaviour of this filter when the variance changes and increases. After some simulations, the corresponding results are presented in Table 4.17, following the same scheme as before and the same heights, z_1 =1.35 m and z_2 = 1.93 m. It is possible to observe that, when the variance increases, the size of the cloud of the estimated positions becomes bigger, consequently the accuracy decreases.

σ (m)	z_1	z_2
0.02	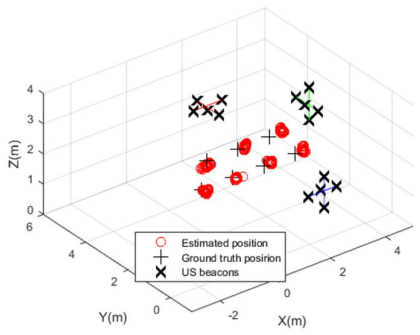	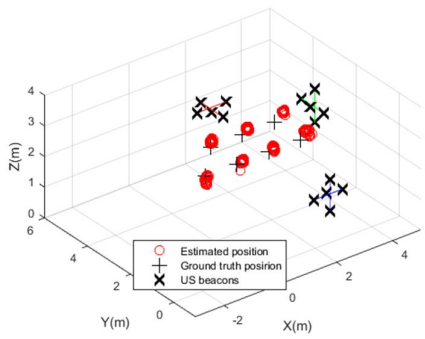
	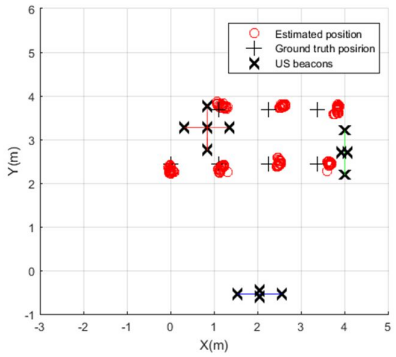	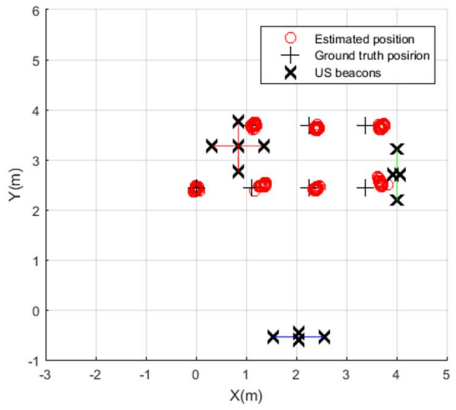

	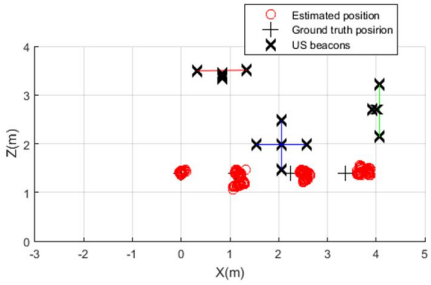 Estimated position Ground truth posirion US beacons Z(m) X(m)	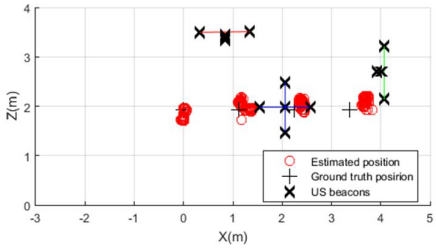 Estimated position Ground truth posirion US beacons Z(m) X(m)
0.2	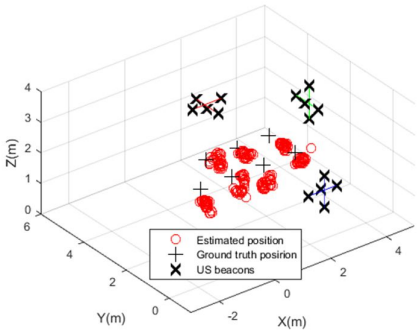 Estimated position Ground truth posirion US beacons Z(m) Y(m) X(m)	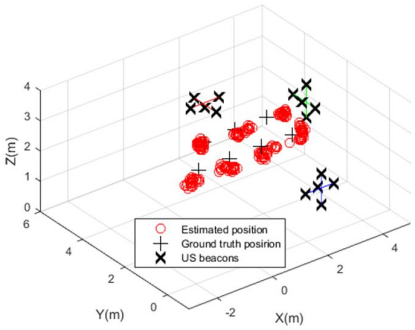 Estimated position Ground truth posirion US beacons Z(m) Y(m) X(m)
	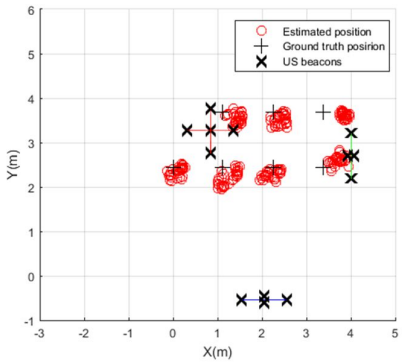 Estimated position Ground truth posirion US beacons Y(m) X(m)	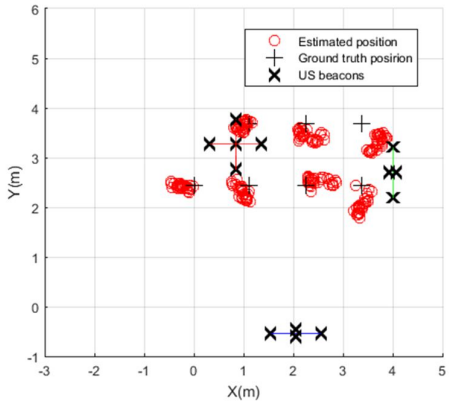 Estimated position Ground truth posirion US beacons Y(m) X(m)

	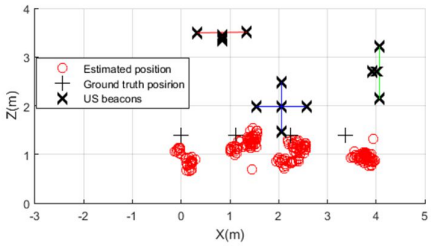 Estimated position Ground truth posirion US beacons Z(m) X(m)	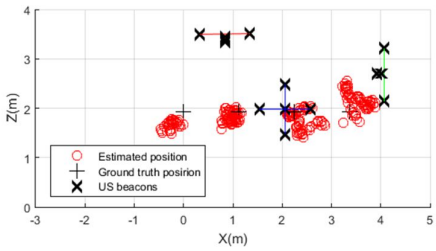 Estimated position Ground truth posirion US beacons Z(m) X(m)
0.5	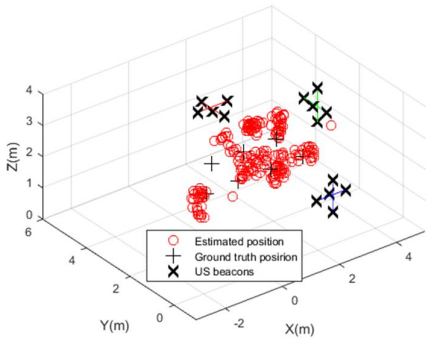 Estimated position Ground truth posirion US beacons Z(m) Y(m) X(m)	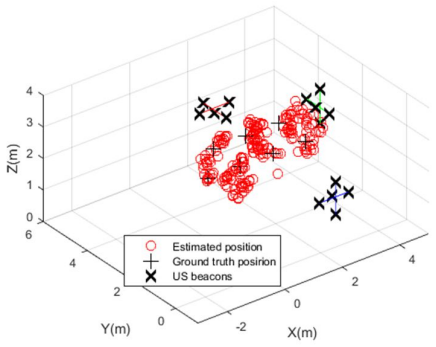 Estimated position Ground truth posirion US beacons Z(m) Y(m) X(m)
	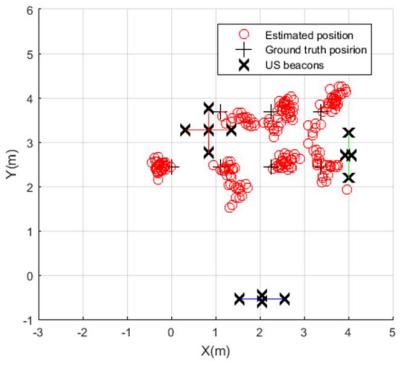 Estimated position Ground truth posirion US beacons Y(m) X(m)	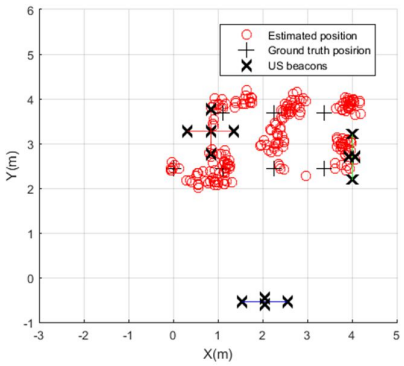 Estimated position Ground truth posirion US beacons Y(m) X(m)

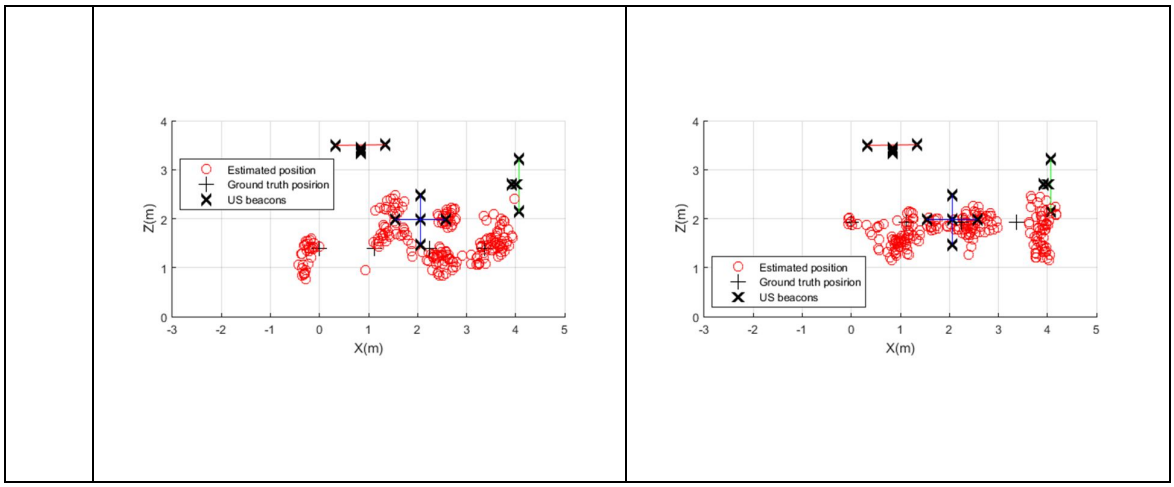

Table 4.18. Results of the EKF fusion for one ULPS and the corresponding plane projection for various variances σ.

Table 4.19 depicts the particular case when implementing EKF for the ULPS-1 installed in the ceiling, as well as employing a variance σ=0.02 m, providing the mean error and standard deviations for the set of seven positions (P'1-P'7).

The cloud of the estimated positions are more or less equal for all the seven positions, no matter the axis or the position, although the size of those clouds decreases from z_1 to z_2, as happened before. At z_2, the lowest mean errors and standard deviation, as well as the smallest errors ellipsoid, are for P'1, P'2 and P'5, the most central points in the covered volume of ULPS-1. Hence, the worst results are obtained for P'3, P'4, P'6 and P'7, where there is some bias caused by their long distance from the central axis of the coverage volume of the ULPS-1.

σ=0.02m	z_1						z_2					
	Mean error (m)			*Standard deviation (m)*			*Mean error (m)*			*Standard deviation (m)*		
Points	*x*	*y*	*z*	*x*	*y*	*z*	*x*	*y*	*z*	*x*	*y*	*z*
P'1	0.027	0.164	0.032	0.028	0.047	0.020	0.025	0.041	0.118	0.018	0.030	0.087
P'2	0.052	0.103	0.041	0.045	0.058	0.025	0.226	0.047	0.020	0.050	0.027	0.034
P'3	0.285	0.054	0.035	0.203	0.045	0.023	0.194	0.033	0.085	0.258	0.021	0.051
P'4	0.367	0.027	0.046	0.454	0.025	0.053	0.384	0.096	0.120	0.426	0.052	0.051
P'5	0.091	0.087	0.231	0.053	0.042	0.036	0.041	0.027	0.149	0.024	0.020	0.047
P'6	0.324	0.090	0.084	0.040	0.024	0.046	0.154	0.044	0.165	0.029	0.023	0.039
P'7	0.460	0.064	0.052	0.025	0.031	0.031	0.317	0.027	0.233	0.037	0.020	0.027

Table 4.19. Mean error and standard deviation for the estimated position with only one ULPS and the EKF for σ =0.02m.

The CDF has been calculated for various variances (0.02 m, 0.2 m, 0.5 m) using an EKF for ULPS-1, plotted in Table 4.20. The mean of the CDF error for the seven positions is 0.3 m for

z_1 and 0.28 m for z_2, taking into account the bias values. Similar results have been extracted for the second value of σ =0.2 m, where the mean of the CDF error increases to 0.51 m at z_1 and 0.42 m at z_2. Finally, for σ =0.5 m the mean of the CDF error keeps increasing up to 0.6 m for z_1 and 0.62m for z_2.

σ(m)	z_1	z_2
0.02	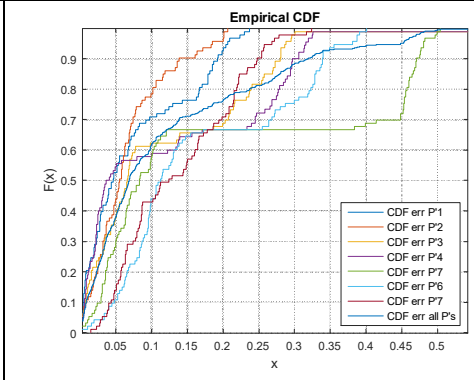	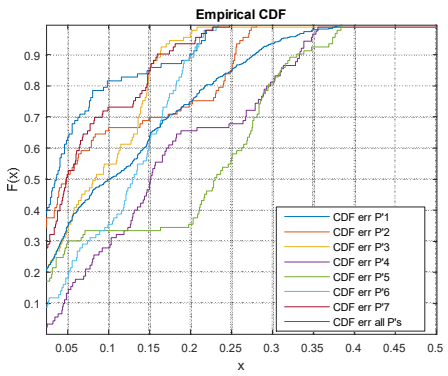
0.2	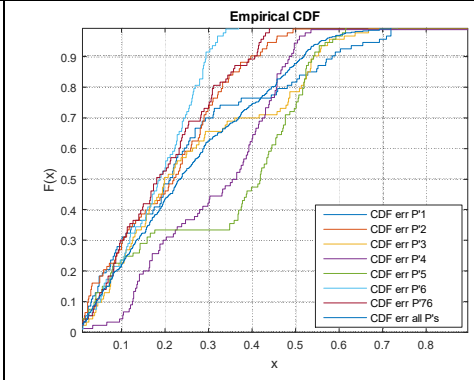	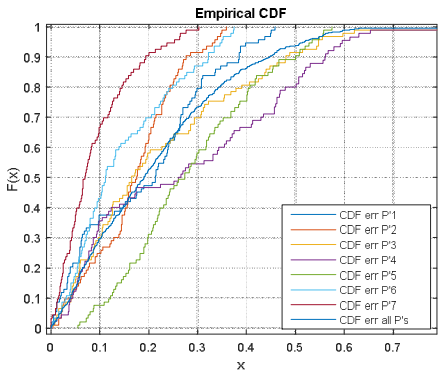
0.5	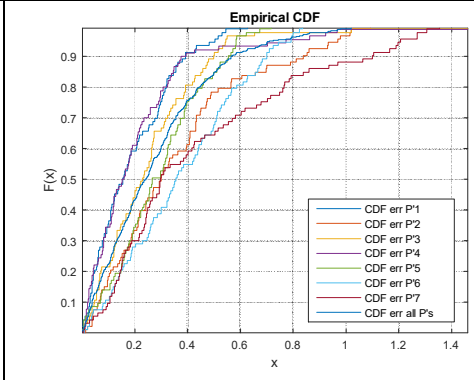	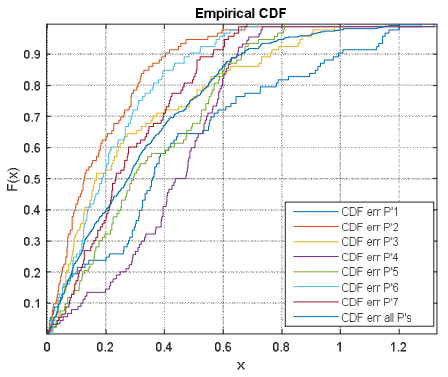

Table 4.20. CDF of the positioning errors in all the space, applying the EKF for one ULPS in the ceiling using multiple variances σ={0.02 m,0.2 m, 0.5 m} in z_1 and z_2 for the three coordinates x, y and z, for the grid of positions (P'1-P'7) .

b. Three Independent ULPSs

Here, three EKFs are used to fuse the three independent ULPSs placed at various planes: the ceiling, and on two perpendicular walls, following the procedure shown in Fig. 4.27. Hereinafter, for clarity's sake, the variance of the estimated positions will be σ=0.2 m.

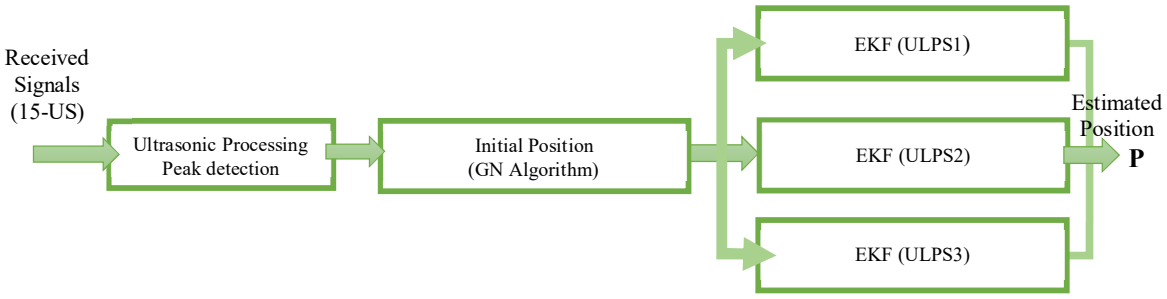

Fig. 4.27. Block diagram of the three independent EKFs for three ULPSs.

Therefore, the estimated positions will be updated by the way of three independent EKF using the distances measured from the ultrasonic transmissions. Some simulations have been applied, and results are presented in Table 4.21. Three different clouds of estimated positions have been detected per point, one cloud per ULPS. Those clouds are plotted with different colours, where the red are from ULPS-1, the green are from ULPs-2 and blue are from ULPs-3. Again, the same heights are considered for the receiver, z_1 =1.35 m and z_2 =1.93m. As it is possible to observe, the variance dispersion of the seven clouds is roughly the same.

z_1	z_2
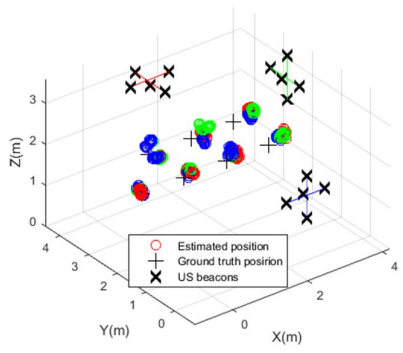	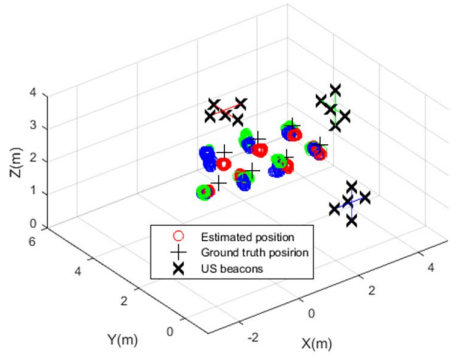

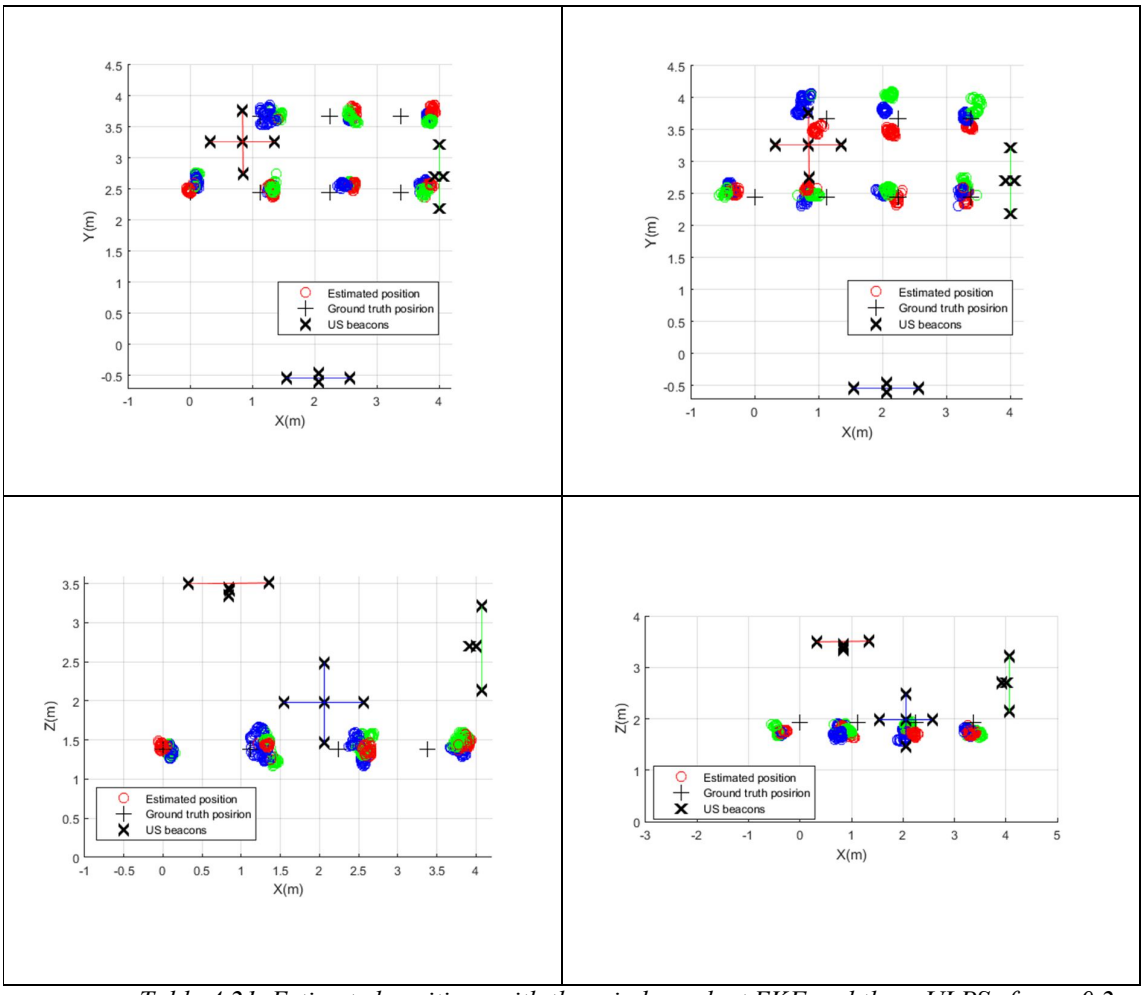

Table 4.21. Estimated positions with three independent EKF and three ULPSs for σ=0.2m.

In this instance, the mean error and the standard deviations are computed and mentioned in Table 4.22 for the set of seven positions (P'1-P'7). The points P'3, P'4, P'6 and P'7 are the least accurate positions. Furthermore, the positions P'1, P'2, P'5 and P'6 are the best at z_1 because they are just below ULPS-1. Likewise, atz_2, P'1, P'2 and P'6 are the least accurate positions. Generally, all the mean errors and the standard deviations for three independent EKF (three ULPSs) are higher than those with one EKF and ULPS-1.

Points	z_1						z_2					
	Mean error (m)			*Standard deviation (m)*			*Mean error (m)*			*Standard deviation (m)*		
	x	*y*	*z*	*x*	*y*	*z*	*x*	*y*	*z*	*x*	*y*	*z*
P'1	0.099	0.169	0.047	0.179	0.192	0.034	0.395	0.125	0.184	0.099	0.184	0.051
P'2	0.196	0.073	0.062	0.033	0.046	0.032	0.272	0.071	0.182	0.072	0.044	0.059
P'3	0.330	0.118	0.061	0.229	0.033	0.053	0.174	0.084	0.202	0.184	0.042	0.089
P'4	0.527	0.121	0.048	0.460	0.022	0.039	0.158	0.073	0.210	0.464	0.026	0.030

P'5	0.190	0.063	0.161	0.105	0.044	0.057	0.298	0.206	0.185	0.116	0.098	0.079
P'6	0.352	0.055	0.115	0.046	0.039	0.062	0.151	0.239	0.156	0.060	0.105	0.061
P'7	0.477	0.071	0.087	0.040	0.048	0.061	0.062	0.120	0.205	0.042	0.088	0.037

Table 4.22. Mean errors and standard deviations for three ULPSs and three independent EKF with σ =0.2m.

The CDF errors for 90% of the obtained estimated positions for 90% of cases in z_1 is between 0.35m and 0.7m to become more accurate in z_2 where its values become between 0.26m and 0.43m. The CDF errors values are greater than those of one single EKF of ULPS-1 as the use of a combination of three EKF of the independent ULPSs, as plotted in representations of Table 4.23.

z_1	z_2
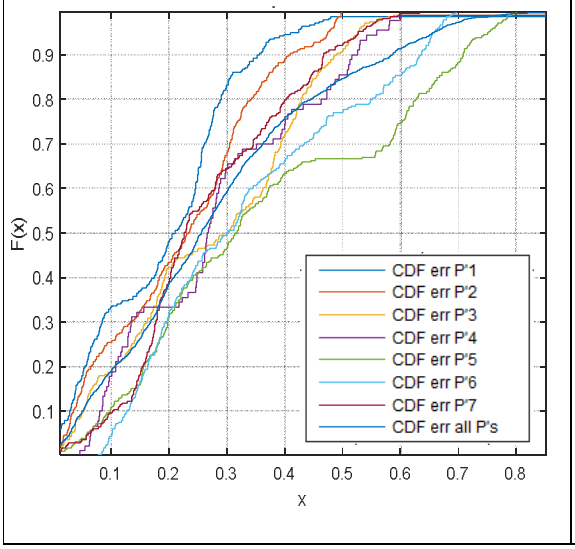	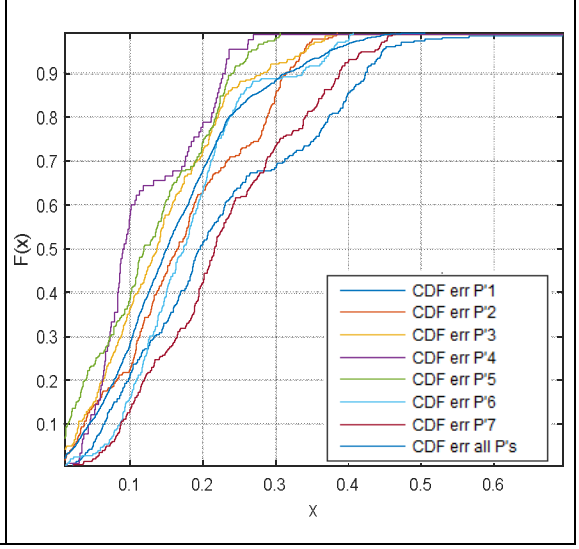

Table 4.23. CDF of the positioning with three independent EKFs and three ULPSs for σ=0.2m, for the three coordinates x, y and z, for the grid of positions (P'1-P'7).

c. Tree Fused ULPSs

Finally, only one EKF is used to fuse the measurements from three ULPSs emitting up to fifteen ultrasonic signals, according to Fig. 4.28 where a block diagram of the algorithm is shown.

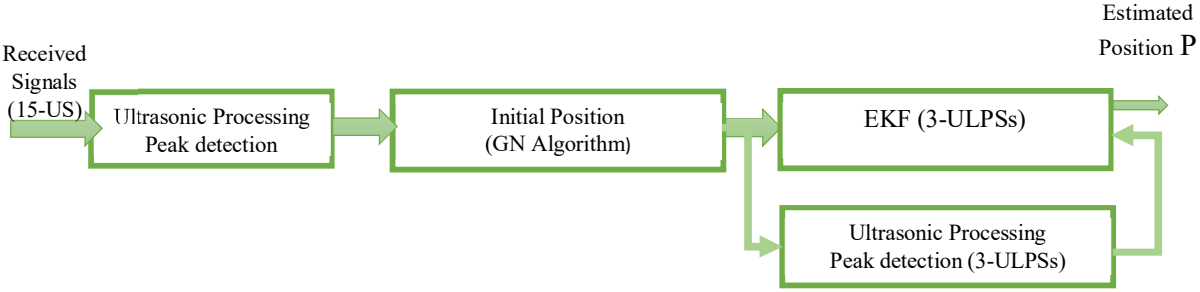

Fig. 4.28. Block diagram of a single EKF for three merged ULPSs.

Simulations have been carried out for the seven positions (P'1-P'7) at z_1 and z_2, with a variance of σ =0.2 m. As plotted in Table 4.24, the clouds of the seven positions are more concentrated around the ground-truth points, whereas their dispersions are low as well.

z_1	z_2
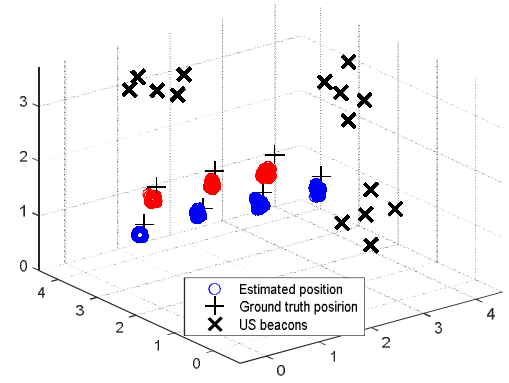	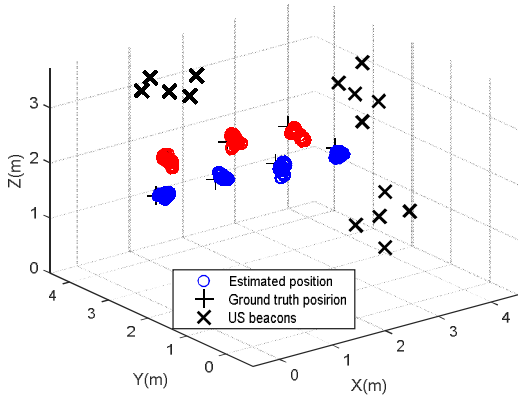
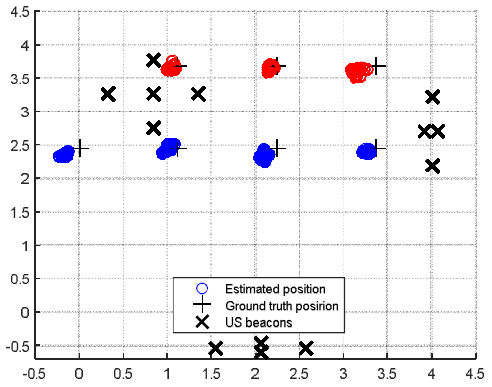	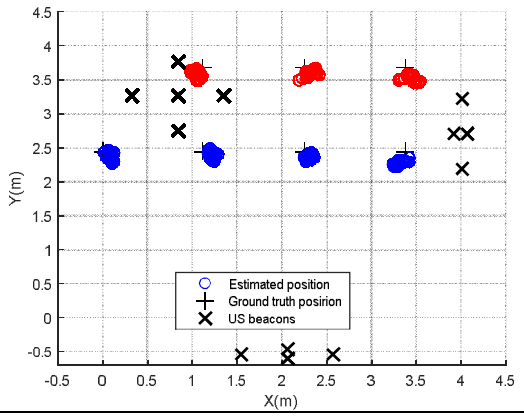
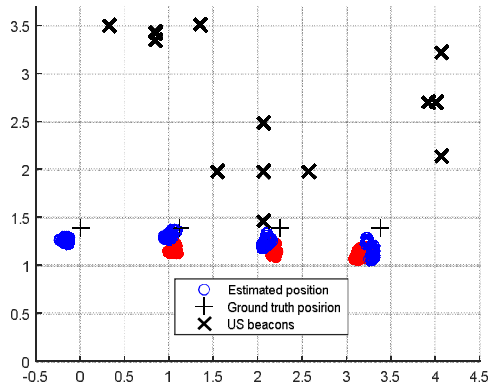	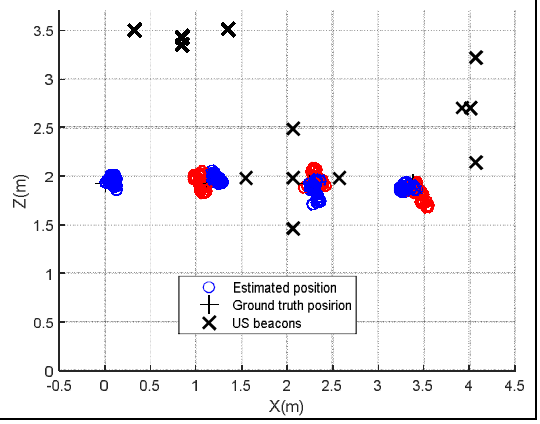

Table 4.24. Estimated positions with a single EKF and three ULPSs for σ=0.2m.

The mean error and the standard deviation are calculated and considered in Table 4.25 for the seven positions (P'1-P'7).

Points	z_1						z_2					
	Mean error (m)			*Standard deviation(m)*			*Mean error (m)*			*Standard deviation (m)*		
	x	y	z	x	y	z	x	y	z	x	y	z
P'1	0.163	0.098	0.117	0.021	0.020	0.021	0.084	0.079	0.029	0.026	0.053	0.027
P'2	0.119	0.034	0.076	0.030	0.021	0.026	0.109	0.066	0.041	0.029	0.045	0.027
P'3	0.143	0.112	0.131	0.027	0.046	0.032	0.053	0.097	0.069	0.035	0.033	0.058
P'4	0.108	0.052	0.223	0.028	0.013	0.076	0.076	0.179	0.051	0.041	0.030	0.024
P'5	0.065	0.037	0.210	0.027	0.018	0.030	0.064	0.095	0.057	0.038	0.049	0.037
P'6	0.070	0.029	0.216	0.020	0.024	0.046	0.078	0.091	0.047	0.043	0.044	0.042
P'7	0.223	0.069	0.267	0.040	0.040	0.041	0.070	0.155	0.102	0.043	0.041	0.067

Table 4.25. Mean errors and standard deviations for three ULPS and a single EKF (σ =0.2 m).

The CDF errors for 90% of the cases for the seven studied points (P'1-P'7) are between 0.107m and 0.3 m at z_1, and between 0.105 m and 0.2m at z_2, as plotted in Table 4.26.

	z_1	z_2
CDF error (90% of positions)	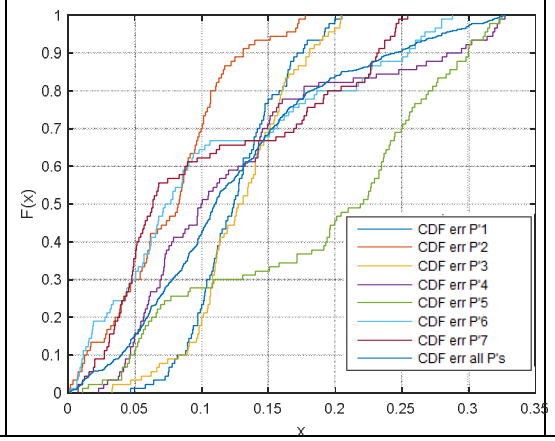	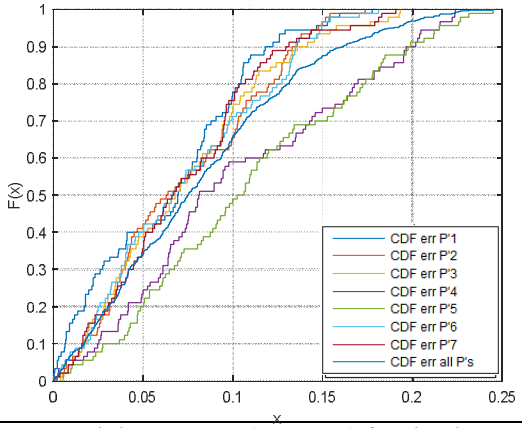

Table 4.26. CDF of the positioning errors, for one EKF and three ULPS (σ=0.2 m) for the three coordinates x, y and z, for the grid of positions (P'1-P'7).

.

4.5.2 High Sampling Frequency Approach

In this configuration, we assume that the mobile receiver computes and estimates its positions in a short range of time, when the emission period of ultrasounds is 10 ms and the receiver moves a distance of 0.228 m per period, so its velocity becomes 2.238m/s. These estimated positions become too close to each other to make a tracking way of its shifting and velocities. The same trajectory, composed of the seven points (P'1-P'7), is used. Additionally, the fusion

of three ULPSs by only one EKF is applied. Simulations have been done using a variance of 0.2m at z_1 and z_2. The resulting estimations are plotted in Table 4.27.

It is possible to observe that, even when the sampling frequency increases, the positioning performance is not affected, and the positioning system keeps tracking its way with suitable accuracies, especially for z_2 where the Z-axis errors improve.

z_1	z_2
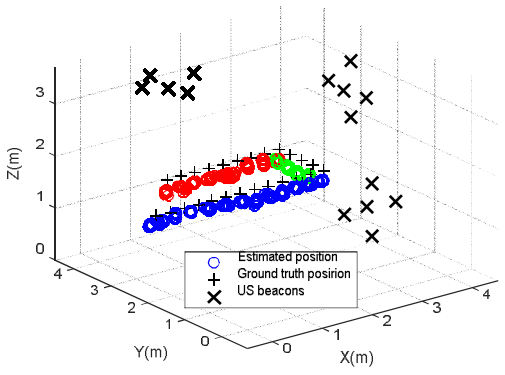	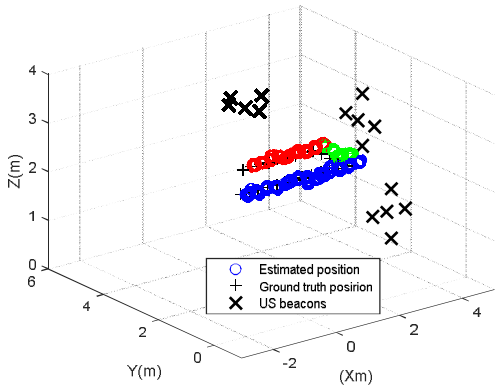
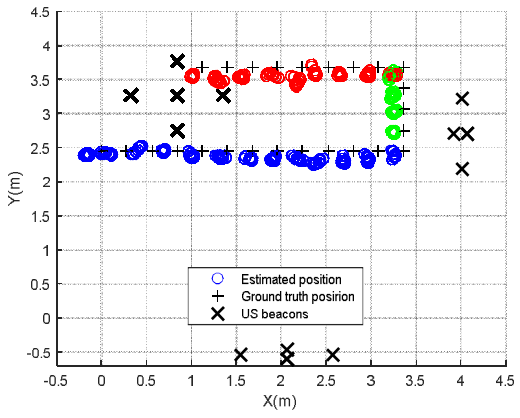	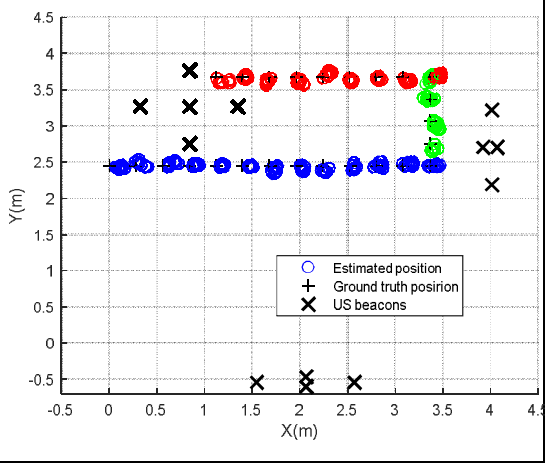

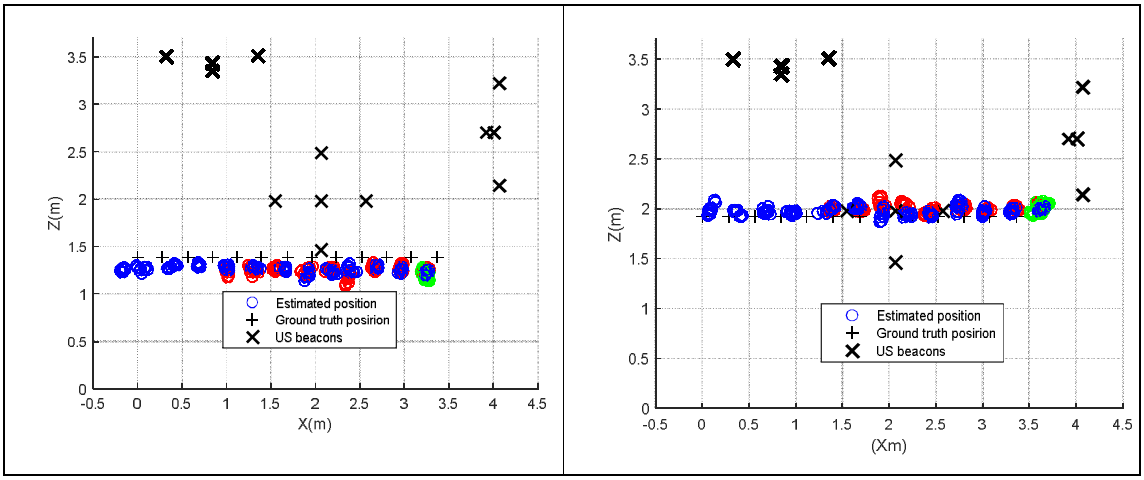

Table 4.27. Positioning performance with high sampling frequency based on the fusion of three ULPSs with only one EKF.

4.5 Summary

The performance of a 3D ultrasonic positioning systems has been studied, firstly developed with a structure and characteristics for 2D positioning, then adapted to be deployed for 3D positioning. This study has covered the use of various ULPSs configurations, considering synchronous and asynchronous measurements. The comparison has been carried out and based on the estimation of the PDOP, by using a grid of points that covers all the volume of interest (a room of 8x8x8 m^3). The use of synchronous measurements from different ULPSs is better in terms of accuracy, but it needs synchronization between ULPSs and the receiver. On the other hand, with the asynchronous measurements for each ULPS, these problems can be avoided and still achieve an accuracy in the range of centimetres and decimetres for many applications.

The selected 3D positioning configuration is composed by three ULPS units placed on perpendicular walls (planes). Simulated analyses have been implemented when at least one ULPs is available. In the case of having more than one ULPS available, two merging method have been used. The first approach is based on the fusion of the obtained positions with the so-called loosely fusion method. In these methods, different algorithms have been applied, such as MLE/Mean, Linear Kalman Filter and Adaptive Kalman Filter. Another fusion approach employed is the so-called tightly coupled fusion. Three different algorithms have been implemented here: Extended Kalman Filter, three independent EKF for three ULPSs, and a single EKF for three ULPSs. Table 4.28 summarizes the CDF errors for 90% of the estimated positions. It is possible to observe that the tightly coupled methods are more accurate than the loosely coupled ones.

CDF Error (m)		z_1			z_2		
		Min	*Max*	*Mean*	*Min*	*Max*	*Mean*
Loosely coupled fusion	MLE/Mean	0.225	0.529	0.344	0.102	0.646	0.21
	KF	0.5	0.78	0.5	0.1	0.4	0.25
	AKF	0.2	0.82	0.4	0.1	0.34	0.2
Tightly coupled fusion	EKF (one ULPS)	0.3	0.6	0.57	0.2	0.56	0.45
	EKF (three ind. ULPSs)	0.35	0.7	0.58	0.26	0.43	0.3
	EKF (three fused ULPSs)	0.107	0.3	0.22	0.105	0.2	0.152

Table 4.28. Summary of the CDF errors for the 90% of the estimated positions.

Chapter 5

Experimental Results

In this chapter, some experimental results are presented and detailed using the same simulated fusion algorithms, which were described in previous chapters. Two different scenarios in the School of Engineering from the University of Alcala have been used, to apply the described 3D configuration and validate it experimentally. The first location is a small area in a laboratory, used to test the reliability of this configuration and the experimental drawbacks derived from the coexistence of various sensors. Then, a second location is an extensive hall on the second floor, where all the simulations of the previous chapter have been held on. Thus, two receivers have been used, the first one is a 2D ultrasonic receiver and the second one a 3D receiver, as described in the following sections of this chapter. Moreover, the characteristics of the ULPS have been described, as well as the fusion algorithms to process received data and compute the receiver's positions. Finally, a preliminary hardware implementation of the processing associated with the ultrasonic signals has been tackled.

5.1 Structure of the Experimental System

5.1.1 Scenarios and Experimental Setup

To cover the 3D working space, three ULPSs units (ULPS-1, ULPS-2, and ULPS-3) have been used and installed in three orthogonal planes or walls: ULPS-1 on the ceiling, and ULPS-2 and ULPS-3 on two perpendicular walls, consequently obeying typical shapes indoors. Two scenarios have been employed, where the scenario no. 1 is placed in the laboratory on the third floor of the building, as shown in Fig. 5.1.a). The first workspace is a complicated environment for ultrasonic signals considering it has a small size, low ceiling and close walls, a space of $3 \times 4 \times 2.7$ m^3, as well as the existence of a lot of furniture. A scenario no. 2, is used in simulations and shown in Fig. 5.1.b). It is an extended hall located on the second floor of the building, a space of $7 \times 8 \times 3.5$ m^3.

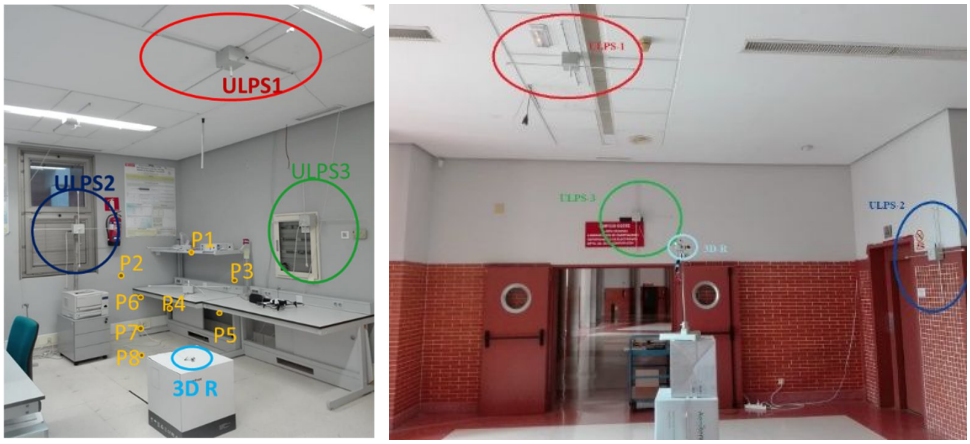

a) b)

Fig. 5.1. General view of the 3D ultrasonic positioning system with three ULPS units installed on three perpendicular planes of the space and a mobile receiver, where experimental tests have been realized: a) scenario no. 1; b) scenario no. 2.

Table 5.1 indicates the coordinates of the central beacons B_1 for every ULPS for the both cases (laboratory and hall); note that ULPS-2 and ULPS-3 are at the same height, as well as in the center of walls in the laboratory, but have different heights and are not placed at the centers of the wall in the hall, due to its complex architecture, since ultrasonic local positioning systems (ULPSs) depend on the environment nature, complexity and size.

ULPS	Coordinates for B_1 in the laboratory (m)	Coordinates for B_1 in the hall (m)
ULPS-1	(1.9773, 3.26, 2.674)	(0.84, 3.267, 3.351)
ULPS-2	(0.077, 1.94, 1.707)	(2.06, −0.458, 1.980)
ULPS-3	(1.707, 0.420, 1.650)	(3.92, 2.7, 2.7)

Table 5.1. Coordinates of the central beacon B1 for every ULPS in the considered workspaces.

This proposal is based on three ULPSs and a mobile receiver (2D-3D), which can be installed on board of a mobile robot in the space, drones, industrial robots, smartphones, people, etc.

The ULPS unit is developed for the LOCATE-US prototype. Its shape is a square with a side of 0.707m, where five ultrasonic beacons, B_i, i=1,2, …5, are located at its four vertices and its centre. Those ultrasonic beacons are not coplanar and present a low height variation: $B_2$and B_4 are included in the ULPS plane which can be ordinarily the ceiling or a wall, $B_3$and B_5 are distant by 10 cm and $B_1$by 20 cm from the ULPS plane, as shown in Fig. 5.2. This variation is to improve the third coordinate's estimation in the direction of the variation of the receiver

positions. The used ultrasonic transducer is the PROWAVE 328ST160, whose bandwidth is around 18 kHz, with a central frequency at 41.667 kHz. The five ultrasonic transducers have the same orientation and cover an equal volume size. This coverage volume is a truncated cone of 53 m^3 when the distance between the small base, a circle including the ULPS with an area about 0.78 m^2, and the large base, a circle around 40 m^2 on the ground, is 3.5 m, considering that the emission angle of each beacon is 120º, as described in previous chapters. The medium access technique for the ultrasonic transmissions can be either Code Division Multiple Access (CDMA) or Time Division Multiple Access (TDMA). Furthermore, the ultrasonic transmissions are encoded with diverse five 1023-bits Kasami sequences (fifteen 1023-bits Kasami sequences are used for the three ULPSs), due to their suitable cross-correlation and auto-correlation properties. These sequences are BPSK (Binary Phase Shift Keying) modulated to fit the available bandwidth. The ultrasonic transmission period is 50 ms, in order to discard possible multipath effects between successive transmissions.

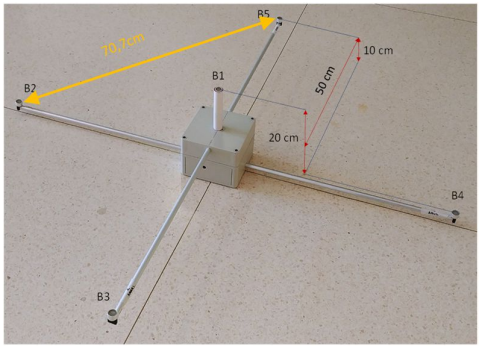

Fig. 5.2. General view of the 3D ULPS emitter unit deployed by the GEINTRA-US/RF group at the University of Alcala.

Fig. 5.3 depicts five ultrasonic transmissions from the five beacons of one ULPS in one emission period. However, in the case of three ULPS the number of ultrasonic transmitted signals will be multiplied by three (15 signals) in the same period of time but with a certain short delay, as the three ULPSs are not synchronized.

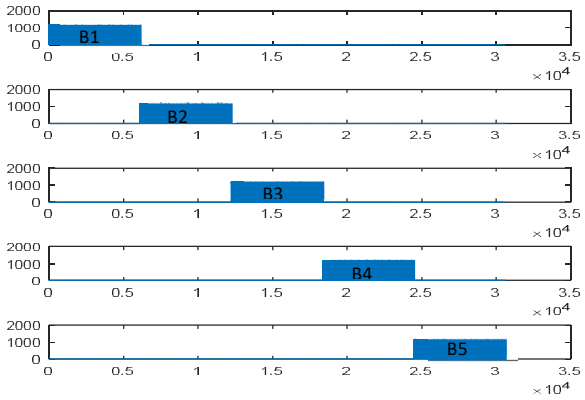

Fig. 5.3. Schemes of beacon transmissions: beacons emission pattern for five different transducers.

For this 3D configuration, the five beacons of each ULPS emitter are synchronized or with known delays between them, which will be discarded later in the algorithm. Also, the receiver does not need to be synchronized with the ULPSs, as the adopted method in the experimental tests is the hyperbolic positioning.

With regard to the reception stage, two types of ultrasonic receivers have been used. The 2D ultrasonic receiver prototype is used to make some preliminary tests of the ULPSs in both workspaces. Then the multiple ultrasonic prototype receiver, called 3D ultrasonic receiver prototype, is considered to realize all the last experimental results. The 3D ultrasonic receiver prototype employs three synchronized 2D ultrasonic receivers placed in the three faces of a triangular pyramid to acquire, at the same instants of time, ultrasonic signals coming from various directions and keeping all the functional properties of the 2D receiver prototype. Note that this 2D ultrasonic receiver prototype is capable of acquiring a data window with a length of 0.1s. Due to the geometry of the beacon units, this single receiver provides good performances whether it is oriented to the ULPS (the optimal acquisition is when the receiver is parallel to the ULPS), so it is possible to acquire the five ultrasonic transmissions involved. The problem arises when there are three ULPSs available in the environment, and where the 2D ultrasonic receiver will not be able to receive all the fifteen transmitted signals coming from various directions. This is the reason why a multiple receiver prototype has been proposed to maximize the probability of acquiring up to fifteen signals coming from the three beacon units, thus improving performance in position estimation, as it was explained in the previous chapter. As can be observed in Fig. 5.4.a), a 2D ultrasonic receiver prototype consists of an omnidirectional microphone, and in Fig. 5.4.b), a 3D ultrasonic receiver prototype consists of three omnidirectional microphones as it is composed of three 2D receivers.

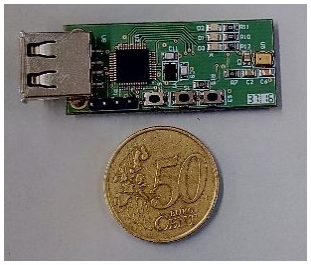

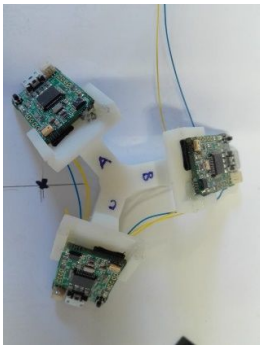

a) b)

Fig. 5.4. General aspect of the ultrasonic receivers modules: a) 2D ultrasonic receiver prototype and b) 3D ultrasonic receiver prototype.

Moreover, each microphone processes its TDOAs in an independent way. So, it is not necessary any synchronization between the microphones. Also, the same processing module is used for the three microphones with a master clock of 50 MHz and an acquisition frequency of 100 kHz (the minimum resolution step in the TDOA determination is then 10 μs).

5.1.2 Estimation of the Receiver's Position

After the installation of the three ULPSs in both environments, it is necessary to calibrate them to cover all the space and sort out the exact coordinates for each beacon in the three ULPSs, with respect to the global coordinate origin. The experimental setup calibration, as well as the ground-truth determination, have been carried out manually, by means of a laser plumb (for angles) and a laser distance meter (for distances).

In the case mentioned before, with three different ULPSs deployed in the environment and the multiple receiver prototype, three incoming received signals, $r_A[n]$, $r_B[n]$ and $r_C[n]$ are acquired, each one containing up to fifteen ultrasonic transmissions. Afterwards, for each one of these three acquired signals, fifteen correlations (45 correlations globally) are performed, involving the different fifteen 1023-bit Kasami sequences used to encode the ultrasonic emissions. These correlation functions and their maximum peaks are used to determine a set of TDOAs. Fig. 5.5 presents an example of the five correlation functions that are obtained at the receiver R_A only for ULPS-1, using different colors for each beacon B_i. As was mentioned before, the window size of the received signal $r_A[n]$ is 10.000 samples, corresponding to 0.1 s long. This size allows at least one emission period to be captured. Fig. 5.6 plots an example of the fifteen correlation functions that are obtained at the receiver R_A for the three ULPSs (ULPS-1, ULPS-2 and ULPS-3).

From the peaks obtained, the TDOAs can be easily obtained, by taking one of the beacons (e.g., beacon B_1) as reference. Finally, by multiplying these TDOAs by the speed of sound in air, we obtain the distance differences used in the hyperbolic positioning algorithm.

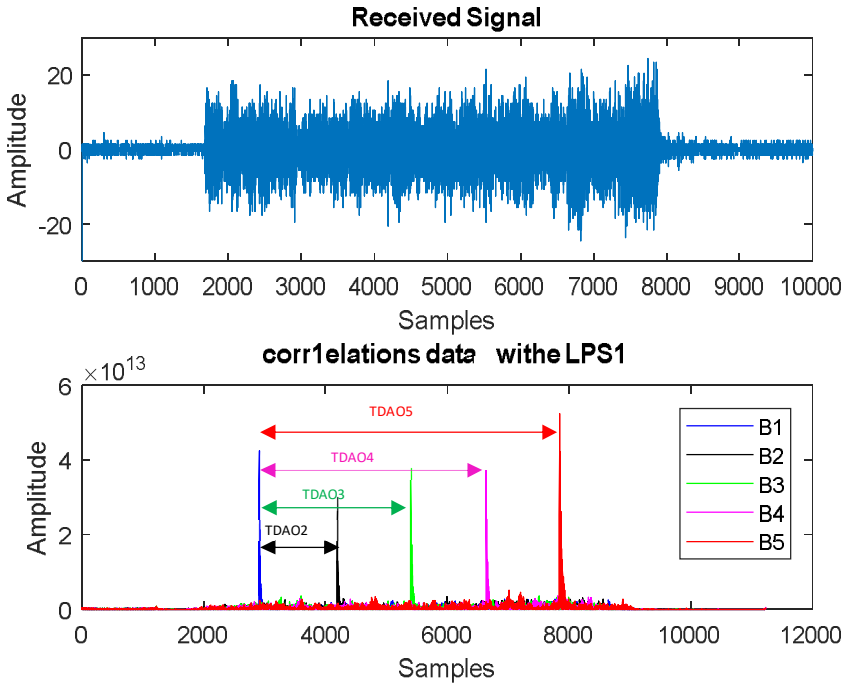

Fig. 5.5. Example of the received signal $r_A[n]$ (top) and the five correlation functions for ULPS-1 (bottom).

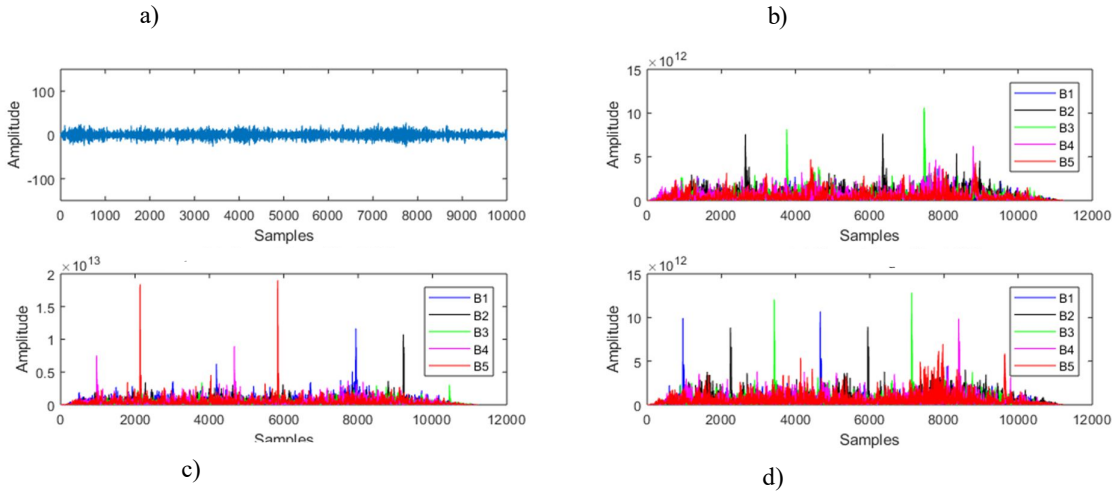

Fig. 5.6. Example of the received signal $r_A[n]$ (a) and the correlation peaks for the three ULPSs, ULPS-1 (b), ULPS-2 (c) and ULPS-3 (d).

The position of each receiver is estimated from these distance differences using a Gauss–Newton algorithm, which implies:

- Defining an initial position p_0 for the receiver (it should be chosen according to the a priori knowledge of the environment — in our case we consider the center of the positioning area). In the following steps of the algorithm, this position will be the previously obtained p_{k-1}.
- Minimizing the following function *f*(*x*, *y*, *z*), the difference of distances function using a Gauss-Newton (GN) minimization algorithm in order to minimize (5.1) on the hyperbolic case:

$$f(x, y, z) = \arg\min \sum_{i=1}^{I} (\Delta r_{1j} - \Delta \hat{r}_{1j}) \quad (5.1)$$

- where $\hat{\Delta} r_{1j} = \hat{r}_1 - \hat{r}_j$ are the theoretical distance differences computed at the last position of the receiver between the reference beacon B_1 and the others B_i (i = 2, …, n);

$$\Delta rij = ri - rj = \sqrt{(x - xi)^2 + (y - yi)^2 + (z - zi)^2} - \sqrt{(x - xj)^2 + (y - yj)^2 + (z - zi)^2} \quad (5.2)$$

- Estimating, at each step k, the new position $p_k = p_{k-1} + \Delta X$, and repeating the process until $\Delta \mathbf{X}$ becomes small enough (according to a pre-defined threshold).

Consequently, for any particular test point *P*, applying this algorithm at each receiver for each one of the three ULPSs, it is possible to obtain up to three different estimated positions for each receiver R_A, R_B and R_C , P_A (x_1, y_1, z_1), P_B (x_2, y_2, z_2) and P_C (x_3, y_3, z_3). Note that every ULPS has beacons emitting different codes and, consequently, the receiver is able to discriminate and calculate a position for each ULPS (if a large enough number of distance differences is obtained). These three resulting positions are merged. Two different fusing method have been applied.

The loosely coupled fusion, where the fusion is done after obtaining the estimated positions. Its whole process is detailed in Fig. 5.7. Three identical branches are applied for the three ultrasonic receivers (R_A, R_B and R_C). It is worth noting that the availability of nine position estimates at the input of the fusion module is optimistic. A last aspect to be considered is the computational load determined by the proposed signal processing. It requires the calculation of three demodulation processes for three input buffers, $r_A[n]$, $r_B[n]$ and $r_C[n]$, with a length of 10,000 samples, and a two-samples demodulation symbol. Afterwards, a total of 45 correlations are implemented, actually 15 per each demodulated signal, where the demodulated signal is still 10,000 samples long and the pattern sequence, assigned to each transmitter, has 1023 samples,

corresponding to the 1023-bit Kasami codes applied to the transmission encoding. A peak detector is performed in the resulting correlated signal, whose peaks are used to determine the partial positions P_A, P_B and P_C. The STM32F103 processor unit manages the acquisition system and the communication with a high-level device (Personal Computer PC, smartphone or tablet) via an USB port. So, all the proposals and tests have been validated hereinafter without real-time constraints.

Three fusion methods have been tested, the hybrid MLE/Mean fusion, the KF and the AKF. Real results will be presented and discussed below in the next section.

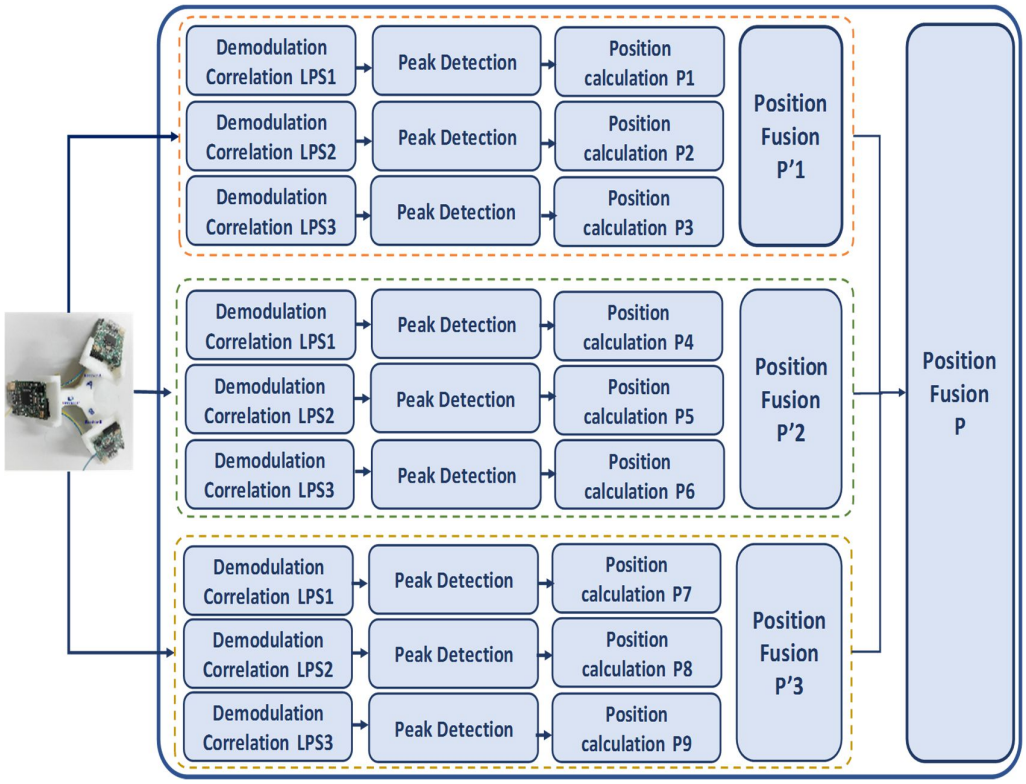

Fig. 5.7. Block diagram of the reception, processing, positioning and fusion of ultrasonic signals for the 3D configuration.

The tightly coupled fusion is applied after making again a BPSK demodulation succeeded by fifteen correlations with fifteen different 1023-bit Kasami sequences per receiver to be 3 BPSK demodulations and 45 correlations for the whole process of the three ultrasonic receivers (R_A, R_B and R_C). When peaks are obtained, the TDOAs and difference of distances can be easily calculated after considering the beacons B_1, always as reference. Finally, distance differences are used in the hyperbolic positioning algorithm, and used to update the previous positions.

Taking in account that the initial point is computed by the Gauss-Newton Algorithm, the principal fusion algorithm is the EKF. This procedure proposed for the tests applies in the following cases: firstly one EKF for only one ULPS in the ceiling; then three EKF modules for the three independent ULPSs; and, finally, only one EKF for the three ULPSs.

5.2 3D Positioning System: Characterizations and Performances

5.2.1 System Characterization: Scenario no. 1

To characterize the 3D ULPS, three asynchronous ULPSs are placed in the lab, which has a small space about 32.5 m^3, where ULPS-1 is fixed on the ceiling, ULPS-2 and ULPS-3 fixed on two perpendicular walls and in their centres as presented in Fig. 5.1.a). Both receivers have been used, the 2D ultrasonic receiver prototype and the 3D ultrasonic receiver prototype. A grid of 8 ground-truth positions in the lab have been tested, five positions (P1, P2, P3, P4 and P5) are at the same height z_1 =1.63 m and three positions (P6, P7 and P8) with different heights z_1 =1.64 m, z_2 =1.17 m and z_3 =0.59 m.

For the 2D ultrasonic receiver prototype, several emitted signals (up to 100) will be received, digitized and stored in a data buffer for the different ground-truth positions. For each signal three estimated positions can be computed, then about 300 estimated positions can be defined from 100 ultrasonic emissions. Whereas, the ideal orientation of the 2D ultrasonic receiver is to be put parallel with the emitter. As in this 3D configuration there are three perpendicular ULPSs so the 2D ultrasonic receiver, which is usually placed opposite to the one in the ceiling (ULPS-1), many signals coming from ULPS-2 and ULPS-3 will be lost. Then the number of the estimated position will be less than the number of emitted signals via different ULPSs. Thus, the number of detected positions is, generally, less than 100 per ULPS. To improve this drawback a 3D receiver ultrasonic is used and some results are presented. Firstly, in the laboratory workspace Fig. 5.8 presents the estimation of the mobile receiver applying ultrasonic signals coming from the three independent ULPSs at a point *P* in the space. Fig. 5.8.b) estimates the position using the 2D ultrasonic receiver prototype, then Fig. 5.8.b) estimates the position using the 3D ultrasonic receiver prototype. The number of estimated positions using the 3D ultrasonic receiver is bigger than using the 2D ultrasonic receiver prototype. As, in real cases, due to geometrical considerations, coverage areas, noise, and other constraints, some ultrasonic transmissions will not be detected at the receivers, thus posing a challenge to obtain the

aforementioned nine estimates. That is why the rest of all the experimental tests will be based on the 3D ultrasonic receiver prototype.

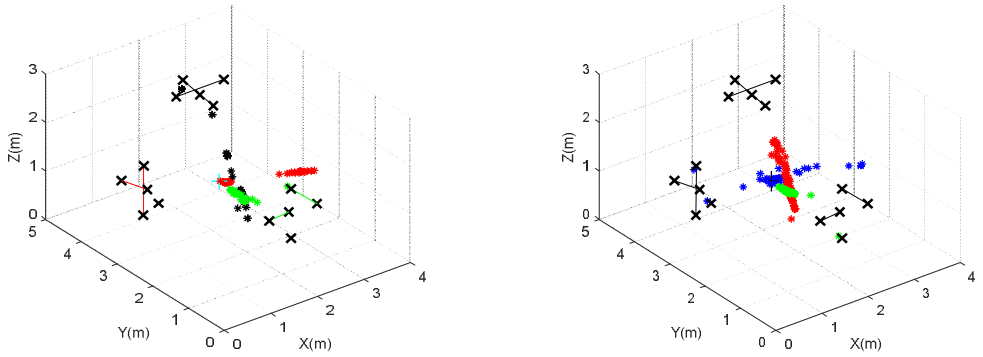

a) b)

Fig. 5.8. Clouds of estimated positions applying three independent ULPSs: a) using a 2D ultrasonic receiver prototype; and b) using a 3D ultrasonic receiver prototype.

It is worth highlighting that the positions to fuse are estimated for each ULPS and not including all the distances from all the ULPSs simultaneously (making a fusion at distance level), because each ULPS operates without a precise synchronization with the others.

Generally speaking, the positioning of any receiver should be carried out in real-time. Nevertheless, in order to use the MLE fusion algorithm, the variances (σ_{ix}^2, σ_{iy}^2, σ_{iz}^2) of the estimated positions in the X, Y and Z axes, where $i = \{1, 2, 3\}$ is the index of the ULPS i, must be known for a set of different ground-truth positions. For that, the final application of the proposal requires a training phase, where the aforementioned variances are obtained off-line for the volume under analysis. These variances are used later during real-time operation to estimate the receiver's position in the MLE/ Mean fusion. In Fig 5.9, a grid of estimated positions (P1, P2, P3, P4 and P5) are plotted in the lab workspace and for various heights in the space.

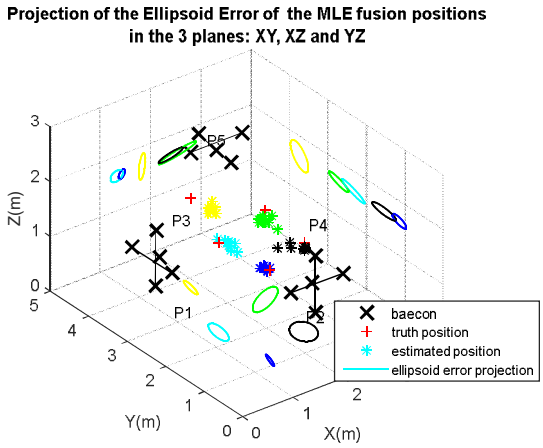

a)

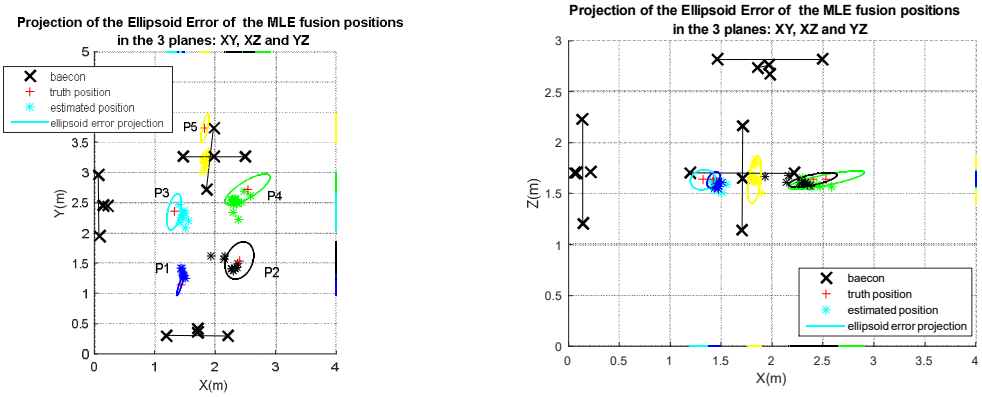

b) c)

Fig. 5. 9. Grid of estimated positions (P1, P2, P3, P4 and P5) after MLE fusion in the lab for the same height z_1 =1.63 m with a projection of the ellipsoid errors: a) 3D presentation; b) its projection in XY-plane; and c) its projection on the XZ-plane.

For the height z_1, the cloud of estimated positions (P1, P2, P3, P4 and P5) results has better accuracy than the estimated positions from the three independent ULPSs. The projection of its errors ellipsoid for 95% of the estimate positions is plotted in Fig. 5.9 using the same colour as the estimated position colour in the three coordinate planes. The error variances are more or less similar for all the estimated positions; P1 presents the lowest variance then better accuracy. The Z-axis mean errors are less than 0.25m at z_1, z_2 and z_3, where the cloud of estimated positions (P6, P7 and P8), after fusion, grows when its height is farther from the ULPSs positions, as shown in Fig. 5.10 and summarized in Table 5.2.

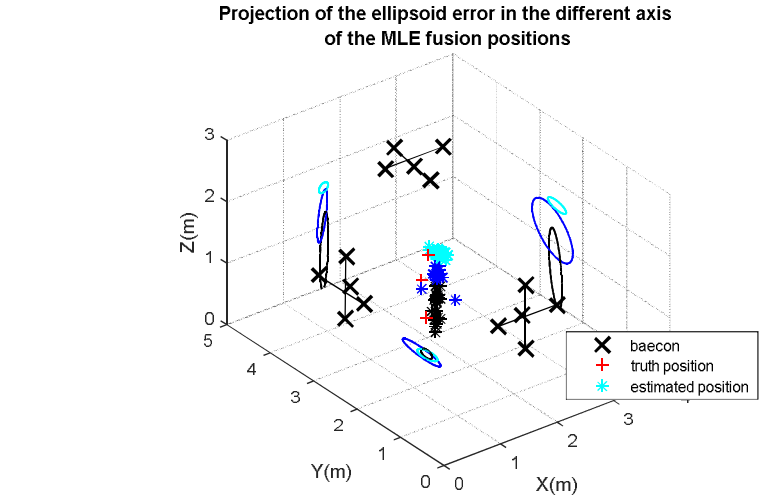

a)

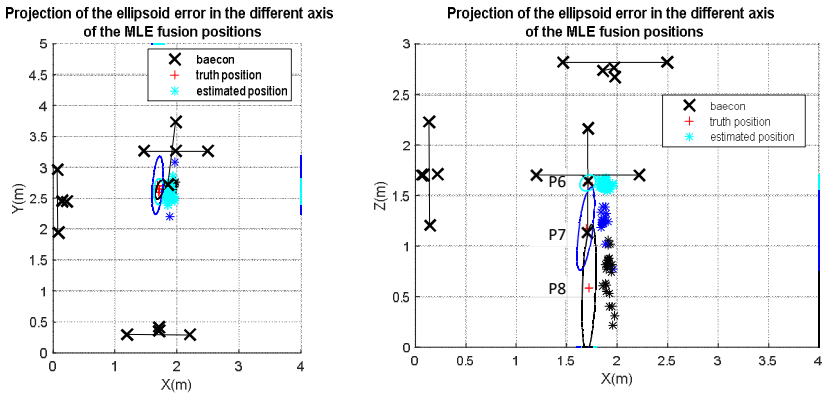

b) *c)*

Fig. 5.10. Grid of estimated positions (P6, P7 and P8) after MLE fusion in the lab for different heights z1=1.62m, z2=1.17m and z3=0.59m with a projection of the ellipsoid errors: a) 3D presentation; b) its projection in the XY-plane; and c) in the XZ-plane.

Some X-axis errors appear due to a calibration error of ULPS-3 and errors in the measuring device. This vertical error is also related to the distance and orientation of the 3D ultrasonic receiver from each ULPS. The error variances are different for all the mobile receiver positions and for the different projections in size and directions when the height changes. Table 5.2 provides a summary about mean error and the standard deviation (Std) per axis for positions (P1, P2, P3, P4 and P5) sharing the same height z_1 and the other positions (P6, P7 and P8) for heights z_1, $z_2$and z_3. In the same way, for the Y-axis, mean errors for points P2, P3, P4 and P5 is between 0.4 m and 0.9m, so they have the less accurate estimated positions whereas P1, P6,

P7 and P8 are the more accurate because their mean errors are less than 0.1m, as they are just below ULPS-1.

			Mean error (m)		Std deviation(m)	
Positions	X(m)	Y(m)	Z(m)	X(m)	Y(m)	Z(m)
P1	0.143	0.075	0.047	0.043	0.075	0.035
P2	0.040	0.177	0.049	0.022	0.064	0.028
P3	0.288	0.750	0.020	0.133	0.091	0.013
P4	0.041	0.965	0.038	0.045	0.110	0.020
P5	0.003	0.534	0.032	0.017	0.083	0.066
P6	0.166	0.009	0.019	0.028	0.055	0.019
P7	0.162	0.007	0.404	0.032	0.139	0.147
P8	0.228	0.045	0.453	0.025	0.036	0.224

Table 5.2. Error mean and std per axis for lab estimated positions after MLE fusion.

Finally, for the Z-axis mean errors and standard deviations, the lowest mean error, standard deviation and also the smallest ellipsoid error is for P1. The greatest mean error, standard deviation and biggest ellipsoid errors are for P7 at z_2 and P8 at z_3, as those positions are farther away from the height of the ULPSs. As well as at z_1, the receiver positions (P1, P2, P3, P4 and P5) have the lowest z-axis mean error, which is due to their position via the positions of ULPS-2 and ULPS-3. So, they present the more accurate positions.

The 90% of the empirical error CDF for various tests in the laboratory workspace are shown in Fig. 5.11. At z_1 =1.63 m, the error CDF are presented by continuous lines and the horizontal positions (P1-P5). Then, the positions (P6-P8) for several heights (z_1- z_3) are plotted with broken lines in a vertical plane. Generally, the worst accuracy is for P3 where its CDF error is below 1.3m, then the CDF for the rest of positions (P1, P2, P4 and P5) is below 0.4 m. The best accuracy is for P1 and P2, where their error is below 0.2m, then for P4 where its error is below 0.55 m, finally the error of P5 which is below 1m. Now changing the height of the mobile receiver, the empirical error for 90% of estimated positions for P6, P7, and P8 (placed successively at z_1 =1.628 m, z_2 =1.17 m, and z_3 =0.59 m) increases when its position height decreases and moves away from the ULPSs height, to be between 0.58m for P8 and 0.18m for P6.

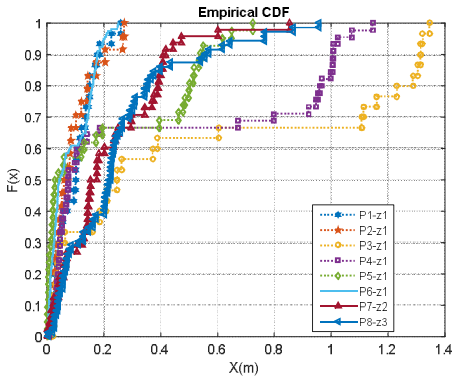

Fig. 5.11 Error CDF of 90% of the estimated positions after the MLE fusion in the lab, solid line for (P6, P7and P8) in various heights z_1, z_2 and z_3, the dotted lines are for (P1,P2, P3,P4 and P5) in the grid of position sharing the same height z_1.

In this section, the 3D positioning system has been experimented in a small workspace (the lab). Several tests have been done to know the ultrasonic proprieties for the proposed ULPSs distribution, as the influence of the directions of the signals on each other, the needed signals strength, the interference phenomena, the multipath effects due to the existed furniture and close walls. Signal proprieties have been adjusted and the 3D positioning system presents good results for the preliminary tests for independent and fused ULPSs (MLE Fused method). This system will be applied later in an extended workspace (the hall) to generalize its properties and its performances.

5.2.2 System Application: Scenario no. 2

New experimental tests have been carried out for the proposed setup, according to scenario no. 2 previously described in Fig. 5.1.b). The three ULPSs have been installed to cover an approximated volume of 196 m^3, on the ceiling and two perpendicular walls. However, in this scenario, the ULPSs are not placed on the center of the three perpendicular walls, due to some architecture drawbacks of the hall. The beacons from the three ULPSs are encoded with fifteen different 1023-bit Kasami sequences, whereas a multiple ultrasonic receiver prototype has been placed on a set of seven measurement points (P'1–P'7); as plotted in Fig. 5.12; at the same heights z_1 = 1.35 m and z_2 = 1.93 m.

Firstly, one hundred measurements have been acquired and stored at each position for the three ULPSs. Those measurements are used to compute the variances of each position via the various

ULPSs, in an offline study, then stored to be used later in the online positioning system, when the variances are needed (in the loosely coupled fusion methods).

Secondly, thirty measurements have been obtained at each point (P'1-P'7), for the online study. Various real results have been obtained in these points, using only one ULPS (e.g., ULPS-1), three independent ULPSs, and then fused to highlight the differences regarding the use of three ULPSs before and after fusion.

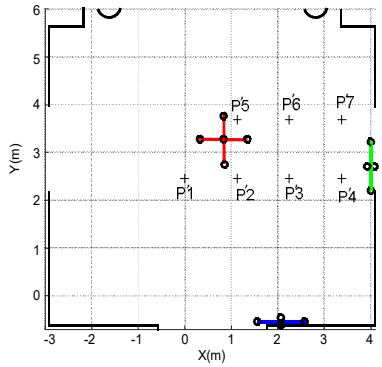

Fig. 5.12. Workspace configuration and the considered grids of positions for the experimental tests of positioning performances.

i. Positioning Performance for a Single ULPS

Particularly for the LOCATE-US ULPS, its accuracy decreases as the receiver gets further away from the center of the coverage area in the perpendicular direction to the ULPS. Several tests have been carried out only for ULPS-1 (the red one on the ceiling), according to the coordinates aforementioned in Table 5.1. For that purpose, a grid of receiver's positions P'1–P'7 has been considered at two different heights (z_1 = 1.35 m and z_2 = 1.93 m), as can be observed in Fig 5.12. Note that, in the analysis developed at this stage, the points are selected to cover a specific area of the second workspace (the hall). At each position P'1–P'7, thirty ultrasonic measurements have been carried out, using hyperbolic trilateration with the Gauss–Newton positioning algorithm described before. Fig.5.13 shows the results for ULPS-1 at both heights z_1 and z_2. Note that the different positions P'1–P'7 have been distinguished by using different colors. There is a significant dispersion along the ultrasonic emission direction. This uncertainty in the determination of coordinate z (the perpendicular axis to the plane where the ULPS-1 is installed) increases when the distance between the ULPS and the receiver does. This is why those results for z_1 and z_2 present more concentrated clouds of points, especially with regard to the coordinate z. For the same reason, ULPS-1 is suitable for the estimation of coordinates x and y, with a

better performance for the points in the center of the coverage zone, such as points P'1, P'2 and P'5 (blue, pink and cyan diamonds in Fig. 5.13). The same behavior can be derived for ULPS-2 and ULPS-3 that are installed on two perpendicular walls, so their highest dispersions are in the *y*-axis and the *x*-axis, respectively.

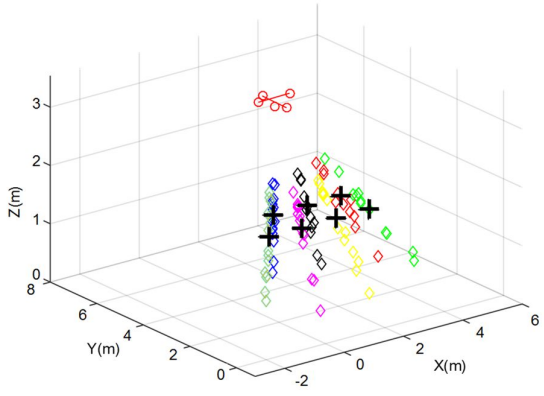

a)

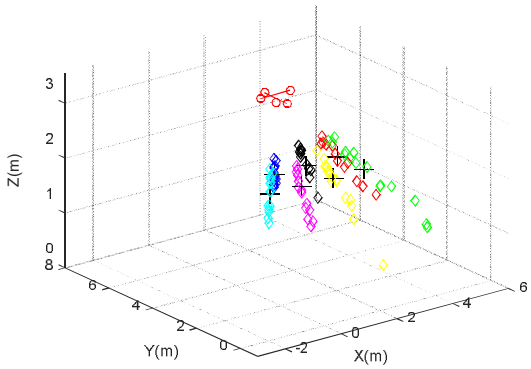

f)

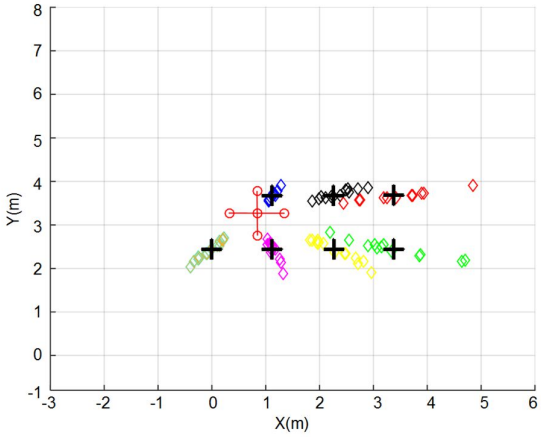

b)

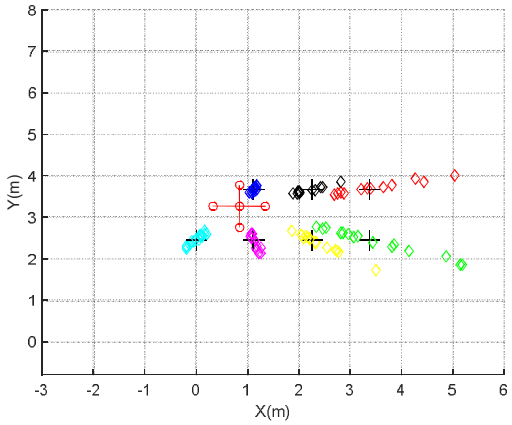

g)

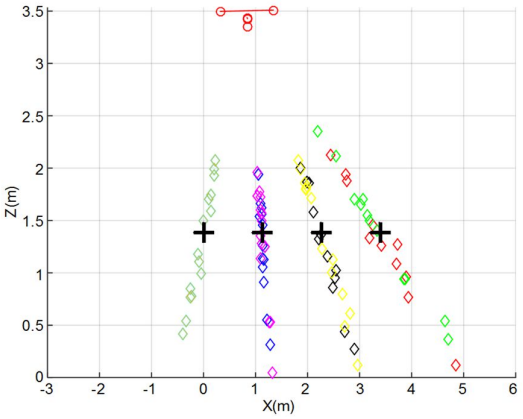

c)

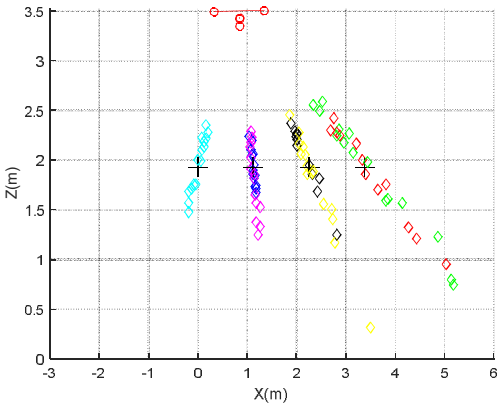

h)

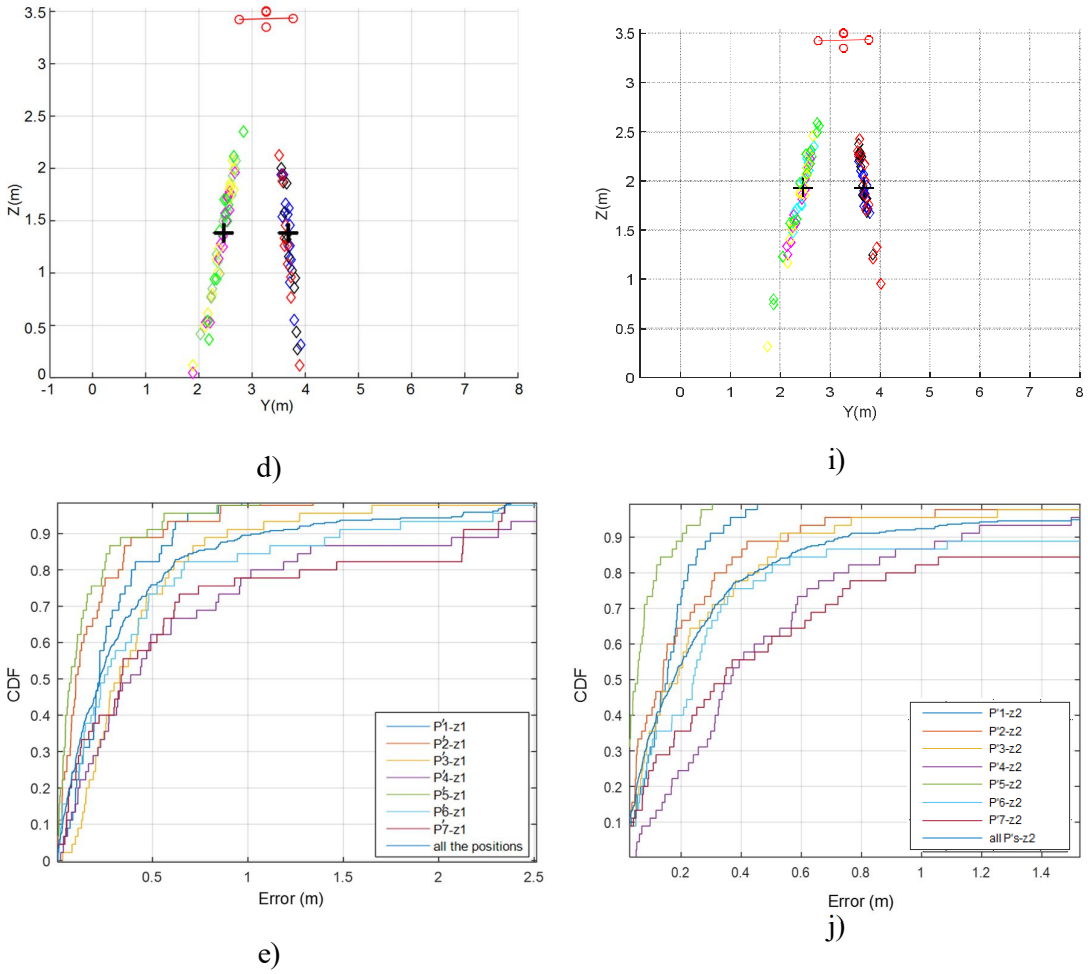

Fig. 5.13. Results obtained in the same test points (P'1–P'7) in the case of using only ULPS-1: (a–e) are the cloud of points and the error CDF for the test-points at z_1 = 1.35 m, whereas (f-j) shows also the cloud of points and the error CDF at z_1 = 1.93 m.

Comparing Fig. 5.13 for both heights, z_1 and z_2, the improvement is clear. For instance, in the error CDFs, considering all the test-points, for 90% of the cases errors are below 1.1 m at z_1 =1.35 m and below 0.75 m for z_2 =1.93 m.

In the Hall scenario, the 3D positioning system is composed also of three ULPSs placed in known positions in three perpendicular planes (the ceiling and two perpendicular walls), and the 3D ultrasonic receiver set in the 7 points (P'1 - P'7). The obtained estimated positions, for independent ULPSs, are dispersed in the space as Expected. Three sets of estimated positions have been calculated from three independent ULPSs: the set of red points are the estimated positions from ULPS-1 (in the ceiling), the set of blue and the green points are successively the

estimated positions from ULPS-2 and ULPS-3 where the dispersion of the estimated positions are high in the direction of emission of each ULP, as plotted in the Fig. 5.14.

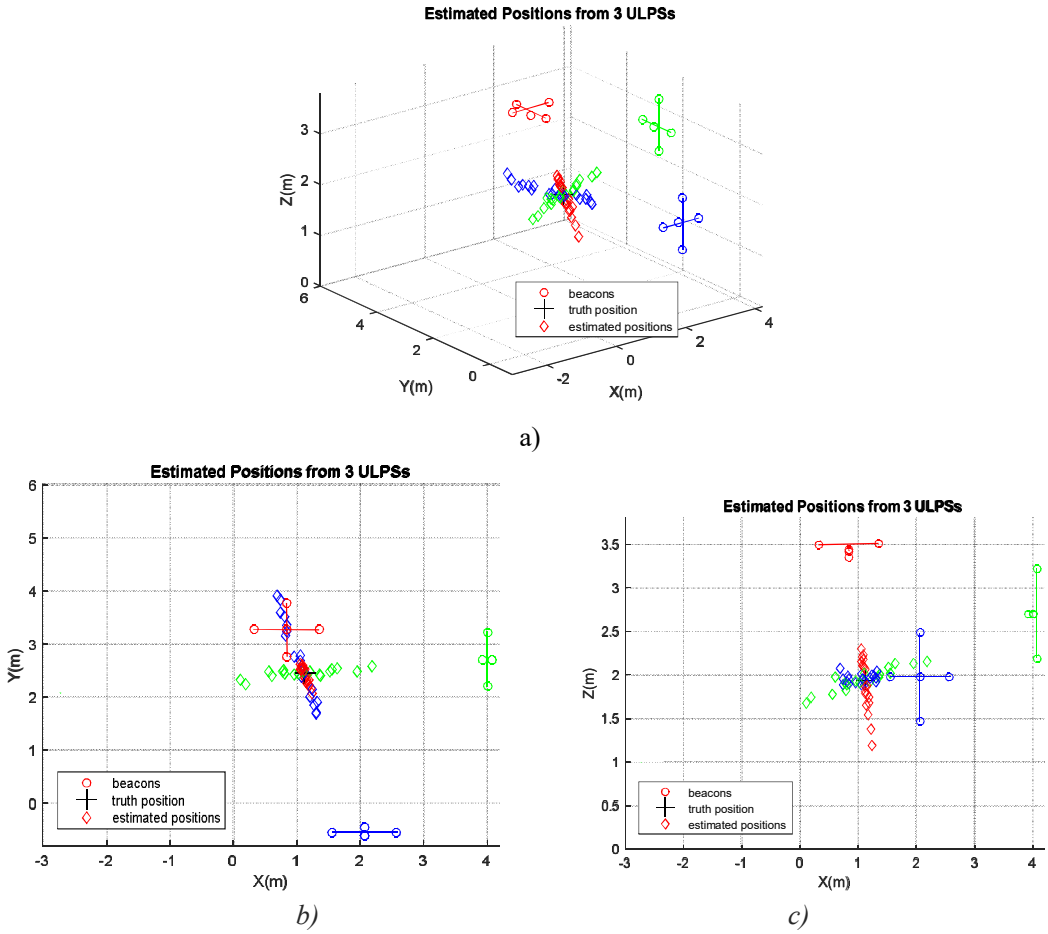

Fig. 5.14. A receiver position and its estimated positions from the three independent ULPSs at =1.94m: a) the 3D estimated positions of the receiver, b) projection of the intersection of the different independent ULPSs positioning in the XY plane and c)) projection of the intersection of the different independent ULPSs positioning in the YZ plane.

Table 5.3 extends these comparisons of errors for 90% of the cases, between the results obtained using only one ULPS at the both heights. The error CDF at z_1 is higher than the error CDF at z_1. Also, it depends on the position of the receiver with respect to the ULPSs to be between the decimeter and the meter ranges.

	z_1			z_2		
Points	*Before Fusion (m)*					
	ULPS-1	*ULPS-2*	*ULPS-3*	*ULPS-1*	*ULPS-2*	*ULPS-3*
P'1	0.608	2.061	1.383	0.297	3.318	4.367
P'2	0.551	1.165	1.246	0.556	1.012	1.293
P'3	0.892	0.872	1.010	0.53	0.762	0.494
P'4	2.313	0.998	0.823	1.134	1.057	0.187
P'5	0.472	0.788	2.578	0.204	2.072	1.091
P'6	1.482	1.165	1.010	1.686	1.65	0.527
P'7	2.130	1.863	0.679	2.049	1.19	0.542

Table 5.3. Positioning error containing 90% of the estimated positions at z_1=1.35 m and z_2=1.93 m.

To improve the accuracy of the final position estimation, several fusion algorithms are used. Some algorithms are applied to the obtained estimated positions and other ones are applied to the difference of distances, as explained in the next sections.

ii. Positioning Performance by merging ULPSs

a. Loosely coupling fusion

- Hybrid MLE/Mean Fusion

It is worth mentioning that all the ULPSs are detected at all the test points (P'1–P'7). Fig. 15 plots all these experimental results after applying the MLE/Mean fusion algorithm. It has been arranged to easily compare results at both heights: z_1 = 1.35 m corresponds to all the subplots on the left and z_2 = 1.93 m to those on the right. Successive rows include the following: Fig. 15.a-e) presents, successively, the 3D representation of the clouds of points obtained around every test point (P'1–P'7), as well as the projections of their corresponding uncertainty ellipsoids on the three coordinate planes; the projections of the clouds of points on the coordinate planes Y-X, Z-X and Z-Y, also the CDFs for the positioning error corresponding to the results obtained at each test point and for all of them. And Fig. 15.f-j) presents the indicated results in z_2.

Note that results for z_2 = 1.93 m are better, as the test points are nearer to the ULPSs and more centred with respect to their coverage area. In fact, the dispersion of results is greater as the test points are further from the centre of the coverage area. Regarding the CDFs, it is straightforward to conclude that the performance of points P'3, P'4 and P'5 are the best, followed by P'6 and P'2 and, finally, P'1 and P`7 (the last is the worst due to its bad coverage from all the ULPSs).

Furthermore, note that, on average for all the test points, errors are always below 0.26 m for z_1 = 1.35 m and below 0.19 m for z_2= 1.93 m, in both cases for 90% of the cases.

Left side: results for height z_1 = 1.35 m.

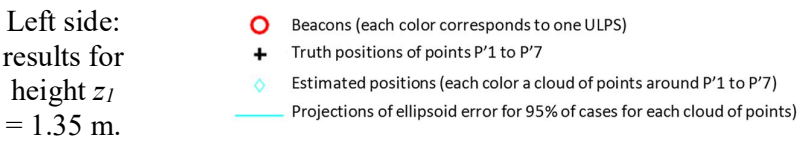

Right side: results for height z_2= 1.93 m.

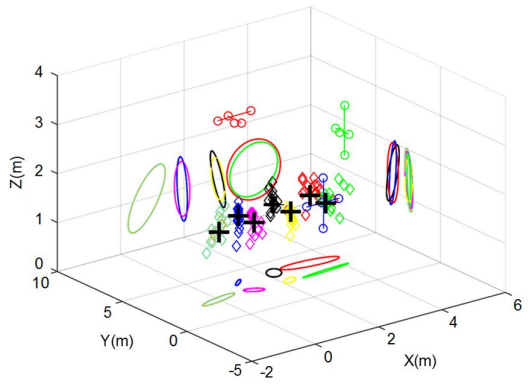

a)

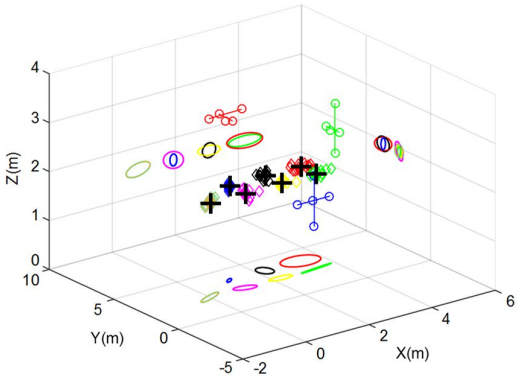

f)

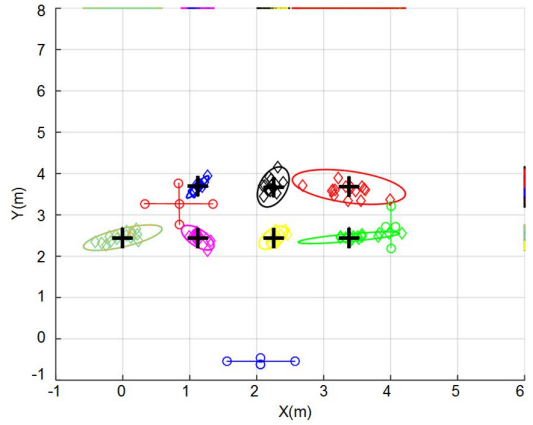

b)

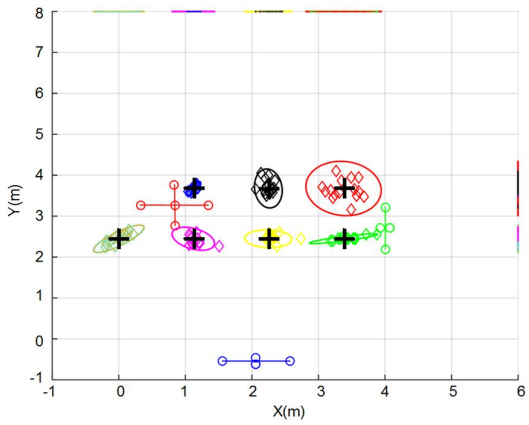

g)

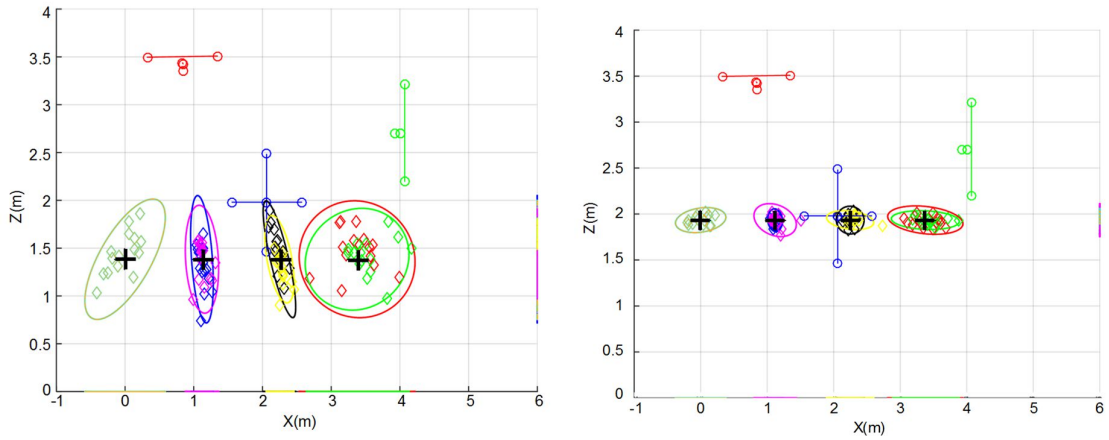

c) h)

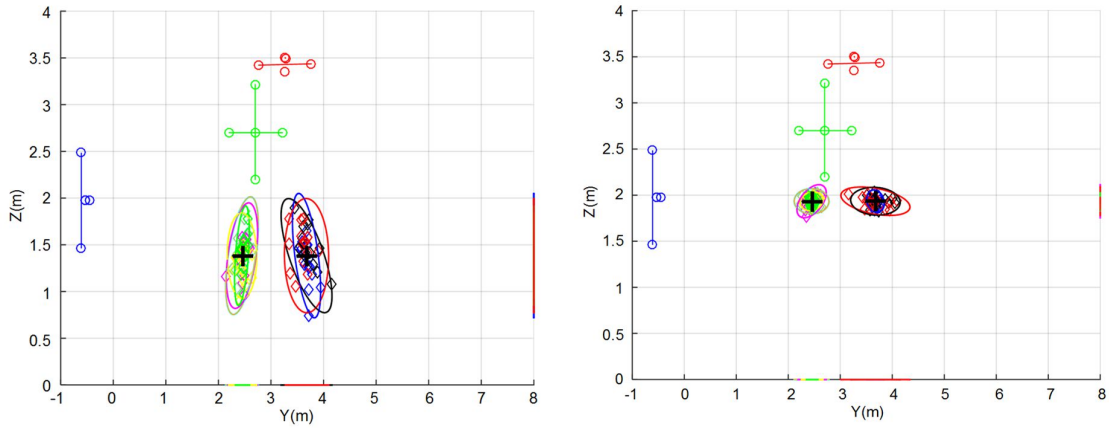

d) i)

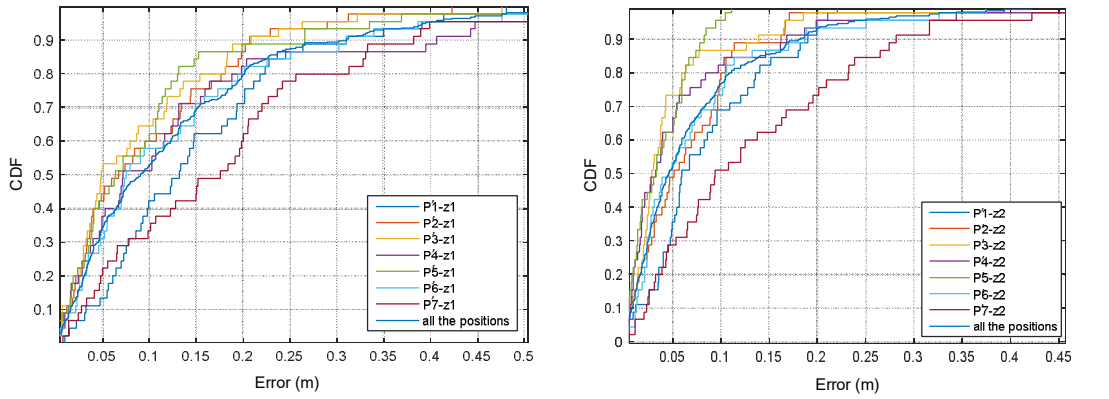

e) j)

Fig. 5.15. Experimental results for the test points (P'1–P'7) for both heights, z_1 = 1.35 m on the left and z_2 = 1.93 m on the right: the clouds of points; its various projections and the experimental CDFs for the results at each test point. All the cases include the projections of their corresponding error ellipsoids with a certainty of 95%, after the average and the maximum likelihood estimation (MLE) fusion.

In summary, the performances of this proposal for both considered heights, z_1 and z_2, are similar, resulting better estimation for z-coordinate at z_2. It can be observed how the fusion improves performance at both heights; the positioning error, for 90% of the cases, remains below 28 cm roughly for all the central test points (at planes z_1 and z_2) and below 28 cm for all cases in plane z_1=1.35m (with the exception of point P'7 that increases to 38 cm). It is important to point out that these are maximum errors for 90% of the cases and not average errors, which, as can be observed in Table 5.4, are below 10 cm in most cases.

	Z_1						Z_2					
Positions	*Mean Error (m)*			*Std Deviation (m)*			*Mean Error (m)*			*Std Deviation (m)*		
	X(m)	*Y(m)*	*Z(m)*	*Y(m)*	*Z(m)*	*Y(m)*	*X(m)*	*Y(m)*	*Z(m)*	*X(m)*	*Y(m)*	*Z(m)*
P'1	0.047	0.046	0.055	0.046	0.055	0.046	0.643	0.112	0.250	0.347	0.072	0.101
P'2	0.014	0.087	0.059	0.087	0.059	0.087	0.762	0.112	0.250	0.347	0.072	0.101
P'3	0.042	0.458	0.052	0.458	0.052	0.458	0.022	0.167	0.019	0.019	0.306	0.031
P'4	0.194	0.346	0.020	0.346	0.020	0.346	0.167	0.296	0.117	0.255	0.474	0.047
P'5	0.025	0.062	0.226	0.161	0.317	0.179	0.161	0.601	0.032	0.088	0.240	0.023
P'6	0.064	0.631	0.005	0.051	0.738	0.068	0.048	0.323	0.045	0.034	0.403	0.021
P'7	0.401	0.756	0.138	0.233	0.901	0.140	0.383	1.129	0.052	0.296	0.942	0.012

Table 5.4. Mean error and standard deviation for the position estimates when applying MLE/Mean fusion method at z_1 = 1.35 m and z_2=1.93 m.

- Kalman Filter Fusion

In this subsection, a Kalman Filter (KF) is used to merge the obtained estimated positions (up to nine) from the three ULPSs, as was explained in chapter 4. Results obtained from the Kalman Filter (KF) are different for the seven points (P'1-P'7). This variation is related to the positions of the mobile receiver with respect to the different ULPSs. Estimated positions after fusion are often better than estimated positions issued from independent ULPSs, as presented in Fig. 5.16. A 3D presentations of the grid of estimated positions are plotted with their different plane projections at z_1 in Fig.5.16.(a-d) and at z_2 in Fig.5.16.(f-i). Also, a CDF error is plotted for both cases, the average CDF error for all the points is 0.72 m at z_1 and 0.34 m at z_2, as plotted in Fig.5.16.e and j.

.

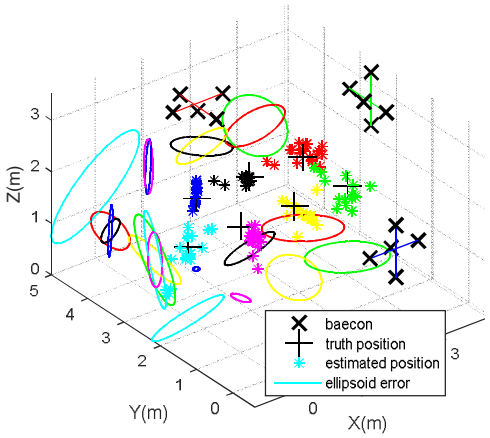
Z(m)
Y(m)
X(m)
baecon
truth position
estimated position
ellipsoid error

a)

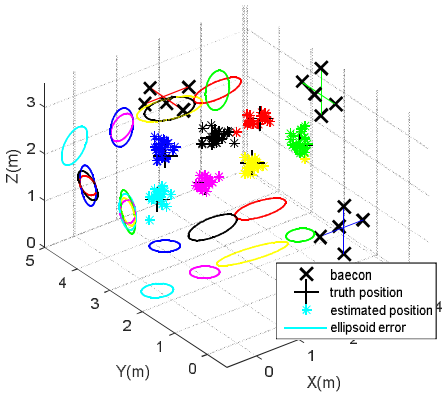
Z(m)
Y(m)
X(m)
baecon
truth position
estimated position
ellipsoid error

f)

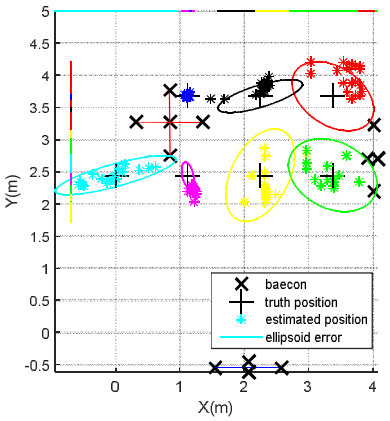
Y(m)
X(m)
baecon
truth position
estimated position
ellipsoid error

b)

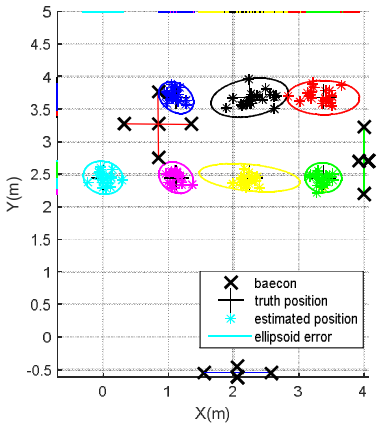
Y(m)
X(m)
baecon
truth position
estimated position
ellipsoid error

g)

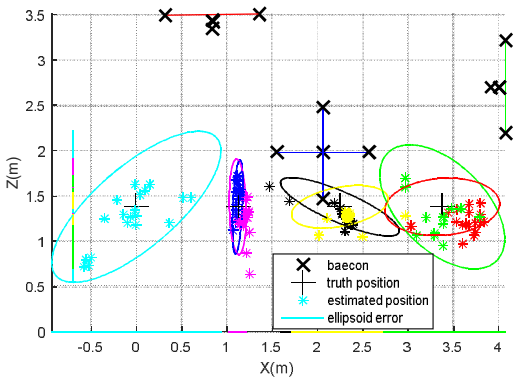
Z(m)
X(m)
baecon
truth position
estimated position
ellipsoid error

c)

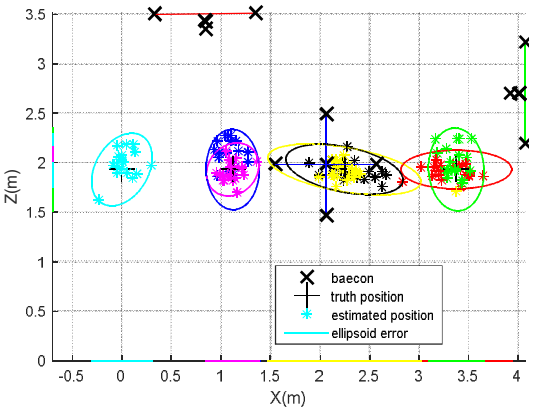
Z(m)
X(m)
baecon
truth position
estimated position
ellipsoid error

h)

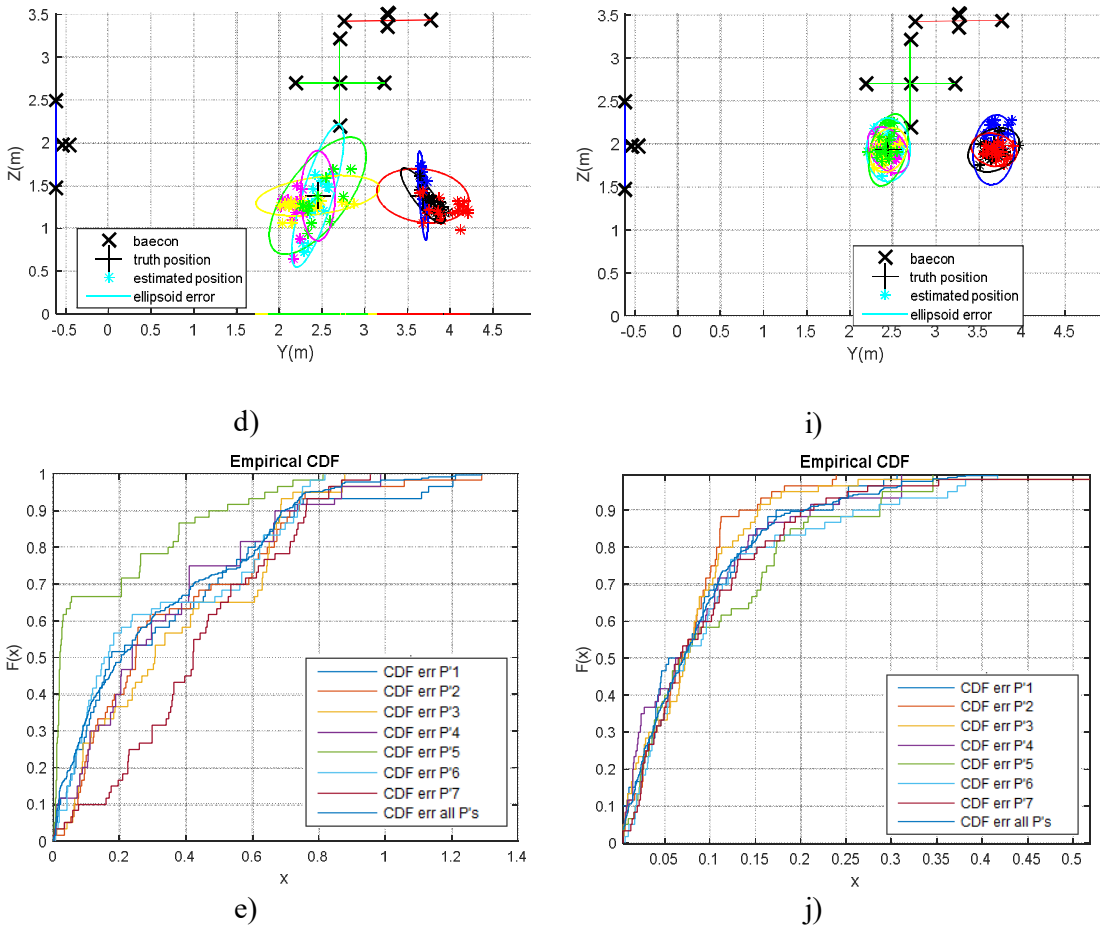

Fig. 5.16. Experimental results for the tested points (P'1–P'7) for both heights, z1= 1.35 m on the left (a-e) and z2 = 1.93 m on the right (f-j): successively 3D representation of clouds of points; Y-X projections; Z-X projections; Z-Y projections and experiment CDFs for the results at each test point after a Linear Kaman Filter fusion.

Table 5.5 shows the mean error and the Std deviation for positions (P'1-P'7) at both heights z_1 and z_2. The value z1presents the less accurate for the z-axis between 0.3 m and 0.08 m, as well as it was improved at $z_2$to become between 0.05 m and 0.11 m. Also, the positions at z_2 are more accurate for the three axes.

	Z_1						Z_2					
Positions	*Mean Error (m)*			*Std Deviation (m)*			*Mean Error (m)*			*Std Deviation (m)*		
	X(m)	*Y(m)*	*Z(m)*	*X(m)*	*Y(m)*	*Z(m)*	*X(m)*	*Y(m)*	*Z(m)*	*X(m)*	*Y(m)*	*Z(m)*
P'1	0.248	0.093	0.658	0.223	0.054	0.298	0.074	0.071	0.110	0.080	0.053	0.089
P'2	0.083	0.254	0.705	0.033	0.071	0.188	0.070	0.073	0.079	0.061	0.042	0.055
P'3	0.140	0.266	0.685	0.149	0.133	0.083	0.140	0.064 0.	0.071	0.238	0.056	0.056
P'4	0.192	0.175	0.608	0.165	0.106	0.244	0.083	0.061	0.119	0.059	0.059	0.115

P'5	0.018	0.016	0.418	0.011	0.012	0.185	0.079	0.068	0.176	0.061	0.058	0.118
P'6	0.132	0.131	0.640	0.191	0.078	0.115	0.165	0.082	0.074	0.140	0.069	0.050
P'7	0.313	0.286	0.714	0.104	0.186	0.113	0.163	0.077	0.058	0.127	0.059	0.041

Table 5.5. Mean errors and standard deviations of estimated positions when applying the Linear Kalman Filter at z_1 = 1.35 m and z_2=1.93 m for all the test points (P'1-P'7).

- Adaptive Kalman Filter

In this subsection, an adaptive Kalman Filter (AKF) is used to merge the obtained estimated positions (up to nine also) from the three independent ULPSs. Fig. 5.17 shows the experimental results for the set of points (P'1-P'7) at both heights z_1 and z_2. Fig.5.17 presents the estimated positions for the grid of points (P'1-P'7) implementing the AKF fusion. The 3D presentation, and the various planes projections at z_1 in Fig.5.17.a-d and at z_2 in Fig.5.17.f-i. For this case also z_2 have the best accuracy, as explained by the CDF errors for 90% of positions. In Fig. 5.17.e, the mean CDF error is 0.346 m at z_1. Whereas, in Fig.5.17.j the mean CDF error is 0.162 m at z_2.

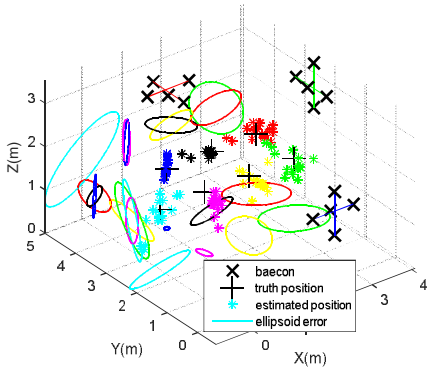

a)

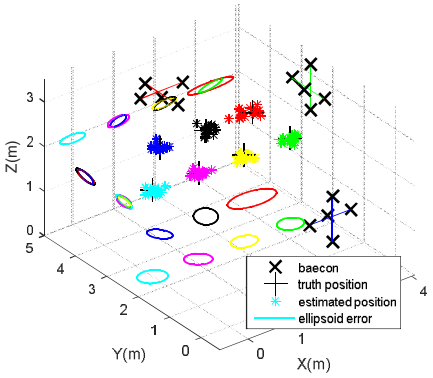

f)

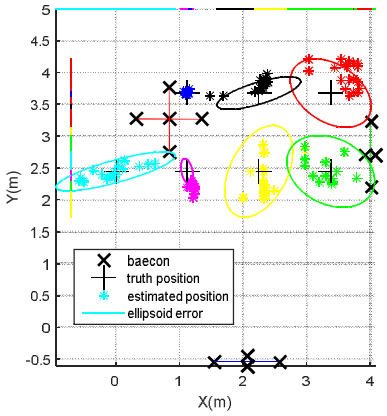

b)

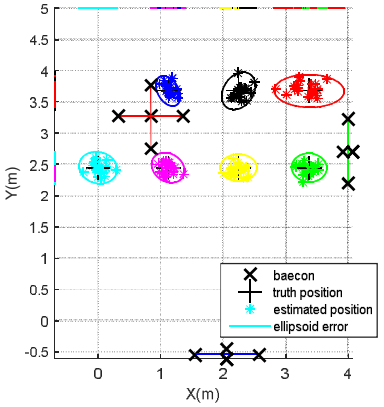

g)

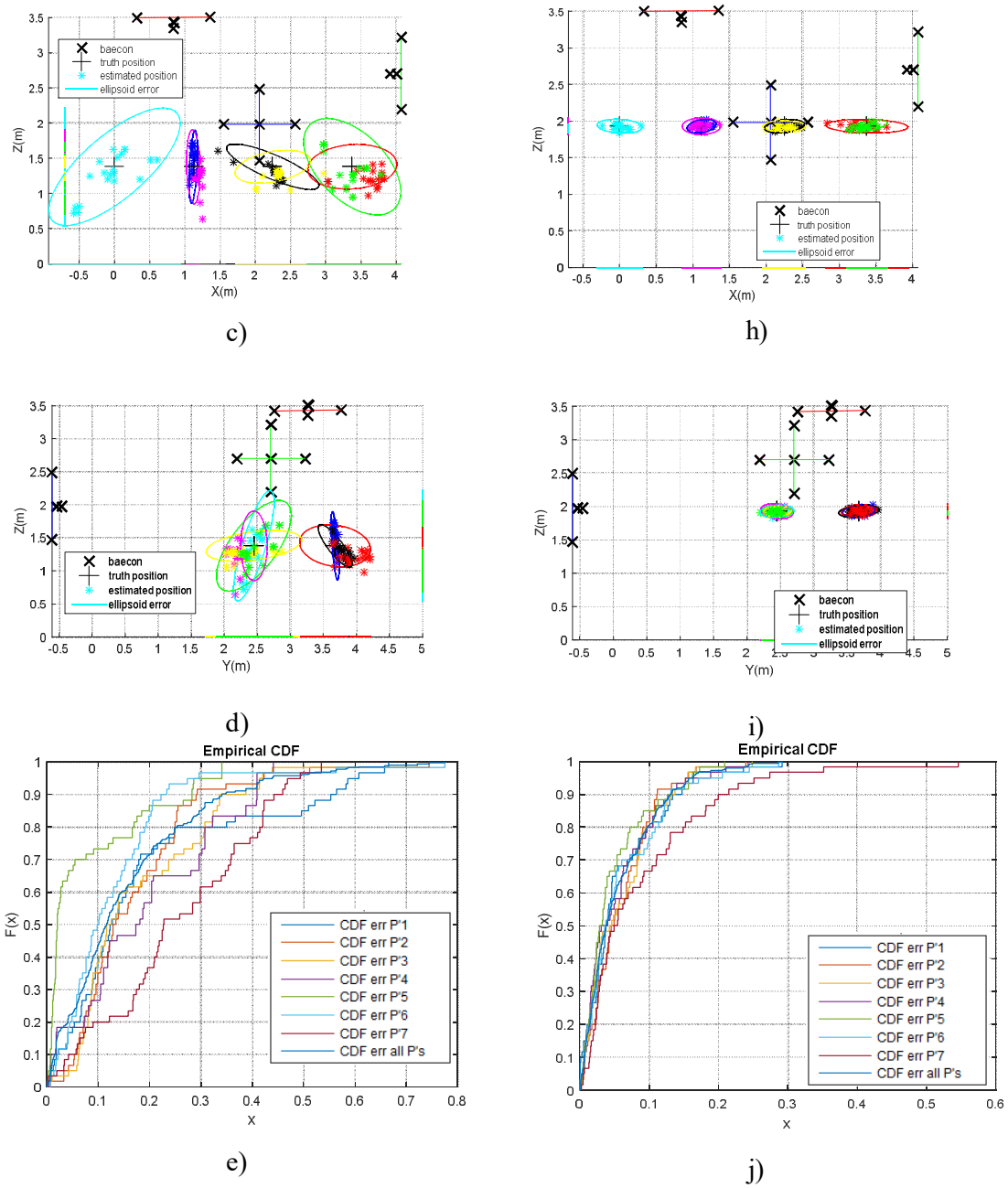

Fig. 5.17. Experimental results for the test points (P'1–P'7) for both heights, z_1= 1.35 m on the left and z_2 = 1.93 m on the right: 3D representation of clouds of points; Y-X projections; Z-X projections; Z-Y projections; experimental CDF errors for the set of points when applying an Adaptive Kaman Filter fusion.

Table 5.6 shows the mean error and the Std deviation for the positions (P'1-P'7) at the both heights z_1 and z_2. The height $z_1$presents a large error in the z-axis, higher than 0.14 m for all the grid, then in the y-axis to be higher than 0.1 m for all the points, whereas at z_2 the z error decreases to less than 0.03 m. The positions at z_2 are always more accurate for the tree axes.

Positions	Z_1						Z_2					
	Mean Error (m)			*Std Deviation (m)*			*Mean Error (m)*			*Std Deviation (m)*		
	X(m)	*Y(m)*	*Z(m)*	*X(m)*	*Y(m)*	*Z(m)*	*X(m)*	*Y(m)*	*Z(m)*	*X(m)*	*Y(m)*	*Z(m)*
P'1	0.248	0.093	0.240	0.223	0.054	0.202	0.074	0.071	0.028	0.080	0.053	0.021
P'2	0.083	0.254	0.177	0.033	0.071	0.170	0.070	0.073	0.033	0.061	0.042	0.021
P'3	0.140	0.266	0.139	0.149	0.133	0.083	0.088	0.064	0.024	0.053	0.056	0.016
P'4	0.192	0.175	0.206	0.165	0.106	0.138	0.083	0.061	0.023	0.059	0.059	0.019
P'5	0.018	0.016	0.198	0.011	0.012	0.100	0.052	0.068	0.024	0.050	0.058	0.023
P'6	0.132	0.131	0.126	0.191	0.078	0.076	0.072	0.082	0.025	0.067	0.061	0.018
P'7	0.313	0.286	0.174	0.104	0.186	0.103	0.163	0.077	0.028	0.127	0.059	0.016

Table 5.6. Mean errors and standard deviations for the estimated positions when applying Adaptive Kalman Filter at z_1 = 1.35 m and z_2=1.93 m.

b. Tightly Coupling Fusion

- Extended Kalman filter for one single ULPS

An EKF is used to fuse only one single ULPSs' signals (ULPS-1), installed on the ceiling. Therefore, after receiving the five ultrasonic transmissions, the algorithm detects the peaks of those five signals and compute the differences of distances (TDOA) to be used later to compute the initial position using the Gauss-Newton algorithm. Thereafter, this position will be updated by the EKF using the range of distances computed from the TDA. In this case, the EKF matrices size is up to 4 x 4 to estimate the new positions. Assuming that the distribution of the estimated positions is Gaussian, where the mean is the ground-truth position and the σ is its variance in the space (σ =0.2 m), to see the behaviour of this filter when this one increases. After some simulations, the corresponding results are presented in Table 5.10, following the same scheme as before and the same heights, z_1 =1.35 m and z_2 = 1.93 m. It is possible to observe that, when the variance increases, the size of the cloud of the estimated positions becomes bigger, consequently the accuracy decreases.

The CDF has been calculated for a variance (0.2 m) using an EKF for ULPS-1, plotted in Fig 5.18 for both heights. The mean of the CDF error for the seven positions when the value of σ =0.2 m, is 0.44 m at $z_1$and 0.432 m at z_2.

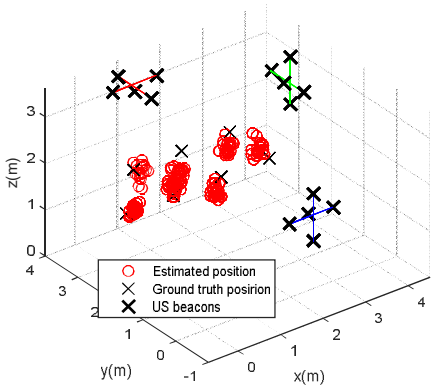
Estimated position
Ground truth posirion
US beacons
z(m)
y(m)
x(m)

a)

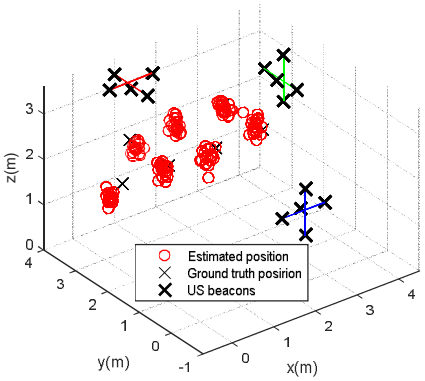
Estimated position
Ground truth posirion
US beacons
z(m)
y(m)
x(m)

e)

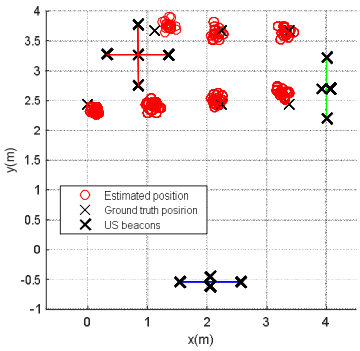
Estimated position
Ground truth posirion
US beacons
y(m)
x(m)

b)

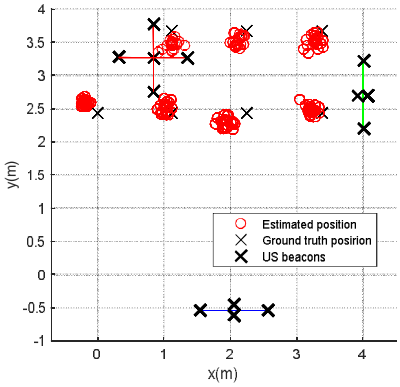
Estimated position
Ground truth posirion
US beacons
y(m)
x(m)

f)

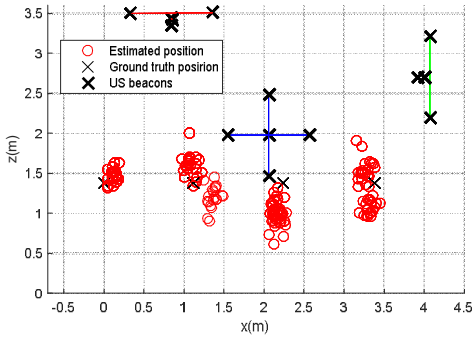
Estimated position
Ground truth posirion
US beacons
z(m)
x(m)

c)

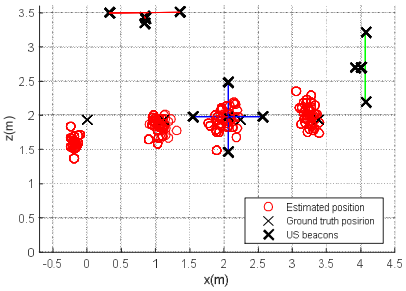
Estimated position
Ground truth posirion
US beacons
z(m)
x(m)

g)

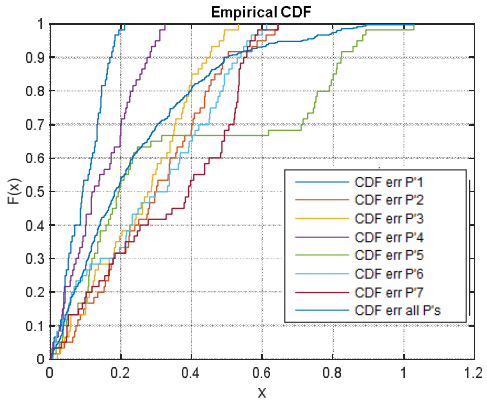

d)

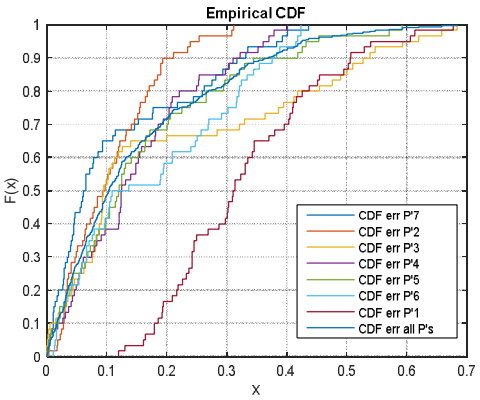

h)

Fig. 5.18. Estimated positions for. a single ULPS (on the ceiling) implementing an EKF, and the CDF error for 90% of the positioning estimates for a variance σ=0.2m.

The cloud of the estimated positions are more or less equal for all the seven positions, no matter the axis or the position, although the size of those clouds decreases from z_1 to z_2, as happened before. At z_1, the lowest mean errors and standard deviation, as well as the smallest errors ellipsoid, are for P'1, P'2 and P'5, the most central points in the covered volume of ULPS-1. Hence, the worst results are obtained for P'3, P'4, P'6 and P'7, where there is some bias caused by their long distance from the central axis of the coverage volume of the ULPS-1.

	Z_1							Z_2					
Positions	*Mean Error (m)*			*Std Deviation (m)*				*Mean Error (m)*			*Std Deviation (m)*		
	X(m)	*Y(m)*	*Z(m)*	*X(m)*	*Y(m)*	*Z(m)*		*X(m)*	*Y(m)*	*Z(m)*	*X(m)*	*Y(m)*	*Z(m)*
P'1	0.027	0.164	0.032	0.028	0.047	0.020	0.025	0.041	0.118	0.018	0.030	0.087	0.027
P'2	0.052	0.103	0.041	0.045	0.058	0.025	0.226	0.047	0.020	0.050	0.027	0.034	0.052
P'3	0.285	0.054	0.035	0.203	0.045	0.023	0.194	0.033	0.085	0.258	0.021	0.051	0.285
P'4	0.367	0.027	0.046	0.454	0.025	0.053	0.384	0.096	0.120	0.426	0.052	0.051	0.367
P'5	0.091	0.087	0.231	0.053	0.042	0.036	0.041	0.027	0.149	0.024	0.020	0.047	0.091
P'6	0.324	0.090	0.084	0.040	0.024	0.046	0.154	0.044	0.165	0.029	0.023	0.039	0.324
P'7	0.460	0.064	0.052	0.025	0.031	0.031	0.317	0.027	0.233	0.037	0.020	0.027	5.7

Table 5.7. Mean error and standard deviation for the estimated position with only one ULPS and the EKF for σ =0.2 m.

- Three independents Extended Kalman filter

Here, three EKFs are used to fuse the three independent ULPSs. Hereinafter, for clarity's sake, the variance of the estimated positions will be σ=0.2 m. Therefore, the estimated positions will

be updated by the three independent EKF using the distances measured from the ultrasonic transmissions. Some experimental tests have been applied, and results are presented in Fig. 5.19. Three various clouds of estimated positions have been detected per point, one cloud per ULPS. Again, the same heights are considered for the receiver, z_1 =1.35 m and z_2 =1.93 m. As it is possible to observe, the variance dispersion of the seven clouds is the same roughly.

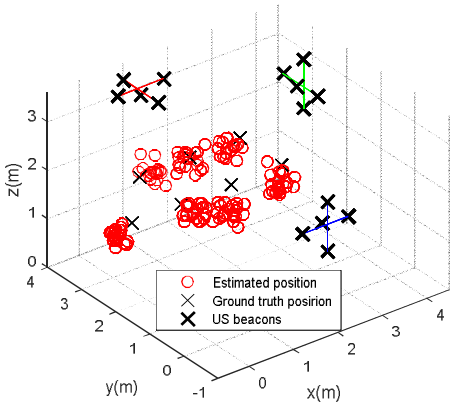

a)

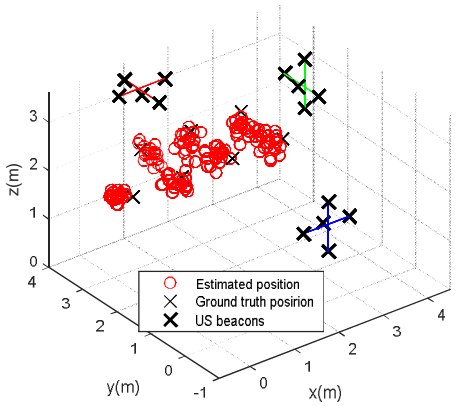

e)

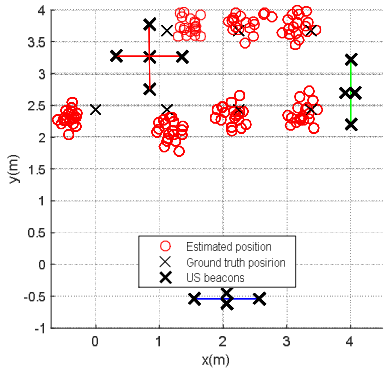

b)

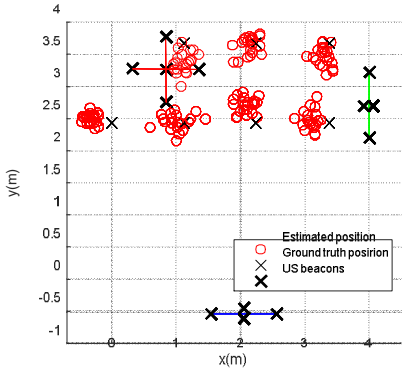

f)

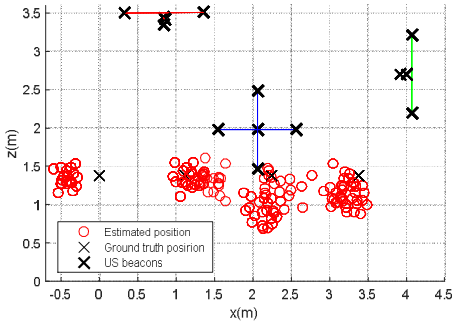

c)

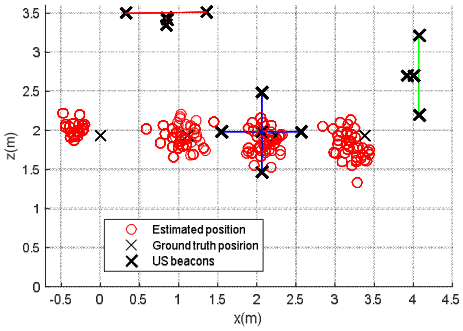

g)

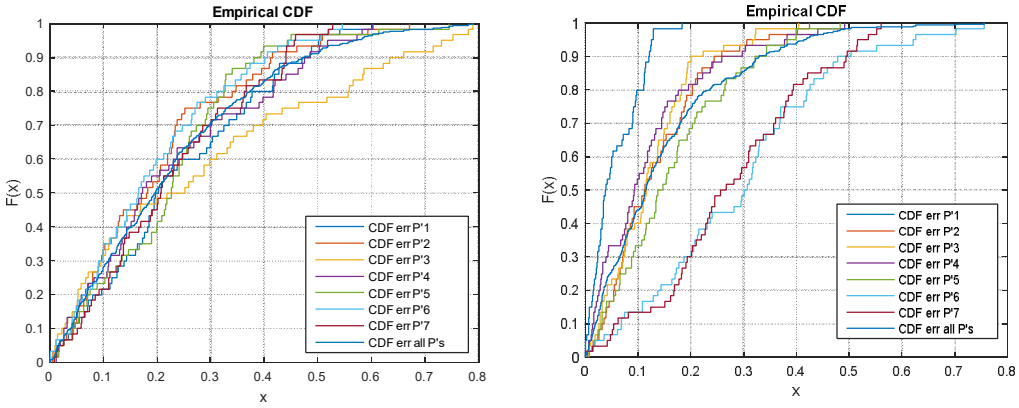

d) h)

Fig. 5.19. Estimated positions and the CDF error for 90% of the estimates with three independent EKFs and three ULPSs for σ=0.2 m.

In this instance, the mean error and the standard deviations are computed and mentioned in Table 5.8 for the set of seven positions (P'1-P'7). The points P'3, P'4, P'6 and P'7 are the least accurate positions. This creates bias as they have furthest distances from ULPS1. Furthermore, the positions P'1 P'2 P'5 and P'6 are the best at z_1 because they are just below ULPS-1. Likewise, at z_2, P'1, P'2 and P'6 are the least accurate positions. Generally, all the mean errors and the standard deviations for three independent EKF (three ULPSs) are higher than those with one EKF and ULPS-1.

	Z_1						Z_2					
Positions	*Mean Error (m)*			*Std Deviation (m)*			*Mean Error (m)*			*Std Deviation (m)*		
	X(m)	*Y(m)*	*Z(m)*	*X(m)*	*Y(m)*	*Z(m)*	*X(m)*	*Y(m)*	*Z(m)*	*X(m)*	*Y(m)*	*Z(m)*
P'1	0.418	0.153	0.148	0.084	0.095	0.092	0.324	0.079	0.394	0.080	0.057	0.090
P'2	0.113	0.355	0.142	0.078	0.149	0.094	0.182	0.094	0.253	0.128	0.075	0.122
P'3	0.131	0.143	0.573	0.116	0.107	0.139	0.284	0.260	0.284	0.117	0.120	0.137
P'4	0.139	0.150	0.394	0.102	0.093	0.163	0.271	0.110	0.278	0.100	0.104	0.140
P'5	0.261	0.140	0.267	0.181	0.102	0.100	0.102	0.210	0.115	0.084	0.142	0.097
P'6	0.132	0.170	0.277	0.098	0.120	0.159	0.136	0.110	0.165	0.100	0.084	0.091
P'7	0.357	0.123	0.197	0.111	0.107	0.095	0.093	0.293	0.352	0.054	0.160	0.141

Table 5.8. Mean errors and standard deviations for three ULPSs and three independent EKF with σ=0.2 m.

The CDF errors for 90% of the obtained estimated positions at z_1 is between 0.35 m and 0.7 m, to become more accurate at z_2 where these values become between 0.26 m and 0.43 m. The

CDF error values are greater than the one single EKF with ULPS-1, as the use of a combination of three EKF and the corresponding independent ULPSs, as plotted in Figs. 5.19.d) and 5.19.h).

- One Extended Kalman filter for the three ULPSs

Experimental results have been carried out for the seven positions (P'1-P'7) at z_1 and z_2, with a variance of σ =0.2 m. As plotted in Fig. 5.20, the clouds of the seven positions are more concentrated around the ground-truth points, whereas their dispersions are low as well.

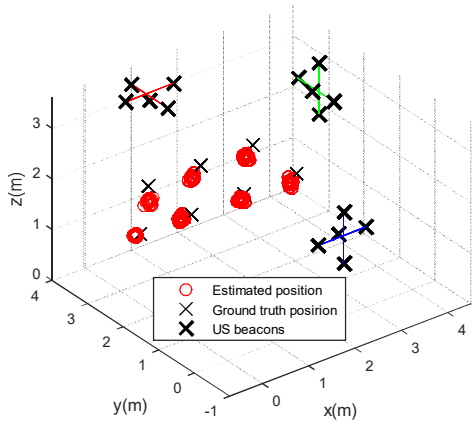

a)

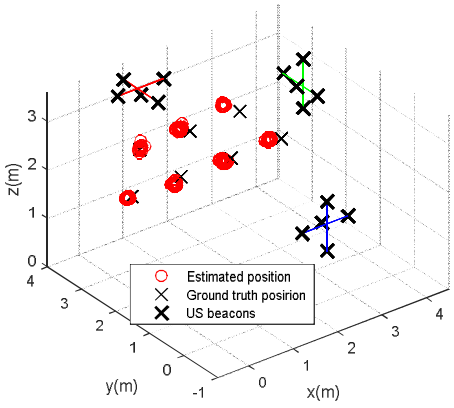

e)

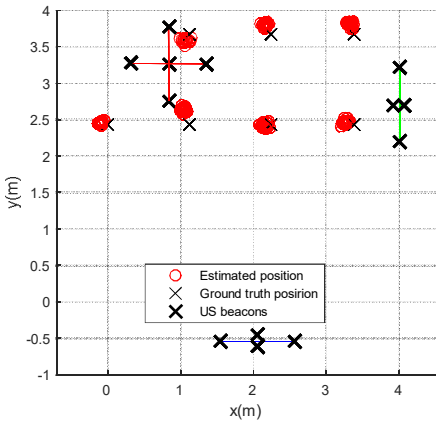

b)

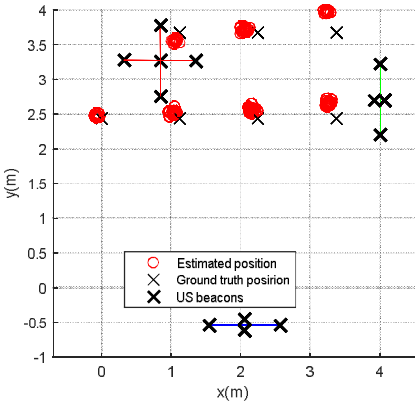

f)

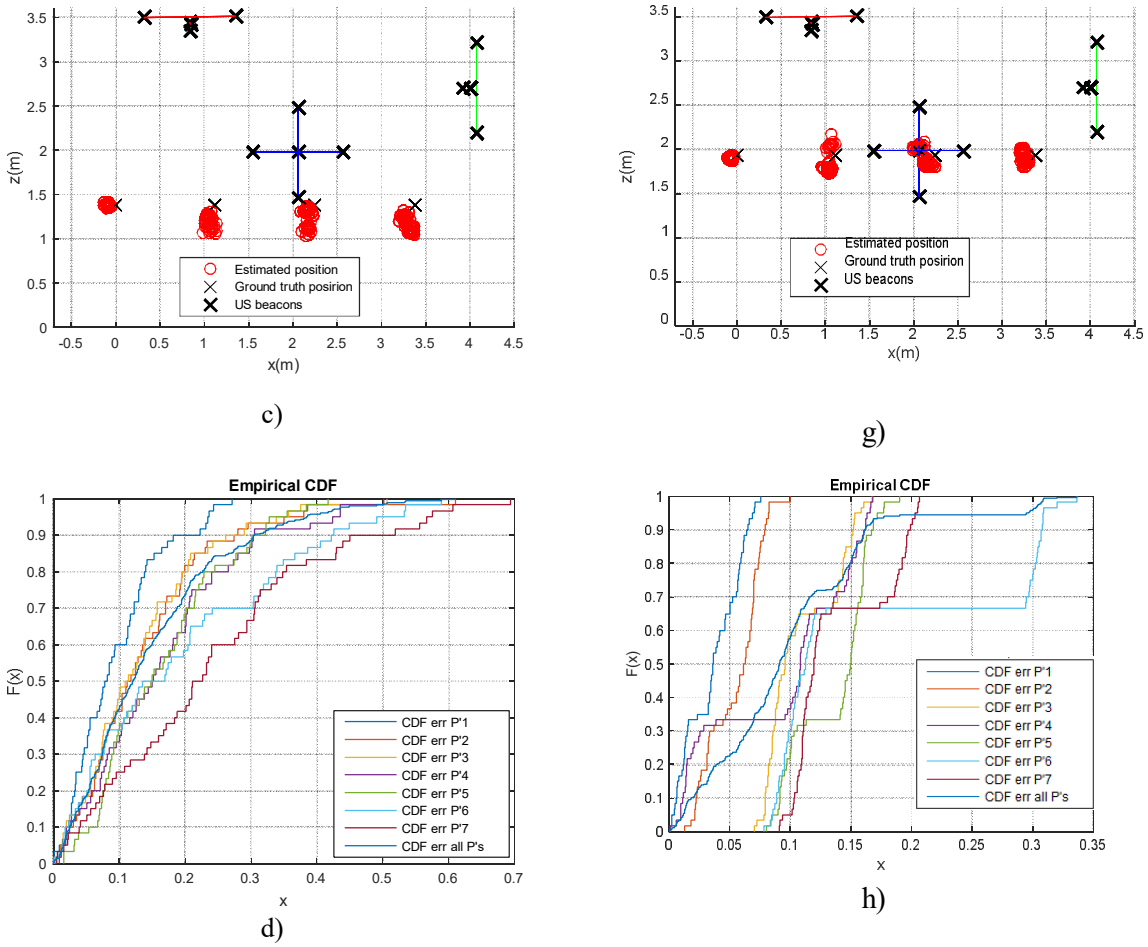

Fig. 5.20. Estimated positions and CDF of the positioning errors (90% of positions), for one EKF and three ULPS (σ=0.2 m); a-d) at z_1 and e-h) at z_2 for σ=0.2 m.

The mean errors and the standard deviations are calculated and considered in Table 5.9 for the seven positions (P'1-P'7). All the axis errors decrease for both heights, especially for z_2, to be less than 0.17 m at z_1 and less than 0.13 m at z_2. The CDF errors for 90% of the cases for the seven studied points (P'1-P'7) are between 0.18 m and 0.45 m at z_1, and between 0.065 m and 0.3 m at z_2, as plotted in Fig. 5.20.d) and 5.20.h).

	Z_1						Z_2					
Positions	*Mean Error (m)*			*Std Deviation (m)*			*Mean Error (m)*			*Std Deviation (m)*		
	X(m)	*Y(m)*	*Z(m)*	*X(m)*	*Y(m)*	*Z(m)*	*X(m)*	*Y(m)*	*Z(m)*	*X(m)*	*Y(m)*	*Z(m)*
P'1	0.143	0.076	0.060	0.067	0.062	0.038	0.061	0.009	0.037	0.006	0.004	0.006
P'2	0.135	0.104	0.176	0.080	0.071	0.151	0.074	0.062	0.027	0.008	0.009	0.007
P'3	0.121	0.168	0.111	0.119	0.097	0.079	0.087	0.090	0.147	0.010	0.010	0.008

P'4	0.140	0.197	0.157	0.100	0.136	0.112	0.108	0.015	0.153	0.006	0.008	0.010
P'5	0.129	0.204	0.155	0.076	0.101	0.103	0.156	0.156	0.095	0.012	0.009	0.007
P'6	0.102	0.337	0.135	0.092	0.142	0.117	0.105	0.098	0.105	0.009	0.011	0.012
P'7	0.225	0.397	0.097	0.109	0.148	0.066	0.110	0.114	0.110	0.008	0.007	0.010

Table 5.9. Mean errors and standard deviations for three ULPS and a single EKF (σ =0.2 m).

iii. High Sampling Frequency Approach

In this configuration, we assume that the receiver computes and estimates its positions in a short range of time, when the emission period of ultrasounds is 10 ms and the receiver moves a distance of 0.228 m per period. These estimated positions become too close to each other to make a tracking way of its shifting and velocities. The same trajectory, composed of the seven points (P'1-P'7), is used. Additionally, the fusion of three ULPSs by only one EKF is applied. Simulations have been done using a variance of 0.2 m at z_1 and z_2. The resulting estimations are plotted in Fig. 5.21. It is possible to observe that, even when the sampling frequency increases, the positioning performance is not affected, and the positioning system keeps tracking its way with suitable accuracies, especially for z_2 where the Z-axis errors improve

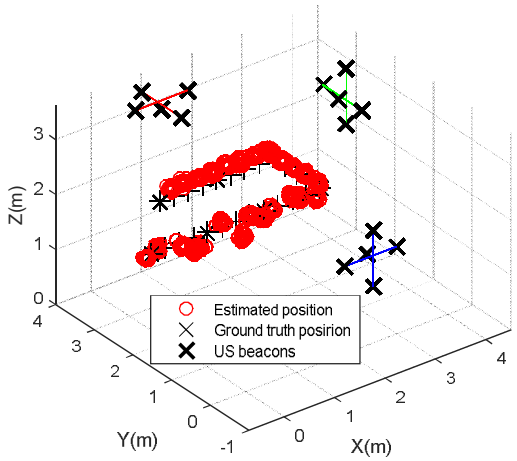

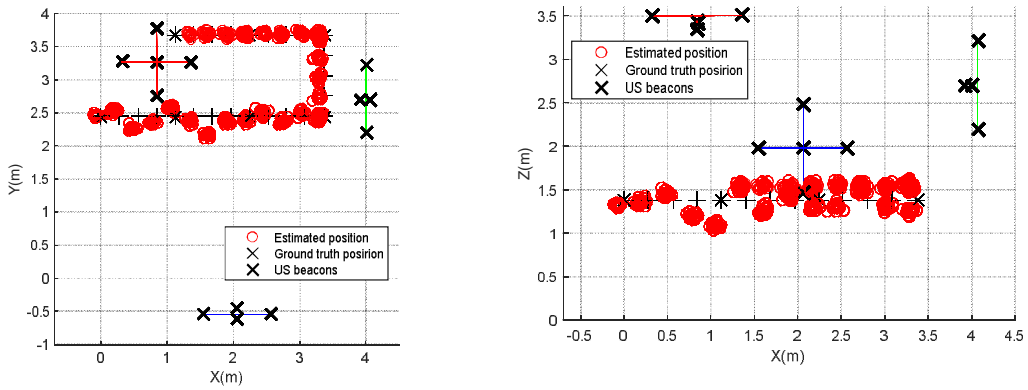

a)

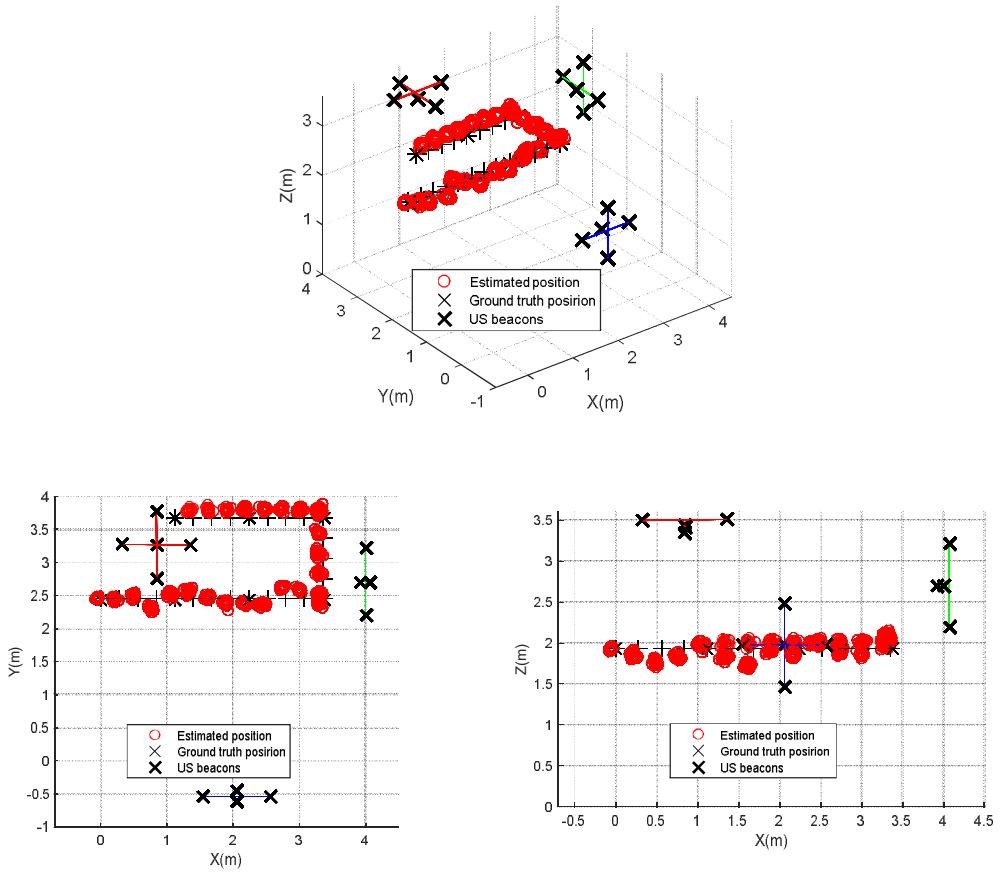

b)

Fig. 5.21. Positioning performance with high sampling frequency based on the fusion of three ULPSs with only one EKF, a) at z_1, and b) at z_2.

iv. Comparison and Discussion

Previous simulated analyses have been implemented experimentally when at least one ULPs is available. In the case of having more than one ULPS available, two merging approaches have been used. The first approach is based on the fusion of the obtained positions with the so-called loosely fusion methods. In these methods, three algorithms have been applied, such as hybrid MLE/Mean, Linear Kalman Filter and Adaptive Kalman filter. The second fusion approach employs the tightly coupled fusion. Also, three algorithms have been implemented here: Extended Kalman Filter for one ULPS, three independent EKF for three ULPSs, and one EKF for three ULPSs. Table 5.10 summarizes the CDF errors for 90% of the estimated positions. It is possible to observe that the tightly coupled method applying one EKF for the three ULPSs has the more accurate estimated positions, where the mean error for the grid of positions is less than 0.3m at z_1 and about 0.15 m at z_2. In addition, this method is capable to compute all the positions. However, for the loosely coupled method this point is not always true. For the loosely coupled approach, the hybrid MLE/Mean presents better results in the accuracy at z_2 than the others (KF and AKF), and AKF is the more accurate at z_2.

CDF Error (m)		z_1			z_2			*% of positions*
		Min	*Max*	*Mean*	*Min*	*Max*	*Mean*	
Loosely coupled fusion	MLE/Mean	0.202	0.429	0.34	0.082	0.28	0.196	90%
	KF	0.48	0.76	0.68	0.16	0.283	0.211	90%
	AKF	0.221	0.574	0.354	0.116	0.227	0.157	90%
Tightly coupled fusion	EKF (one ULPS)	0.18	0.812	0.476	0.156	0.514	0.354	100%
	EKF (three ind. ULPSs)	0.38	0.662	0.472	0.28	0.494	0.46	100%
	EKF (three fused ULPSs)	0.182	0.46	0.302	0.105	0.301	0.151	100%

Table 5.10. Summary of the CDF errors for the 90% of the estimated positions and the present of obtained positions at z_1 and z_2.

5.3 Definition of a Hardware Architecture for the Proposal Implementation

The real-time architecture described hereinafter is just for the 2D ultrasonic receiver prototype, as a starting approach. This implementation becomes a challenge, essentially due to the demanding computational capacity. FPGA (Field-Programmable Gate Array) devices are a suitable architecture for this approach, where the programmable logic allows a parallel design, conceding the development of hardware peripherals dedicated to the implementation of the

processing signals stages. Furthermore, the ARM processor available in the same die implies the possibility of designing SoC (System-on-Chip) architectures, where the processor is in charge of controlling the set of peripherals as well as running some tasks, which can fit more the software approach.

In this subsection, a FPGA-based SoC architecture is defined and oriented to process the ultrasonic signal acquired by a receiver moving inside the coverage volume of an ULPS. It consists of an ARM processor together with a low-level peripheral, which is in charge of processing the ultrasonic signal, by demodulating and performing the correlation functions to determine the TDOAs used in the positioning algorithms. The ARM processor also manages and controls an USB ultrasonic transducer, where the input ultrasonic signal is acquired. Furthermore, encoding techniques can be involved, based on different types of sequences, such as pseudo-random sequences, Kasami sequences, or complementary sets of sequences. Since the Prowave 328ST160 transducer has been installed in the ULPS, it implies a carrier frequency of 41.67 kHz in a BPSK (Binary Phase Shift Keying) modulation with an approximated bandwidth of 18kHz. Furthermore, Kasami codes with a length of 255 bits have been considered, where each one of the five existing beacons/transducers has its own identifying code [Hern2018], [Ureñ2018].

- Ultrasonic Signal Processing

The main module for the implementation is the processing block of the reception stage. After the ultrasonic acquisition realized by the receiver prototype, there is available a set of 10.000 samples with a width of 8 bits, sampled at fs=100 kHz, corresponding to the input signal $r[n]$. The consequent processing aims to compute the correlation functions of the emitted Kasami sequences, so the instants of arrival for the transmissions coming from the ultrasonic beacons can be determined. Fig. 5.22 shows the general block diagram for this low-level processing, mainly based on a BPSK demodulation and the already mentioned correlation functions [Hern2018], [Ureñ2018].

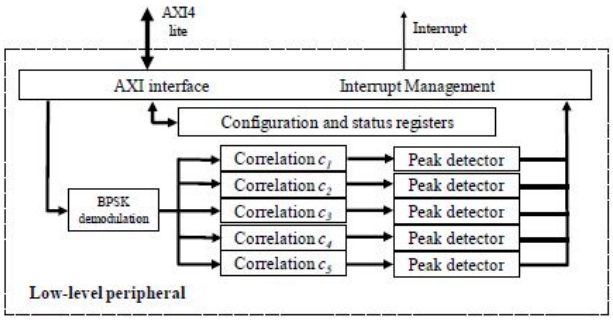

Fig. 5.22. General block diagram proposed for the low-level processing of the acquired signal r[n].

The first block consists of a BPSK demodulation according to (5.1).

$$d[n] = \sum_{m=0}^{M-1} r[n+m].\, s[n] \tag{5.1}$$

Where $d[n]$ is the demodulated signal; $s[n]$ is the modulation symbol; $r[n]$ is the acquired signal; and M is the length of the modulation symbol $s[n]$. Note that the parameter actually represents the oversampling factor, so $M=fs/fc$= 500 kHz/41.67kHz = 12 samples in this case. After the BPSK demodulation (plotted in Fig.5.23.up), a correlation process is carried out (plotted in Fig.5.23.bown), in order to search for the five Kasami sequence transmitted by the corresponding ultrasonic beacons (5.2).

$$t_i[n] = \sum_{l=0}^{L-1} d[l.M+n]\,.\, c_i[n] \tag{5.2}$$

Where $t_i[n]$ is the correlation output searching for the Kasami code c_i; $d[n]$ is still the demodulated signal; and L=255 bits is the length of the Kasami codes [Hern2018].

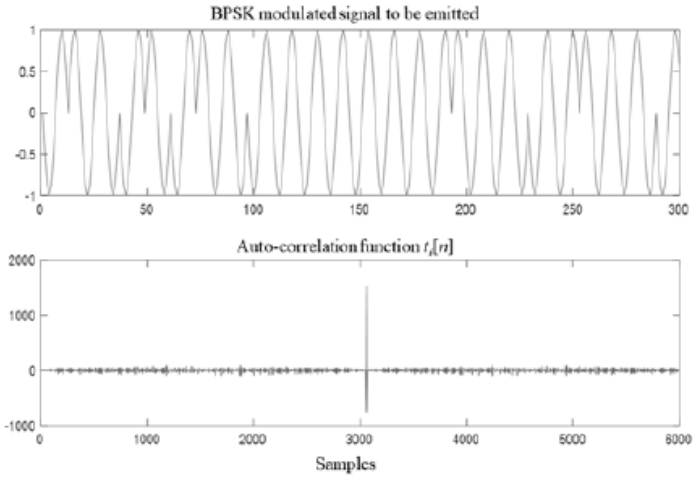

Fig. 5.23. Example of a 255-bits Kasami sequence, BPSK modulated (up), and its auto-correlation function (down).

Note that the correlation maximum values allow the time differences of arrival (TDOA) to be determined. Afterwards, these TDOA are used by a Gauss-Newton positioning algorithm to estimate the point coordinates [Ureñ2018].

- Proposed SOC architecture

Since the implementation of the receiver stage involves the management of the USB ultrasonic receiver together with aforementioned signal processing, a SoC (System-on-Chip) architecture based on a FPGA device has been proposed, as is shown in Fig. 5.24. It has been firstly prototyped on a Zedboard platform, with a Xilinx Zynq xc7z020 device [Hern2018].

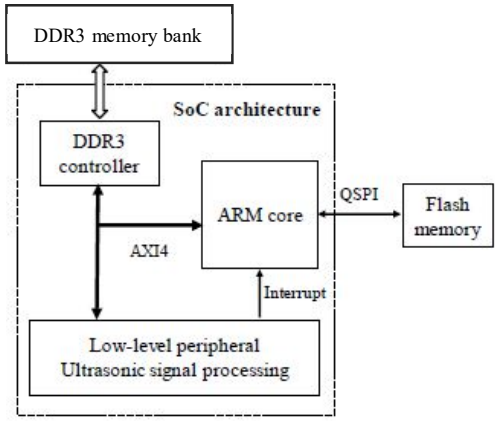

Fig. 5.24. SoC architecture proposed for the receiver module.

The ARM processor is in charge of managing the USB ultrasonic receiver, acquiring a buffer of 10.000 8-bits samples every time a position is desired to be estimated. These samples should be sent then to a low-level peripheral, implemented in the available programmable logic (PL), which carries out the BPSK demodulation and the correlation functions depicted in Fig. 5.23 (up). The low-level peripheral has been specified in HLS to compute the required processing. This design has been pipelined and it is connected to the ARM processor through an AXI-lite bus as a preliminary approach, although this bus is expected to become an AXI-stream in coming versions. Furthermore, the peripheral generates an interrupt signal that allows the processor to be notified whether any processing has been concluded. This peripheral has been specified in fixed-point representation, considering a trade-off between the resource consumption and the resulting quantization error. Table 5.11 shows the number of bits dedicated to the main variables and parameters in the design. With this definition, it has been tested that the absolute quantization error keeps below 0.75, whereas the relative one is below 0.04%. Fig. 5.25 shows an example of the resulting correlation function $t_i[n]$ in floating and fixed point, respectively, as well as the corresponding error [Hern2018].

	Parameter	No. of bits	No. of integer bits
Demod.	Input	8	1
	Symbol	16	1
	Product	24	2
	Accumulator	28	6
	Output	12	5
Corr	Input	12	5
	Accumulator	20	13
	Output	20	13

Table 5.11. Fixed-point representation defined for each parameter in the design of the low-level peripheral.

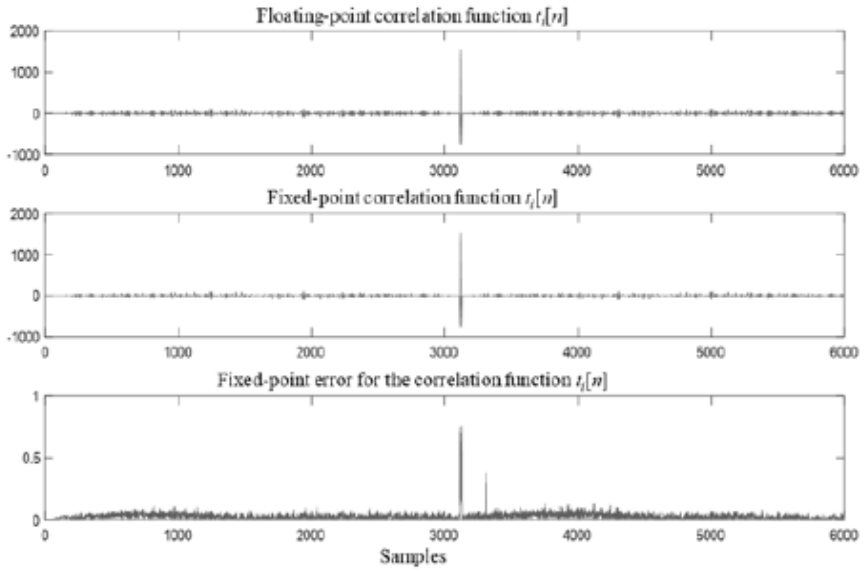

Fig. 5.25. Example of the fixed-point error obtained in the correlation function $t_i[n]$ for the representation defined in Table 5.11.

On the other hand, the ARM processor is running a Petalinux distribution, specifically compiled for this hardware architecture. The use of a Linux operating system implies an easy management of the USB ultrasonic receiver from the user space. In order to make accessible the low-level peripheral in the user space, a device driver has been developed for it, where the peripheral has been integrated as a character device. In this way, the ordinary calls to the *write* function allow the acquired samples from signal $r[n]$ to be sent to the peripheral, whereas the calls to the *read* function make possible to obtain the correlation functions $t_i[n]$. It is worth noting that the device driver also makes the necessary translation from the physical memory addresses in the SoC architecture, where the peripheral is placed, into the virtual addresses assigned for it in a SO memory system. Finally, the device driver includes an interrupt service routine, which manages the peripheral whenever it requires the processor's attention. Fig. 5.26 shows how the device driver has been included in the Linux architecture [Hern2018].

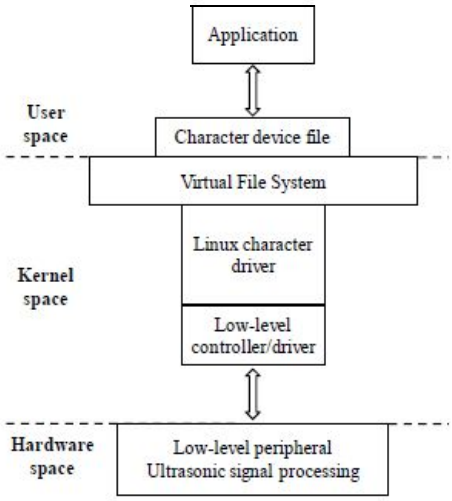

Fig. 5.26. Block diagram of the device driver proposed for the low-level peripheral in a Petalinux distribution.

.

5.3 Conclusions and Discussions

This chapter has presented the structure of the experimental system in order to test the 3D positioning system, as well as the positioning and fusion algorithms developed in this Thesis in previous chapters. This structure is composed of the deployment of three ULPSs installed in three perpendicular walls in the aim of covering almost the whole space of an ordinary room shape. Two different workspaces have been tested, the laboratory which is a small space and contains furniture and noise, and the hall which is an extended space which is a complex shape (not really a cube). Moreover, a 3D ultrasonic receiver prototype is used, to acquire signals coming from various direction emissions.

Then several fusion algorithms have been tested based on two different approaches, the loosely coupled approach and the tightly coupled approach and a comparison have been done. To conclude that, taking into account that two heights have been studied for all the considered algorithms, the height z_2 has the more accurate positions, due to its specific location with respect to the three ULPSs, especially for ULPS-2 and ULPS-3. Also, the tightly coupled approach for the three ULPSs simultaneously is the more accurate approach at both heights z_1 and z_2. However, the hybrid MLE/Mean fusion presents good accuracy for the loosely coupled approach at z_1 and the AKL presents better accuracy results at z_2 (also this approach do not

guarantee to get a position everywhere). Generally, the positioning error is in the decimetre range.

The last section deals with a real-time architecture of the receiver stage, where a SoC have been developed to perform a BPSK demodulation and five correlation functions for one ULPS. This stage must be continued as future work, so all the fusion algorithms might be implemented in the FPGA device.

Chapter 6

Conclusions and Future Work

This chapter introduces a summary of the most relevant contributions obtained from this thesis. In the first section, we outline its principal interventions and results. The second section presents some perspectives and some proposed research lines can be a succession of this thesis work. Finally, it is included those publications in indexed international journals, international and national conferences, all of them derived from this work.

6.1 Conclusions

In this Thesis, a 3D indoor positioning system is developed, employing several ultrasonic emitters and receivers. To deal with the issue of covering an extensive indoor space, several ULPSs have been used and various configurations have been studied. Furthermore, a 3D receiver prototype has been developed to acquire signals coming from different directions. To locate the more accurate position of the mobile receiver, different fusion algorithms have been developed to merge signals coming from those ULPSs. Those points are summarized below:

- Proposal of new 3D configurations deploying multiple ULPSs for positioning in large spaces. These 3D configurations employ several ULPSs placed at fixed positions and a mobile receiver in the space. The first configuration employed three ULPSs installed in three perpendicular planes, in the ceiling and two perpendicular walls in our case. Moreover, the second configuration used four ULPSs installed in the four corners of the principal diagonals of the room space. Then, after adapting the design of the ultrasonic emitter unit (ULPS), utilised previously for 2D positioning, the five ultrasonic beacons have a slight height difference between them, so they are not coplanar anymore, to avoid the positioning errors in its neighbourhood space. Also, a 3D ultrasonic receiver prototype is developed. This receiver is composed of three 2D ultrasonic receivers placed in the three faces of a tetrahedron. This design is employed to facilitate and maximize the reception of ultrasonic signals coming from various directions. The 3D prototype receiver is placed in a grid of positions, then in specific locations at several heights.

- Applying only one ULPS the estimated position had a considered error in the direction of the ULPS emission, from the decimetre range to the metre range. To solve this problem various ULPSs are used. Moreover, two ways of multi-ULPSs are studied.
    - The first way, when the ULPSs are synchronized, so the distribution of the PDOP values in the space and its accuracies are computed after estimating the receiver positions using the spherical Gauss-Newton algorithm, the error decreases to be in the centimetre range and reaches the decimetre range in the farthest receiver positions in the extended spaces.
    - The second way, when the ULPSs are not synchronized, so fusion methods have been applied to obtain the accurate receiver positions, after applying the hyperbolic Gauss-Newton algorithm. Various fusion methods are applied and compared. Some of those methods are using the fusion of the difference of distances computed after the reception of the signal, called tightly coupled method, by basically applying the EKF for a single ULPS or all the ULPSs. Other methods fuse the estimated positions, obtained by the Gauss-Newton algorithm, called loosely coupled fusion. In this method, the MLE fusion or the hybrid MLE/Mean fusion, LKF, and AKF are implemented, for various ULPSs combination. The error is between the centimetre and decimetre range, depending on the location of the mobile receiver and the ULPSs.
- In this thesis, the choice of the three unsynchronized ULPSs to be applied for the experimental tests is due to several factors. It presents better accuracy in the extended spaces as well as a more suitable error distribution in the space. Also, its cost is low, no need to add more devices to synchronize the ULPSs and the receiver.
- For this configuration (three perpendicular ULPSs), the more accurate positions are when the mobile receiver is included in the intersection of the three ULPSs coverage volumes, especially in the intersection of the three coverages volume axes. Afterwards, estimated positions for all the used fusion methods in the nearest areas of the three ULPSs and their intersections present better results and more accurate positions than in the farthest spaces as well as the lack of the coverage spaces of one ULPS or more.
- The tightly coupled fusion based on EKF of the three ULPSs shows the best and the most accurate method for the studied 3D positioning system. Also, after increasing the ultrasonic signals emission frequency (high-speed emission system), this method keeps it's positioning and accuracy proprieties then it can be used for 3D tracking. However,

AKF shows the more accurate positions for just the loosely coupled method in the same height of the ULPSs locations, as well as the hybrid MLE/ mean proves the accurate estimated positions for the loosely coupled method also in the farthest ULPS locations.

- The FPGA device is used to make the real-time implementation of the ultrasonic receivers, as it has a suitable architecture as well as it allows programmable logic in a parallel view to develop the assigned hardware peripherals. The ARM processor implies the possibility of designing SoC (System-on-Chip) architectures, where the processor is in charge of managing the set of peripherals and also running some tasks, which can be more suitable for a software approach. So, a BPSK demodulation and five correlation functions of the emitted Kasami sequences have been implemented in the SoC architectures to determine the instants of arrival for the transmissions coming from the ultrasonic beacons, then providing the time differences of arrival (TDOA), which will be used later by the Gauss-Newton positioning algorithm to estimate the position coordinates.

6.2 Future Works

The research lines developed in this Thesis can be extended to the following works:

- Determining the optimal number of ULPS units, their optimal installation positions as well as their orientations to get the optimal and uniform accuracy, in this extended space (room shape), then in a complex space as whole building with various floors. To do it, several algorithms can be utilised, such as artificial intelligence or genetic algorithms.
- Using hybrid technologies to improve the accuracy, as the combination of the ultrasonic beacons (ULPS) and Wi-Fi or light, as they exist everywhere and no need to buy specific devices for the emission; just the reception devices will be developed to receive and process the existing technologies.
- Finishing the development of the SoC architecture by adding the Gauss-Newton positioning algorithm and the multi-sensors fusion methods, as well as adapting a specific SoC architecture where the use of the FPGA resources will be optimal. Also, the energy consumption must be low to keep the battery life of the mobile system as long as possible.
- It is also possible to develop another ultrasonic emitter unit with a new design, form, number of ultrasonic beacons, and several other emission parameters, where is PDOP

values will be smaller and with synchronization to permit a real implementation of spherical trilateration.

6.3 Publications Derived from the Thesis

The scientific contributions procured from this Thesis are the following:

6.3.1 International Journals

- **K. Mannay**, J. Ureña, Á. Hernández, M. Machhout, "Performance of Location and Positioning Systems: a 3D-Ultrasonic System Case", *Advances in Science, Technology and Engineering Systems Journal*, Vol. 3, no. 2, pp. 106-118, 2018.
- **K. Mannay**, J. Ureña, Á. Hernández, M. Machhout, T. Aguili, "Characterization of an Ultrasonic Local Positioning System for 3D Measurements", *Sensors*, vol. *20*, pp. 2794, 2020.

6.3.2 International Conferences

- **K. Mannay**, N. Benhadjyoussef, M. Machhout and J. Ureña, "Location and Positioning Systems: Performance and comparison", *2016 4th International Conference on Control Engineering & Information Technology (CEIT)*, Hammamet, 2016, pp. 1-6.
- **K. Mannay**, J. Ureña, Á. Hernández, D. Gualda, and J. M. Villadangos, "Analysis of performance of Ultrasonic Local Positioning Systems for 3D Spaces", *8th International Conference on Indoor Positioning and Indoor Navigation (IPIN)*, Sapporo, 2017, vol. 1, pp. 1-5.
- **K. Mannay**, J. Ureña, Á. Hernández, D. Gualda, J. M. Villadangos, M. Machhout and T. Aguili, "Testing an Ultrasonic Local Positioning System for 3D Spaces", *9th International Conference on Indoor Positioning and Indoor Navigation (IPIN),* Nantes, 2018, pp. 1-5.
- Á. Hernández, J. Ureña, J. M. Villadangos and **K. Mannay**, "SoC Architecture for an Ultrasonic Receiver applied to Local Positioning Systems," *2018 Conference on Design of Circuits and Integrated Systems (DCIS)*, Lyon, France, 2018, pp. 1-5.

6.2.3 National Conferences

- J. Ureña, **K. Mannay**, Á. Hernández, D. Gualda, J. M. Villadangos , "Adaptation of an Ultrasonic Positioning System for Operation with Low-Speed Drones in Limited Areas", *Actas de las XXXIX Jornadas de Automática*, Badajoz, Spain, 2018, pp. 1-7.
- **K. Mannay**, J. Ureña, Á. Hernández, M. Machhout and T. Aguili, "3D Ultrasonic Indoor Local Positioning System: Study and Implementation", *Journées 5G&SC 2019*, Tunis, Tunisia, 2019, pp.1-5.

6.2.4 Workshop

- "Study of ULPS distributions for 3D positioning", *Workshop de Posicionamiento y Navegación (REPNIN)*, Alcala de Henares, Madrid, Spain, 2017.

References

[Ampl2012] Amplified SiSonicTM Microphone, SPU0414HR5H-SB, Product Specification, 2012.

[Bak2013] BAKSHI, Aditya, SHARMA, A. K., and MISHRA, Atul. Significance of mobile AD-HOC networks (MANETS). International Journal of Innovative Technology and Exploring Engineering (IJITEE), 2013, vol. 2, no 4, p. 1-5.

[Bat2018] BATISTIĆ, Luka and TOMIC, Mladen. Overview of indoor positioning system technologies. In: 2018 41st International Convention on Information and Communication Technology, Electronics and Microelectronics (MIPRO). IEEE, 2018. p. 0473-0478.

[Ben2012] BENINI, Alessandro, MANCINI, Adriano, MARINELLI, Alessio, and al. A biased extended kalman filter for indoor localization of a mobile agent using low-cost imu and uwb wireless sensor network. IFAC Proceedings Volumes, 2012, vol. 45, no 22, p. 735-740.

[Bha2019] BHATIA, Dinesh and PAUL, Sudip. Sensor fusion and control techniques for biorehabilitation. In : Bioelectronics and Medical Devices. Woodhead Publishing, 2019. p. 615-634.

[Bre2017] BRENA, Ramon F., GARCÍA-VÁZQUEZ, Juan Pablo, GALVÁN-TEJADA, Carlos E., and al. Evolution of indoor positioning technologies: A survey. Journal of Sensors, 2017, vol. 2017, p. 1-22.

[Cas2013] CASTANEDO, Federico. A review of data fusion techniques. The Scientific World Journal, 2013, vol. 2013, p. 1-20.

[Cho2017] CHOY, Suelynn, KUCKARTZ, Joost, DEMPSTER, Andrew G., and al. GNSS satellite-based augmentation systems for Australia. GPS Solutions, 2017, vol. 21, no 3, p. 835-848.

[Co1964] COX, Henry. On the estimation of state variables and parameters for noisy dynamic systems. IEEE Transactions on automatic control, 1964, vol. 9, no 1, p. 5-12.

[Dar2018] DARI, Yohanes Erwin, SUYOTO, Suyoto Suyoto, and PRANOWO, Pranowo Pranowo. CAPTURE: A mobile based indoor positioning system using wireless indoor positioning system. International Journal of Interactive Mobile Technologies (iJIM), 2018, vol. 12, no 1, p. 61-72.

[Daw2011] DAWES, Brett and CHIN, Kwan-Wu. A comparison of deterministic and probabilistic methods for indoor localization. Journal of Systems and Software, 2011, vol. 84, no 3, p. 442-451.

[DeA2015] DE ANGELIS, Alessio, MOSCHITTA, Antonio, CARBONE, Paolo, and al. Design and characterization of a portable ultrasonic indoor 3-D positioning system. IEEE Transactions on Instrumentation and Measurement, 2015, vol. 64, no 10, p. 2616-2625.

[Del] Dellaert, Frank. Sensor Fusion as Weighted Averaging, Technical Report, Center for Robotics and Intelligent Machines, Georgia Institute of Technology, p. 1-5.

[Gan2001] GAN, Qiang and HARRIS, Chris J. Comparison of two measurement fusion methods for Kalman-filter-based multisensor data fusion. IEEE Transactions on Aerospace and Electronic systems, 2001, vol. 37, no 1, p. 273-279.

[Ge2007] GENG, Yanrui, COLE, Anthony, DEMPSTER, A. G., and al. Developing a low-cost MEMS IMU/DGPS integrated system for robust machine automation. Proceedings of ION-GNSS 2007, 2007, p. 1618-1624.

[Gro2015] GROVES, Paul D. Principles of GNSS, inertial, and multisensor integrated navigation systems, [Book review]. IEEE Aerospace and Electronic Systems Magazine, 2015, vol. 30, no 2, p. 26-27.

[Gu2016] GU, Wenjun, AMINIKASHANI, Mohammadreza, DENG, Peng, and al. Impact of multipath reflections on the performance of indoor visible light positioning systems. Journal of Lightwave Technology, 2016, vol. 34, no 10, p. 2578-2587.

[Gua2014] GUALDA, David, UREÑA, Jesús, GARCÍA, Juan C., and al. Locally-referenced ultrasonic–LPS for localization and navigation. Sensors, 2014, vol. 14, no 11, p. 21750-21769.

[Gua2019] GUALDA, David, UREÑA, Jesús, GARCÍA, Juan C., and al. Simultaneous calibration and navigation (SCAN) of multiple ultrasonic local positioning systems. Information Fusion, 2019, vol. 45, p. 53-65.

[Hall2001] HALL, David and LLINAS, James (ed.). Multisensor data fusion. CRC press, 2001.

[Hau2012] HAUG, Anton J. Bayesian estimation and tracking: a practical guide. John Wiley & Sons, 2012.

[Hel2018] HELLMERS, Hendrik, KASMI, Zakaria, NORRDINE, Abdelmoumen, and al. Accurate 3D positioning for a mobile platform in non-line-of-sight scenarios based on IMU/magnetometer sensor fusion. Sensors, 2018, vol. 18, no 1, p. 126-145.

[Her2017] HERNÁNDEZ, Álvaro, GARCÍA, Enrique, GUALDA, David, and al. FPGA-based architecture for managing ultrasonic beacons in a local positioning system. IEEE Transactions on Instrumentation and Measurement, 2017, vol. 66, no 8, p. 1954-1964.

[Hern2018] HERNÁNDEZ, Álvaro, UREÑA, Jesús, VILLADANGOS, José M., and al. SoC Architecture for an Ultrasonic Receiver applied to Local Positioning Systems. In: 2018 Conference on Design of Circuits and Integrated Systems (DCIS). IEEE, 2018. p. 1-5.

[Ji2016] JIANG, Qideng, MA, Yongtao, LIU, Kaihua, and al. A probabilistic radio map construction scheme for crowdsourcing-based fingerprinting localization. IEEE Sensors Journal, 2016, vol. 16, no 10, p. 3764-3774.

[Jim2010] JIMÉNEZ, Antonio Ramón, SECO, Fernando, PRIETO, José Carlos, and al. Indoor pedestrian navigation using an INS/EKF framework for yaw drift reduction and a foot-mounted IMU. In: 2010 7th Workshop on Positioning, Navigation and Communication. IEEE, 2010. p. 135-143.

[Kal1961] KALMAN, Rudolph E. and BUCY, Richard S. New results in linear filtering and prediction theory. 1961.

[Kap2016] KAPOOR, Rohan, RAMASAMY, Subramanian, GARDI, Alessandro, and al. A novel 3D multilateration sensor using distributed ultrasonic beacons for indoor navigation. Sensors, 2016, vol. 16, no 10, p. 1637-1650.

[Kap2020] KAPOOR, Rohan, GARDI, Alessandro, and SABATINI, Roberto. Acoustic Positioning and Navigation System for GNSS Denied/Challenged Environments. In: 2020 IEEE/ION Position, Location and Navigation Symposium (PLANS). IEEE, 2020. p. 1280-1285.

[Kho2009] KHOURY, Hiam M. and KAMAT, Vineet R. Evaluation of position tracking technologies for user localization in indoor construction environments. Automation in construction, 2009, vol. 18, no 4, p. 444-457.

[Khy2012] KHYAM, Md Omar, ALAM, Md Jahangir, LAMBERT, Andrew J., and al. High precision ultrasonic positioning using phase correlation. In : 2012 6th International Conference on Signal Processing and Communication Systems. IEEE, 2012. p. 1-6.

[Kil2014] KILANI, Moez Ben, RAYMOND, Alexandre J., GAGNON, François, and al. RSSI-based indoor tracking using the extended Kalman filter and circularly polarized antennas. In: 2014 11th Workshop on Positioning, Navigation and Communication (WPNC). IEEE, 2014. p. 1-6.

[Kit2010] KITT, Bernd, GEIGER, Andreas, and LATEGAHN, Henning. Visual odometry based on stereo image sequences with ransac-based outlier rejection scheme. In: 2010 ieee intelligent vehicles symposium. IEEE, 2010. p. 486-492.

[Kol2017] KOLODZIEJ, Krzysztof W. and HJELM, Johan. Local positioning systems: LBS applications and services. CRC press, 2017.

[Kum2013] KUMAR, Mohit and MISHRA, Rashmi. An overview of MANET: History, challenges and applications. Indian Journal of Computer Science and Engineering (IJCSE), 2012, vol. 3, no 1, p. 121-125.

[Li2019] LIN, Qiongzheng, AN, Zhenlin, and YANG, Lei. Rebooting ultrasonic positioning systems for ultrasound-incapable smart devices. In : The 25th Annual International Conference on Mobile Computing and Networking. 2019. p. 1-16.

[Lor2004] LORINCZ, Konrad and WELSH, Matt. A robust, decentralized approach to rf-based location tracking. Harvard University, Cambridge, MA, Tech. Rep. TR-19-04, 2004, p.1-13.

[Lop2012] LOPES, Sergio Ivan, VIEIRA, Jose Manuel Neto, and ALBUQUERQUE, Daniel. High accuracy 3D indoor positioning using broadband ultrasonic signals. In: 2012 IEEE 11th International Conference on Trust, Security and Privacy in Computing and Communications. IEEE, 2012. p. 2008-2014.

[Lu2017] LU, Shaoping, XU, Chen, ZHONG, Ray Y., and al. A RFID-enabled positioning system in automated guided vehicle for smart factories. Journal of Manufacturing Systems, 2017, vol. 44, p. 179-190.

[Man2017] MANNAY, Khaoula, URENA, Jesús, HERNANDEZ, A., and al. Analysis of performance of ultrasonic local positioning systems for 3D spaces. In: 2017 International Conference on Indoor Positioning and Indoor Navigation (IPIN 2017). 2017, vol. 1, p. 1-5.

[Man2018] MANNAY, Khaoula, UREÑA, Jesus, HERNÁNDEZ, Álvaro, and al. Performance of Location and Positioning Systems: a 3D-Ultrasonic System Case. Advances in Science, Technology and Engineering Systems Journal (ASTESJ), 2018, vol. 3, no 2, p. 106-118.

[Man2020] MANNAY, Khaoula, UREÑA, Jesús, HERNÁNDEZ, Álvaro, and al. Characterization of an Ultrasonic Local Positioning System for 3D Measurements. Sensors, 2020, vol. 20, p. 1-23,

[Mann2018] MANNAY, Khaoula, URENA, Jesús, HERNANDEZ, A., and al, Testing an Ultrasonic Local Positioning System for 3D Spaces. In: 2018 International Conference on Indoor Positioning and Indoor Navigation (IPIN 2018). 2018, vol. 1, p. 1-5.

[Mau2012] MAUTZ, Rainer. Indoor positioning technologies. 2012.

[Me2012] MENG, Weixiao, HE, Ying, DENG, Zhian, and al. Optimized access points deployment for WLAN indoor positioning system. In: 2012 IEEE Wireless Communications and Networking Conference (WCNC). IEEE, 2012. p. 2457-2461.

[Med2013] MEDINA, Carlos, SEGURA, José Carlos, and DE LA TORRE, Angel. Ultrasound indoor positioning system based on a low-power wireless sensor network providing sub-centimeter accuracy. Sensors, 2013, vol. 13, no 3, p. 3501-3526.

[Men2019] MENDOZA-SILVA, Germán Martín, TORRES-SOSPEDRA, Joaquín, and HUERTA, Joaquín. A meta-review of indoor positioning systems. Sensors, 2019, vol. 19, no 20, p. 4507-4532.

[Mir2017] MIRAGLIA, Giovanni, MALEKI, K. Niki, and HOOK, Loyd R. Comparison of two sensor data fusion methods in a tightly coupled UWB/IMU 3-D localization system. In: 2017 International Conference on Engineering, Technology and Innovation (ICE/ITMC). IEEE, 2017. p. 611-618.

[Moh1999] MOHAMED, A. H. and SCHWARZ, K. P. Adaptive Kalman filtering for INS/GPS. Journal of geodesy, 1999, vol. 73, no 4, p. 193-203.

[Mou2018] MOUSA, Farag IK, ALMAADEED, Noor, BUSAWON, Krishna, and al. Indoor visible light communication localization system utilizing received signal strength indication technique and trilateration method. Optical Engineering, 2018, vol. 57, no 1, p. 016107-016128.

[Na2010] NAKAMURA, Shigeki, SATO, Tomohiko, SUGIMOTO, Masanori, and al. An accurate technique for simultaneous measurement of 3D position and velocity of a moving object using a single ultrasonic receiver unit. In : 2010 International Conference on Indoor Positioning and Indoor Navigation. IEEE, 2010. p. 1-7.

[Nur2017] NURMI, Jari, LOHAN, Elena-Simona, WYMEERSCH, Henk, and al. (ed.). Multi-technology positioning. Springer, 2017.

[PRI2005] PRIYANTHA, Nissanka Bodhi. The cricket indoor location system. 2005. Thèse de doctorat. Massachusetts Institute of Technology.

[Pri2009] PRIETO, José Carlos, JIMÉNEZ, Antonio Ramón, GUEVARA, Jorge, and al. Performance evaluation of 3D-LOCUS advanced acoustic LPS. IEEE transactions on instrumentation and measurement, 2009, vol. 58, no 8, p. 2385-2395.

[Pro2014] Pro-Wave Electronics Corporation, Air Ultrasonic Ceramis Transducers 328ST/R160, Product Specification, 2014.

[Pue2013] PUÉRTOLAS MONTAÑÉS, José Antonio, MENDOZA RODRÍGUEZ, Adriana, and SANZ PRIETO, Iván. Smart indoor positioning/location and navigation: A lightweight

approach. 2013, International Journal of Interactive Multimedia and Artificial Intelligence, 2013, vol. 2, p. 43-50.

[Raj2014] RAJAGOPAL, Niranjini, LAZIK, Patrick, and ROWE, Anthony. Visual light landmarks for mobile devices. In: IPSN-14 proceedings of the 13th international symposium on information processing in sensor networks. IEEE, 2014. p. 249-260.

[Rhu2012] RHUDY, Matthew, GROSS, Jason, GU, Yu, and al. Fusion of GPS and redundant IMU data for attitude estimation. In: AIAA Guidance, Navigation, and Control Conference. 2012. p. 5030-5043.

[Ro2015] ROY, Sudipto and NENE, Manisha J. A security framework for military application on infrastructure based wireless sensor network. In: 2015 IEEE International Conference on Research in Computational Intelligence and Communication Networks (ICRCICN). IEEE, 2015. p. 369-376.

[Rod2017] RODRÍGUEZ-NAVARRO, David, LÁZARO-GALILEA, José Luis, DE-LA-LLANA-CALVO, Álvaro, and al. Indoor positioning system based on a PSD detector, precise positioning of agents in motion using AoA techniques. Sensors, 2017, vol. 17, no 9, p. 2124-2150.

[Roo2002] ROOS, Teemu, MYLLYMÄKI, Petri, TIRRI, Henry, and al. A probabilistic approach to WLAN user location estimation. International Journal of Wireless Information Networks, 2002, vol. 9, no 3, p. 155-164.

[S2012] SAAD, Mohamed M., BLEAKLEY, Chris J., BALLAL, Tarig, and al. High-accuracy reference-free ultrasonic location estimation. IEEE Transactions on Instrumentation and Measurement, 2012, vol. 61, no 6, p. 1561-1570.

[Sab2013] SABATINI, Roberto, MOORE, Terry, and HILL, Chris. A new avionics-based gnss integrity augmentation system: Part 1–fundamentals. The Journal of Navigation, 2013, vol. 66, no 3, p. 363-384.

[Sah2015] SAHA, Nirzhar, IFTHEKHAR, Md Shareef, LE, Nam Tuan, and al. Survey on optical camera communications: challenges and opportunities. Iet Optoelectronics, 2015, vol. 9, no 5, p. 172-183.

[Sak2017] SAKPERE, Wilson, ADEYEYE-OSHIN, Michael, and MLITWA, Nhlanhla BW. A state-of-the-art survey of indoor positioning and navigation systems and technologies. South African Computer Journal, 2017, vol. 29, no 3, p. 145-197.

[Sal2008] SALAHSHOOR, Karim, MOSALLAEI, Mohsen, and BAYAT, Mohammadreza. Centralized and decentralized process and sensor fault monitoring using data fusion based on adaptive extended Kalman filter algorithm. Measurement, 2008, vol. 41, no 10, p. 1059-1076.

[Sam2009] SAMESHIMA, Harry S. and KATZ, Ed. Experiences with Cricket/Ultrasound Technology for 3-Dimensional Locationing within an Indoor Smart Environment. 2009. p. 1-14.

[Sat2011] SATO, Tomohiko, NAKAMURA, Shigeki, TERABAYASHI, Kotaro, and al. Design and implementation of a robust and real-time ultrasonic motion-capture system. In : 2011 International Conference on Indoor Positioning and Indoor Navigation. IEEE, 2011. p. 1-6.

[Sc2010] SCHWEINZER, Herbert and SYAFRUDIN, Mohammad. LOSNUS: An ultrasonic system enabling high accuracy and secure TDoA locating of numerous devices. In : 2010 International Conference on Indoor Positioning and Indoor Navigation. IEEE, 2010. p. 1-8.

[Se2012] SERTATIL, Cem, ALTINKAYA, Mustafa A., and RAOOF, Kosai. A novel acoustic indoor localization system employing CDMA. Digital Signal Processing, 2012, vol. 22, no 3, p. 506-517.

[Sert2012] SERTATIL, Cem, ALTINKAYA, Mustafa A., and RAOOF, Kosai. A novel acoustic indoor localization system employing CDMA. Digital Signal Processing, 2012, vol. 22, no 3, p. 506-517.

[Sil2018] SILVIA, Zuin, MARTINA, Calzavara, FABIO, Sgarbossa, and al. Ultra Wide Band Indoor Positioning System: analysis and testing of an IPS technology. IFAC-PapersOnLine, 2018, vol. 51, no 11, p. 1488-1492.

[Suz2009] SUZUKI, Akimasa, IYOTA, Taketoshi, CHOI, Yongwoon, and al. Measurement accuracy on indoor positioning system using spread spectrum ultrasonic waves. In: 2009 4th International Conference on Autonomous Robots and Agents. IEEE, 2009. p. 294-297.

[Tor2010] TORRES-SOLIS, Jorge, FALK, Tiago H., and CHAU, Tom. A review of indoor localization technologies: towards navigational assistance for topographical disorientation. INTECH Open Access Publisher, 2010. p. 1-34.

[Ure2016] UREÑA, J., VILLADANGOS, J. M., GUALDA, D., and al. Technical description of locate-US: An ultrasonic local positioning system based on encoded beacons. In: Proc. Int. Conf. Indoor Positioning Indoor Navigat. (IPIN). 2016. p. 1-4.

[Ure2018] UREÑA, Jesus, HERNÁNDEZ, Álvaro, GARCÍA, J. Jesús, and al. Acoustic local positioning with encoded emission beacons. Proceedings of the IEEE, 2018, vol. 106, no 6, p. 1042-1062.

[V1997] VARSHNEY, Pramod K. Multisensor data fusion. Electronics & Communication Engineering Journal, 1997, vol. 9, no 6, p. 245-253.

[Wa2014] WAWRZYNIAK, Piotr, KORBEL, Piotr, SKULIMOWSKI, Piotr, and al. Mixed-mode wireless indoor positioning system using proximity detection and database correlation. In : 2014 Federated Conference on Computer Science and Information Systems. IEEE, 2014. p. 1035-1042.

[Wa2013] WANG, Yapeng, YANG, Xu, ZHAO, Yutian, and al. Bluetooth positioning using RSSI and triangulation methods. In: 2013 IEEE 10th Consumer Communications and Networking Conference (CCNC). IEEE, 2013. p. 837-842.

[Xie2017] XIE, Lang, HEEGAARD, Poul E., and JIANG, Yuming. Survivability analysis of a two-tier infrastructure-based wireless network. Computer Networks, 2017, vol. 128, p. 28-40.

[Yan2006] YANG, Yuanxi and GAO, Weiguang. An optimal adaptive Kalman filter. Journal of Geodesy, 2006, vol. 80, no 4, p. 177-183.

[Yuc2012] YUCEL, Hikmet, EDIZKAN, Rifat, OZKIR, Taha, and al. Development of indoor positioning system with ultrasonic and infrared signals. In: 2012 International Symposium on Innovations in Intelligent Systems and Applications. IEEE, 2012. p. 1-4.

[Zaf2019] ZAFARI, Faheem, GKELIAS, Athanasios, and LEUNG, Kin K. A survey of indoor localization systems and technologies. IEEE Communications Surveys & Tutorials, 2019, vol. 21, no 3, p. 2568-2599.

[Zek2011] ZEKAVAT, Reza and BUEHRER, R. Michael. Handbook of position location: Theory, practice and advances. John Wiley & Sons, 2011.

[Zen2019] ZENG, Qingxi, LIU, Dehui, and LV, Chade. UWB/Binocular VO Fusion Algorithm Based on Adaptive Kalman Filter. Sensors, 2019, vol. 19, no 18, p. 4044-4063.

What feels like the End
is often the Beginning